BOUNDARY ELEMENT METHOD SOLUTION OF INITIAL AND BOUNDARY VALUE PROBLEMS IN FLUID DYNAMICS AND MAGNETOHYDRODYNAMICS

CANAN BOZKAYA

JUNE 2008

BOUNDARY ELEMENT METHOD SOLUTION OF INITIAL AND BOUNDARY VALUE PROBLEMS IN FLUID DYNAMICS AND MAGNETOHYDRODYNAMICS

A THESIS SUBMITTED TO
THE GRADUATE SCHOOL OF NATURAL AND APPLIED SCIENCES
OF
MIDDLE EAST TECHNICAL UNIVERSITY

BY

CANAN BOZKAYA

IN PARTIAL FULFILLMENT OF THE REQUIREMENTS
FOR
THE DEGREE OF DOCTOR OF PHILOSOPHY
IN
MATHEMATICS

JUNE 2008

Approval of the thesis:

BOUNDARY ELEMENT METHOD SOLUTION OF INITIAL AND BOUNDARY VALUE PROBLEMS IN FLUID DYNAMICS AND MAGNETOHYDRODYNAMICS

submitted by **CANAN BOZKAYA** in partial fulfillment of the requirements for the degree of **Doctor of Philosophy in Mathematics Department, Middle East Technical University** by,

Prof. Dr. Canan Özgen _____
Dean, Graduate School of **Natural and Applied Sciences**

Prof. Dr. Zafer Nurlu _____
Head of Department, **Mathematics**

Prof. Dr. Münevver Tezer _____
Supervisor, **Mathematics Dept., METU**

Examining Committee Members:

Prof. Dr. Hasan Taşeli _____
Mathematics Dept., METU

Prof. Dr. Münevver Tezer _____
Mathematics Dept., METU

Prof. Dr. Cahit Çıray _____
Aerospace Engineering Dept., METU

Prof. Dr. Ali Yazıcı _____
Computer Engineering Dept., TOBB

Assoc. Prof. Dr. I. Hakan Tarman _____
Engineering Sciences Dept., METU

Date: June 5th, 2008

I hereby declare that all information in this document has been obtained and presented in accordance with academic rules and ethical conduct. I also declare that, as required by these rules and conduct, I have fully cited and referenced all materials and results that are not original to this work.

Name, Last name : Canan Bozkaya

Signature :

ABSTRACT

BOUNDARY ELEMENT METHOD SOLUTION OF INITIAL AND BOUNDARY VALUE PROBLEMS IN FLUID DYNAMICS AND MAGNETOHYDRODYNAMICS

Bozkaya, Canan
Ph.D., Department of Mathematics
Supervisor: Prof. Dr. Münevver Tezer

June 2008, 188 pages

In this thesis, the two-dimensional initial and boundary value problems involving convection and diffusion terms are solved using the boundary element method (BEM). The fundamental solution of steady magnetohydrodynamic (MHD) flow equations in the original coupled form which are convection-diffusion type is established in order to apply the BEM directly to these coupled equations with the most general form of wall conductivities. Thus, the solutions of MHD flow in rectangular ducts and in infinite regions with mixed boundary conditions are obtained for high values of Hartmann number, M.

For the solution of transient convection-diffusion type equations the dual reciprocity boundary element method (DRBEM) in space is combined with the differential quadrature method (DQM) in time. The DRBEM is applied with the fundamental solution of Laplace equation treating all the other terms in the equation as nonhomogeneity. The use of DQM eliminates the need of iteration and very small time increments since it is unconditionally stable. Applications include unsteady MHD duct flow and elastodynamic problems. The transient Navier-Stokes equations which are nonlinear in nature are also solved with the DRBEM in space - DQM in time procedure iteratively in terms of stream function

and vorticity. The procedure is applied to the lid-driven cavity flow for moderate values of Reynolds number. The natural convection cavity flow problem is also solved for high values of Rayleigh number when the energy equation is added.

Keywords: BEM, DRBEM, DQM, fundamental solutions, MHD flow.

ÖZ

AKIŞKANLAR MEKANİĞİ VE MAGNETOHİDRODİNAMİK BAŞLANGIÇ VE SINIR DEĞER PROBLEMLERİNİN SINIR ELEMANLAR YÖNTEMİ İLE ÇÖZÜMÜ

Bozkaya, Canan
Doktora, Matematik Bölümü
Tez Yöneticisi: Prof. Dr. Münevver Tezer

Haziran 2008, 188 sayfa

Bu tezde, konveksiyon ve difüzyon terimlerini içeren iki boyutlu başlangıç ve sınır değer problemleri sınır elemanlar yöntemi kullanılarak çözülmüştür. Sınır elemanlar yönteminin durgun, birbirine bağlı magnetohidrodinamik denklemlere direkt olarak uygulanabilmesi amaçlanmıştır. En genel duvar iletkenlik koşulları ile verilmiş ve orijinal formu konveksiyon-difüzyon tipinde olan bu denklemlere sınır elemanlar yöntemi için gereken temel çözüm türetilmiştir. Böylece, gerek dikdörtgen kesitli kanal içerisinde gerekse sonsuz bölgelerde tanımlı magnetohidrodinamik akış problemlerinin çözümleri, karma sınır koşulları altında, büyük Hartmann sayıları, M, için elde edilmiştir.

Zaman bağımlı konveksiyon-difüzyon tipindeki denklemleri çözmek için, uzay koordinatlarının ve zaman parametresinin ayrıklaştırılmasında sırasıyla karşılıklı sınır elemanlar ve diferansiyel kuadratür yöntemleri birarada kullanılmıştır. Karşılıklı sınır elemanlar yöntemi Laplace denkleminin temel çözümü alınarak uygulanmış ve diğer bütün terimler sağ taraf fonsiyonu olarak kabul edilmiştir. Diferansiyel kuadratür koşulsuz kararlı bir yöntem olduğu için iterasyon ve küçük zaman aralığı kullanma gerekliliğini ortadan kaldırmaktadır. Zaman bağımlı magnetohidrodinamik kanal akış ve elastodinamik problemleri uygulamalar içerisinde-

dir. Aynı yöntem ile lineer olmayan, zamana bağlı Navier-Stokes denklemleri de stream fonksiyonu ve vorticity cinsinden çözülmüştür. Yöntemin uygulaması olarak üst kapağı hareketli kare kesitli kanal akış problemi ele alınmış, çözümler orta değerdeki Reynolds sayıları için elde edilmiştir. Akabinde, bu denklemlerle birlikte enerji denklemini de içeren doğal konveksiyon kanal problemi yüksek Rayleigh sayıları için çözülmüştür.

Anahtar Kelimeler: Sınır elemanlar yöntemi, karşılıklı sınır elemanlar yöntemi, diferansiyel kuadratür yöntemi, temel çözümler, MHD akış.

To my parents, Şerife and Ahmet,
my sisters, Nurhan and Nuray,
and my brother, Emre

ACKNOWLEDGMENTS

I would like to express my sincere gratitude to the following people for their contribution to the completion of my Ph.D. program.

First, I thank my supervisor Prof. Dr. Münevver Tezer for her precious guidance, continuous encouragement and persuasive support throughout the research. Her great enthusiasm and confidence in me make this study possible. Beyond being a supervisor, she is a good friend that I always feel myself free to share my anxieties and delights with her. Under her invaluable supervision, I have a chance to develop myself in both academic and personal subjects.

I would also like to thank the members of my defense committee, Assoc. Prof. Dr. Hakan Tarman, Prof. Dr. Hasan Taşeli, Prof. Dr. Cahit Çıray and Prof. Dr. Ali Yazıcı, for their valuable suggestions and reviewing my work. I thank Prof. Dr. Cem Tezer for his help in English and his helpful advice. My gratitude is extended to my friends and the members of the Department of Mathematics. Especially, I am grateful to my friends; Selçuk for his sincere friendship and his help in programming; Zeynep for always being a funny and understanding roommate with her smiling face; Didem and Gökçe for making me feel never alone with their endless friendships.

The financial support of The Scientific and Technical Research Council of Turkey (TÜBİTAK) is also acknowledged.

I offer my special thanks to my mother, Şerife, and my father, Ahmet, for their love, support and encouragement that provide me the success in my personal and consequently in my academic life. I thank my sister Nurhan, her husband Alparslan and my brother Emre for their frienships and encouragements during the research; and my pretty niece Ayşe Nihan and my lovely nephew Mehmet Çağrı for making my life more colorful.

Last, but not the least, I would like to express my deepest gratitude to my sister, Nuray, for always being near me when I need someone to talk and for sharing all the ups and downs of the life with me. I am thankful for her continuous support, motivation and understanding.

TABLE OF CONTENTS

ABSTRACT iv

ÖZ vi

ACKNOWLEDGMENTS ix

TABLE OF CONTENTS x

LIST OF TABLES xiii

LIST OF FIGURES xiv

LIST OF SYMBOLS xix

CHAPTER

1 INTRODUCTION 1

1.1 Fundamental Solution to Coupled Magnetohydrodynamic Equations 3

1.2 DRBEM in Space-DQM in Time Domains for Unsteady Problems 7

1.3 Plan of the Thesis 14

2 THE BOUNDARY ELEMENT METHOD AND THE FUNDAMENTAL SOLUTIONS 16

2.1 Fundamental Solutions 16

2.1.1 Fundamental solution of Laplace equation 18

2.1.2 Fundamental solutions of Helmholtz and modified Helmholtz equations 20

2.1.3 Fundamental solution of convection-diffusion equation . . . 23

2.2 Boundary Element Method 24
2.2.1 Discretization of the boundary in 2-D 27

3 BOUNDARY ELEMENT METHOD SOLUTION OF THE MAGNETOHYDRODYNAMIC FLOW EQUATIONS 34
3.1 Governing Equations for the MHD Flow 35
3.2 Derivation of the Fundamental Solution to Coupled MHD Flow Equations 40
3.3 Application of the Boundary Element Method 47
3.4 Numerical Results and Discussions 50
3.4.1 Pressure driven MHD flow in a rectangular duct 51
3.4.2 Electrically driven MHD flow on the upper half plane . . . 83

4 APPLICATION OF DUAL RECIPROCITY BOUNDARY ELEMENT METHOD WITH DIFFERENTIAL QUADRATURE TIME INTEGRATION SCHEME TO THE TRANSIENT CONVECTION-DIFFUSION TYPE EQUATIONS 106
4.1 Dual Reciprocity Boundary Element Method 108
4.1.1 DRBEM for Poisson equation 109
4.1.2 DRBEM for the equation $\nabla^2 = b(x, y, t, u, u_x, u_y, u_t)$ . . . 113
4.2 Differential Quadrature Method 117
4.2.1 The weighting coefficients in one-dimensional polynomial differential quadrature 117
4.2.2 DQM for the initial value problems 119
4.3 Numerical Solutions and Discussions 122
4.3.1 Diffusion and convection-diffusion problems 122
4.3.2 Unsteady magnetohydrodynamic duct flow 131
4.3.3 Transient elastodynamic problems 136

5 SOLUTION OF INCOMPRESSIBLE VISCOUS FLUIDS BY COUPLING OF DIFFERENTIAL QUADRATURE INTEGRATION SCHEME

WITH DUAL RECIPROCITY BOUNDARY ELEMENT METHOD 148
5.1 Method of Solution 152
5.1.1 Application of DRBEM to vorticity transport and stream function equations 152
5.1.2 Application of the DQM to vorticity transport equation . . 158
5.2 Numerical Results 161
5.2.1 Navier-Stokes equations in a square 161
5.2.2 Lid-driven cavity flow 164
5.2.3 Natural convection in a square cavity 170

6 CONCLUSION 175

REFERENCES 178

VITA 185

LIST OF TABLES

5.1 Numerical results of natural convection for $Ra = 10^3$, 10^4 and 10^5 174

LIST OF FIGURES

2.1 Geometric representation of the constant c_i 26
2.2 Constant and linear boundary elements 27

3.1 MHD duct flow with insulating walls 52
3.2 Velocity lines for $M = 50$ and $N = 80$ ($\alpha = \pi/2$) 54
3.3 Induced magnetic field lines for $M = 50$ and $N = 80$ ($\alpha = \pi/2$) . . 54
3.4 Velocity lines for $M = 300$ and $N = 300$ ($\alpha = \pi/2$) 55
3.5 Induced magnetic field lines for $M = 300$ and $N = 300$ ($\alpha = \pi/2$) 55
3.6 MHD duct flow under an external oblique magnetic field 56
3.7 Velocity lines for $M = 50$ and $N = 72$ ($\alpha = \pi/4$) 57
3.8 Induced magnetic field lines for $M = 50$ and $N = 72$ ($\alpha = \pi/4$) . . 58
3.9 Velocity lines for $M = 300$ and $N = 300$ ($\alpha = \pi/4$) 58
3.10 Induced magnetic field lines for $M = 300$ and $N = 300$ ($\alpha = \pi/4$) 59
3.11 Velocity lines for $M = 50$ and $N = 72$ ($\alpha = \pi/3$) 59
3.12 Induced magnetic field lines for $M = 50$ and $N = 72$ ($\alpha = \pi/3$) . . 60
3.13 Velocity lines for $M = 300$ and $N = 300$ ($\alpha = \pi/3$) 60
3.14 Induced magnetic field lines for $M = 300$ and $N = 300$ ($\alpha = \pi/3$) 61
3.15 MHD duct flow with a conducting part on $x = 0$ 62
3.16 Velocity lines for $M = 50$ and $N = 76$ ($l = 0.15$) 63
3.17 Velocity lines for $M = 50$ and $N = 76$ ($l = 0.25$) 64
3.18 Velocity lines for $M = 50$ and $N = 76$ ($l = 0.35$) 64
3.19 Induced magnetic field lines for $M = 50$ and $N = 76$ ($l = 0.15$) . . 65
3.20 Induced magnetic field lines for $M = 50$ and $N = 76$ ($l = 0.25$) . . 65
3.21 Induced magnetic field lines for $M = 50$ and $N = 76$ ($l = 0.35$) . . 66
3.22 Velocity lines for $M = 100$ and $N = 92$ ($l = 0.15$) 67
3.23 Velocity lines for $M = 100$ and $N = 92$ ($l = 0.25$) 67
3.24 Velocity lines for $M = 100$ and $N = 92$ ($l = 0.35$) 68
3.25 Induced magnetic field lines for $M = 100$, $N = 92$ ($l = 0.15$) . . . 68

3.26 Induced magnetic field lines for $M = 100$, $N = 92$ ($l = 0.25$) . . . 69
3.27 Induced magnetic field lines for $M = 100$, $N = 92$ ($l = 0.35$) . . . 69
3.28 Velocity lines for $M = 300$ and $N = 180$ ($l = 0.15$) 70
3.29 Velocity lines for $M = 300$ and $N = 180$ ($l = 0.25$) 70
3.30 Velocity lines for $M = 300$ and $N = 180$ ($l = 0.35$) 71
3.31 Induced magnetic field lines for $M = 300$ and $N = 180$ ($l = 0.15$) 71
3.32 Induced magnetic field lines for $M = 300$ and $N = 180$ ($l = 0.25$) 72
3.33 Induced magnetic field lines for $M = 300$ and $N = 180$ ($l = 0.35$) 72
3.34 Velocity and induced magnetic field lines for $M = 100$ and $N = 48$ ($l = 0.35$) 73
3.35 Velocity and induced magnetic field lines for $M = 100$ and $N = 184$ ($l = 0.35$) 73
3.36 Velocity and induced magnetic field lines for $M = 100$ and $N = 360$ ($l = 0.35$) 74
3.37 MHD duct flow with a conducting walls parallel to B_0 75
3.38 Velocity lines for $M = 10$, $N = 80$ 77
3.39 Induced magnetic field lines for $M = 10$, $N = 80$ 77
3.40 Velocity lines for $M = 100$, $N = 100$ 78
3.41 Induced magnetic field lines for $M = 100$, $N = 100$ 78
3.42 Velocity lines for $M = 300$, $N = 312$ 79
3.43 Induced magnetic field lines for $M = 300$, $N = 312$ 79
3.44 Velocity level curves for $M = 10$, $N = 80$ 80
3.45 Velocity level curves for $M = 50$, $N = 80$ 80
3.46 Velocity level curves for $M = 200$, $N = 212$ 81
3.47 Induced magnetic field level curves for $M = 10$, $N = 80$ 81
3.48 Induced magnetic field level curves for $M = 50$, $N = 80$ 82
3.49 Induced magnetic field level curves for $M = 200$, $N = 212$ 82
3.50 Geometry of Problem 1 89
3.51 Variation of V and B with the length of the boundary elements . 90
3.52 Variation of V and B with the length of computational interval on Γ_x 91
3.53 Velocity lines for $M = 10$, $N = 20$ 91

3.54 Induced magnetic field lines for $M = 10$, $N = 20$ 92
3.55 Velocity lines for $M = 300$, $N = 68$ 92
3.56 Induced magnetic field lines for $M = 300$, $N = 68$ 93
3.57 Details of Figure 3.55 93
3.58 Details of Figure 3.56 94
3.59 Velocity lines for $M = 700$, $N = 100$ 94
3.60 Induced magnetic field lines for $M = 700$, $N = 100$ 95
3.61 Geometry of Problem 2 96
3.62 Velocity lines for $M = 50$, $N = 28$, $a = 0.1$ 97
3.63 Velocity lines for $M = 50$, $N = 28$, $a = 0.3$ 98
3.64 Induced magnetic field lines for $M = 50$, $N = 28$, $a = 0.1$ 98
3.65 Induced magnetic field lines for $M = 50$, $N = 28$, $a = 0.3$ 99
3.66 Velocity lines for $M = 400$, $N = 80$, $a = 0.1$ 99
3.67 Velocity lines for $M = 400$, $N = 80$, $a = 0.3$ 100
3.68 Induced magnetic field lines for $M = 400$, $N = 80$, $a = 0.1$ 100
3.69 Induced magnetic field lines for $M = 400$, $N = 80$, $a = 0.3$ 101
3.70 Velocity lines for $M = 700$, $N = 100$, $a = 0.1$ 101
3.71 Velocity lines for $M = 700$, $N = 100$, $a = 0.3$ 102
3.72 Induced magnetic field lines for $M = 700$, $N = 100$, $a = 0.1$ 102
3.73 Induced magnetic field lines for $M = 700$, $N = 100$, $a = 0.3$ 103
3.74 Variation of Hartmann boundary layer thickness 104
3.75 Variation of secondary layer thickness 105

4.1 Solution of diffusion equation in a circular region at varying time levels for $r = 0$, 0.5 and 1.0 respectively, $N = 24$, $L = 10$ 125
4.2 Solution of convection-diffusion equation at several T' s for $d_3 = 1$ at $y = 0.6$, $N = 112$ 127
4.3 Solution of convection-diffusion equation for $d_3 = 20$ at $y = 0.6$, $T = 1.0$, $N = 180$, $L = 20$ 127
4.4 Solution of convection-diffusion equation for $d_3 = 40$ at $y = 0.6$, $T = 1.0$, $N = 240$, $L = 35$ 128

4.5 Solution of convection-diffusion type equation with FDM and DQM for $d_3 = 1$ at $y = 0.6$, $N = 112$, $L = 7$ 129
4.6 Solution of convection-diffusion type equation with FEM and DQM for $d_3 = 10$ at $y = 0.6$, $T = 1.0$, $N = 140$, $L = 13$ 129
4.7 Solution of convection-diffusion type equation with FEM and DQM for $d_3 = 20$ at $y = 0.6$, $T = 1.0$, $N = 180$, $L = 20$ 130
4.8 Solution of convection-diffusion type equation with variable coefficients at $T = 0.5$ and $T = 5.0$ respectively, $N = 200$, $K = 5$ 131
4.9 Velocity and induced magnetic field lines for $M = 5$, $N = 92$ . . . 134
4.10 Velocity and induced magnetic field lines for $M = 20$, $N = 108$. 135
4.11 Velocity and induced magnetic field lines for $M = 50$, $N = 240$, $y = 0$ 135
4.12 Displacement curve at the point (0.5, 0.5) for free vibration of membrane, $\lambda = 0$ 139
4.13 Traction curve at the point (1, 0.5) for free vibration of membrane, $\lambda = 0$ 139
4.14 Square plate subjected to outer force 140
4.15 Displacement curve at point B, $\lambda = 0$ 141
4.16 Traction curve at point C, $\lambda = 0$ 141
4.17 Displacement curve at point B, $\lambda = \pi/10$ 142
4.18 Traction curve at point C, $\lambda = \pi/10$ 142
4.19 Displacement curve for vibration of square plate subjected to Heaviside impact load for several N at the point (1.0, .5), $\lambda = 0$ 144
4.20 Relative error of displacement for several N at the point (1.0, .5), $\lambda = 0$ 145
4.21 Displacement curve for vibration of square plate subjected to Heaviside impact load for several K at the point (1.0, .5), $\lambda = 0$ 145
4.22 Relative error of displacement for several K at the point (1.0, .5), $\lambda = 0$ 146
4.23 Displacement curve at the point (1.0, .5) for vibration of square plate subjected to Heaviside impact load , $\lambda = 0$ 146

5.1 Stream function and vorticity contours for $Re = 500$, $N = 64$, $K = 4$, $T = 10$ 163
5.2 Stream function and vorticity contours for $Re = 1500$, $N = 72$, $K = 4$, $T = .5$ 163
5.3 Stream function and vorticity contours for $Re = 2000$, $N = 80$, $K = 4$, $T = 1$ 164
5.4 Boundary conditions for the lid-driven cavity problem 165
5.5 ψ values on the boundary mesh points 166
5.6 Stream function and vorticity contours for $Re = 100$, $N = 56$, $K = 3$ 168
5.7 Stream function and vorticity contours for $Re = 500$, $N = 88$, $K = 2$ 168
5.8 Stream function and vorticity contours for $Re = 1000$, $N = 112$, $K = 2$ 169
5.9 u-velocity along vertical line ($x = 0.5$) 169
5.10 v-velocity along horizontal line (y=0.5) 170
5.11 Boundary conditions for the natural convection flow 172
5.12 Stream function, vorticity and temperature contours: $(a1 - a3)$ $Ra = 10^3$, $N = 48$, $K = 3$; $(b1 - b3)$ $Ra = 10^4$, $N = 64$, $K = 2$ and $(c1 - c3)$ $Ra = 10^5$, $N = 100$, $K = 2$ 173

LIST OF SYMBOLS

$a_{ij}^{(m)}$	weighting coefficients for the mth order derivative of a function with respect to time in DQM
B_0	inductance of external imposed magnetic field
c	velocity of light in vacuum, wave propagation velocity
E	Young' s modulus
$\mathbf{E}$	electric field (vector)
$\mathbf{F}^{(em)}$	electromagnetic force (vector)
g	gravitational acceleration
$\boldsymbol{\mathcal{H}}$	induced magnetic field (vector)
$\mathcal{H}_0$	imposed magnetic field intensity
$H_\nu^{(n)}(z)$	Bessel function of the third kind (Hankel) of order ν
$\mathbf{J}$	electric current density (vector)
k	diffusivity constant
$K_\nu(z)$	modified Bessel function of the second kind of order ν
$\mathcal{L}$	differential operator
$\boldsymbol{\mathcal{L}}$	matrix differential operator
L_0, $L^{'}$	characteristic length
M	Hartmann number
Nu_0	Nusselt number on the boundary of the cavity at $x = 0$
$\overline{Nu}$	average Nusselt number throughout the cavity
p, p'	pressure
Pr	Prandtl number
Ra	Rayleigh number
Re	Reynold' s number
T_s	surface temperature (temperature of the wall)
T_∞	quiescent temperature (fluid temperature far from the surface of the object)

α	an angle, thermal diffusivity
β	thermal expansion coefficient
$\gamma^{'}$, ν	kinematic viscosity
Γ	problem boundary
$\delta(x)$	Kronecker delta function
$\Delta(x)$	Dirac delta function
η	magnetic diffusivity
λ	coefficient of viscous damping
μ, μ'	coefficient of viscosity
μ_e	magnetic permeability
ν_0, $U^{'}$	characteristic velocity
Ω	computational domain
ρ, ρ'	density
σ	electrical conductivity
θ_i	internal angle at the point i

CHAPTER 1

INTRODUCTION

A wide range of ordinary or partial differential equations which are the mathematical model of engineering or physical problems can only be solved in an approximate manner due to their complexity. The best known approximate techniques are the finite difference method (FDM) and the finite element method (FEM). These methods are called domain discretization methods since they require the discretization of the domain of the problem under consideration into a number of elements or cells.

Finite difference technique approximates the governing differential equation using truncated Taylor series expansion, which results in a system of algebraic equations. Although the method employs a comparatively straightforward internal discretization scheme and it is computationally economical, main difficulties of the technique lie in the consideration of curved geometries and the insertion of boundary conditions in this case.

Finite element method was developed in order to obtain a better representation of the geometry of the problem and to simplify the incorporation of the boundary conditions. The method uses polynomial interpolation functions to approximate the terms in the equations over small parts of domains, called elements. By assembling all of the influence matrices which express the properties of each element, a global matrix is obtained. This enables a simpler way than the one used in FDM for the insertion of the boundary conditions. The disadvantages of FEM are that large quantities of data are required to discretize the full domain, and that there are also difficulties when modelling infinite regions and moving boundary problems.

The boundary element method (BEM) is a well-established numerical technique for solving boundary value problems. The method provides an efficient

alternative to the prevailing finite difference and finite element methods by offering important advantages over them. The basic idea of the technique is the transformation of the original differential equation describing the behaviour of the unknown both inside and on the boundary of the domain, into an equivalent integral equation only on the boundary. This boundary integral relates boundary unknown solution values and their normal derivatives on the boundary. The main advantage of the BEM is its boundary-only nature. That is, BEM requires only the boundary discretization, which reduces the dimensionality of the problem under consideration by one. Thus, a smaller system of equations is obtained in comparison with the numerical methods requiring domain discretization, and then the boundary conditions can be applied in a similar way as is done in finite elements. Consequently, the solution is carried out very efficiently with substantial savings in computer time and storage. Another important advantage of the method is that it is also well suited for free and moving surface problems and for the problems defined on infinite regions for which the classical domain methods are unsuitable.

The origin of the boundary element method can be traced to the work on the application of boundary integral equations to potential flow and stress analysis problems in the 1960' s. The modern definition of boundary elements that is used nowadays was then introduced in 1978 by Brebbia [1] and his research group [2, 3]. Since 1978 the popularity of the boundary element method has increased. The first comprehensive work on the BEM and its applications in the various fields of engineering science is represented in the book of Banerjee and Butterfield [4]. The method has become a widely used technique with the applications around in many areas of engineering such as general potential theory, fluid mechanics, creep and fracture problems on solid mechanics, inelastic problems, elastodynamics, electrodynamics and magnetohydrodynamics problems. Further, transient heat conduction, wave propagation and other time dependent problems are also treated by BEM, [1, 2, 3].

The boundary element method, like finite elements, can be obtained as a special case of the general weighted residual statement [2]. The advantage of using weighted residual technique is its generality which allows the extension of

the method to the solution of more complex partial differential equations and it helps to clarify its relationship to other numerical techniques such as finite elements. Actually, the errors introduced if the analytical solution of the problem is replaced by an approximate solution, can be minimized by orthogonalizing them with respect to a weight (weighting) function. A special type of weighting function, called the fundamental solution of the differential equation defining the problem, is used in order to transform the weighted residual formula involving domain integrals into a boundary integral equation.

1.1 Fundamental Solution to Coupled Magnetohydrodynamic Equations

The fundamental solution represents the field generated by a concentrated unit source acting at a point x_i. The effect of this source is propagated from x_i to infinity without any consideration of boundary conditions. Because of this, the fundamental solution u^* satisfies the following equation, [5, 6],

$$\mathcal{L}u^* = -\Delta(x - x_i) \tag{1.1}$$

where $\mathcal{L}$ is the differential operator of the given initial and/or boundary value problem. The term $\Delta(x - x_i)$ represents the Dirac delta function which tends to infinity at the source point x_i and is equal to zero elsewhere.

Fundamental solutions are very useful in the theory of differential equations. They are used in solving nonhomogeneous equations and give the information about the regularity and growth of the solutions. The general existence and uniqueness theorems about the fundamental solutions are given in the books by Kythe [5] and Pozrikidis [6].

The fundamental solution is needed for the boundary element method solution, because BEM is a numerical technique which makes intensive use of a fundamental solution of differential equation defining the problem. The boundary integral equation corresponding to an initial and/or boundary value problem

is obtained by the choice of the weight function equivalent to the fundamental solution of the problem in question through the weighted residual procedure. Therefore, not to lose the most significant advantage of BEM, the boundary-only nature, fundamental solutions of the problem under consideration must be known. For most of the differential equations, including Laplace, Helmholtz, modified Helmholtz and convection-diffusion equations, the fundamental solutions exist in the literature. However, in the case of the coupled partial differential equations, e.g. magnetohydrodynamic (MHD) flows and original form of the Navier-Stokes equations, the fundamental solutions are not available to our knownledge.

In this thesis, the fundamental solution of the original coupled magnetohydrodynamic flow equations is derived and it is used in the boundary element method to obtain an efficient and accurate solution to these equations. This is one of the basic contributions in the thesis.

Magnetohydrodynamics studies the dynamics of electrically conducting fluids and their interactions with magnetic fields. In magnetohydrodynamics, magnetic field can induce currents in a moving conducting fluid, which create Lorentz force in turn on the fluid, and also change the magnetic field itself. Thus, one has to consider both the fluid mechanics equations and the electromagnetic field equations simultaneously. This makes most MHD problems both theoretically and practically difficult to study. Magnetohydrodynamics is a challenging subject due to its important applications in varies fields. It occurs naturally in the Earth's interior constituting the dynamo that produces the Earth's magnetic field, in the magnetosphere that surrounds the Earth, and throughout astrophysics. In the laboratory, magnetohydrodynamics is important in the magnetic confinement of plasmas in experiments on controlled thermonuclear fusion. Magnetohydrodynamic principles are also used for the propulsion and flight control in rocket and hypersonic aerodynamic vehicles, for pumping of conducting liquids, and for magnetohydrodynamic power generation.

The design of the MHD generators, pumps, brakes and accelerators requires an understanding of the flow of a conducting fluid down a duct having finitely conducting walls driven by a pressure gradient. The situation may be approximated by the pressure driven flow down a rectangular duct (a straight duct

of rectangular cross-section) under an applied transverse magnetic field imposed parallel to one pair of sides of the duct. The MHD flow which is laminar, steady and incompressible, of a viscous and electrically conducting fluid through pipes of rectangular cross-section is considered. Special emphasis is given to the ducts which have partly insulated partly conducting walls as well as to inclined applied magnetic field. Some problems of laminar flow of a viscous electrically conducting fluid on the upper half plane are also studied with the emphasis on the mixed boundaries due to the electrodes placed on the x-axis. These MHD flows constitute electrically driven MHD problems in infinite regions.

The motion of a nonconducting fluid through a duct can only be maintained by some cause of mechanical nature, such as a pressure gradient along the duct, a given upstream motion, the gravitational field, etc. These causes transfer a certain energy. Conducting fluids having an additional property give us the possibility of slowing down or accelerating the motion through the external action of an electromagnetic field. Moreover, the external magnetic field determines the appearance within the fluid of an induced current which can be made to flow in an external circuit. In this manner, some of the internal energy of the fluid is given up to the exterior as utilizable electrical energy (MHD generators). These are some of the reasons for the motion through ducts to be of considerable theoretical and practical importance.

The set of equations which describe MHD is a combination of the Navier-Stokes equations of fluid dynamics and Maxwell's equations of electromagnetism through Ohm' s law. These coupled system of differential equations have to be solved simultaneously. Due to the coupling of the MHD equations in velocity and induced magnetic field, analytical solutions are available only for some simple geometries under simple boundary conditions [7, 8]. Therefore, several numerical techniques such as FDM, FEM and BEM have been used to obtain approximate solutions for the MHD flow problems.

Singh and Lal [9, 10] have used FDM to solve MHD flow through channels of triangular cross-section for small values of Hartmann number, M. There is an extensive study on the numerical solution of MHD duct flow problems using FEM. Singh and Lal [11, 12], Gardner and Gardner [13] presented FEM solu-

tions for arbitrary cross-section of ducts but for Hartmann numbers less than 10. Tezer-Sezgin and Köksal [14] extended these studies to moderate Hartmann numbers up to 100 using standard FEM with linear and quadratic elements. Further, Demendy and Nagy [15] have used the analytical finite element method to obtain their numerical solution in the range of the Hartmann number $M \leq 1000$. Barrett [16] obtained FEM solution for high values of M by using very fine mesh within the Hartmann layers but as the author himself indicated the method is computationally very expensive, memory and time consuming. Later, Neslitürk and Tezer-Sezgin [17, 18] solved MHD flow equations in rectangular ducts by using a stabilized FEM with residual free buble functions. Thus, it was possible to increase M up to 1000 and also to use general wall conductivities.

The BEM applications for solving MHD flow problems arise from the difficulties of solving huge systems and high computational cost in FEM because of the domain discretization. Singh and Agarwal [19], Tezer-Sezgin [20], Liu and Zhu [21], Tezer-Sezgin and Han Aydın [22] and Carabineanu et al [23]' s papers are some studies on the BEM solutions of MHD duct flow problems. All these BEM solutions have been obtained for small and moderate values of Hartmann number ($M \leq 50$). On the other hand the duct walls are taken as insulated (the induced magnetic field is zero at the walls) which enables to decouple the MHD equations [20, 22]. The decoupled MHD equations then are treated with the dual reciprocity BEM, making use of the fundamental solution of Laplace or modified Helmholtz equations. But the original MHD equations are coupled convection-diffusion type equations and are convection dominated equations for large values of Hartmann number. Treating these equations in dual reciprocity BEM with the fundamental solution of decoupled equations loses this dominance and is the main reason of obtaining the solutions only for small and moderate values of Hartmann number. The solution procedure is also restricted to the simple case of insulated duct boundary, however most of the physical MHD flow applications need partly conducting and partly insulated duct walls. We consider here the direct BEM solution of MHD equations in coupled form. Thus, the derivation of the fundamental solution of coupled MHD equations which are convection-diffusion type is certainly required and given in this thesis.

The fundamental solution derived in the thesis for the coupled MHD equations is used in the boundary element solution of some MHD flows in rectangular duct. First, the duct with insulating wall is taken for comparing the results with the exact solution which is available only for this insulated boundary case, [8]. Then, the same problem is solved when the applied magnetic field is inclined, making angles with the axes. Special emphasis is given to the solution of MHD flow in ducts with partly insulating and partly conducting walls which was not possible to obtain before with BEM, since the equations can not be decoupled due to the mixed boundary conditions. Now, the original coupled MHD equations can be treated directly with the fundamental solution obtained here in using BEM. The MHD flow in rectangular duct with perfectly conducting walls parallel to the external magnetic field is also solved with the derived fundamental solution. In this case, the MHD equations can not also be decoupled since then the boundary conditions are coupled, [20]. In all these duct problems we have considered flows which are pressure driven. The MHD flows which are driven by imposed electric currents on the upper half plane of partly insulating and partly conducting x-axis are also solved by the BEM with the fundamental solution derived for coupled MHD equations. This fundamental solutions make possible to obtain solutions for large values of Hartmann number in MHD ducts and MHD infinite region problems. In the infinite region (upper half plane) MHD flow problem, the boundary layer thicknesses are also computed directly from the BEM integral formulations of the velocity and the induced magnetic field.

1.2 DRBEM in Space-DQM in Time Domains for Unsteady Problems

In the second part of the thesis, we consider unsteady problems as diffusion, convection-diffusion, unsteady MHD duct flow and elastodynamic problems. The time-dependent Navier-Stokes and the natural convection flow equations are also solved in a square cavity. In all of these problems, the first or second order time derivatives of the unknown functions are involved. Therefore, in the use of BEM,

finding the corresponding fundamental solutions is not an easy task. There are BEM studies using time dependent fundamental solution, [24, 25, 26], but then some domain integrals are encountered in the BEM formulation destroying the boundary only nature of the BEM applications. One of the procedure to deal with the time derivatives and some nonlinear terms in the BEM applications is the dual reciprocity boundary element method (DRBEM).

The dual reciprocity boundary element method was introduced by Nardini and Brebbia [27] in 1982 for elastodynamic problems and extended by Wrobel and Brebbia [28] to time-dependent diffusion in 1986. The method was further extended to more general problems by Partridge and Brebbia [29] and Partridge and Wrobel [30].

The dual reciprocity BEM uses the fundamental solution of the dominating differential operator (Laplace operator in the problems considered here) and treats the time and space derivatives, nonlinear terms as nonhomogeneity, [31]. In the thesis, the DRBEM is developed for the Poisson equation in which the nonhomogeneous term is a known function of space. Then, the method is extended to the time-dependent problems in which the right hand side of the governing equation is taken as an unknown function of the problem variable as well as a function of space and time derivatives. The right hand side is approximated using linear and quadratic radial basis (coordinate) functions, [22].

In the applications, the numerical solutions to transient convection-diffusion problems containing variable coefficients with Dirichlet and/or Neumann type boundary conditions are obtained. First, the solution of the diffusion problem in a circular region with mixed type boundary conditions, [32], is obtained. Then the rotating pulse problem with homogeneous Dirichlet boundary condition, [33], is solved in a square region. The solution of the unsteady MHD duct flow problem with insulating walls is also available with the DRBEM procedure since the equations are convection-diffusion type. Then, the transient elastodynamic problems, the only difference being the existence of the second order time derivative of the unknown, are solved with the DRBEM procedure, [34, 35]. The problems of free vibration of a square membrane [36], longitudinal vibration of a plate subjected to a periodic plane force [37] and Heaviside impact load [38], and longitudinal

vibration of damped plate subjected to Heaviside impact load [39] are solved.

DRBEM application to convection-diffusion and elastodynamic equations gives rise to initial value problems represented by systems of first and second order ordinary differential equations in time, respectively. These initial value problems need a time integration scheme for obtaining the discrete solution at a required time level or at steady-state. There are several time integration schemes mostly iterative in nature.

Singh and Kalra [40] provided a comprehensive comparative study of various different time integration algorithms indicating that all these algorithms for first order system of initial value problems encountered loss of accuracy in solving problems with Dirichlet boundary conditions. Later, in Singh and Kalra [41], a least square finite element scheme in the time domain was presented and it was found that the one step least squares scheme is more accurate than other one step schemes but it is not suitable for stiff initial value problems.

Recently, Chawla and Al-Zanaidi [42] have described a locally one-dimensional time integration scheme which is third order in time and is unconditionally stable for the diffusion equation in two space dimensions based on the extended trapezoidal formula. The method of fundamental solutions with dual reciprocity was applied to solve convection-diffusion equation by Partridge and Sensale [43]. The time integration scheme is also the finite difference with a relaxation procedure which is iterative in nature and needs carefully taken time increment. The combined application of dual reciprocity boundary element method (DRBEM) for the spatial partial derivatives and differential quadrature method for the time derivative in solving diffusion problems was presented by Tanaka and Chen [44]. The resulting Lyapunov matrix equation was solved by Bartels-Stewart algorithm to reduce the computing effort of solving such matrix equations. As the authors themselves indicate, the computing effort is nearly the same as that in the step by step integration algorithms since their procedure needs similarity transformations for the matrices in the differential system and this is quite time consuming computationally. Also, the method performs very well only for Dirichlet type boundary conditions in solving diffusion problems.

For the elastodynamic problems the finite difference approximations, such as

Houbolt and Newmark scheme that are implicit and unconditionally stable algorithms, have been used in the DRBEM solutions by Nardini and Brebbia [34] and Loeffer and Mansur [45]. They have concluded that the Houbolt scheme should be preferred for time marching in order to remove disturbing effects that higher modes introduce in the response. It has been also noticed that the accuracy and computational effort of the solutions depend greatly on the proper choice of the time step size and the number of employed internal nodes and subregions. Besides these commonly used traditional time integration methods, many researchers have used the finite element method in the discretization of the time domain. Chien et. al. [46] applied the time discontinuous Galerkin finite element method in time domain to solve the transient elastodynamic problems and showed that their solution technique is more stable and more accurate than the solution procedure based on the Houbolt method using step-by-step time integration algorithm.

In this thesis the differential quadrature method (DQM) is used for the solution of the resulting initial value problems in time, since it is known that it is unconditionally stable, [47]. The differential quadrature method was presented by R.E. Bellman and his associates in early 1970' s and since then, the technique has been succesfully employed in a variety of problems in engineering and physical science.

Differential quadrature provides a global approach to numerical discretization, which approximates the partial derivative of a function. The DQ method is based on the idea of conventional integral quadrature. Since the weighting coefficients only depend on the grid spacing, they do not relate to any special problem. Thus, any partial differential equation can easily be reduced to a set of algebraic equations using these coefficients. The key to DQM is to determine the weighting coefficients for the discretization of a derivative of any order. Several approaches, e.g. polynomial-based and Fourier expansion-based differential quadrature, have been introduced in order to obtain the weighting coefficients in [48, 49].

When the DQM discretizes the system of ordinary differential equations in time direction, we finally obtain a large system of linear equations for the unknown nodal values containing both discretized space and time points. This system gives the solution vector at any required time level since it contains spatial

nodal solution at all interior time levels between the initial and the final. These interior time levels may be either equally spaced or the Gauss-Chebyshev-Lobatto (GCL) points. This way, the resulting linear system of equations can be solved by any direct (Gaussian type) or iterative (Gauss-Seidel, SOR) solver without any special treatment like the use of Bartels-Stewart algorithm in the solution of Lyapunov matrix equations. Also, our solution procedure can be used with large time increments directly in the system of linear equations and does not need an iterative algorithm in the time direction. The other time integration schemes (Singh and Kalra [40]) mostly need very small time increments for stability and convergence and thus they are expensive computationally.

The last problem of this section is the DRBEM in space - DQM in time domains solution of the Navier-Stokes equations. Applications are on the solution of lid-driven cavity flow problem, and natural convection flow in a square cavity which includes the temperature equation as well. Four alternative formulations of the Navier-Stokes equations are given earlier. These are (i) the velocity-pressure formulation, (ii) the vorticity-stream function formulation, (iii) the stream function fourth order equation and (iv) the velocity-vorticity formulation. For two dimensional and also for axi-symmetric flows it is convenient to use the vorticity-stream function formulation where the equation of continuity is automatically satisfied. Of course, the resulting system consists of two coupled equations. Aside from the fact that one of these coupled equations, the vorticity transport equation, is nonlinear, there are several other difficulties associated with their solution. A major difficulty arises from the boundary conditions of the problem. In practice only the velocity on the boundaries is prescribed, while for the numerical solution of the equation in the vorticity-stream function formulation we require the values of the vorticity on the boundaries as well. The advantage of using the velocity-pressure formulation is that we are dealing with the primitive variables. However, in the velocity-pressure formulation it becomes necessary to solve a rather complicated pressure equation, introducing additional difficulties. A third possibility is to solve the fourth order formulation of the Navier-Stokes equations. Although there is only one nonlinear equation that is to be solved, it must be realized that one is now faced with a higher order nonlinear equation.

One of the boundary conditions is given in terms of the normal derivatives which also complicates the numerical procedure.

There are many studies on the numerical solutions of the Navier-Stokes equations in these formulations. Wong and Chan [50] have given numerical verifications of the mixed finite element consistent splitting scheme for solving Navier-Stokes equations in primitive variables. Their numerical simulation for the double lid-driven cavity by using fine mesh with 513×513 points for high Reynolds number, Re. The Navier-Stokes equations in stream function-vorticity formulation are solved using a fine uniform grid mesh of 601×601 for high Re by Erturk et. al. [51]. Wu and Liao [52] have applied the domain decomposition method and the general BEM to solve the laminar viscous flow in a driven cavity in terms of stream function and vorticity. Sousa and Sobey [53] have developed a global iteration matrix formulation for the stream function-vorticity equations for examining the effect on numerical stability of boundary vorticity discretization. Two dimensional time-dependent incompressible Navier-Stokes equations in stream function-vorticity formulation are solved by uncoupling the variables, linearizing the advective terms and using Euler type implicit time discretization by Ghadi [54] et al. A numerical solution by using differential quadrature method has been developed by Lo et al. [55] for 2D Navier-Stokes equations in velocity-vorticity form and this numerical algorithm has been implemented successfully to study natural convection in a differentially heated cavity. For the time derivative an iterative second-order time stepping of finite difference type has been used. Ding et al. [56] also presented a mesh free finite difference scheme based on the use of a weighted least-square aproximation to solve 2D natural convection in a square cavity. Moreover, the global methof of generalized differential quadrature is applied to simulate the natural convection in a square cavity by Shu and Xue [57]. In these two studies also iterative time integration schemes have been used.

Most of the studies on the discretization of time derivative in the vorticity transport equation are based on finite difference approximations. Erturk et al. [51] used an implicit Euler time scheme which is first order accurate, Wong and Chan [50] used a fully implicit second order backward differentiation formula since it is stable. Kobayashi et al. [58] have chosen an explicit fourth order accu-

rate Runge-Kutta method for solving the unsteady fourth order stream function equation. It is known that the above mentioned methods need iterations with a proper choice of time increment Δt for obtaining the solution at a required time level. Since all the equations obtained from space discretization must be solved in each iteration the whole solution procedure is usually computationally expensive.

In this thesis, we follow the stream function-vorticity formulation of the Navier-Stokes equations, and use the DRBEM treating the time derivatives and nonlinear terms as the nonhomogeneity in the vorticity transport and the energy equations. In the stream function equation the nonhomogeneity is the previous value of vorticity and these two equations are solved iteratively. We obtain the vorticity boundary conditions from the Taylor series expansion of stream function equation in terms of boundary and interior stream function values. The approximations for the vorticity boundary conditions affect the accuracy and convergence of the whole solution procedure. The formula we use involves the unknown values of stream function at the distances ph and qh away from the boundary (p and q are integers and h is the mesh distance). The DRBEM application to vorticity transport equation results in system of first-order initial value problem in time. We use the DQM in discretizing the time derivative in this initial value problem. The DQM gives the solution at any required time level at one stroke with a minimal number of discretized points between the initial and the required time level. By taking these results as initial values we solve the system for obtaining the solution at another required time level. This way, we reach iteratively to the steady state by solving the system in time blocks. These time blocks are discretized with very small number of Gauss-Chebyshev-Lobatto points since it is known that it gives better accuracy than the use of equally spaced points, [47]. Our solution procedure has been tested first on solving Navier-Stokes equations when a force term is present for which an exact solution is available. Then, the lid-driven cavity and natural-convection cavity problems are solved for Reynolds number up to 1000 and Rayleigh number up to 10^5, respectively. These two benchmark problems have occupied the attention of many scientists in developing computational algorithms for solving the Navier-Stokes and energy equations.

1.3 Plan of the Thesis

In Chapter 2, we give the derivations of fundamental solutions for Laplace, Helmholtz, modified-Helmholtz and convection-diffusion type differential equations. These are the basic studies in developing the fundamental solution for coupled convection-diffusion type differential equations which is necessary in obtaining BEM formulation of the MHD flow problems. The boundary element method is explained on Laplace equation giving the corresponding boundary integral equation. Discretization of the boundary is performed by using constant and linear elements and the resulting system of algebraic equations is obtained.

Chapter 3 presents the boundary element method solution of the magnetohydrodynamic flow equations. The governing equations of a laminar, steady and fully developed MHD flow of a viscous, incompressible and electrically conducting fluid are formulated in nondimensional form. Then, the derivation procedure in Chapter 2 is extended to establish the fundamental solution of these coupled MHD flow equations which are convection-diffusion type. With this fundamental solution, the MHD flow equations are transformed into the boundary integral equations. In Section 3.4 applications are given on the pressure driven MHD flows in rectangular ducts and electrically driven MHD flows in infinite regions. The first, involves flow which is driven by means of a constant pressure gradient and is subjected to a constant and uniform imposed magnetic field. We consider here four MHD flow problems in a rectangular duct with insulating and/or conducting, and partly insulating partly conducting walls. The latter includes the flow which is driven by the electrodes through external circuits. Two sample problems with partly insulating and partly perfectly conducting walls are solved on the upper half plane.

In the last two chapters of the thesis a numerical method, which is the coupling of the DRBEM with the DQM, is introduced for solving the transient convection-diffusion type and elastodynamic problems, and also for the solution of unsteady Navier-Stokes equations. The dual reciprocity BEM is used for the discretization of the spatial domain whereas the DQM discretizes the time domain.

Chapter 4 presents the theory of DRBEM on the Poisson equation with a

right hand side function containing the unknown itself, and its space and time derivatives. Thus, the application of DRBEM with the fundamental solution of the Laplace equation to these unsteady differential equations yields systems of first or second order (in transient elastodynamic problems) initial value problems in time. The differential quadrature method is made use of in solving resulting initial value problems in Section 4.2. The applications of the proposed coupled method are given in Section 4.3. The method is first applied to the diffusion equation in a circular region and then the transient convection-diffusion type equations with variable coefficients are solved. Then, the method is used for the solution of unsteady MHD flow problem with insulating walls, which also contains coupled convection-diffusion type equations. The last application in this chapter is the solution of the transient elastodynamic problems which involve second order time derivative of the solution as well.

In Chapter 5, the unsteady Navier-Stokes equations are solved in terms of stream function and vorticity by using the procedure given in Chapter 4. The stream function equation is solved with the dual reciprocity BEM and the coupling of DRBEM in space - DQM in time is made use of for solving the vorticity transport equation. Numerical results are given in Section 5.2 for the laminar flow of an incompressible, viscous fluid in a lid-driven cavity and for the natural convection flow in a square cavity. The natural convection flow contains also the energy equation which is of the same type of vorticity transport equation.

CHAPTER 2

THE BOUNDARY ELEMENT METHOD AND THE FUNDAMENTAL SOLUTIONS

In this chapter a unified treatment of the derivation of fundamental solutions for some differential equations and the basic formulation of the boundary element method for solving the model problem governed by the Laplace equation are presented. The first part of the chapter, Section 2.1, makes reference to the fundamental solution together with its properties. Furthermore, the derivation of the fundamental solutions for the Laplace, Helmholtz, modified Helmholtz and convection-diffusion type differential equations is demonstrated. Section 2.2 deals with the development of the general integral equation by weighting the Laplace equation over the domain of the problem. A corresponding boundary integral equation is obtained by using the fundamental solution together with the application of Divergence theorem. After the discretization of the boundary by constant, linear, quadratic or cubic elements, the problem is finally expressed as an algebraic system of equations which can be solved for discrete unknown boundary values after the insertion of the boundary conditions. The solution then, can be obtained at any required interior point by revising the same integral equation for interior region.

2.1 Fundamental Solutions

Fundamental solutions are very useful in the theory of differential equations. They are used in solving nonhomogeneous equations and tell us about the regularity and growth of solutions. The general existence and uniqueness theorems

about fundamental solutions are given in the books by Kythe [5] and Pozrikidis [6].

Let $\mathcal{L}$ be a differential operator, i.e.

$$\mathcal{L}u = f(x), \qquad x \in \Omega\,. \tag{2.1}$$

If $f(x) = -\Delta(x - x_i)$, the solution of equation (2.1), if it exists, is called the fundamental solution for the operator $\mathcal{L}$, and it is denoted by u^*, i.e.

$$\mathcal{L}u^* = -\Delta(x - x_i)\,. \tag{2.2}$$

The Dirac delta function, $\Delta(x - x_i)$, is defined as

$$\Delta(x - x_i) = \begin{cases} 0\,, & \text{if} \quad x \neq x_i \\ \infty\,, & \text{if} \quad x = x_i \end{cases}$$

and is also constrained to satisfy the identity

$$\int_\Omega \Delta(x - x_i)\, d\Omega = 1$$

where Ω is the domain contaning the point x_i. The Dirac delta function has the fundamental property that

$$\int_\Omega \Phi(x)\Delta(x - x_i)\, d\Omega = \begin{cases} \Phi(x_i), & \text{if} \quad x_i \in \Omega \\ 0, & \text{if} \quad x_i \notin \Omega \end{cases}$$

where $\Phi(x)$ is any function continuous at x_i.

In other words, the fundamental solution represents the field generated by a concentrated unit source acting at a point $x = x_i$. The effect of this source is propagated from $x = x_i$ to infinity without any consideration of boundary conditions.

The fundamental solution is necessary for the application of the boundary element method to the differential equations, because BEM is a numerical technique which makes intensive use of a fundamental solution of the problem in

question in order to reach the boundary-only merit of the method. Therefore, we derive fundamental solutions for some classical linear operators, namely Laplace, Helmholtz, modified Helmholtz and convection-diffusion operators, which help us also to find the fundamental solutions of some coupled differential equations in progress.

2.1.1 Fundamental solution of Laplace equation

The solution of potential flow problems governed by Laplace or Poisson equations is one of the most important application area of the boundary element method. In this thesis, especially in Chapters 4 and 5, some differential equations in which the Laplacian is the dominating differential operator will be considered. In order to transform these differential equations into boundary integrals, the fundamental solution of the Laplace equation is made use of. This section concentrates on the derivation of the fundamental solution of firstly two- and three-dimensional Laplace equation, and then a general form is given for the n-dimensional case [5, 6].

2-D Laplace Equation

The two-dimensional (2-D) Laplace equation is governed by

$$\frac{\partial^2 u}{\partial x^2} + \frac{\partial^2 u}{\partial y^2} = 0 \tag{2.3}$$

in the $xy-$coordinate system. By the substitution $r = |\mathbf{x}| = \sqrt{x^2 + y^2}$, equation (2.3) can be written in polar coordinates for the axisymmetric case as follows

$$\frac{1}{r}\frac{\partial}{\partial r}\left(r\frac{\partial u}{\partial r}\right) = 0\,. \tag{2.4}$$

The fundamental solution u^* of 2-D Laplace equation is the solution of

$$\nabla^2 u^* = -\Delta(\mathbf{x}) \tag{2.5}$$

where $\Delta(\mathbf{x})$ is the Dirac delta function concentrated at origin. For $\mathbf{x} \neq \mathbf{0}$, u^* will satisfy the homogeneous equation

$$\nabla^2 u^* = 0 \tag{2.6}$$

which has a general solution

$$u^* = A \ln(r) + B \tag{2.7}$$

where A and B are constants. By setting arbitrarily $B = 0$, equation (2.7) will have the form

$$u^* = A \ln(r) \, . \tag{2.8}$$

In order to determine the coefficient A, take into account the magnitude of the source at $\mathbf{x} = \mathbf{0}$. Integrating equation (2.5) over a small circle of radius ϵ center at origin, we obtain $A = -\dfrac{1}{2\pi}$.

Hence, the fundamental solution for 2-D Laplace equation is given by

$$u^* = -\frac{1}{2\pi} \ln(r) = \frac{1}{2\pi} \ln\left(\frac{1}{|\mathbf{x}|}\right) \, . \tag{2.9}$$

In a similar way, the fundamental solution of the 3-D Laplace equation can be easily obtained as

$$u^* = -\frac{1}{4\pi r} = -\frac{1}{4\pi |\mathbf{x}|} \tag{2.10}$$

in which the magnitude r of the vector $\mathbf{x} = (x, y, z)$ is given by $r = \sqrt{x^2 + y^2 + z^2}$.

n-D Laplace Equation

The n-dimensional Laplace equation in polar coordinates with the absence of angle dependence is given by

$$\frac{1}{r^{n-2}} \frac{\partial}{\partial r} \left(r^{n-1} \frac{\partial u}{\partial r} \right) = 0, \qquad n > 2 \tag{2.11}$$

where $r = |\mathbf{x}| = \sqrt{x_1^2 + x_2^2 + \cdots + x_n^2}$. By a similar procedure given for the two-dimensional case, the general solution of the homogeneous equation corresponding to the equation

$$\nabla^2 u^* = -\Delta(\mathbf{x}) \tag{2.12}$$

is obtained as, [59],

$$u^* = \frac{A}{r^{n-2}(n-2)} + B \tag{2.13}$$

for $\mathbf{x} \neq \mathbf{0}$, in which A and B are constants. By setting arbitrarily $B = 0$, equation (2.13) will have the form

$$u^* = \frac{A}{r^{n-2}(n-2)}\,. \tag{2.14}$$

One can determine the coefficient A as $A = -1/S_n(1)$ by integrating equation (2.12) over a unit radius spherical domain centered at origin, where $S_n(1)$ is the surface area of the spherical domain. Hence, the fundamental solution for n-dimensional Laplace equation is obtained as

$$u^* = -\frac{1}{r^{n-2} S_n(1)(n-2)} \quad \text{for } n > 2\,. \tag{2.15}$$

2.1.2 Fundamental solutions of Helmholtz and modified Helmholtz equations

Helmholtz and modified Helmholtz equations are also basic differential equations like Laplace in the sense that their fundamental solutions are beneficial to obtain the fundamental solutions of convection-diffusion type equations which is derived in the following Section 2.1.3. First, the derivation of the two-dimensional case is sketched out in details and then the form for three-dimension is given.

2-D Helmholtz and modified Helmholtz equations

The two-dimensional Helmholtz and modified Helmholtz equations in the cartesian coordinate system are given by

$$\frac{\partial^2 u}{\partial x^2} + \frac{\partial^2 u}{\partial y^2} + \lambda^2 u = 0 \tag{2.16}$$

and

$$\frac{\partial^2 u}{\partial x^2} + \frac{\partial^2 u}{\partial y^2} - \lambda^2 u = 0 \tag{2.17}$$

respectively. These two equations differ only with the sign of the term $\lambda^2 u$, with an arbitrary constant λ.

The substitution $r = |\mathbf{x}| = \sqrt{x^2 + y^2}$ leads to the equation

$$r^2 \frac{d^2 u}{dr^2} + r\frac{du}{dr} \pm \lambda^2 r^2 u = 0 \tag{2.18}$$

in polar coordinates for both of equations (2.16) and (2.17). The fundamental solutions u^* of 2-D Helmholtz and modified Helmholtz equations satisfy the equation

$$\nabla^2 u^* \pm \lambda^2 u^* = -\Delta(\mathbf{x}) \tag{2.19}$$

respectively, for the plus and minus signs in the equation.

For $\mathbf{x} \neq \mathbf{0}$, u^* will satisfy the homogeneous equation

$$\nabla^2 u^* \pm \lambda^2 u^* = 0 \tag{2.20}$$

which have general solutions

$$u^* = \begin{cases} AH_0^{(1)}(\lambda r) + BH_0^{(2)}(\lambda r) & \text{for Helmholtz equation} \\ \\ AH_0^{(1)}(i\lambda r) + BH_0^{(2)}(i\lambda r) & \text{for modified Helmholtz equation} \end{cases} \tag{2.21}$$

where $H_0^{(1)}$ and $H_0^{(2)}$ are the Bessel functions of the third kind and of order zero, A and B are constants. Since u^* is bounded as $r \to \infty$, we must take $A = 0$ for Helmholtz equation and $B = 0$ for Modified Helmholtz equation, then

$$u^* = \begin{cases} BH_0^{(2)}(\lambda r) & \text{for Helmholtz equation} \\ \\ AH_0^{(1)}(i\lambda r) & \text{for Modified Helmholtz equation .} \end{cases} \tag{2.22}$$

In order to determine the coefficients A and B, apply Divergence theorem to

the integral of equation (2.19) over Ω, so we have

$$\int_{\partial\Omega} \frac{du^*}{dr}\, dS = -1 \tag{2.23}$$

or

$$\lim_{r\to 0}\left(\frac{du^*}{dr}\, 2\pi r\right) = -1 \ . \tag{2.24}$$

Then, $A = i/4$ and $B = -i/4$. Hence, the fundamental solutions for two-dimensional Helmholtz and modified Helmholtz equations are obtained as

$$u^* = \begin{cases} -\dfrac{i}{4}\, H_0^{(2)}(\lambda r) & \text{for Helmholtz equation} \\ \\ \dfrac{i}{4}\, H_0^{(1)}(i\lambda r) = \dfrac{1}{2\pi} K_0(\lambda r) & \text{for modified Helmholtz equation} \end{cases} \tag{2.25}$$

where K_0 is the modified Bessel function of the second kind and of order zero.

In the same manner the fundamental solutions for three-dimensional case can be derived and they are given by, [5],

$$u^* = \begin{cases} -\dfrac{\lambda}{4\pi i}\sqrt{\dfrac{\pi}{2\lambda r}}\, H_{1/2}^{(2)}(\lambda r) & \text{for Helmholtz equation} \\ \\ \dfrac{\lambda}{2\pi^2}\sqrt{\dfrac{\pi}{2\lambda r}}\, K_{1/2}(\lambda r) & \text{for modified Helmholtz equation} \end{cases} \tag{2.26}$$

or

$$u^* = \begin{cases} -\dfrac{\lambda}{4\pi i}\dfrac{i}{\lambda r} e^{-i\lambda r} = -\dfrac{e^{-i\lambda r}}{4\pi r} & \text{for Helmholtz equation} \\ \\ \dfrac{\lambda}{2\pi^2}\dfrac{\pi}{2\lambda r} e^{-\lambda r} = \dfrac{e^{-\lambda r}}{4\pi r} & \text{for modified Helmholtz equation} \end{cases} \tag{2.27}$$

where $H_{1/2}$, $I_{1/2}$ and $K_{1/2}$ are spherical Bessel function of the third kind, modified spherical Bessel functions of the first and second kind, respectively.

2.1.3 Fundamental solution of convection-diffusion equation

This section deals with the derivation of the fundamental solution of the two-dimensional convection diffusion equation which is going to be used in Chapter 3 to derive the fundamental solution of the coupled convection-diffusion type equations. The two-dimensional convection-diffusion equation is given as

$$k\nabla^2 u = U_x \frac{\partial u}{\partial x} + U_y \frac{\partial u}{\partial y} \tag{2.28}$$

where $\mathbf{U} = (U_x, U_y)$ is the constant velocity vector and k is the diffusivity constant.

Introducing a new variable $v = v(x, y)$ as follows, [5],

$$u = \frac{1}{k} \exp\left(\frac{\mathbf{U}.\mathbf{x}}{2k}\right) v \,, \tag{2.29}$$

one obtains a differential equation in the form of a modified Helmholtz equation

$$\nabla^2 v - \lambda^2 v = 0 \tag{2.30}$$

where $\lambda = \dfrac{|\mathbf{U}|}{2k}$ and $|.|$ denotes the magnitude of a vector.

Equation (2.30) is a 2-D modified Helmholtz equation with the fundamental solution

$$v^* = \frac{1}{2\pi} K_0(\lambda|\mathbf{x}|) \tag{2.31}$$

given as in Section 2.1.2. Now substituting v^* back in equation (2.29), we obtain

$$u^* = \frac{1}{2\pi k} \exp\left(\frac{\mathbf{U}.\,\mathbf{x}}{2k}\right) K_0(\frac{|\mathbf{U}|}{2k}\,|\mathbf{x}|) \tag{2.32}$$

which is the fundamental solution for 2-D convection-diffusion equation.

2.2 Boundary Element Method

The boundary element formulation for the solution of boundary value problems can be deduced as a weighted residual technique as mentioned before. To illustrate this, we follow the procedure in [1, 3] to find the solution of Laplace equation in a two- or three-dimensional domain Ω,

$$\nabla^2 u = 0, \qquad \text{in } \Omega \tag{2.33}$$

with the following boundary conditions:

i. *Essential* conditions of type $u = \bar{u}$ on Γ_1

ii. *Natural* conditions such as , $q = \dfrac{\partial u}{\partial n} = \bar{q}$ on Γ_2

where n is the outward normal to the boundary $\Gamma = \Gamma_1 + \Gamma_2$ and the bars indicate known values.

The errors ϵ introduced in the above equations if the exact values of u and q are replaced by the approximate values $\hat{u}$ and $\hat{q}$, can be minimized by orthogonalizing them with respect to a weight function [1, 3].

Thus, one can obtain the following residuals

$$\begin{aligned} \epsilon &= \nabla^2 \hat{u} \neq 0 && \text{in } \Omega \\ \epsilon_1 &= \hat{u} - \bar{u} \neq 0 && \text{on } \Gamma_1 \\ \epsilon_2 &= \frac{\partial \hat{u}}{\partial n} - \bar{q} \neq 0 && \text{on } \Gamma_2 \ . \end{aligned} \tag{2.34}$$

These residuals can be weighted as in the method of weighted residuals, so that we have the following integral equation

$$\int_\Omega \epsilon \, u^* \, d\Omega + \int_{\Gamma_1} \epsilon_1 \, \bar{u}^* \, d\Gamma + \int_{\Gamma_2} \epsilon_2 \, \bar{\bar{u}}^* \, d\Gamma = 0 \tag{2.35}$$

where u^*, $\bar{u}^*$ and $\bar{\bar{u}}^*$ are the weight functions. After the substitution of the residuals in equation (2.35), we have

$$\int_\Omega (\nabla^2 \hat{u}) u^* \, d\Omega + \int_{\Gamma_1} (\hat{u} - \bar{u}) \, \bar{u}^* \, d\Gamma + \int_{\Gamma_2} \left(\frac{\partial \hat{u}}{\partial n} - \bar{q} \right) \bar{\bar{u}}^* \, d\Gamma = 0 \ . \tag{2.36}$$

Now, applying the Divergence theorem

$$-\int_{\Omega}\frac{\partial\hat{u}}{\partial n}\frac{\partial u^*}{\partial n}\,d\Omega+\int_{\Gamma_1+\Gamma_2}\frac{\partial\hat{u}}{\partial n}\,u^*\,d\Gamma+\int_{\Gamma_1}(\hat{u}-\bar{u})\,\bar{u}^*\,d\Gamma+\int_{\Gamma_2}\left(\frac{\partial\hat{u}}{\partial n}-\bar{q}\right)\bar{\bar{u}}^*\,d\Gamma=0 \tag{2.37}$$

and choosing $u^*=-\bar{\bar{u}}^*$, we have

$$-\int_{\Omega}\frac{\partial\hat{u}}{\partial n}\frac{\partial u^*}{\partial n}\,d\Omega+\int_{\Gamma_1}\frac{\partial\hat{u}}{\partial n}\,u^*\,d\Gamma+\int_{\Gamma_1}(\hat{u}-\bar{u})\,\bar{u}^*\,d\Gamma+\int_{\Gamma_2}\bar{q}\,u^*\,d\Gamma=0\ . \tag{2.38}$$

Application of the Divergence theorem once more and choosing $\bar{u}^*=\partial u^*/\partial n$, equation (2.38) becomes

$$\int_{\Omega}\hat{u}\,\nabla^2u^*\,d\Omega-\int_{\Gamma_2}\hat{u}\,\frac{\partial u^*}{\partial n}\,d\Gamma+\int_{\Gamma_1}\frac{\partial\hat{u}}{\partial n}\,u^*\,d\Gamma-\int_{\Gamma_1}\bar{u}\,\frac{\partial u^*}{\partial n}\,d\Gamma+\int_{\Gamma_2}\bar{q}\,u^*\,d\Gamma=0\,. \tag{2.39}$$

To eliminate the domain integral $\displaystyle\int_{\Omega}\hat{u}\,\nabla^2u^*\,d\Omega$, we choose u^* such that

$$\nabla^2u^*=-\Delta(\mathbf{r}-\mathbf{r_i}) \tag{2.40}$$

where $\Delta(\mathbf{r}-\mathbf{r_i})$ is the Dirac delta function concentrated at the point $i=(x_i,y_i)$, $\mathbf{r}$ and $\mathbf{r_i}$ are the distance vectors of the field point (x,y) and the source point (x_i,y_i), respectively. Substituting equation (2.40) into equation (2.39) and by the integral property of the Dirac delta function, we have

$$-c_i\,\hat{u}_i+\int_{\Gamma_1}\frac{\partial\hat{u}}{\partial n}\,u^*\,d\Gamma+\int_{\Gamma_2}\bar{q}\,u^*\,d\Gamma-\int_{\Gamma_1}\bar{u}\,\frac{\partial u^*}{\partial n}\,d\Gamma-\int_{\Gamma_2}\hat{u}\,\frac{\partial u^*}{\partial n}\,d\Gamma=0\,. \tag{2.41}$$

Defining

$$\tilde{u}=\begin{cases}\bar{u}, & \text{if}\quad i\in\Gamma_1\\ \hat{u}, & \text{if}\quad i\in\Gamma_2\end{cases}$$

$$\tilde{q}=\begin{cases}\bar{q}, & \text{if}\quad i\in\Gamma_2\\ \hat{q}, & \text{if}\quad i\in\Gamma_1\,.\end{cases}$$

where $\hat{q} = \partial\hat{u}/\partial n$ and $q^* = \partial u^*/\partial n$, we have

$$c_i\,\tilde{u}_i + \int_\Gamma \tilde{u}\,q^*\,d\Gamma - \int_\Gamma \tilde{q}\,u^*\,d\Gamma = 0\,. \tag{2.42}$$

The constant c_i is equal to

$$c_i = \begin{cases} \dfrac{\theta_i}{2\pi}, & \text{if } i \in \Gamma \\ 1, & \text{if } i \in \Omega/\Gamma \end{cases}$$

with θ_i denoting the internal angle at point i in radians, as shown in Figure 2.1.

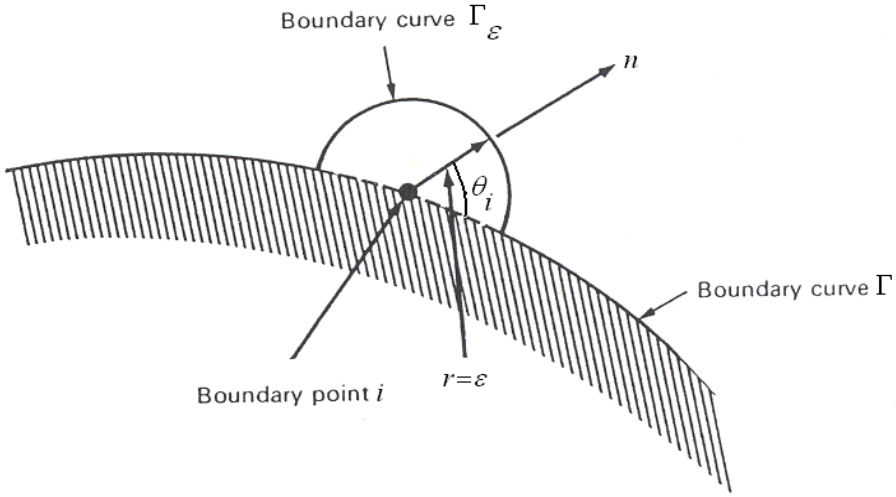

Figure 2.1: Geometric representation of the constant c_i

The weight function u^* is the fundamental solution of the given differential equation which is the Laplace equation in this case. For two- and three-dimensional Laplace equation the weight functions are derived in Section 2.1.1 and given respectively by

$$u^* = \frac{1}{2\pi}\ln\left(\frac{1}{r}\right)$$

and

$$u^* = \frac{1}{4\pi r}$$

with the distance r between the source and field points.

2.2.1 Discretization of the boundary in 2-D

We consider now how the boundary integral equation (2.42) can be discretized to find the system of equations from which the boundary values are calculated. In BEM, discretization is made on the boundary by dividing it into small portions which are called *boundary elements*, [1, 3]. The points where the unknown values are considered are called *nodes*. If the node is taken in the middle of the element, the method is called *constant element method*. The method with the nodes at the extremes or ends of the element is the *linear element method* (see Figure (2.2)). Higher order elements can be obtained by adding nodes to the elements (e.g. center and end points for a cubic element).

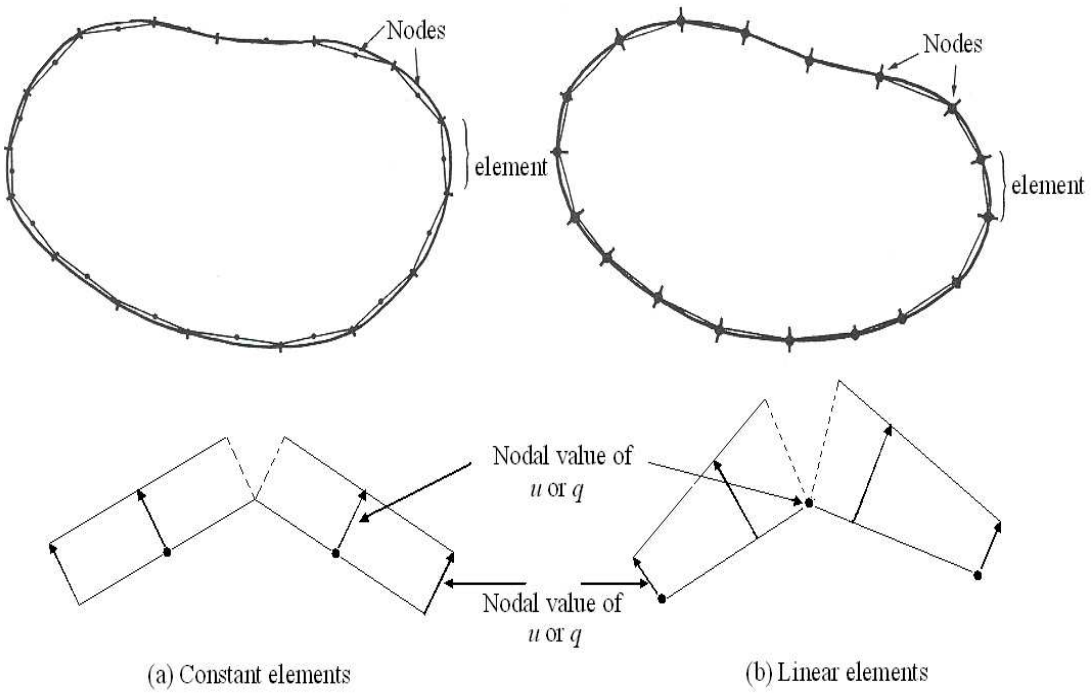

Figure 2.2: Constant and linear boundary elements

The discretization with constant and linear elements of equation (2.42) is performed by using u and q for the approximate solution and its normal derivative

respectively instead of $\tilde{u}$ and $\tilde{q}$ for simplifying the notation. That is,

$$c_i\, u_i + \int_\Gamma u\, q^*\, d\Gamma - \int_\Gamma q\, u^*\, d\Gamma = 0\,. \tag{2.43}$$

Constant element case

The boundary is assumed to be divided into N elements. In the case of the constant elements the values of u and q are assumed to be constant over each element and equal to the value at the mid-element node. The points at the ends of the elements are used only for defining the geometry of the problem. Note that for the type of constant element the boundary is always *smooth* at the nodes as these are located at the center of the elements, hence the constant c_i is always $\frac{1}{2}$.

Equation (2.43) can be discretized for a given point i before applying any boundary conditions, as follows

$$\frac{1}{2}\, u_i + \sum_{j=1}^{N} \int_{\Gamma_j} u q^*\, d\Gamma_j - \sum_{j=1}^{N} \int_{\Gamma_j} q u^*\, d\Gamma_j = 0 \tag{2.44}$$

where the point i is on the boundary and Γ_j is the boundary of the jth element. The u and q values can be taken out of the integral since they are constants over each element j and they are denoted as u_j and q_j. Hence,

$$\frac{1}{2}\, u_i + \sum_{j=1}^{N} \hat{H}_{ij} u_j = \sum_{j=1}^{N} G_{ij} q_j \tag{2.45}$$

where $\hat{H}_{ij} = \displaystyle\int_{\Gamma_j} q^*\, d\Gamma_j$ and $G_{ij} = \displaystyle\int_{\Gamma_j} u^*\, d\Gamma_j$. These integrals are related to the node i where the fundamental solution is applied, to any other node j. The entries $\hat{H}_{ij}$ and G_{ij} are given particularly for the two-dimensional problems with the fundamental solution of 2-D Laplace equation as follows, [1, 3]

$$\hat{H}_{ij} = \frac{1}{2\pi} \int_{\Gamma_j} \frac{(\mathbf{r} - \mathbf{r_i}).\mathbf{n}}{|\mathbf{r} - \mathbf{r_i}|^{\mathbf{2}}}\, d\Gamma_j$$

and

$$G_{ij} = \frac{1}{2\pi} \int_{\Gamma_j} \ln \frac{1}{|\mathbf{r} - \mathbf{r_i}|} \, d\Gamma_j$$

where $\mathbf{r} = (x, y)$ and $\mathbf{r_i} = (x_i, y_i)$ are the free (field) and fixed (source) points, respectively. The symbol $|.|$ denotes the norm of a vector and $\mathbf{n}$ is the outward unit normal vector on the boundary Γ_j.

The matrix-vector form of equation (2.45) is

$$\mathbf{Hu} = \mathbf{Gq} \tag{2.46}$$

where $\mathbf{u}$ and $\mathbf{q}$ are vectors of length N and $\mathbf{H}$ and $\mathbf{G}$ are the $N \times N$ matrices. The entries of the matrix $\mathbf{H}$ are given as

$$H_{ij} = \frac{1}{2}\delta_{ij} + \hat{H}_{ij}$$

where δ is the Kronecker delta function defined as

$$\delta_{ij} = \begin{cases} 1, & \text{if } i = j \\ 0, & \text{if } i \neq j \, . \end{cases}$$

Notice that N_1 values of u and N_2 values of q are known on Γ_1 and Γ_2 respectively ($N_1 + N_2 = N$), hence there are only N unknowns in the system of equations (2.46). To introduce these boundary conditions into system (2.46) one has to rearrange the system by moving columns of $\mathbf{H}$ and $\mathbf{G}$ from one side to the other. Once all unknowns are passed to the left hand side one can write

$$\mathbf{A}'\mathbf{x} = \mathbf{b} \tag{2.47}$$

where $\mathbf{x}$ is the vector of unknown boundary values of u and q, and $\mathbf{b}$ is found by multiplying the corresponding columns of $\mathbf{H}$ or $\mathbf{G}$ by the known values of u or q. It is interesting to point out that the unknowns are now a mixture of the potential u and its normal derivative q, rather than the potential only as in finite element method. This is a consequence of the boundary element method being a *mixed* formulation, and constitutes an important advantage over finite elements.

Equation (2.47) can now be solved and all the boundary values will then be known. Once this is done it is also possible to calculate internal values of u at any point i by using equation (2.43) with $c_i = 1$, which after the discretization become

$$u_i = \sum_{j=1}^{N} q_j G_{ij} - \sum_{j=1}^{N} u_j \hat{H}_{ij} \, . \tag{2.48}$$

Notice that now, the fundamental solution is considered to be acting on an internal point i and that all values of u and q are already known. The entries $\hat{H}_{ij}$ and G_{ij} in (2.48), in which the indices i and j denote the fixed node in the interior of the domain and jth element on the boundary respectively, have to be calculated for each different internal point.

The coefficients $\hat{H}_{ij}$ and G_{ij} can be calculated using analytical or numerical integration such as Gauss quadrature formula for the case $i \neq j$. In the case $i = j$ the singularity of the fundamental solution requires a more accurate integration rule or a special formula such as logarithmic integration. For constant element case $\hat{H}_{ii}$ and G_{ii} can be calculated analytically. The entries $\hat{H}_{ii} = 0$ due to the orthogonality of the distance vector $\mathbf{r}$ and the normal vector $\mathbf{n}$. The integrals G_{ii} require special handling. For a two-dimensional element, for instance, they are of the form

$$G_{ii} = \int_{\Gamma_i} u^* d\Gamma_i = \frac{1}{2\pi} \int_{\Gamma_i} \ln\left(\frac{1}{r}\right) d\Gamma_i \, . \tag{2.49}$$

In order to integrate the above expression one can perform a change of coordinates such that

$$r = \left|\frac{\ell}{2}\zeta\right|, \qquad d\Gamma_i = dr = \frac{\ell}{2} d\zeta \tag{2.50}$$

where ℓ is the length of the element. Hence, taking into account symmetry,

equation (2.49) can be written as, [1, 3]

$$
\begin{aligned}
G_{ii} = \frac{1}{2\pi}\int_{\text{Point 1}}^{\text{Point 2}} \ln\left(\frac{1}{r}\right) d\Gamma_i &= \frac{1}{\pi}\int_{\text{node } i}^{\text{Point 2}} \ln\left(\frac{1}{r}\right) d\Gamma_i \\
&= \frac{\ell}{2\pi}\int_0^1 \ln\left(\frac{2}{\ell\zeta}\right) d\zeta \qquad (2.51)\\
&= \frac{\ell}{2\pi}\left\{\ln\left(\frac{2}{\ell}\right) + \int_0^1 \ln\left(\frac{1}{\zeta}\right)\right\} .
\end{aligned}
$$

Thus,

$$
G_{ii} = \frac{\ell}{2\pi}\left(\ln\frac{2}{\ell} + 1\right) . \qquad (2.52)
$$

Linear element case

In this case we consider a linear variation of u and q for which the nodes are taken to be at the ends of the boundary element. After the discretization of the boundary into N elements, the boundary integral equation (2.43) can be written as

$$
c_i u_i + \sum_{j=1}^{N}\int_{\Gamma_j} uq^*\, d\Gamma_j = \sum_{j=1}^{N}\int_{\Gamma_j} qu^*\, d\Gamma_j . \qquad (2.53)
$$

The integrals in this equation are more difficult to evaluate than those for the constant element as u and q vary linearly over each element Γ_j and hence it is not possible to take them out of integrals. The values of u and q at any point on the element can be defined in terms of their nodal values and two linear interpolation functions ϕ_1 and ϕ_2 as follows

$$
\begin{aligned}
u(\xi) = \phi_1 u_1 + \phi_2 u_2 = [\phi_1 \quad \phi_2]\begin{bmatrix} u_1 \\ u_2 \end{bmatrix} \\
q(\xi) = \phi_1 q_1 + \phi_2 q_2 = [\phi_1 \quad \phi_2]\begin{bmatrix} q_1 \\ q_2 \end{bmatrix}
\end{aligned} \qquad (2.54)
$$

where ξ is the dimensionless coordinate varying from -1 to $+1$ and the two interpolation functions are

$$\phi_1 = \frac{1}{2}(1-\xi), \qquad \phi_2 = \frac{1}{2}(1+\xi)\,. \tag{2.55}$$

The integral over an element j given on the left hand side of equation (2.53) can be written as

$$\int_{\Gamma_j} uq^*\,d\Gamma_j = \int_{\Gamma_j} [\phi_1 \quad \phi_2]\,q^*\,d\Gamma_j \begin{bmatrix} u_1 \\ u_2 \end{bmatrix} = [h_{ij}^1 \quad h_{ij}^2] \begin{bmatrix} u_1 \\ u_2 \end{bmatrix} \tag{2.56}$$

where for each jth element we have two components

$$h_{ij}^1 = \int_{\Gamma_j} \phi_1 q^*\,d\Gamma_j, \qquad h_{ij}^2 = \int_{\Gamma_j} \phi_2 q^*\,d\Gamma_j\,. \tag{2.57}$$

Similarly, the integral on the right hand side of (2.53) gives

$$\int_{\Gamma_j} qu^*\,d\Gamma_j = \int_{\Gamma_j} [\phi_1 \quad \phi_2]\,u^*\,d\Gamma_j \begin{bmatrix} q_1 \\ q_2 \end{bmatrix} = [g_{ij}^1 \quad g_{ij}^2] \begin{bmatrix} q_1 \\ q_2 \end{bmatrix} \tag{2.58}$$

where

$$g_{ij}^1 = \int_{\Gamma_j} \phi_1 u^*\,d\Gamma_j, \qquad g_{ij}^2 = \int_{\Gamma_j} \phi_2 u^*\,d\Gamma_j\,. \tag{2.59}$$

Substituting the integrals in (2.56) and (2.58) for each jth element into (2.53) one obtains the following equation for node i

$$c_i u_i + [\hat{H}_{i1}\ \hat{H}_{i2}\ \ldots \hat{H}_{iN}\,] \begin{bmatrix} u_1 \\ u_2 \\ \vdots \\ u_n \end{bmatrix} = [\hat{G}_{i1}\ \hat{G}_{i2}\ \ldots \hat{G}_{iN}\,] \begin{bmatrix} q_1 \\ q_2 \\ \vdots \\ q_n \end{bmatrix} \tag{2.60}$$

where $\hat{H}_{ij}$ is equal to the h_{ij}^1 term of element j plus $h_{i,j-1}^2$ term of element $j-1$ and similarly for G_{ij}. Hence, equation (2.60) represents the assembled equation

for node i and it can be written as

$$\sum_{j=1}^{N} H_{ij}\, u_j = \sum_{j=1}^{N} G_{ij}\, q_j \tag{2.61}$$

where j defines the nodes in between elements and $H_{ij} = c_i \delta_{ij} + \hat{H}_{ij}$. Then, the matrix-vector form becomes

$$\mathbf{Hu} = \mathbf{Gq} \tag{2.62}$$

which can be solved for the unknown $\mathbf{u}$ and $\mathbf{q}$ values after the insertion of boundary conditions as explained in the constant element case.

This chapter is closed with the standart derivation procedures of the fundamental solutions for Laplace, Helmholtz, modified Helmholtz and convection-diffusion equations. The boundary element method is explained on the solution of Laplace equation for showing the general steps of the method. Thus, these basic ideas are going to be used in deriving the fundamental solution of coupled magnetohydrodynamic equations and the corresponding BEM application in the next chapter, which constitutes the main original part of the thesis.

The boundary element method can easily be used to study problems with more than one boundary, such as the case of a region with holes in it (multiply connected regions). In order to define an external or internal boundary we need to identify the direction of the normal. For external boundary the numbering scheme is defined in the counterclockwise direction whereas for internal boundary it is defined in the clockwise direction.

CHAPTER 3

BOUNDARY ELEMENT METHOD SOLUTION OF THE MAGNETOHYDRODYNAMIC FLOW EQUATIONS

Magnetohydrodynamics is the academic discipline which studies the dynamics of electrically conducting fluids and their interactions with magnetic fields. The idea of MHD is that magnetic fields can induce currents in a moving conductive fluid, which create forces on the fluid, and also change (through Ohm' s law) the magnetic field itself. Qualitatively, the magnetohydrodynamic interactions tend to link the fluid and the field lines so as to make them move together.

The governing equations of MHD flow are the Navier-Stokes equations of fluid dynamics and Maxwell' s equations of electromagnetism. The coupling of these equations is due to Ohm' s Law and makes it necessary to solve them simultaneously. These coupled MHD equations can be solved analytically in terms of velocity and induced magnetic field only for some simple geometries under simple boundary conditions as completely insulated or conducting, [7]. The previous boundary element method solution procedures given in the literature are also restricted to the simple case of insulated boundaries, since the equations can be decoupled, [20]-[23]. Our aim is to solve the MHD equations by using boundary element method with a fundamental solution which treats the equations in coupled form. Thus, one can able to solve MHD flow problems with partly insulated and partly conducting walls, and for large values of Hartmann number.

In the present chapter, the solution of the MHD flow equations by using the

boundary element method is explained. Section 3.1 gives the basic equations that govern the magnetohydrodynamic flow problems. In Section 3.2, the fundamental solution of MHD flow equations in the original coupled form which are convection-diffusion type is established to be able to apply the BEM directly to these coupled equations with the most general form of wall conductivities. This constitutes one of the main original contributions to the thesis. Section 3.3 concentrates on how the boundary element method is applied to transform these coupled MHD flow equations into the boundary integrals by using the fundamental solution derived in Section 3.2. Thus, the dimensionality of the problem is reduced by one and the constant elements are used in order to discretize the boundary of the domain under consideration. The resulting system of linear equations is solved after the insertion of boundary conditions. In the last section, Section 3.4, pressure driven MHD flows in rectangular ducts with insulating and/or conducting, partly insulating partly conducting walls, and electrically driven MHD flows on the upper half plane are solved.

3.1 Governing Equations for the MHD Flow

The equations governing all the magnetohydrodynamic problems considered in this chapter are the same. The problems differ only in either the boundary conditions, the direction of the imposed magnetic field or the geometry of the regions. So, the equations will be derived in general as in Dragoş [7] or Shercliff [8], for the duct problems and for the flow between parallel plates, and then the nondimensionalization will be performed.

We consider the problem in a region on the xy-plane in which the fluid velocity is in the z-direction, and the imposed uniform magnetic field $\mathcal{H}_0$ existing outside the fluid acts in a direction lying in the xy-plane but forming an angle α with the y-axis.

All physical quantities in our problems, except pressure, are independent of z, the velocity vector $\mathbf{V}$ has only a z-component, $V_z(x, y)$, and the magnetic field vector takes the form $\boldsymbol{\mathcal{H}} = (\mathcal{H}_x, \mathcal{H}_y, \mathcal{H}_z(x, y))$, in which $\mathcal{H}_x = \mathcal{H}_0 \sin\alpha$ and $\mathcal{H}_y = \mathcal{H}_0 \cos\alpha$. We also assume that displacement currents are negligible and

there is no net flow of current in the z-direction. The flow is steady, laminar and the fluid is viscous, incompressible.

On neglecting displacement currents, in the steady-state, Maxwell' s equations governing the electrodynamic field become, [7],

$$\text{curl } \mathbf{E} = 0 \tag{3.1}$$

$$\text{curl } \boldsymbol{\mathcal{H}} = \mathbf{J} \tag{3.2}$$

$$\text{div } \boldsymbol{\mathcal{H}} = 0 \tag{3.3}$$

where $\mathbf{E}$ is the electric field intensity and $\mathbf{J}$ is the electric current density[1].

By taking the curl of Ohm' s law, which is

$$\mathbf{J} = \sigma(\mathbf{E} + \mu_e \mathbf{V} \times \boldsymbol{\mathcal{H}}) \tag{3.4}$$

where σ and μ_e are known as the electrical conductivity and magnetic permeability, respectively, we obtain from equations (3.1) and (3.2)

$$\text{curl } \mathbf{J} = \text{curl curl } \boldsymbol{\mathcal{H}} = \sigma\mu_e \,\text{curl } (\mathbf{V} \times \boldsymbol{\mathcal{H}}) \,. \tag{3.5}$$

Using the following two vector identities

$$\text{curl curl } \boldsymbol{\mathcal{H}} = \text{grad div } \boldsymbol{\mathcal{H}} - \nabla^2 \boldsymbol{\mathcal{H}}$$

and

$$\text{curl } (\mathbf{V} \times \boldsymbol{\mathcal{H}}) = (\boldsymbol{\mathcal{H}}.\nabla)\mathbf{V} - (\mathbf{V}.\nabla)\boldsymbol{\mathcal{H}} + \mathbf{V} \text{ div } \boldsymbol{\mathcal{H}} - \boldsymbol{\mathcal{H}} \text{ div } \mathbf{V}$$

[1]Divergence of a vector function $\mathbf{f} = (f_1, f_2, f_3)$ is given by

$$\text{div } \mathbf{f} = \nabla.\mathbf{f} = \frac{\partial f_1}{\partial x} + \frac{\partial f_2}{\partial y} + \frac{\partial f_3}{\partial z}$$

and curl of a vector function $\mathbf{f} = (f_1, f_2, f_3)$ is given by

$$\text{curl } \mathbf{f} = \nabla \times \mathbf{f} = (\frac{\partial f_3}{\partial y} - \frac{\partial f_2}{\partial z})\mathbf{i} + (\frac{\partial f_1}{\partial z} - \frac{\partial f_3}{\partial x})\mathbf{j} + (\frac{\partial f_2}{\partial x} - \frac{\partial f_1}{\partial y})\mathbf{k}$$

and noting that the divergence of $\boldsymbol{\mathcal{H}}$ and $\mathbf{V}$ both vanish. Since μ_e is constant and the fluid is incompressible, we deduce the equation[2]

$$\nabla^2\boldsymbol{\mathcal{H}} + \sigma\mu_e\left[(\boldsymbol{\mathcal{H}}.\nabla)\mathbf{V} - (\mathbf{V}.\nabla)\boldsymbol{\mathcal{H}}\right] = 0\,. \tag{3.6}$$

The Navier-Stokes equation (equation of motion) for the steady-state in the absence of the body forces is given as (since div $\mathbf{V} = 0$),[8],

$$\mathbf{F}^{(em)} - \text{grad } p + \mu\nabla^2\mathbf{V} = \rho(\mathbf{V}.\text{grad})\mathbf{V}\,. \tag{3.7}$$

When the given medium is simple, the electromagnetic force $\mathbf{F}^{(em)}$ is reduced to Lorentz force $\mathbf{J} \times \mu_e\boldsymbol{\mathcal{H}}$. From equations (3.2) and (3.7) we get

$$\mu_e(\text{curl } \boldsymbol{\mathcal{H}}) \times \boldsymbol{\mathcal{H}} - \text{grad } p + \mu\nabla^2\mathbf{V} = \rho(\mathbf{V}.\text{grad})\mathbf{V} \tag{3.8}$$

where μ and ρ are the coefficient of viscosity and the density of the fluid, respectively, p is the pressure in the fluid.

Since

$$(\text{curl } \boldsymbol{\mathcal{H}}) \times \boldsymbol{\mathcal{H}} = (\boldsymbol{\mathcal{H}}.\text{grad})\boldsymbol{\mathcal{H}} - \frac{1}{2}\text{grad } |\boldsymbol{\mathcal{H}}|^2$$

equation (3.8) becomes

$$\mu_e(\boldsymbol{\mathcal{H}}.\text{grad})\boldsymbol{\mathcal{H}} - \mu_e\frac{1}{2}\text{grad } |\boldsymbol{\mathcal{H}}|^2 - \text{grad } p + \mu\nabla^2\mathbf{V} = \rho(\mathbf{V}.\text{grad})\mathbf{V}\,. \tag{3.9}$$

Since the conditions are invariant in the z-direction, apart from a pressure gradient, differentiating the above equation with respect to z shows that grad$(\partial p/\partial z)$

[2]The cross product of two vectors $\mathbf{A} = (A_1, A_2, A_3)$ and $\mathbf{B} = (B_1, B_2, B_3)$ is

$$\mathbf{A} \times \mathbf{B} = (A_2B_3 - A_3B_2)\mathbf{i} + (A_3B_1 - A_1B_3)\mathbf{j} + (A_1B_2 - A_2B_1)\mathbf{k}\,,$$

the dot product is given by

$$\mathbf{A}.\mathbf{B} = A_1B_1 + A_2B_2 + A_3B_3\,.$$

The gradient of a scalar ϕ is $\nabla\phi = \dfrac{\partial\phi}{\partial x}\mathbf{i} + \dfrac{\partial\phi}{\partial y}\mathbf{j} + \dfrac{\partial\phi}{\partial z}\mathbf{k}$.

The Laplacian operator is $\nabla^2 = \dfrac{\partial^2}{\partial x^2} + \dfrac{\partial^2}{\partial y^2} + \dfrac{\partial^2}{\partial z^2}$.

vanishes. Hence $\partial p/\partial z$ is a constant.

Since $V_x = 0$, $V_y = 0$, $\mathcal{H}_x = \mathcal{H}_0 \sin\alpha$, $\mathcal{H}_y = \mathcal{H}_0 \cos\alpha$ where $\mathcal{H}_0$ is a constant, then $J_z = 0$, $\boldsymbol{\mathcal{H}}.\text{grad} = \mathcal{H}_x \dfrac{\partial}{\partial x} + \mathcal{H}_y \dfrac{\partial}{\partial y}$, and $\mathbf{V}.\text{grad} = 0$.

Thus, the z-components of equations (3.6) and (3.9) become

$$\begin{aligned} \mu\nabla^2 V_z + \mu_e \mathcal{H}_0 \sin\alpha \frac{\partial \mathcal{H}_z}{\partial x} + \mu_e \mathcal{H}_0 \cos\alpha \frac{\partial \mathcal{H}_z}{\partial y} &= \frac{\partial p}{\partial z} \\ \nabla^2 \mathcal{H}_z + \sigma\mu_e \mathcal{H}_0 \sin\alpha \frac{\partial V_z}{\partial x} + \sigma\mu_e \mathcal{H}_0 \cos\alpha \frac{\partial V_z}{\partial y} &= 0\,. \end{aligned} \tag{3.10}$$

By taking $\eta = \dfrac{1}{\sigma\mu_e}$, which is known as magnetic diffusivity, equation (3.10) becomes

$$\begin{aligned} \mu\nabla^2 V_z + \mu_e \mathcal{H}_0 \sin\alpha \frac{\partial \mathcal{H}_z}{\partial x} + \mu_e \mathcal{H}_0 \cos\alpha \frac{\partial \mathcal{H}_z}{\partial y} &= \frac{\partial p}{\partial z} \\ \eta\nabla^2 \mathcal{H}_z + \mathcal{H}_0 \sin\alpha \frac{\partial V_z}{\partial x} + \mathcal{H}_0 \cos\alpha \frac{\partial V_z}{\partial y} &= 0\,. \end{aligned} \tag{3.11}$$

By using the relationship

$$\mathbf{D} = \epsilon\mathbf{E}, \quad \mathbf{B} = \mu_e \boldsymbol{\mathcal{H}} \tag{3.12}$$

where $\mathbf{D}$ is the electric induction, $\mathbf{B}$ is the magnetic induction and ϵ is the electrical permitivity, one can write equation (3.11) in terms of induced magnetic field $\mathbf{B}$.

In vacuum, equation (3.12) become

$$\mathbf{D} = \epsilon_0\mathbf{E}, \quad \mathbf{B} = \mu_0 \boldsymbol{\mathcal{H}}$$

where ϵ_0 and μ_0 are constants, and for a simple medium,

$$\epsilon\mu_e \approx \epsilon_0\mu_0$$

and $c = \dfrac{1}{(\mu_0\epsilon_0)^{1/2}}$ =velocity of light in vacuum.

Now, equations (3.11) are written in terms of $\mathbf{B}$ as

$$\begin{aligned} \mu\nabla^2 V_z + \frac{B_0}{\mu_e}\sin\alpha\frac{\partial B_z}{\partial x} + \frac{B_0}{\mu_e}\cos\alpha\frac{\partial B_z}{\partial y} &= \frac{\partial p}{\partial z} \\ \eta\nabla^2 B_z + B_0\sin\alpha\frac{\partial V_z}{\partial x} + B_0\cos\alpha\frac{\partial V_z}{\partial y} &= 0 \end{aligned} \tag{3.13}$$

where B_0 is the inductance of the applied magnetic field.

Introducing dimensionless variables

$$V = \frac{1}{\nu_0}V_z,\ B = \frac{1}{\nu_0\mu_e}(\sigma\mu)^{-1/2}B_z,\ x' = \frac{x}{L_0},\ y' = \frac{y}{L_0}$$

where

$$\nu_0 = -L_0^2(\frac{\partial p}{\partial z})/\mu$$

is the characteristic velocity (mean axis velocity) and L_0 is the characteristic length, and substituting in equation (3.13) ($x' = x$, $y' = y$ substituted), we obtain the following equations for the velocity $V(x, y)$ and the induced magnetic field $B(x, y)$:

$$\begin{aligned} \nabla^2 V + M\sin\alpha\frac{\partial B}{\partial x} + M\cos\alpha\frac{\partial B}{\partial y} &= -1 \\ \nabla^2 B + M\sin\alpha\frac{\partial V}{\partial x} + M\cos\alpha\frac{\partial V}{\partial y} &= 0 \end{aligned} \tag{3.14}$$

where $M = B_0 L_0\sqrt{\sigma}/\sqrt{\mu}$ is the Hartmann number, which was first used by Hartmann when dealing with flow between parallel non-conducting planes. In other words, the Hartmann number M is the magnitude of the vector $\boldsymbol{M} = (M_x, M_y)$ in which

$$\begin{aligned} M_x &= M\sin\alpha \\ M_y &= M\cos\alpha\,. \end{aligned} \tag{3.15}$$

Thus, equation (3.14) becomes

$$\begin{aligned} \nabla^2 V + M_x \frac{\partial B}{\partial x} + M_y \frac{\partial B}{\partial y} &= -1 \\ \nabla^2 B + M_x \frac{\partial V}{\partial x} + M_y \frac{\partial V}{\partial y} &= 0 \end{aligned} \tag{3.16}$$

which describes two coupled second order linear partial differential equations. For each problem which is solved in this chapter, the geometry, the direction of the applied magnetic field and the boundary conditions will be explained in Section 3.4. Also, the characteristic length L_0 will be taken differently for each problem considered and specified according to the geometry of the problem. For all of the problems considered, the walls are a combination of insulators ($\sigma \approx 0$) and perfect conductors ($\sigma \approx \infty$). The effect of the conducting part and the value of the Hartmann number on the velocity field and induced magnetic field will be discussed for each problem.

3.2 Derivation of the Fundamental Solution to Coupled MHD Flow Equations

For the BEM solution of equations (3.16) which are the convection-diffusion type coupled equations, the fundamental solution is needed because BEM is a numerical technique which makes intensive use of a fundamental solution of the problem in question.

The MHD equations (3.16) are first transformed to the matrix-vector form

$$\boldsymbol{\mathcal{L}}\,\mathbf{u} = \mathbf{f} \tag{3.17}$$

where $\boldsymbol{\mathcal{L}}$ is the matrix containing both diffusion and convection operators

$$\boldsymbol{\mathcal{L}} = \begin{bmatrix} \nabla^2 & M_x \dfrac{\partial}{\partial x} + M_y \dfrac{\partial}{\partial y} \\ M_x \dfrac{\partial}{\partial x} + M_y \dfrac{\partial}{\partial y} & \nabla^2 \end{bmatrix} \tag{3.18}$$

and

$$\mathbf{u} = \begin{bmatrix} V \\ B \end{bmatrix} \quad , \quad \mathbf{f} = \begin{bmatrix} -1 \\ 0 \end{bmatrix} \quad . \tag{3.19}$$

Weighting this equation over the domain of the problem, Ω, in the Galerkin principle [3],

$$\int_\Omega \mathbf{w}^T \boldsymbol{\mathcal{L}}\, \mathbf{u}\, d\Omega = \int_\Omega \mathbf{w}^T \mathbf{f}\, d\Omega \tag{3.20}$$

where $\mathbf{w^T}$ is the transpose of the vector weight function $\mathbf{w} = \begin{bmatrix} V^* \\ B^* \end{bmatrix}$, gives the integral equation

$$\int_\Omega \begin{bmatrix} V^* & B^* \end{bmatrix} \begin{bmatrix} \nabla^2 & M_x \dfrac{\partial}{\partial x} + M_y \dfrac{\partial}{\partial y} \\ M_x \dfrac{\partial}{\partial x} + M_y \dfrac{\partial}{\partial y} & \nabla^2 \end{bmatrix} \begin{bmatrix} V \\ B \end{bmatrix} d\Omega$$

$$= \int_\Omega \begin{bmatrix} V^* & B^* \end{bmatrix} \begin{bmatrix} -1 \\ 0 \end{bmatrix} d\Omega \ .$$

This is actually one equation containing three integrals in the form

$$I_1 + I_2 = I_3 \tag{3.21}$$

where

$$I_1 = \int_\Omega V^* \left(\nabla^2 V + M_x \frac{\partial B}{\partial x} + M_y \frac{\partial B}{\partial y} \right) d\Omega$$

$$I_2 = \int_\Omega B^* \left(\nabla^2 B + M_x \frac{\partial V}{\partial x} + M_y \frac{\partial V}{\partial y} \right) d\Omega$$

and

$$I_3 = -\int_\Omega V^* d\Omega \ .$$

After the application of Green's second identity, the integrals I_1 and I_2 reduce to

$$I_1 = \int_\Omega V \nabla^2 V^* d\Omega + \int_\Gamma \left(V^* \frac{\partial V}{\partial n} - V \frac{\partial V^*}{\partial n} \right) d\Gamma + I_4 \tag{3.22}$$

$$I_2 = \int_\Omega B\nabla^2 B^* d\Omega + \int_\Gamma \left(B^* \frac{\partial B}{\partial n} - B\frac{\partial B^*}{\partial n} \right) d\Gamma + I_5 \tag{3.23}$$

where Γ is the boundary of the domain Ω,

$$I_4 = \int_\Omega V^* \left(M_x \frac{\partial B}{\partial x} + M_y \frac{\partial B}{\partial y} \right) d\Omega$$

and

$$I_5 = \int_\Omega B^* \left(M_x \frac{\partial V}{\partial x} + M_y \frac{\partial V}{\partial y} \right) d\Omega \, .$$

Now, we rewrite

$$V^* \left(M_x \frac{\partial B}{\partial x} + M_y \frac{\partial B}{\partial y} \right) = M_x \left((V^* B)_{,\,x} - V^*_{,\,x} B \right) + M_y \left((V^* B)_{,\,y} - V^*_{,\,y} B \right)$$

$$B^* \left(M_x \frac{\partial V}{\partial x} + M_y \frac{\partial V}{\partial y} \right) = M_x \left((B^* V)_{,\,x} - B^*_{,\,x} V \right) + M_y \left((B^* V)_{,\,y} - B^*_{,\,y} V \right)$$

and substitute in the integrals I_4 and I_5. The subscripts $_{,\,x}$, $_{,\,y}$ denote the x and y derivatives, respectively. Moreover, with the application of the Divergence theorem, the integrals I_4 and I_5 become

$$I_4 = \int_\Gamma \left(M_x V^* B n_x + M_y V^* B n_y \right) d\Gamma - \int_\Omega \left(M_x B V^*_{,\,x} + M_y B V^*_{,\,y} \right) d\Omega$$

$$I_5 = \int_\Gamma \left(M_x B^* V n_x + M_y B^* V n_y \right) d\Gamma - \int_\Omega \left(M_x V B^*_{,\,x} + M_y V B^*_{,\,y} \right) d\Omega \ .$$

By the substitution of I_4 and I_5 in equations (3.22) and (3.23) respectively, equation (3.21) becomes,

$$\int_\Omega V \left(\nabla^2 V^* - M_x \frac{\partial B^*}{\partial x} - M_y \frac{\partial B^*}{\partial y} \right) d\Omega + \int_\Omega B \left(\nabla^2 B^* - M_x \frac{\partial V^*}{\partial x} - M_y \frac{\partial V^*}{\partial y} \right) d\Omega$$

$$+ \int_\Gamma \left(V^* \frac{\partial V}{\partial n} - V \frac{\partial V^*}{\partial n} \right) d\Gamma + \int_\Gamma \left(B^* \frac{\partial B}{\partial n} - B \frac{\partial B^*}{\partial n} \right) d\Gamma$$

$$+ \int_\Gamma M_x \left(V^* B + B^* V \right) n_x d\Gamma + \int_\Gamma M_y \left(V^* B + B^* V \right) n_y d\Gamma = - \int_\Omega V^* d\Omega \tag{3.24}$$

where $\mathbf{n} = (n_x, n_y)$ is the outward unit normal vector on Γ.

To omit the region integrals on the left hand side of equation (3.24), we need to consider two cases:

First case:

$$\begin{aligned} \nabla^2 V^* - M_x \frac{\partial B^*}{\partial x} - M_y \frac{\partial B^*}{\partial y} &= -\Delta(A, P) \\ \nabla^2 B^* - M_x \frac{\partial V^*}{\partial x} - M_y \frac{\partial V^*}{\partial y} &= 0 \end{aligned}$$

where A and P are the fixed and the variable points in Ω respectively. The solution for this case is denoted as

$$\begin{bmatrix} V_1^* \\ B_1^* \end{bmatrix} .$$

Second case:

$$\begin{aligned} \nabla^2 V^* - M_x \frac{\partial B^*}{\partial x} - M_y \frac{\partial B^*}{\partial y} &= 0 \\ \nabla^2 B^* - M_x \frac{\partial V^*}{\partial x} - M_y \frac{\partial V^*}{\partial y} &= -\Delta(A, P) \end{aligned}$$

and denote the solution as

$$\begin{bmatrix} V_2^* \\ B_2^* \end{bmatrix} .$$

These two cases transform equation (3.24) into the following integral equations

$$-c_A V(A) + \int_\Gamma \left(V_1^* \frac{\partial V}{\partial n} - V \frac{\partial V_1^*}{\partial n} \right) d\Gamma + \int_\Gamma \left(B_1^* \frac{\partial B}{\partial n} - B \frac{\partial B_1^*}{\partial n} \right) d\Gamma$$

$$+ \int_\Gamma M_x \left(V_1^* B + B_1^* V \right) n_x d\Gamma + \int_\Gamma M_y \left(V_1^* B + B_1^* V \right) n_y d\Gamma \tag{3.25}$$

$$= - \int_\Omega V_1^* d\Omega$$

where c_A is a constant equals to $\dfrac{\theta}{2\pi}$, θ being the internal angle at the source point A, and

$$-c_A B(A) + \int_\Gamma \left(V_2^* \frac{\partial V}{\partial n} - V \frac{\partial V_2^*}{\partial n} \right) d\Gamma + \int_\Gamma \left(B_2^* \frac{\partial B}{\partial n} - B \frac{\partial B_2^*}{\partial n} \right) d\Gamma$$

$$+ \int_\Gamma M_x \left(V_2^* B + B_2^* V \right) n_x d\Gamma + \int_\Gamma M_y \left(V_2^* B + B_2^* V \right) n_y d\Gamma \tag{3.26}$$

$$= - \int_\Omega V_2^* d\Omega.$$

Let the matrix $\mathbf{G}^*$ be formed as

$$\mathbf{G}^* = \begin{bmatrix} V_1^* & V_2^* \\ B_1^* & B_2^* \end{bmatrix} \tag{3.27}$$

which is the fundamental solution for the adjoint operator

$$\boldsymbol{\mathcal{L}}^* = \begin{bmatrix} \nabla^2 & -M_x \dfrac{\partial}{\partial x} - M_y \dfrac{\partial}{\partial y} \\ -M_x \dfrac{\partial}{\partial x} - M_y \dfrac{\partial}{\partial y} & \nabla^2 \end{bmatrix} \tag{3.28}$$

of $\boldsymbol{\mathcal{L}}$. That is,

$$\boldsymbol{\mathcal{L}}^* \boldsymbol{G}^* = -\Delta(A, P)\mathbf{I}$$

and $\mathbf{I}$ is the 2×2 identity matrix.

Therefore, the fundamental solution $\mathbf{G}^*$ becomes

$$\mathbf{G}^* = \begin{bmatrix} \nabla^2 & M_x\dfrac{\partial}{\partial x} + M_y\dfrac{\partial}{\partial y} \\ M_x\dfrac{\partial}{\partial x} + M_y\dfrac{\partial}{\partial y} & \nabla^2 \end{bmatrix} \begin{bmatrix} 1 & 0 \\ 0 & 1 \end{bmatrix} \Phi \tag{3.29}$$

where Φ is the fundamental solution of the biharmonic equation

$$\left(\nabla^4 - M_x^2\frac{\partial^2}{\partial x^2} - 2M_xM_y\frac{\partial^2}{\partial x\partial y} - M_y^2\frac{\partial^2}{\partial y^2}\right) u = 0\,.$$

This can be partitioned into two convection-diffusion equations

$$\left(\nabla^2 - M_x\frac{\partial}{\partial x} - M_y\frac{\partial}{\partial y}\right)\Psi_1 = -\Delta(A,P) \tag{3.30}$$

and

$$\left(\nabla^2 + M_x\frac{\partial}{\partial x} + M_y\frac{\partial}{\partial y}\right)\Psi_2 = -\Delta(A,P) \tag{3.31}$$

where

$$\Psi_1 = \left(\nabla^2 + M_x\frac{\partial}{\partial x} + M_y\frac{\partial}{\partial y}\right)\Phi \tag{3.32}$$

and

$$\Psi_2 = \left(\nabla^2 - M_x\frac{\partial}{\partial x} - M_y\frac{\partial}{\partial y}\right)\Phi\ . \tag{3.33}$$

It is clear that Ψ_1 and Ψ_2 are the fundamental solutions of the convection-diffusion type equations (3.30) and (3.31) respectively, of which the derivations are given in Section 2.1.3. Therefore,

$$\Psi_1 = \frac{1}{2\pi}\, e^{\mathbf{M}.\,\mathbf{r}/2} K_0(\frac{M}{2}\,r) \tag{3.34}$$

and

$$\Psi_2 = \frac{1}{2\pi}\, e^{-\mathbf{M}.\,\mathbf{r}/2} K_0(\frac{M}{2}\,r) \tag{3.35}$$

where $\mathbf{M}$ is the vector with components (M_x, M_y) and $\mathbf{r} = (r_x, r_y)$ is the distance vector between the source and field points. The Hartmann number M and r are the modulus of the vectors $\mathbf{M}$ and $\mathbf{r}$ respectively.

With the relationships between Φ and the fundamental solutions Ψ_1 and Ψ_2, we have

$$M_x \frac{\partial \Phi}{\partial x} + M_y \frac{\partial \Phi}{\partial y} = \frac{\Psi_1 - \Psi_2}{2} \tag{3.36}$$

$$\nabla^2 \Phi = \frac{\Psi_1 + \Psi_2}{2} \tag{3.37}$$

where

$$\frac{\Psi_1 - \Psi_2}{2} = \frac{1}{2\pi} K_0(\frac{M}{2} r) \sinh(\frac{\mathbf{M}.\mathbf{r}}{2})$$

and

$$\frac{\Psi_1 + \Psi_2}{2} = \frac{1}{2\pi} K_0(\frac{M}{2} r) \cosh(\frac{\mathbf{M}.\mathbf{r}}{2}) \, .$$

Thus, the fundamental solution $\mathbf{G}^*$ for the adjoint operator $\boldsymbol{\mathcal{L}}^*$ is finally obtained as

$$\mathbf{G}^* = \begin{bmatrix} \frac{1}{2\pi} K_0(\frac{M}{2} r) \cosh(\frac{\mathbf{M}.\mathbf{r}}{2}) & \frac{1}{2\pi} K_0(\frac{M}{2} r) \sinh(\frac{\mathbf{M}.\mathbf{r}}{2}) \\ \frac{1}{2\pi} K_0(\frac{M}{2} r) \sinh(\frac{\mathbf{M}.\mathbf{r}}{2}) & \frac{1}{2\pi} K_0(\frac{M}{2} r) \cosh(\frac{\mathbf{M}.\mathbf{r}}{2}) \end{bmatrix} \tag{3.38}$$

with its entries from (3.27) as

$$\begin{aligned} V_1^* &= B_2^* = \frac{1}{2\pi} K_0(\frac{M}{2} r) \cosh(\frac{\mathbf{M}.\mathbf{r}}{2}) \\ V_2^* &= B_1^* = \frac{1}{2\pi} K_0(\frac{M}{2} r) \sinh(\frac{\mathbf{M}.\mathbf{r}}{2}) \, . \end{aligned} \tag{3.39}$$

3.3 Application of the Boundary Element Method

Having found the fundamental solutions $V_1^* = B_2^*$ and $B_1^* = V_2^*$, equations (3.25) and (3.26) can be rewritten,

$$\begin{aligned} -c_A V(A) + \int_\Gamma \left(M_x B_1^* n_x + M_y B_1^* n_y - \frac{\partial V_1^*}{\partial n} \right) V d\Gamma \\ + \int_\Gamma \left(M_x V_1^* n_x + M_y V_1^* n_y - \frac{\partial B_1^*}{\partial n} \right) B d\Gamma + \int_\Gamma V_1^* \frac{\partial V}{\partial n} \, d\Gamma + \int_\Gamma B_1^* \frac{\partial B}{\partial n} \, d\Gamma \\ = - \int_\Omega V_1^* d\Omega \end{aligned} \tag{3.40}$$

and

$$\begin{aligned} -c_A B(A) + \int_\Gamma \left(M_x V_1^* n_x + M_y V_1^* n_y - \frac{\partial B_1^*}{\partial n} \right) V d\Gamma \\ + \int_\Gamma \left(M_x B_1^* n_x + M_y B_1^* n_y - \frac{\partial V_1^*}{\partial n} \right) B d\Gamma + \int_\Gamma B_1^* \frac{\partial V}{\partial n} \, d\Gamma + \int_\Gamma V_1^* \frac{\partial B}{\partial n} \, d\Gamma \\ = - \int_\Omega B_1^* d\Omega \, . \end{aligned} \tag{3.41}$$

Thus, after the discretization of the boundary Γ of the domain of the problem by using the constant elements, boundary element matrix equations for the unknowns, the velocity V and the induced magnetic field B and their normal derivatives, can now be obtained by the evaluation of the boundary integrals in equations (3.40) and (3.41). The matrix-vector form is

$$\begin{bmatrix} -c_A \mathbf{V}(A) \\ -c_A \mathbf{B}(A) \end{bmatrix} + \begin{bmatrix} \mathbf{H} & \mathbf{G} \\ \mathbf{G} & \mathbf{H} \end{bmatrix} \begin{bmatrix} \mathbf{V} \\ \mathbf{B} \end{bmatrix} + \begin{bmatrix} \mathbf{H}^1 & \mathbf{G}^1 \\ \mathbf{G}^1 & \mathbf{H}^1 \end{bmatrix} \begin{bmatrix} \dfrac{\partial \mathbf{V}}{\partial n} \\ \\ \dfrac{\partial \mathbf{B}}{\partial n} \end{bmatrix} = \begin{bmatrix} F_1 \\ F_2 \end{bmatrix} \tag{3.42}$$

where $\mathbf{H}$, $\mathbf{G}$, $\mathbf{H}^1$ and $\mathbf{G}^1$ are the matrices with the entries

$$\begin{aligned} h_{ij} &= \int_{\Gamma_j} \left(M_x B_1^* n_x + M_y B_1^* n_y - \frac{\partial V_1^*}{\partial n} \right) d\Gamma_j \\ g_{ij} &= \int_{\Gamma_j} \left(M_x V_1^* n_x + M_y V_1^* n_y - \frac{\partial B_1^*}{\partial n} \right) d\Gamma_j \\ h_{ij}^1 &= \int_{\Gamma_j} V_1^* \, d\Gamma_j \\ g_{ij}^1 &= \int_{\Gamma_j} B_1^* \, d\Gamma_j \end{aligned} \tag{3.43}$$

and $\mathbf{F} = \begin{bmatrix} F_1 \\ F_2 \end{bmatrix}$ is the right hand side vector with the entries containing domain integrals

$$\begin{aligned} F_1 &= -\int_\Omega V_1^* d\Omega \\ F_2 &= -\int_\Omega B_1^* d\Omega \, . \end{aligned} \tag{3.44}$$

The subscripts i and j indicate the fixed node i and the jth element on the boundary respectively. $\mathbf{r} = (r_x, r_y)$ is the vector between the boundary nodes i and j. After the substitution of the fundamental solutions V_1^* and B_1^* and their normal derivatives in equations (3.43) and (3.44), the entries of $\mathbf{H}$, $\mathbf{G}$, $\mathbf{H}^1$, $\mathbf{G}^1$ and $\mathbf{F}$ become;

$$
\begin{aligned}
h_{ij} &= \frac{1}{4\pi}\int_{\Gamma_j}\left(K_0(\frac{M}{2}r)\sinh(\frac{\mathbf{M}.\mathbf{r}}{2})\mathbf{M}.\mathbf{n} + MK_1(\frac{M}{2}\,r)\cosh(\frac{\mathbf{M}.\mathbf{r}}{2})\,\frac{\partial r}{\partial n}\right)d\Gamma_j \\
g_{ij} &= \frac{1}{4\pi}\int_{\Gamma_j}\left(K_0(\frac{M}{2}\,r)\cosh(\frac{\mathbf{M}.\mathbf{r}}{2})\mathbf{M}.\mathbf{n} + MK_1(\frac{M}{2}\,r)\sinh(\frac{\mathbf{M}.\mathbf{r}}{2})\,\frac{\partial r}{\partial n}\right)d\Gamma_j \\
h^1_{ij} &= \frac{1}{2\pi}\int_{\Gamma_j}K_0(\frac{M}{2}\,r)\cosh(\frac{\mathbf{M}.\mathbf{r}}{2})\,d\Gamma_j \\
g^1_{ij} &= \frac{1}{2\pi}\int_{\Gamma_j}K_0(\frac{M}{2}\,r)\sinh(\frac{\mathbf{M}.\mathbf{r}}{2})\,d\Gamma_j \\
F_1 &= -\int_{\Omega}K_0(\frac{M}{2}\,r)\cosh(\frac{\mathbf{M}.\mathbf{r}}{2})\,d\Omega \\
F_2 &= -\int_{\Omega}K_0(\frac{M}{2}\,r)\sinh(\frac{\mathbf{M}.\mathbf{r}}{2})\,d\Omega
\end{aligned}
\tag{3.45}
$$

where K_1 is the modified Bessel function of the second kind and of order one.

The constant c_A is $1/2$ or 1 when the fixed point A is on the straight boundary or inside respectively. The problem is solved first for the values of unknowns V, B and their normal derivatives $\dfrac{\partial V}{\partial n}$, $\dfrac{\partial B}{\partial n}$ on the boundary, so equation (3.42) becomes

$$
\begin{bmatrix} \bar{\mathbf{H}} & \mathbf{G} \\ \mathbf{G} & \bar{\mathbf{H}} \end{bmatrix}\begin{bmatrix} \mathbf{V} \\ \mathbf{B} \end{bmatrix} + \begin{bmatrix} \mathbf{H}^1 & \mathbf{G}^1 \\ \mathbf{G}^1 & \mathbf{H}^1 \end{bmatrix}\begin{bmatrix} \dfrac{\partial \mathbf{V}}{\partial n} \\ \\ \dfrac{\partial \mathbf{B}}{\partial n} \end{bmatrix} = \begin{bmatrix} F_1 \\ F_2 \end{bmatrix} \tag{3.46}
$$

where $\bar{\mathbf{H}}$ is the matrix with the entries

$$
\bar{h}_{ij} = -\frac{1}{2}\,\delta_{ij} + h_{ij}\ .
$$

This linear system of equations (3.46) is going to be solved for values of $\dfrac{\partial V}{\partial n}$ on Γ, B on Γ_2 and $\dfrac{\partial B}{\partial n}$ on Γ_1. Having found (V, B) and $(\dfrac{\partial V}{\partial n}, \dfrac{\partial B}{\partial n})$ everywhere on

the boundary, one can obtain the values of V and B at any point of the domain Ω by using equation (3.42) with c_A equals to one. This is given by

$$\begin{bmatrix} \mathbf{V} \\ \mathbf{B} \end{bmatrix} = \begin{bmatrix} \mathbf{HI} & \mathbf{GI} \\ \mathbf{GI} & \mathbf{HI} \end{bmatrix} \begin{bmatrix} \mathbf{V} \\ \mathbf{B} \end{bmatrix} + \begin{bmatrix} \mathbf{HI}^1 & \mathbf{GI}^1 \\ \mathbf{GI}^1 & \mathbf{HI}^1 \end{bmatrix} \begin{bmatrix} \dfrac{\partial \mathbf{V}}{\partial n} \\ \\ \dfrac{\partial \mathbf{B}}{\partial n} \end{bmatrix} - \begin{bmatrix} F_1 \\ F_2 \end{bmatrix}. \qquad (3.47)$$

The entrices of the matrices $\mathbf{HI}$, $\mathbf{GI}$, $\mathbf{HI}^1$ and $\mathbf{GI}^1$ are in the same form with the ones of $\mathbf{H}$, $\mathbf{G}$, $\mathbf{H}^1$ and $\mathbf{G}^1$. But, this time in the entries of $\mathbf{HI}$, $\mathbf{GI}$, $\mathbf{HI}^1$ and $\mathbf{GI}^1$, i indicates the fixed node in the domain and j indicates the jth element on the boundary. Thus, the vector $\mathbf{r}$ is computed between the inside node i and the boundary node j.

3.4 Numerical Results and Discussions

In this section we discuss the solution of the magnetohydrodynamic flow equations by using the boundary element method. In all of the problems considered in this section, the fluid is taken as viscous, incompressible and having uniform electrical conductivity. The first part includes the flow which is driven by means of a *constant pressure gradient* in a rectangular duct and throughtout its passage the flow is subjected to a constant and uniform imposed magnetic field. Then, in the second part, the flow on the half-plane which is driven by *the electrodes through external circuits* is considered. We further assume that, in both of the cases, the fluid motion is fully developed (i.e. the ducts are assumed to be of infinite length and end-effects are neglected), steady and laminar. The geometry and boundary conditions of each problem will be given in detail in the parts where they belong.

The computations are performed by using programs written in FORTRAN language and MATLAB is made use of in drawing graphics. For the evaluation of the modified Bessel functions, K_0 and K_1, the routines S18ACF and S18ADF, which are based on Chebyshev expansions, from the NAG library are used respec-

tively. The solution of resulting algebraic linear system of equations is obtained by using LU factorization. The routine F04ATF from the NAG library which applies iterative refinement is used.

3.4.1 Pressure driven MHD flow in a rectangular duct

The magnetohydrodynamic flow of an incompressible, viscous, electrically conducting fluid, driven down the duct by a constant pressure gradient, subjected to a constant and uniform magnetic field is considered. In the BEM discretization for the domain, the constant boundary elements are used. We give four MHD flow test problems in a rectangular duct with different types of wall conductivities and the numerical results for both the velocity and the induced magnetic field are visualized in terms of graphics.

Problem 1: Insulating wall duct

The magnetohydrodynamic flow in a rectangular duct, the cross-section of which is shown in Figure 3.1, is considered. The axis of the duct is chosen as the z-axis. A uniform magnetic field of strength B_0 is directed along the x-axis (i.e. $\alpha = \pi/2$).

The basic equations governing the MHD duct flow subjected to a magnetic field parallel to x-direction (in nondimensionalized form) are

$$\begin{aligned} \nabla^2 V + M\frac{\partial B}{\partial x} &= -1 \\ \nabla^2 B + M\frac{\partial V}{\partial x} &= 0 \end{aligned} \tag{3.48}$$

where $V(x, y)$ and $B(x, y)$ are the velocity and the induced magnetic field respectively, both of which have only one component in the z-direction. M is the Hartmann number. The walls of the duct are insulated ($B = 0$) and the velocity is zero on the solid walls (Figure 3.1). The analytical solution of this problem exits [7, 8], which gives the opportunity to be able to compare the obtained boundary element results with the exact ones.

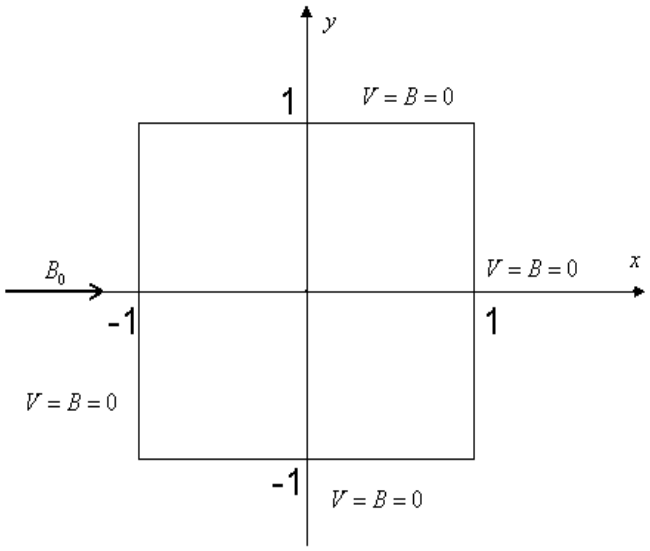

Figure 3.1: MHD duct flow with insulating walls

The coupled nonhomogeneous MHD flow equations (3.48) are expressed in matrix differential operator form

$$\boldsymbol{\mathcal{L}}\,\mathbf{u} = \mathbf{f}$$

where

$$\boldsymbol{\mathcal{L}} = \begin{bmatrix} \nabla^2 & M\dfrac{\partial}{\partial x} \\ M\dfrac{\partial}{\partial x} & \nabla^2 \end{bmatrix}, \quad \mathbf{u} = \begin{bmatrix} V \\ B \end{bmatrix}, \quad \mathbf{f} = \begin{bmatrix} -1 \\ 0 \end{bmatrix}$$

for which the corresponding homogeneous equations can be obtained by using the particular solution

$$\mathbf{u_p} = \begin{bmatrix} V_p \\ B_p \end{bmatrix}$$

where $V_p = 0$ and $B_p = -x/M$.

By taking

$$\mathbf{u} = \mathbf{u_h} + \mathbf{u_p}$$

the homogeneous solution $\mathbf{u_h} = \begin{bmatrix} V_h \\ B_h \end{bmatrix}$ satisfies

$$\begin{aligned} \nabla^2 V_h + M\frac{\partial B_h}{\partial x} &= 0 \\ \nabla^2 B_h + M\frac{\partial V_h}{\partial x} &= 0 \end{aligned} \qquad \text{in } \Omega \tag{3.49}$$

with the boundary conditions

$$V_h = 0, \qquad B_h = \frac{x}{M}, \qquad \text{on} \quad \Gamma \ . \tag{3.50}$$

Thus, the evaluation of the domain integrals on the right hand side in equations (3.46) and (3.47) is omitted.

The fundamental solution for the adjoint equation

$$\boldsymbol{\mathcal{L}}^* \, \mathbf{u} = \mathbf{f}$$

takes the form in (3.38)

$$\mathbf{G}^* = \begin{bmatrix} \frac{1}{2\pi} K_0(\frac{M}{2}\, r) \cosh(\frac{M}{2}\, r_x) & \frac{1}{2\pi} K_0(\frac{M}{2}\, r) \sinh(\frac{M}{2}\, r_x) \\ \frac{1}{2\pi} K_0(\frac{M}{2}\, r) \sinh(\frac{M}{2}\, r_x) & \frac{1}{2\pi} K_0(\frac{M}{2}\, r) \cosh(\frac{M}{2}\, r_x) \end{bmatrix} . \tag{3.51}$$

The BEM is applied to solve homegeneous equations (3.49) with boundary conditions (3.50). The square boundary is discretized by using $N = 80$ and $N = 300$ constant elements for the values of Hartmann number $M = 50$ and $M = 300$, respectively. Figures 3.2-3.3 and 3.4-3.5 depict the agreement of the numerical solution with the exact solution for both the velocity and the induced magnetic field in terms of velocity and induced magnetic field lines (equivelocity and current lines), respectively for $M = 50$ and $M = 300$. It is noted that as M increases the velocity becomes uniform at the center of the duct and the boundary layer formation starts for both the velocity and the induced magnetic field.

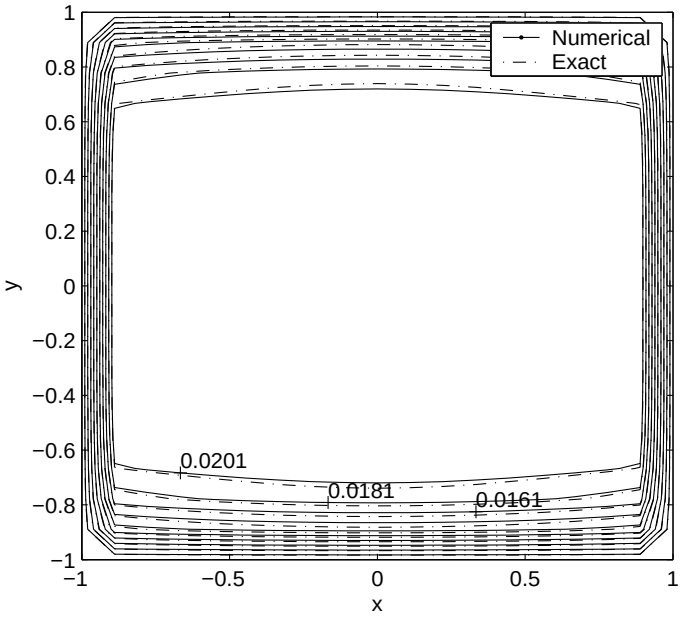

Figure 3.2: Velocity lines for $M = 50$ and $N = 80$ ($\alpha = \pi/2$)

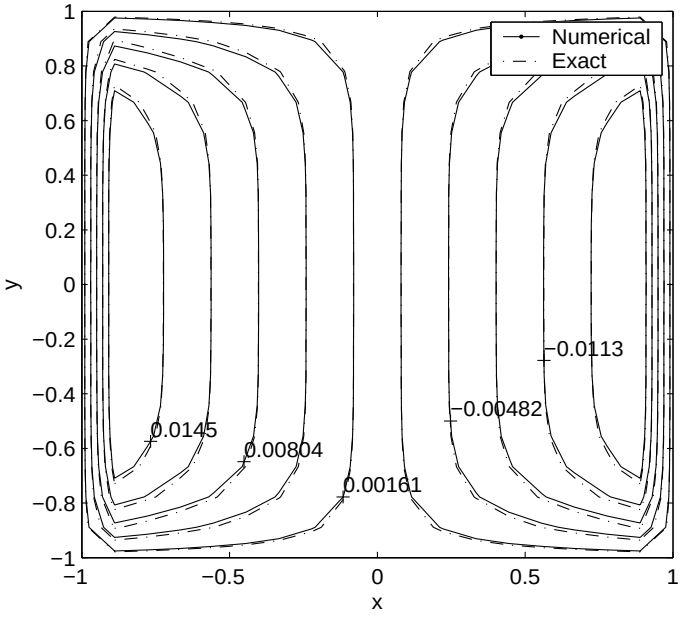

Figure 3.3: Induced magnetic field lines for $M = 50$ and $N = 80$ ($\alpha = \pi/2$)

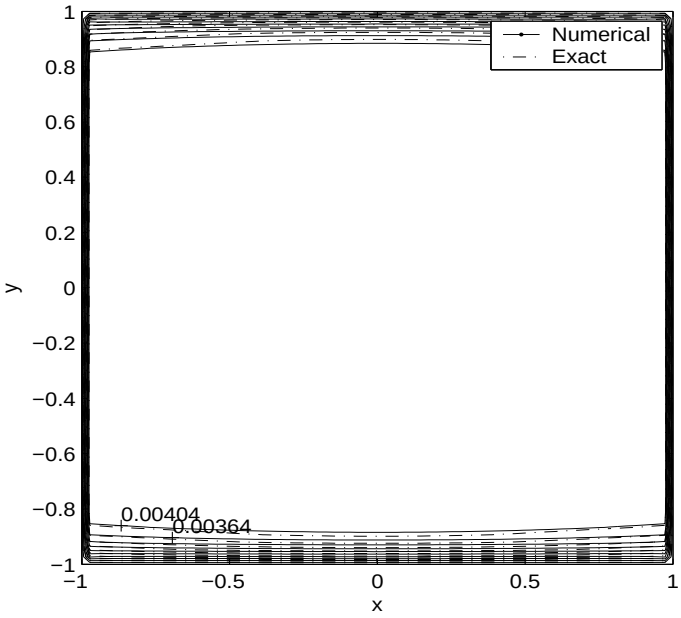

Figure 3.4: Velocity lines for $M = 300$ and $N = 300$ ($\alpha = \pi/2$)

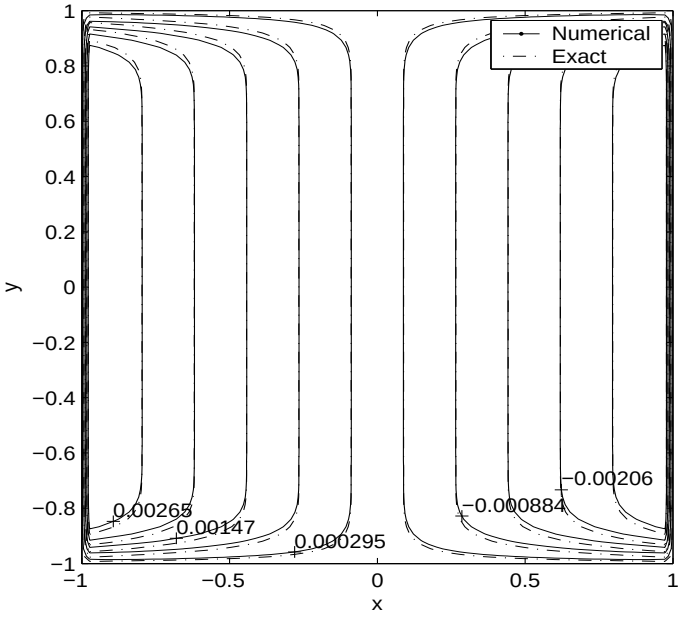

Figure 3.5: Induced magnetic field lines for $M = 300$ and $N = 300$ ($\alpha = \pi/2$)

Problem 2: Insulating wall duct under oblique magnetic field

The steady laminar flow of an incompressible, viscous, electrically conducting fluid in a rectangular duct subjected to an externally oblique magnetic field of strength B_0 making a positive angle with the y-axis is considered. The governing partial differential equations (in nondimensionalized form) in terms of velocity V and induced magnetic field B are

$$\begin{aligned} \nabla^2 V + M_x \frac{\partial B}{\partial x} + M_y \frac{\partial B}{\partial y} &= -1 \\ \nabla^2 B + M_x \frac{\partial V}{\partial x} + M_y \frac{\partial V}{\partial y} &= 0\,. \end{aligned} \tag{3.52}$$

The boundary conditions are homogeneous for both the velocity and the induced magnetic field. The cross-section of the square domain $|x| \leq 1$, $|y| \leq 1$ is drawn in Figure (3.6).

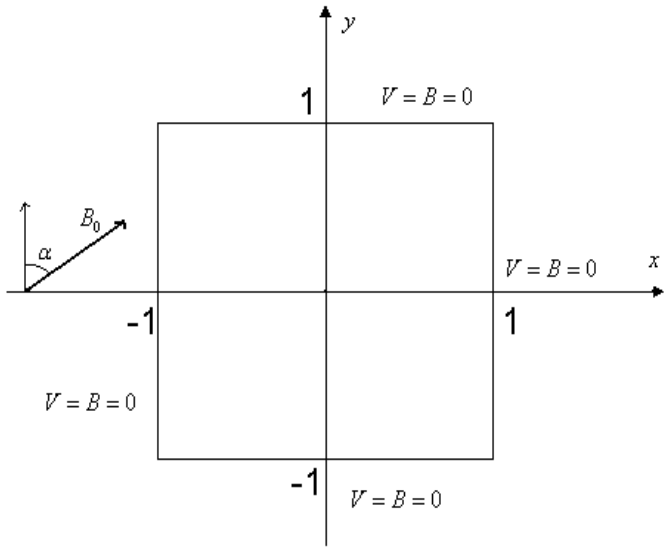

Figure 3.6: MHD duct flow under an external oblique magnetic field

Similar to Problem 1 we take the particular solution $\mathbf{u_p} = \begin{bmatrix} 0 \\ -x/M_x \end{bmatrix}$ for reducing the problem in (3.52) to homogeneous equations with non-homogeneous boundary conditions. Computations are carried out with $N = 72$ and 300 constant boundary elements for the values of Hartmann number $M = 50$ and 300 respectively. In Figures 3.7-3.8 and 3.9-3.10, the velocity-induced magnetic field lines are presented with $\alpha = \pi/4$ for the values of Hartmann number $M = 50$ and $M = 300$, respectively. Similarly, the velocity-induced magnetic field lines are drawn in Figures 3.11-3.12 and 3.13-3.14 with $\alpha = \pi/3$ for $M = 50$ and 300, respectively. The boundary layer formation close to the walls for both the velocity and the induced magnetic field is well observed for increasing Hartmann number. Velocity again becomes uniform at the center of the duct and the flow becomes stagnant. The boundary layers are concentrated near the corners in the direction of the applied oblique magnetic field for both the velocity and the induced magnetic field. These are the well-known characteristics of the magnetohydrodynamic flow.

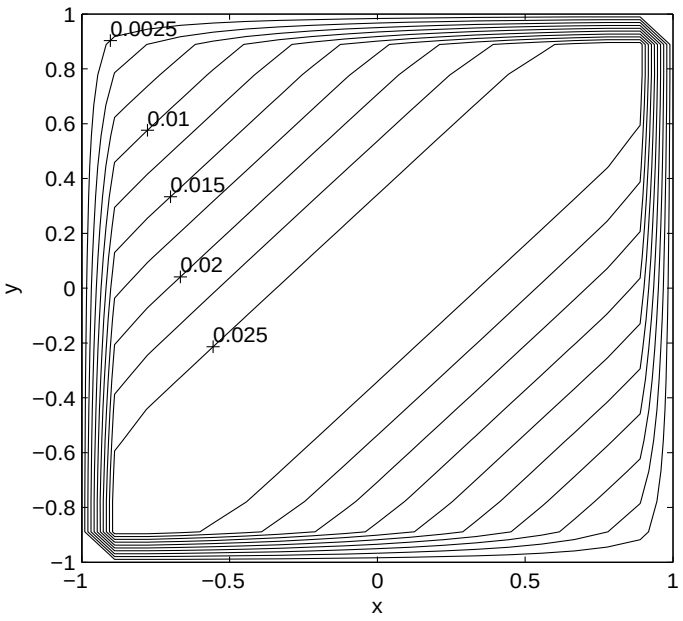

Figure 3.7: Velocity lines for $M = 50$ and $N = 72$ ($\alpha = \pi/4$)

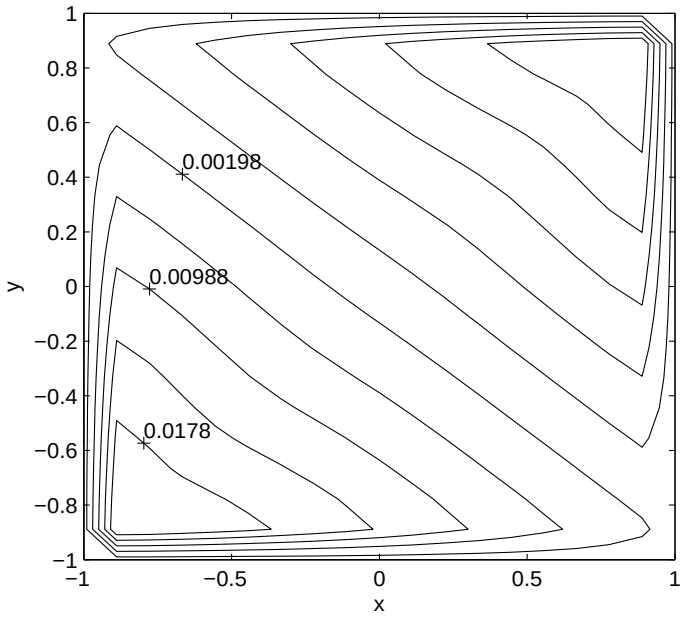

Figure 3.8: Induced magnetic field lines for $M = 50$ and $N = 72$ ($\alpha = \pi/4$)

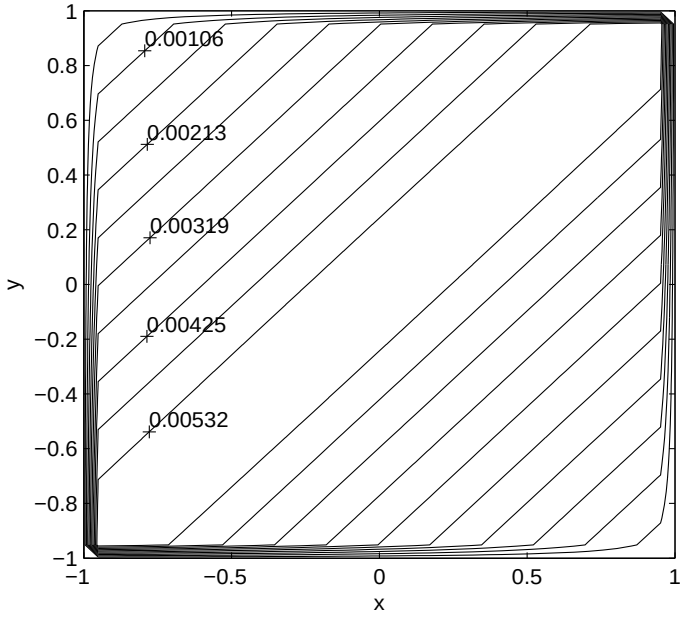

Figure 3.9: Velocity lines for $M = 300$ and $N = 300$ ($\alpha = \pi/4$)

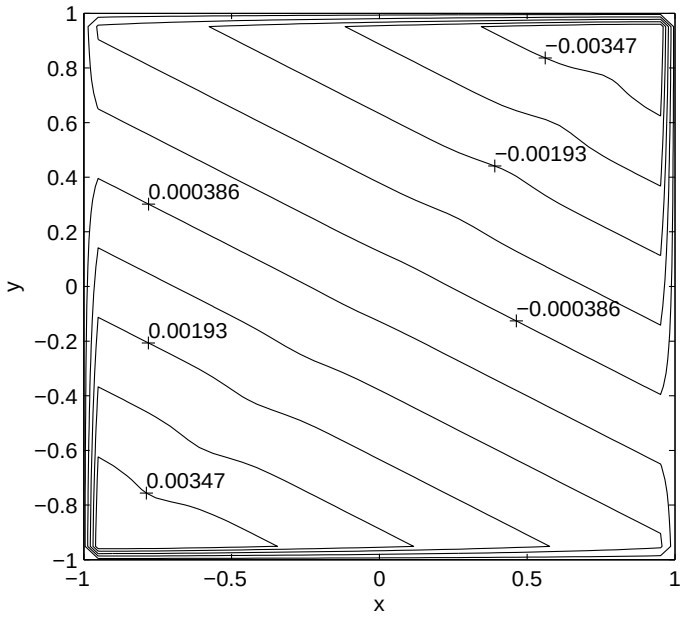

Figure 3.10: Induced magnetic field lines for $M = 300$ and $N = 300$ ($\alpha = \pi/4$)

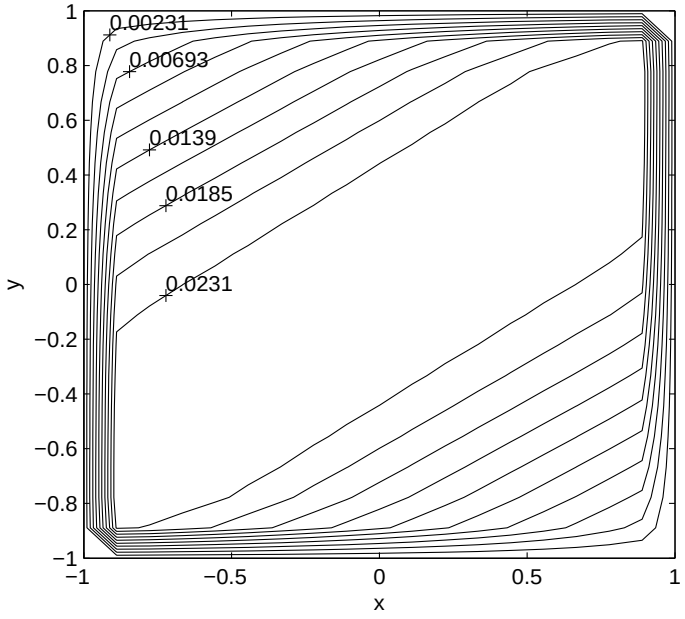

Figure 3.11: Velocity lines for $M = 50$ and $N = 72$ ($\alpha = \pi/3$)

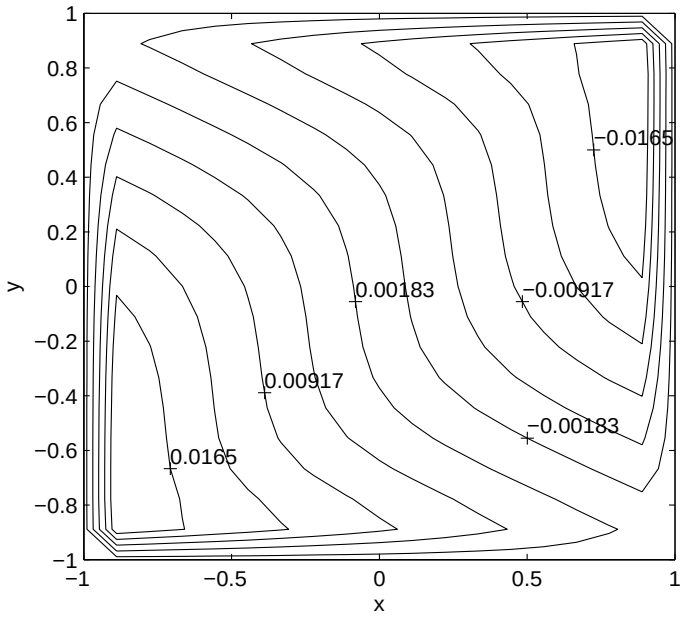

Figure 3.12: Induced magnetic field lines for $M = 50$ and $N = 72$ ($\alpha = \pi/3$)

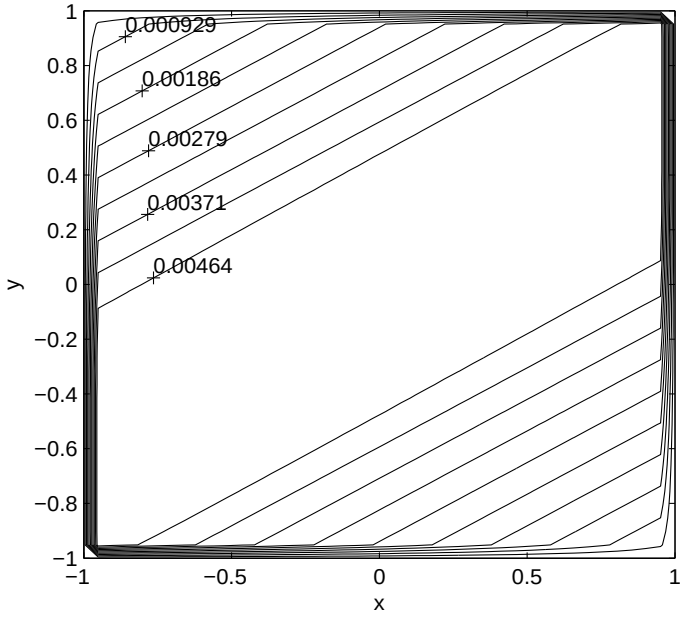

Figure 3.13: Velocity lines for $M = 300$ and $N = 300$ ($\alpha = \pi/3$)

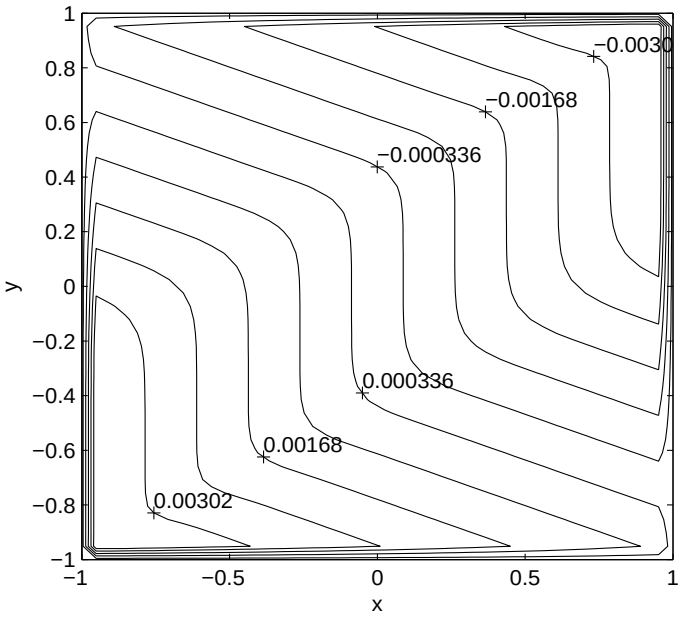

Figure 3.14: Induced magnetic field lines for $M = 300$ and $N = 300$ ($\alpha = \pi/3$)

Problem 3: Duct with partly insulating partly conducting walls

The magnetohydrodynamic flow, subjected to an external magnetic field of strength B_0 in the direction of x-axis in a rectangular duct with a cross section $0 \leq x \leq a$, $-b/2 \leq y \leq b/2$ where a and b are the lengths of the sides in x and y-directions, is considered. It is assumed that the sides of the duct parallel to the magnetic field are electrically insulated, while the perpendicular side $x = 0$ is conducting symmetrically about the x-axis for a length l from the origin, the rest of the same side is assumed to be insulated. The side $x = a$ is insulated completely (see Figure 3.15).

The basic equations governing the MHD duct flow are given as

$$\begin{aligned} \nabla^2 V + M\frac{\partial B}{\partial x} &= -1 \\ \nabla^2 B + M\frac{\partial V}{\partial x} &= 0 \end{aligned} \tag{3.53}$$

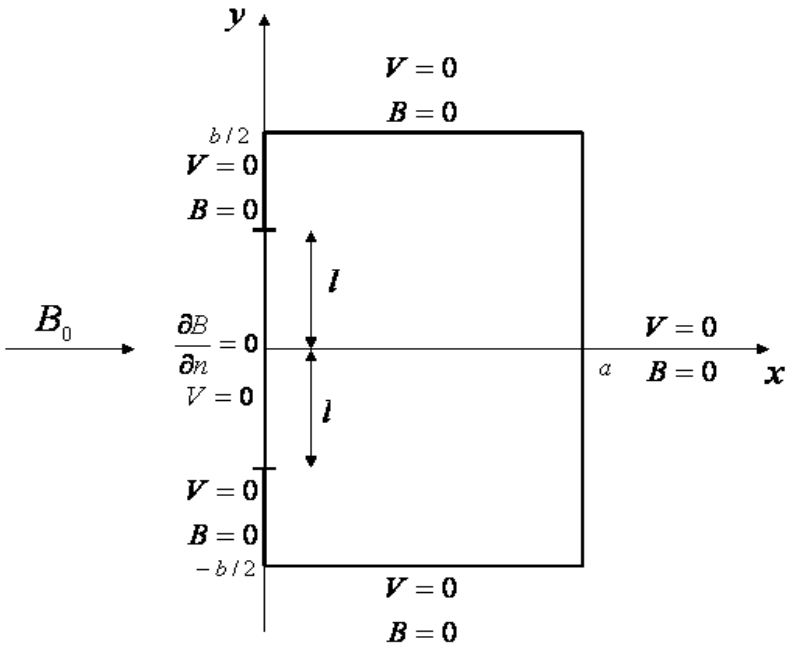

Figure 3.15: MHD duct flow with a conducting part on $x = 0$

in terms of the velocity V and the induced magnetic field B with the Hartmann number $M = M_x$. There is only one component of the velocity and induced magnetic field in the z-direction. These nonhomogeneous equations are reduced to homogeneous partial differential equations (3.49) with the nonhomogeneous boundary conditions (3.50) by using the same particular solution $\mathbf{u_p} = \begin{bmatrix} 0 \\ -x/M \end{bmatrix}$ given in Problem 1. In the computations the lengths a and b are taken as one.

Boundary element method solutions are carried out for the values of Hartmann number $M = 50$, 100 and 300 and for several values of length of the conducting part of the boundary l by discretizing the boundary of the problem with appropriate numbers of constant elements. Equal velocity and induced magnetic field lines are drawn in Figures 3.16-3.33 for $M = 50$, 100 and 300 and for the values of $l = 0.15$, 0.25 and 0.35 . In Figures 3.17, 3.23 and 3.29, the equal velocity lines are depicted for $M = 50$, 100 and 300, respectively. In each of the figures l is kept fixed ($l = 0.25$). One can notice from these graphs that as Hartmann number

M is increased Hartmann layer formation starts to take place at the insulated parts of the boundary. The thickness of the Hartmann layer is of the order of M^{-1} at the walls $x = 0$, a and of order of $1/\sqrt{M}$ at the walls $y = \pm b/2$ (Shercliff [8]). Also the parabolic boundary layer emanating from the discontinuity points $y = \pm l$ in the direction of applied magnetic field starts to form with increasing M, and is more pronounced, higher the value of l or M. For small l or M, the two layers coming from the two points of discontinuity tend to interfere with each other in the middle, while for large l or M, they stay seperate and are, therefore, more easily displayed.

The effect of varying M on the induced magnetic field lines are demonstrated in Figures 3.20, 3.26 and 3.32 for $M = 50$, 100 and 300, respectively. The length of the conducting portion l is kept fixed ($l = 0.25$). As M increases, the region for which $B > 0$, keeps on increasing. The maximum value of the induced magnetic field, B, takes place in front of the conducting part.

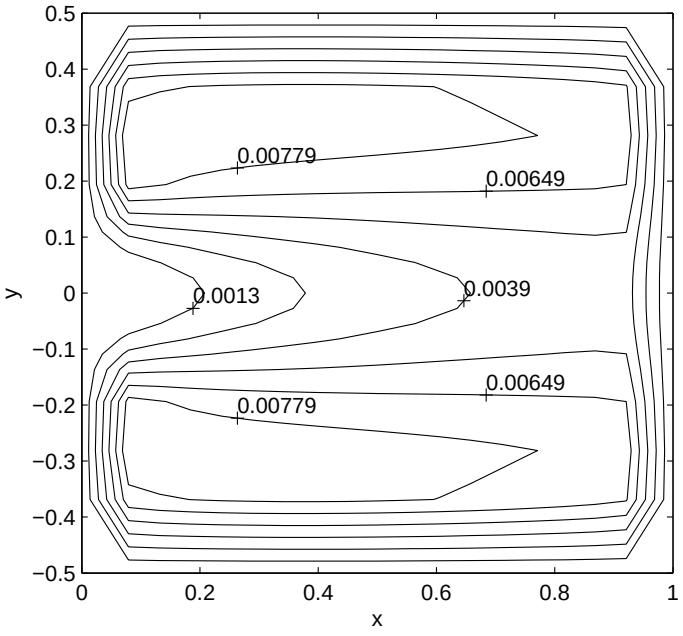

Figure 3.16: Velocity lines for $M = 50$ and $N = 76$ ($l = 0.15$)

To see the effect of the increase in the length of the conducting part on the

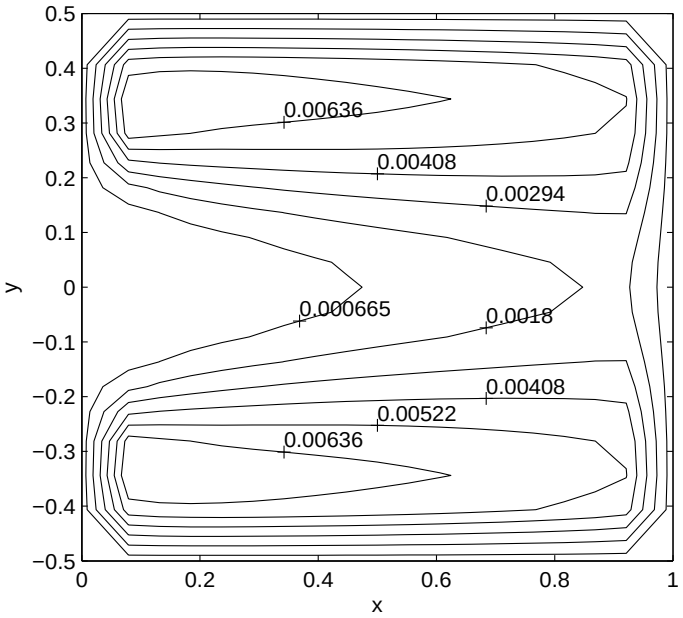

Figure 3.17: Velocity lines for $M = 50$ and $N = 76$ ($l = 0.25$)

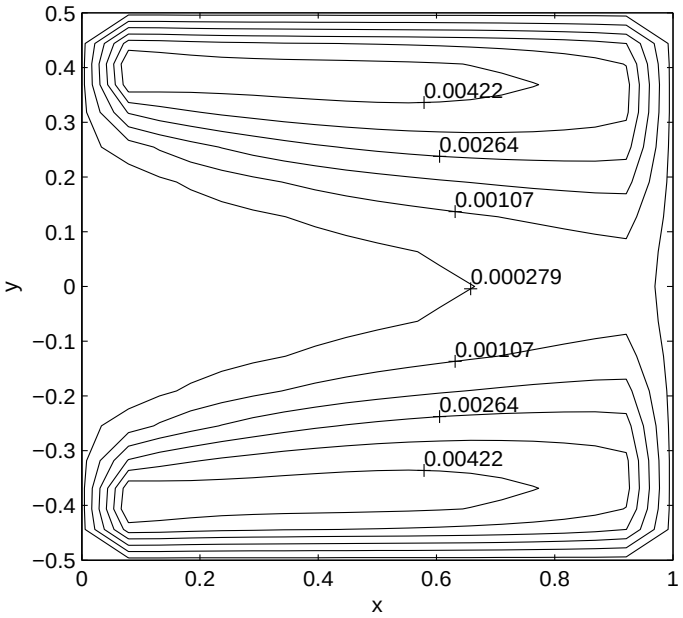

Figure 3.18: Velocity lines for $M = 50$ and $N = 76$ ($l = 0.35$)

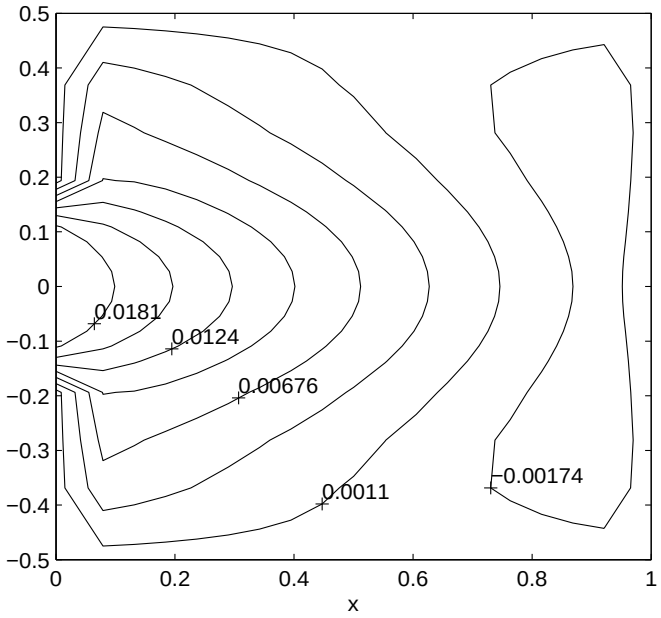

Figure 3.19: Induced magnetic field lines for $M = 50$ and $N = 76$ ($l = 0.15$)

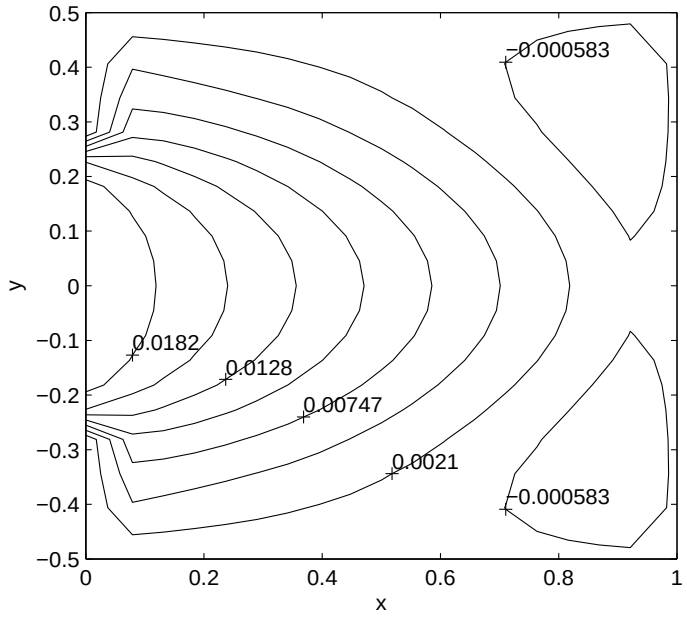

Figure 3.20: Induced magnetic field lines for $M = 50$ and $N = 76$ ($l = 0.25$)

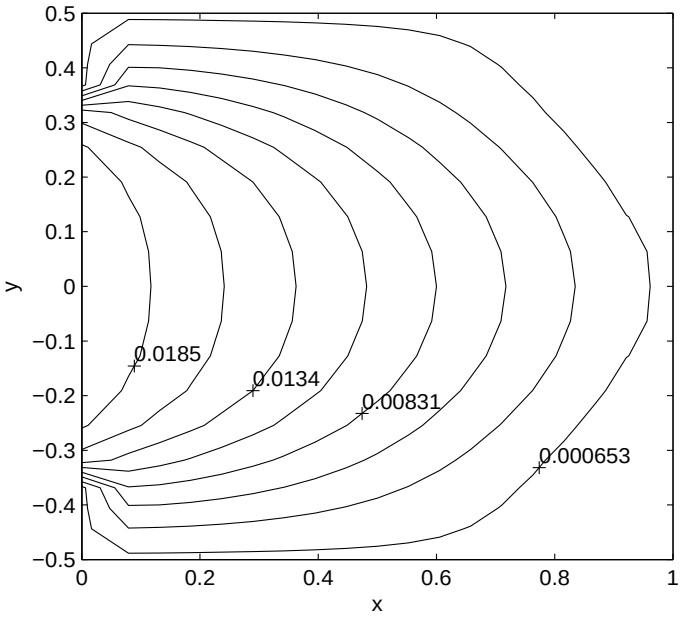

Figure 3.21: Induced magnetic field lines for $M = 50$ and $N = 76$ ($l = 0.35$)

velocity field, equivelocity lines in Figures 3.22, 3.23 and 3.24 are plotted for $M = 100$ and $l = 0.15$, 0.25 and 0.35, respectively. We observe that the increase in the value of l results in the expansion of the region in which the fluid is nearly stagnant. This region is in the neighbourhood of the conducting part. The other features remain essentially the same. An increase in the length of the conducting part l has a similar effect with an increase in Hartmann number M on the induced magnetic field lines. This is shown in Figures 3.25, 3.26 and 3.27 where M is fixed ($M = 100$) and l varies as $l = 0.15$, 0.25 and 0.35, respectively.

The numerical accuracy of the results for this problem is validated by increasing the number of the boundary elements, N, used in the computations. Especially at the discontinuity points $y = \mp l$, $l = 0.35$, much more refined elements are used as presented in Figures 3.34, 3.35 and 3.36 respectively for $N = 48$, 184 and 360 for the value of Hartmann number $M = 100$. The convergence and the formation of the parabolic boundary layers emanating from the discontinuity points are well observed when the number of boundary elements is increased.

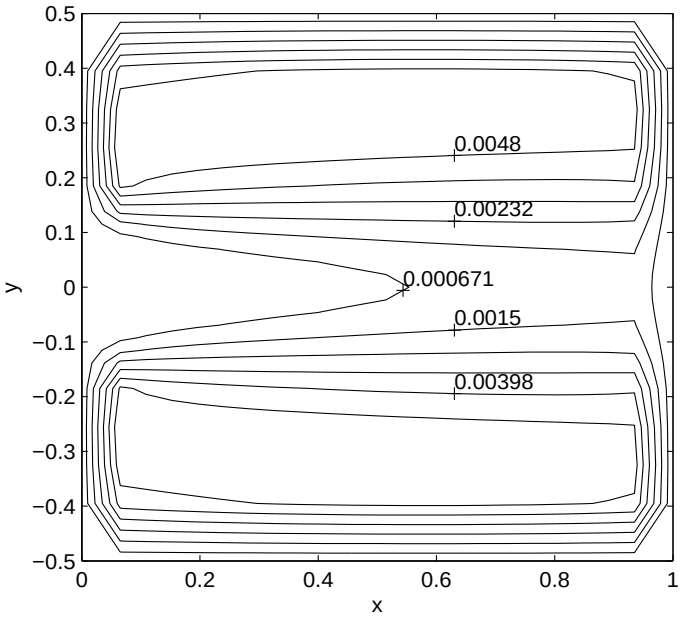

Figure 3.22: Velocity lines for $M = 100$ and $N = 92$ ($l = 0.15$)

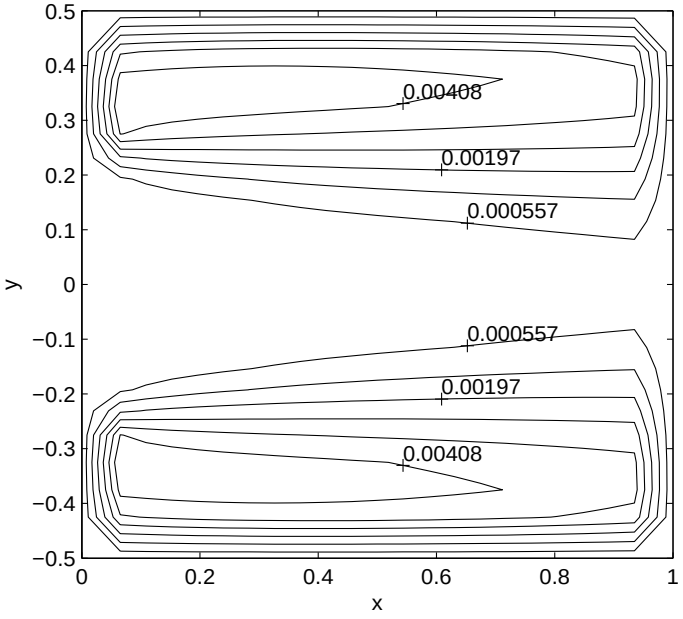

Figure 3.23: Velocity lines for $M = 100$ and $N = 92$ ($l = 0.25$)

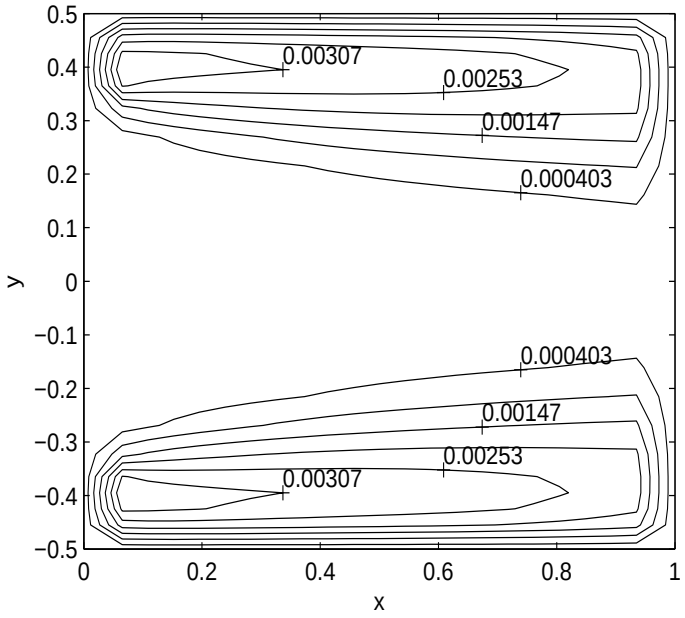

Figure 3.24: Velocity lines for $M = 100$ and $N = 92$ ($l = 0.35$)

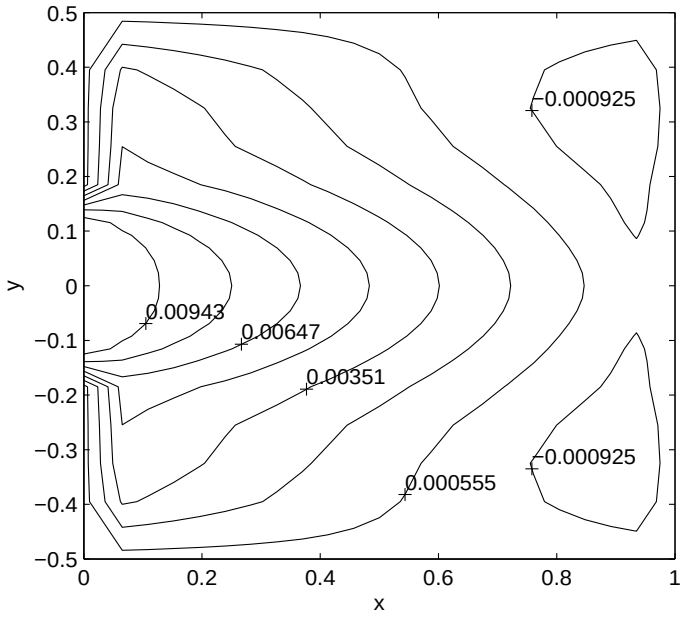

Figure 3.25: Induced magnetic field lines for $M = 100$, $N = 92$ ($l = 0.15$)

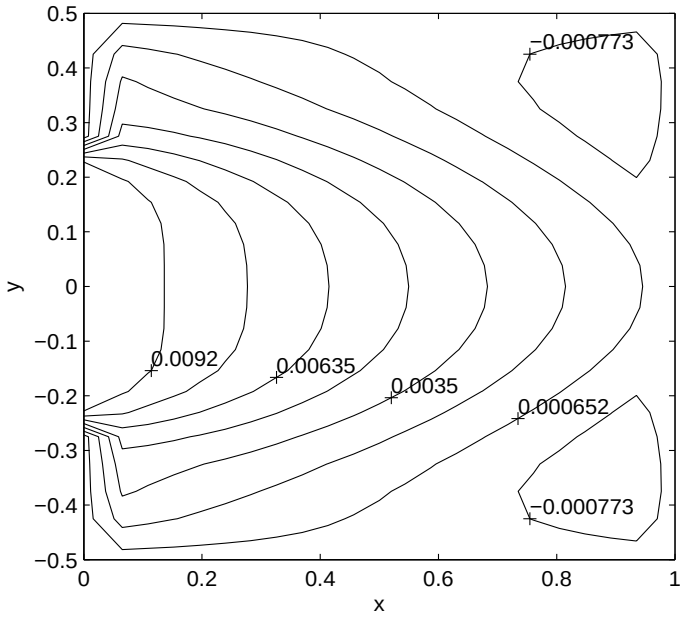

Figure 3.26: Induced magnetic field lines for $M = 100$, $N = 92$ ($l = 0.25$)

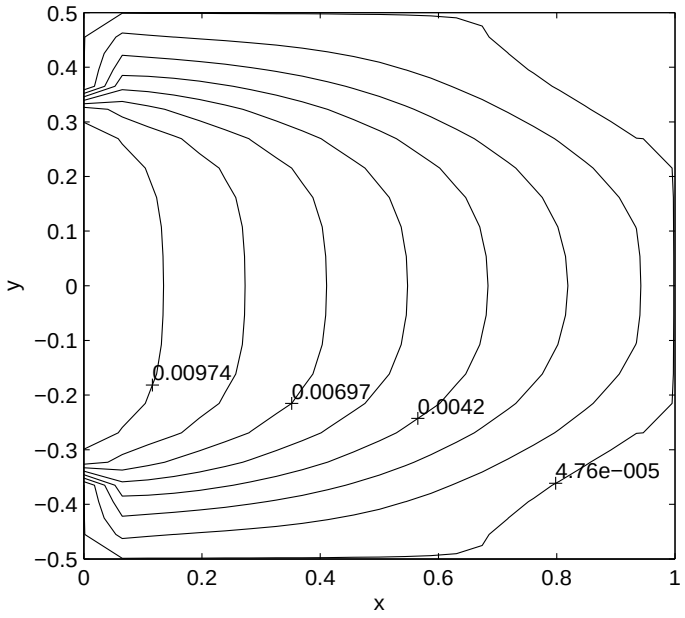

Figure 3.27: Induced magnetic field lines for $M = 100$, $N = 92$ ($l = 0.35$)

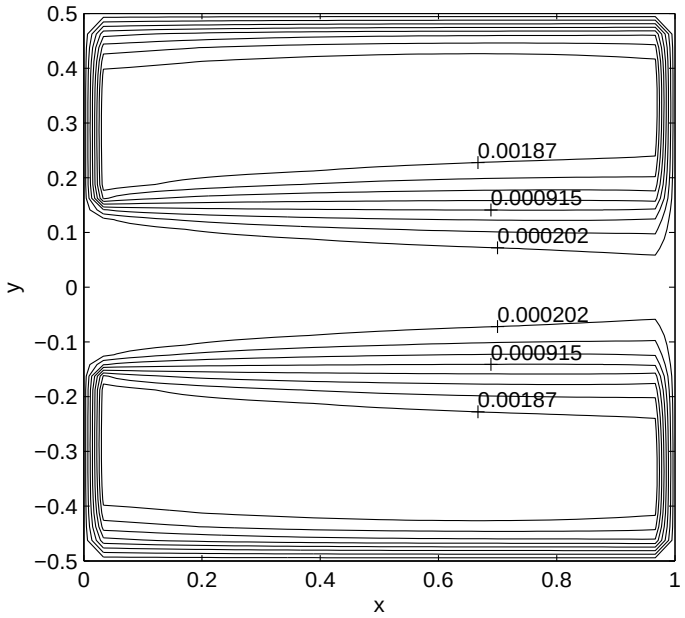

Figure 3.28: Velocity lines for $M = 300$ and $N = 180$ ($l = 0.15$)

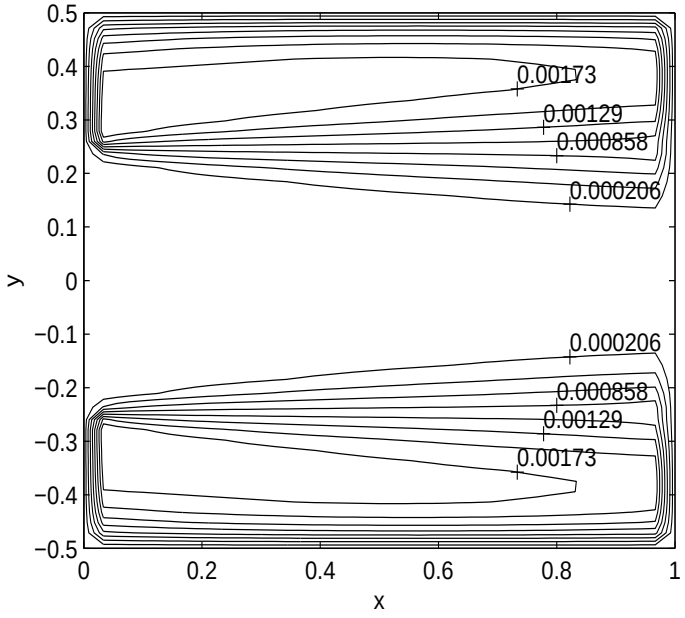

Figure 3.29: Velocity lines for $M = 300$ and $N = 180$ ($l = 0.25$)

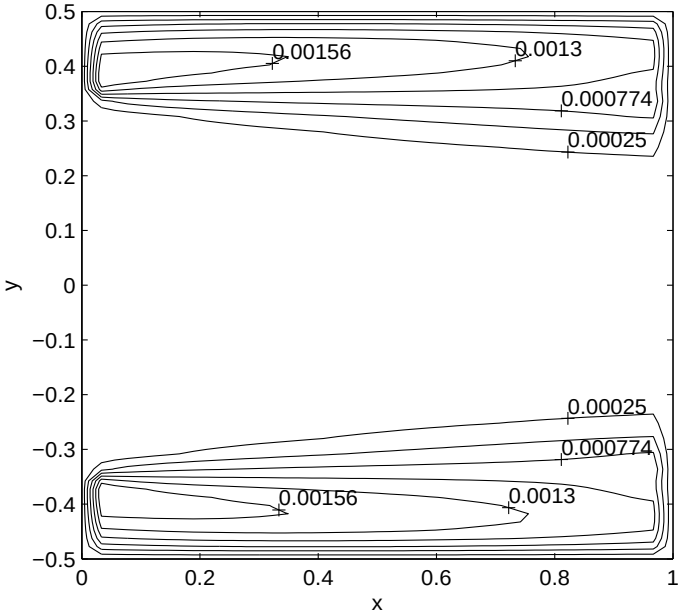

Figure 3.30: Velocity lines for $M = 300$ and $N = 180$ ($l = 0.35$)

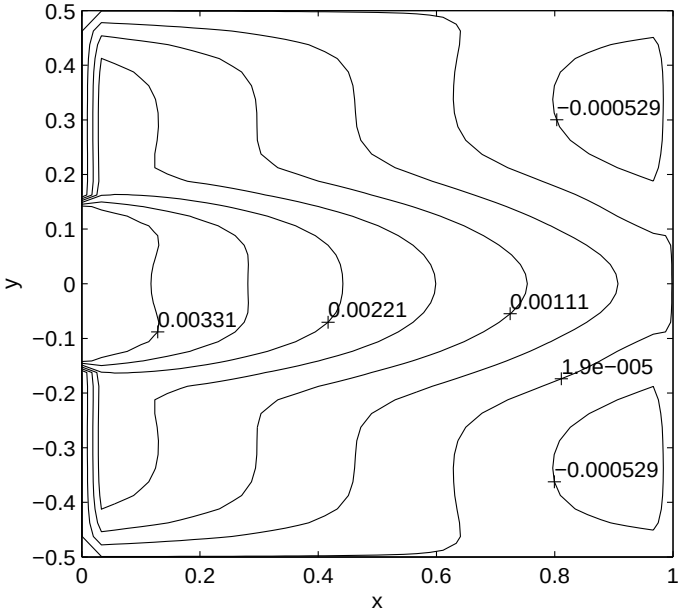

Figure 3.31: Induced magnetic field lines for $M = 300$ and $N = 180$ ($l = 0.15$)

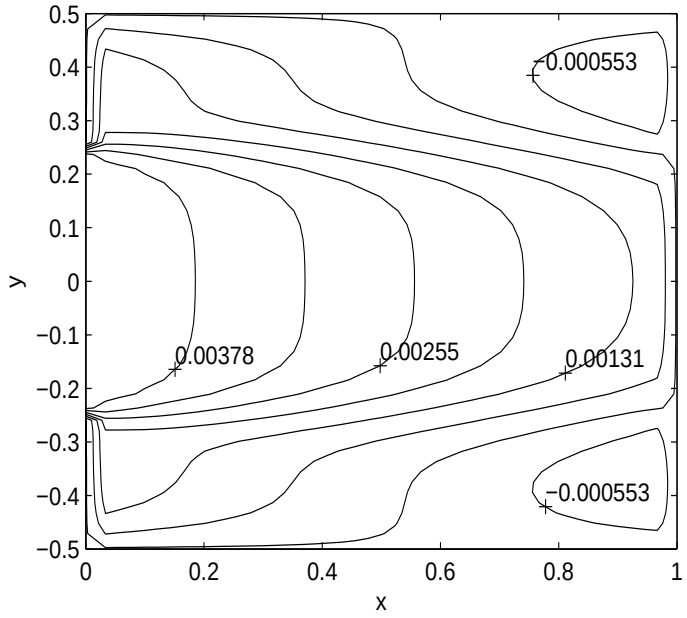

Figure 3.32: Induced magnetic field lines for $M = 300$ and $N = 180$ ($l = 0.25$)

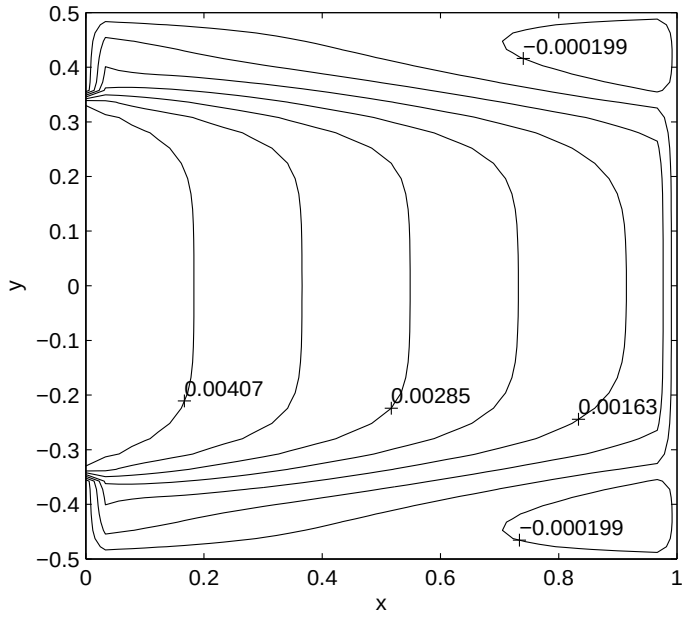

Figure 3.33: Induced magnetic field lines for $M = 300$ and $N = 180$ ($l = 0.35$)

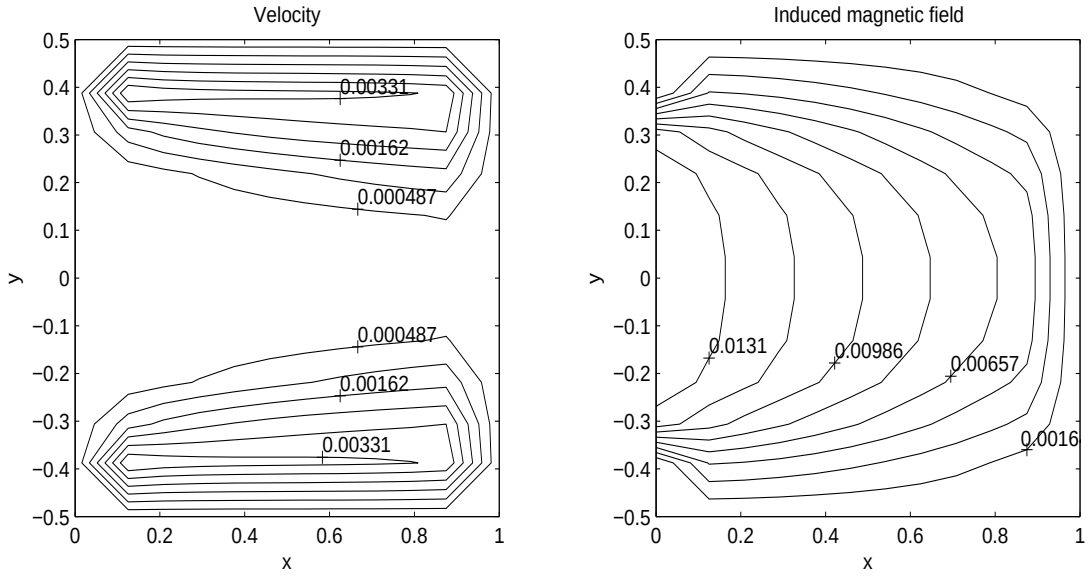

Figure 3.34: Velocity and induced magnetic field lines for $M = 100$ and $N = 48$ ($l = 0.35$)

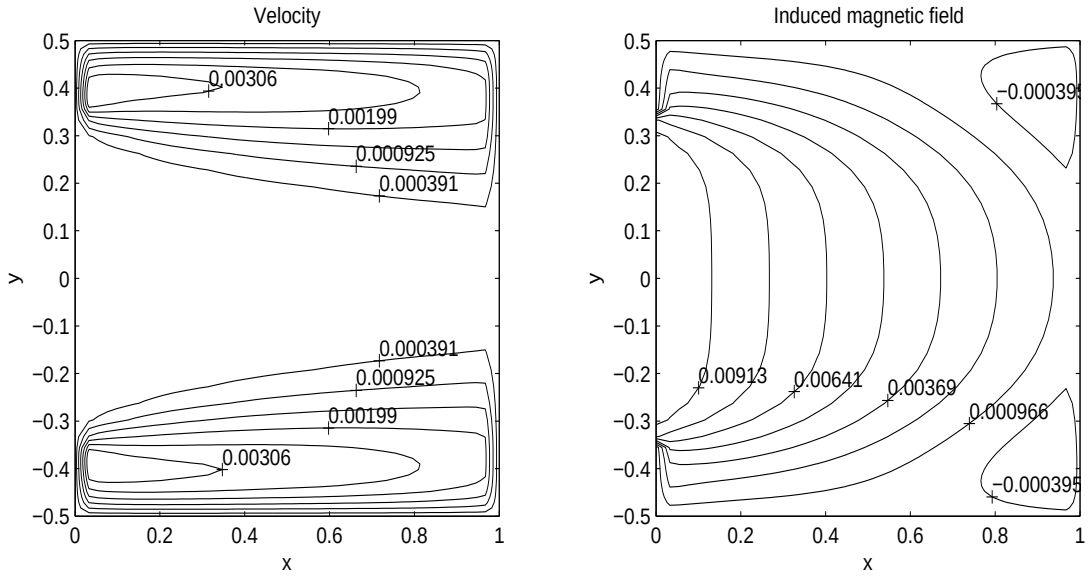

Figure 3.35: Velocity and induced magnetic field lines for $M = 100$ and $N = 184$ ($l = 0.35$)

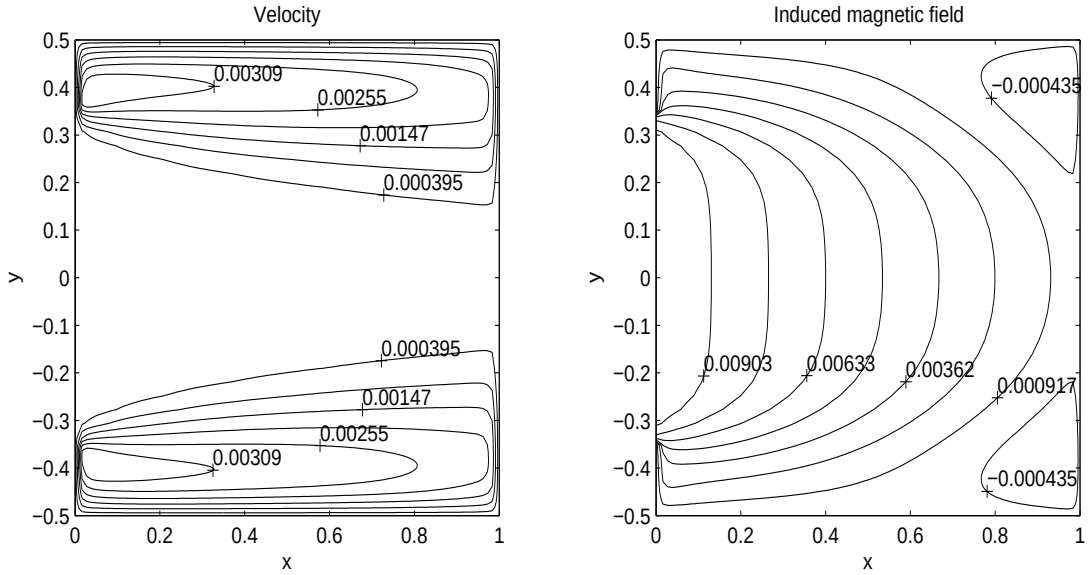

Figure 3.36: Velocity and induced magnetic field lines for $M = 100$ and $N = 360$ ($l = 0.35$)

Problem 4: Duct with conducting walls parallel to applied magnetic field

MHD flow in a rectangular duct with perfectly conducting walls parallel to the applied magnetic field and insulated walls perpendicular to the field is solved. Although a rigorous solution in terms of double infinite series has been established by Greenberg and given in Dragoş [7], its practical usefulness is limited. Thus, efficient numerical solutions are needed in terms of computational cost and time.

In the present problem the external magnetic field is applied in a parallel direction to the conducting walls, whereas in the previous test problem, Problem 3, it is perpendicular to the conducting portion of the boundary. The equations governing these MHD duct flow subjected to an external magnetic field B_0 in the direction of y-axis are given as,

$$\begin{aligned} \nabla^2 V + M\frac{\partial B}{\partial y} &= -1 \\ & \qquad \text{in } \Omega \\ \nabla^2 B + M\frac{\partial V}{\partial y} &= 0 \end{aligned} \tag{3.54}$$

where $\Omega \subset \mathbb{R}^2$ denotes the section of the duct ($-1 \leq x,\, y \leq 1$) and $M = M_y$. The external magnetic field B_0 is applied parallel to the conducting walls at $x = \mp 1$ and perpendicular to the horizontal insulated walls at $y = \mp 1$. The fluid is driven down the duct by means of a constant pressure gradient. The boundary conditions for the unknowns $V(x, y)$ and $B(x, y)$ are

$$\begin{aligned} &V(\mp 1, y) = 0, \qquad \left.\frac{\partial B}{\partial x}\right|_{x=\mp 1} = 0, \qquad |y| \leq 1 \\ &V(x, \mp 1) = 0, \qquad B(x, \mp 1) = 0, \qquad |x| \leq 1 \end{aligned} \tag{3.55}$$

as shown in Figure 3.37.

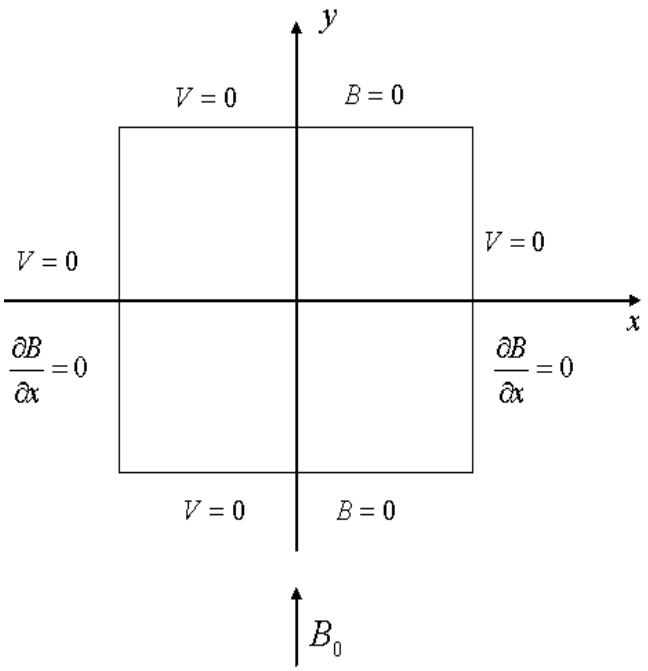

Figure 3.37: MHD duct flow with a conducting walls parallel to B_0

The MHD problem considered here is of considerable theoretical and practical importance. The external magnetic field determines the appearance within the fluid of an induced current which can be made to flow in an external circuit through the conducting walls. In this manner, some of the internal energy of the fluid is given up to the exterior as utilizable electrical energy. But, the BEM

must be applied directly to coupled equations since they can not be decoupled because of the conducting walls. For this, the fundamental solution $\mathbf{G}^*$ to coupled equations,

$$\mathbf{G}^* = \frac{1}{2\pi} K_0(\frac{M}{2}\, r) \begin{bmatrix} \cosh(\frac{M}{2}\, r_y) & \sinh(\frac{M}{2}\, r_y) \\ \\ \sinh(\frac{M}{2}\, r_y) & \cosh(\frac{M}{2}\, r_y) \end{bmatrix} \tag{3.56}$$

which is derived as in Section 3.2, is used.

The boundary of the square duct is discretized by using $N = 80$ to $N = 312$ constant elements for the values of Hartmann number ranging from $M = 10$ to $M = 300$. It is observed that the higher the Hartmann number is, the more the number of boundary elements is needed for obtaining accurate solutions. Figures 3.38-3.39, 3.40-3.41 and 3.42-3.43 show the velocity-induced magnetic field lines for Hartmann numbers $M = 10$, 100 and 300 respectively. When M is increasing, the boundary layer formation for the velocity close to the insulated walls is much faster than the one close to the conducting walls. It is also known from the MHD duct flow theory that the boundary layer thickness is $1/M$ on the walls perpendicular to the external field whereas it is $1/\sqrt{M}$ on the walls parallel to the field, [60]. For the induced magnetic field also, the boundary layers are formed near the insulated walls for increasing value of Hartmann number. The symmetry for both the velocity and the induced magnetic field with respect to y-axis is observed from the graphics since the problem and the boundary conditions are invariant under the transformation $x \rightarrow -x$. The induced magnetic field is antisymmetric with respect to x-axis, although the velocity is symmetric.

In Figures 3.44-3.46 and 3.47-3.49 the velocity and the induced magnetic field level curves are depicted respectively for values of $M = 10$, 50 and 200. One can notice that as M increases a flattening tendency is observed for both the velocity and the induced magnetic field. Induced magnetic field lines are emanating from the conducting walls orthogonally satisfying the condition $\partial B/\partial n = 0$ there. Finally, the fluid is almost stagnant at the center of the duct when M increases. These are all the well known characteristics of the MHD duct flow.

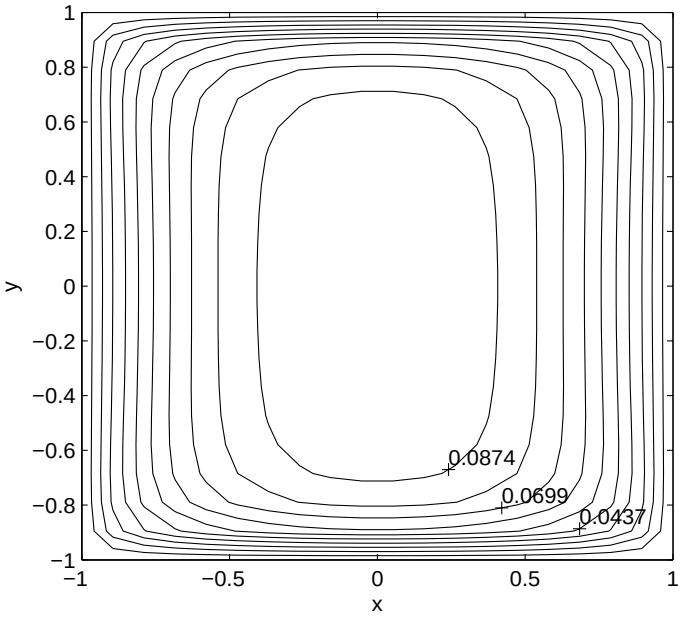

Figure 3.38: Velocity lines for $M = 10$, $N = 80$

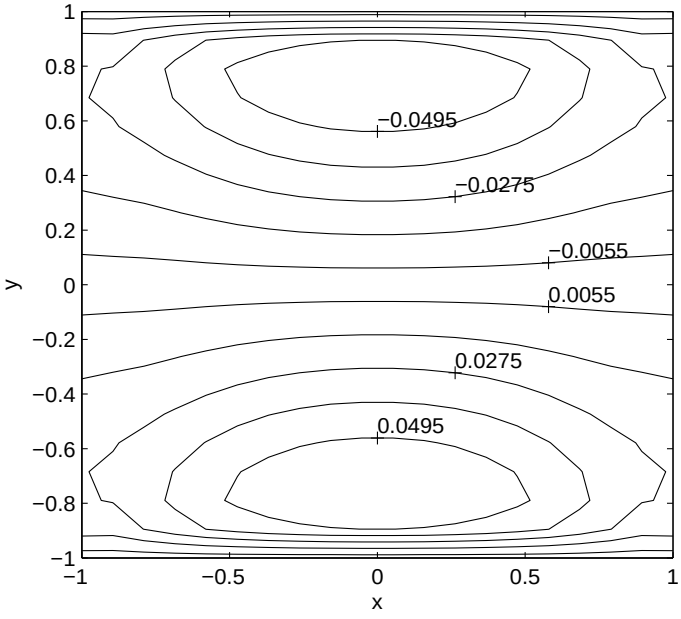

Figure 3.39: Induced magnetic field lines for $M = 10$, $N = 80$

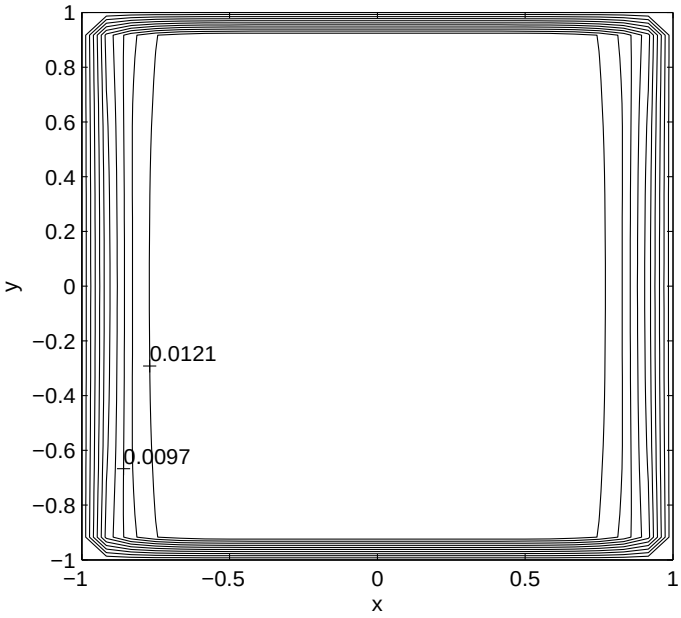

Figure 3.40: Velocity lines for $M = 100$, $N = 100$

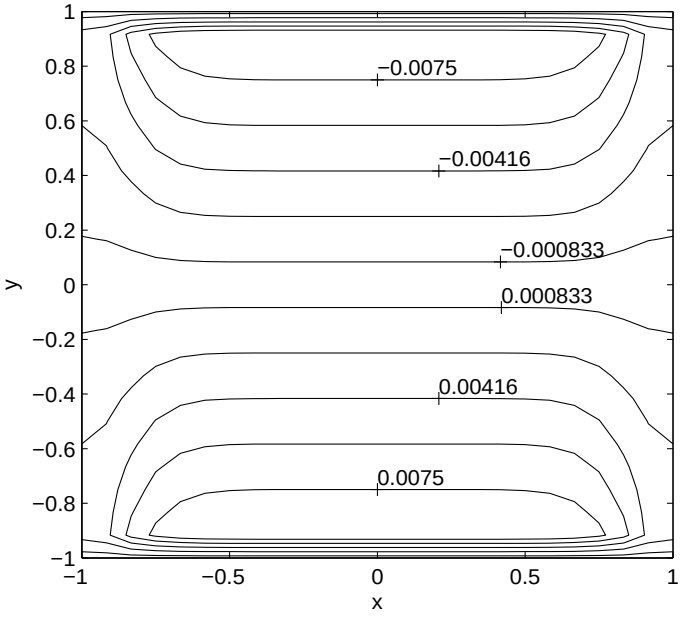

Figure 3.41: Induced magnetic field lines for $M = 100$, $N = 100$

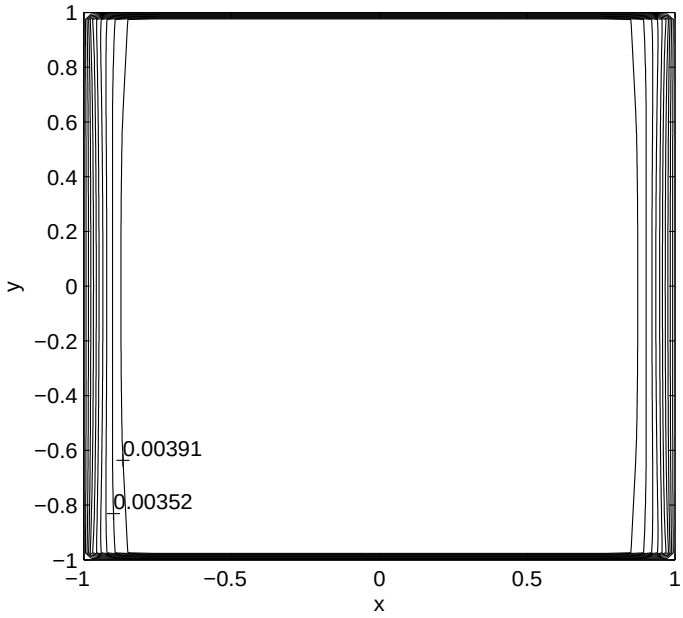

Figure 3.42: Velocity lines for $M = 300$, $N = 312$

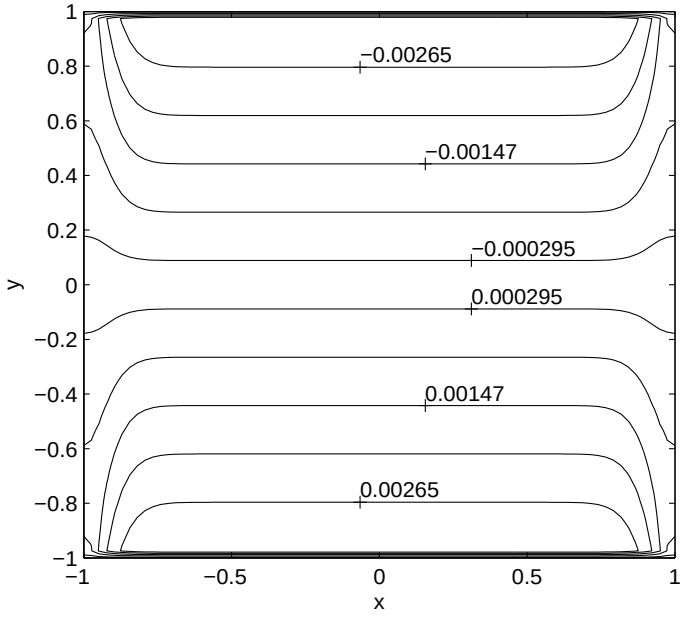

Figure 3.43: Induced magnetic field lines for $M = 300$, $N = 312$

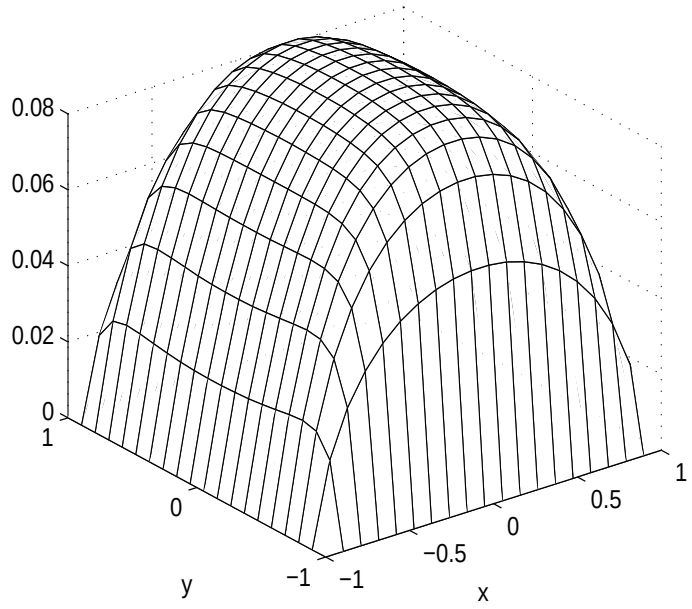

Figure 3.44: Velocity level curves for $M = 10$, $N = 80$

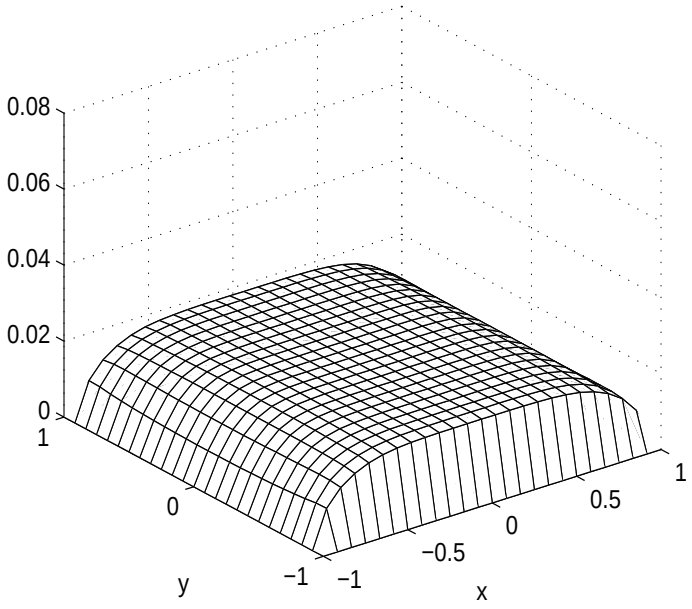

Figure 3.45: Velocity level curves for $M = 50$, $N = 80$

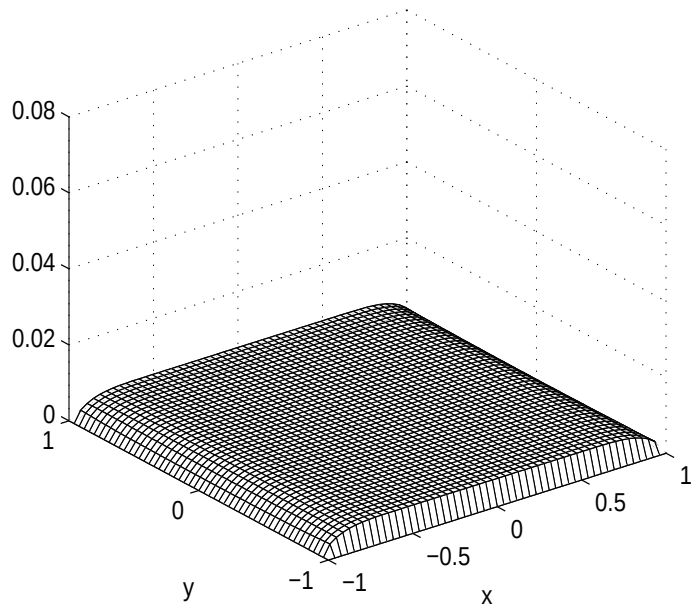

Figure 3.46: Velocity level curves for $M = 200$, $N = 212$

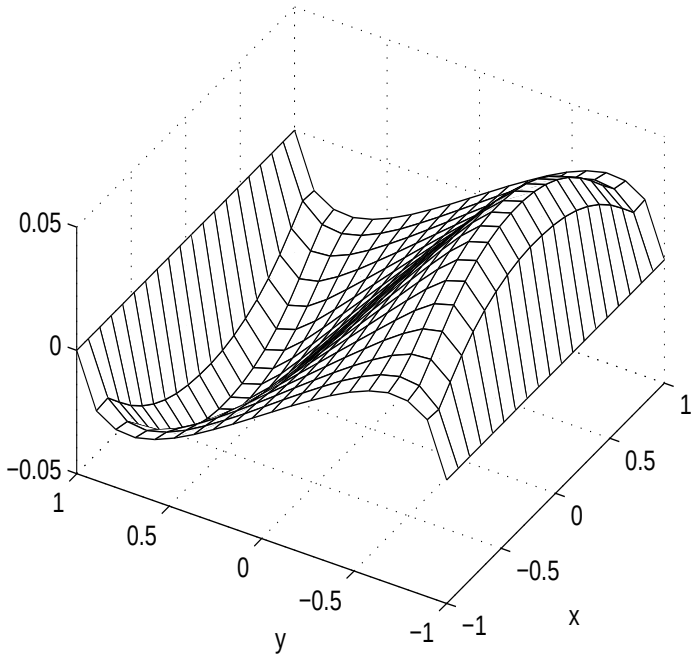

Figure 3.47: Induced magnetic field level curves for $M = 10$, $N = 80$

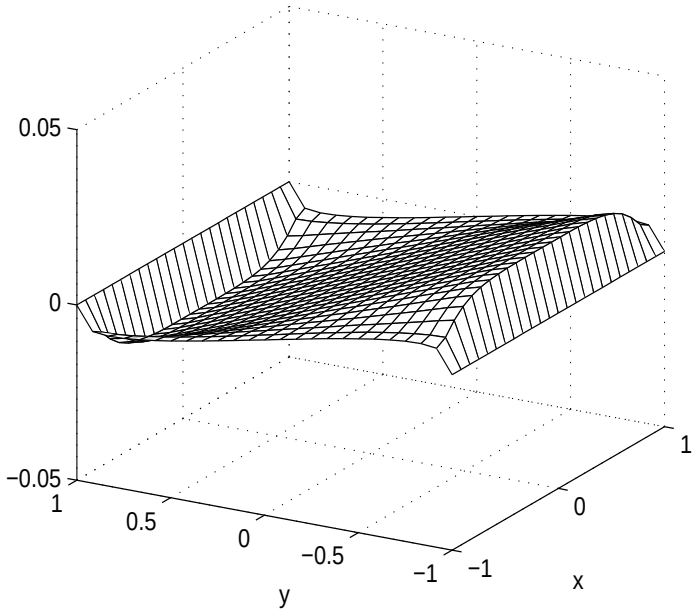

Figure 3.48: Induced magnetic field level curves for $M = 50$, $N = 80$

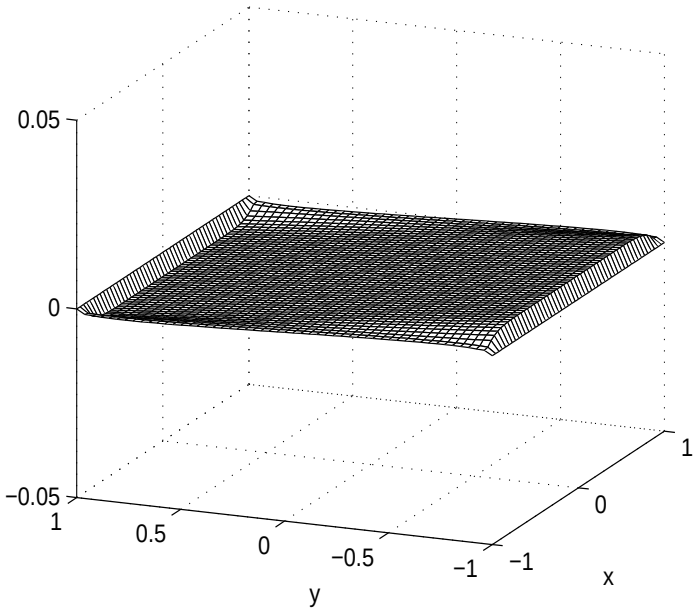

Figure 3.49: Induced magnetic field level curves for $M = 200$, $N = 212$

3.4.2 Electrically driven MHD flow on the upper half plane

In the previous section, Section 3.4.1, we consider flows which are pressure driven in a rectangular duct. The purpose of this section is to solve the MHD flows which are driven by imposed electric currents (without pressure gradient) on the upper half plane of partly insulated and partly conducting x-axis. It may be considered as the MHD flow along a flat plate ($y = 0$ line) with a transverse external magnetic field applied perpendicular to the plate. The coupled equations are solved with the boundary element method by using the fundamental solution (derived in Section 3.2) which treats the equations in coupled form. The use of this fundamental solution makes it possible to obtain the solution for large values of Hartmann number as $M \leq 700$. It is important to increase M in the solution procedure since the higher the value of M means the stronger the applied magnetic field is. Thus, the behaviour of the velocity and that of the induced magnetic field are greatly affected and the action takes place in very narrow regions close to the insulated walls and also inside of narrow parabolas in front of the discontinuity points. The flow is almost stagnant in front of the conducting portion of the boundary.

The boundary element method is a technique which offers a great advantage to analyse stationary problems with infinite domains. Due to the regularity conditions, it is possible to limit the discretization to a finite interval on the x-axis (infinite flat plate). The coupled MHD equations on the upper half plane restrict the integral equations only to the $y = 0$ line by using the properties of Bessel functions for large arguments. The advantage of the BEM lies in the need of discretization of only a finite lenght on the x-axis. In domain discretization methods, a closed region is assumed with a fictitious boundary taken far from the x-axis and this closed region is discretized with quite a number of elements. The computational economy makes very attractive the present numerical procedure.

We consider the steady and laminar flow of an incompressible fluid which is driven by the interaction of imposed electric currents and a uniform, transverse magnetic field B_0 applied perpendicular to the x-axis. There is only one component of velocity and induced magnetic field (in the z-direction). All these physical

variables, including pressure, and the boundary conditions are functions of x and y only.

So, the partial differential equations describing such flows are the same as those MHD duct flows where pressure gradient is taken as zero and they are given by (in nondimensionalized form), [7],

$$\begin{aligned} \nabla^2 V + M\frac{\partial B}{\partial y} &= 0 \\ & \qquad \text{in } \Omega \\ \nabla^2 B + M\frac{\partial V}{\partial y} &= 0 \end{aligned} \tag{3.57}$$

where Ω is the upper half plane (i.e. infinite region bounded by a regular plane containing all sufficiently distant points) and $M = M_y$.

The general form of the boundary conditions which are suitable in practice for the MHD flow in an infinite region can be expressed as

$$\begin{aligned} & V(x,0) = 0 && -\infty < x < \infty \\ & B(x,0) = \bar{B} && \text{on } \Gamma_I \\ & \frac{\partial B}{\partial y}(x,0) = 0 && \text{on } \Gamma_C \\ & |V(x,y)| < \infty,\ |B(x,y)| < \infty && \text{as } x^2 + y^2 \to \infty \\ & \left|\frac{\partial V}{\partial n}\right| < \infty,\ \left|\frac{\partial B}{\partial n}\right| < \infty && \text{as } x^2 + y^2 \to \infty \\ & \left|\frac{\partial V}{\partial n}\right| \to 0,\ \left|\frac{\partial B}{\partial n}\right| \to 0 && \text{as } y \to \infty \text{ in the vicinity of discontinuity points} \end{aligned} \tag{3.58}$$

where $\Gamma = \Gamma_I + \Gamma_C$ is the whole x-axis with $\Gamma_I \cap \Gamma_C = \emptyset$. Γ_I and Γ_C are the insulated and conducting parts of the boundary Γ respectively. The points where the conductivity changes abrubtly are called discontinuity points. $\bar{B}$ is a known value.

The application of the boundary element method to equation (3.57) leads to

the following homogeneous boundary integral equations

$$-c_A V(A) + \int_\Gamma \left(M B_1^* n_y - \frac{\partial V_1^*}{\partial n} \right) V d\Gamma + \int_\Gamma \left(M V_1^* n_y - \frac{\partial B_1^*}{\partial n} \right) B d\Gamma + \int_\Gamma V_1^* \frac{\partial V}{\partial n}\, d\Gamma + \int_\Gamma B_1^* \frac{\partial B}{\partial n}\, d\Gamma = 0 \tag{3.59}$$

and

$$-c_A B(A) + \int_\Gamma \left(M V_1^* n_y - \frac{\partial B_1^*}{\partial n} \right) V d\Gamma + \int_\Gamma \left(M B_1^* n_y - \frac{\partial V_1^*}{\partial n} \right) B d\Gamma + \int_\Gamma B_1^* \frac{\partial V}{\partial n}\, d\Gamma + \int_\Gamma V_1^* \frac{\partial B}{\partial n}\, d\Gamma = 0 \tag{3.60}$$

which are similar to equations (3.40) and (3.41), respectively, with $\mathbf{M} = (M_x = 0, M_y = M)$. The components V_1^* and B_1^* of the fundamental solution $\mathbf{G}^*$ defined in (3.39) are reduced to

$$\begin{aligned} V_1^* &= \frac{1}{2\pi} K_0(\frac{M}{2}\, r) \cosh(\frac{M}{2}\, r_y) \\ B_1^* &= \frac{1}{2\pi} K_0(\frac{M}{2}\, r) \sinh(\frac{M}{2}\, r_y) \end{aligned} \tag{3.61}$$

with their normal derivatives

$$\begin{aligned} \frac{\partial V_1^*}{\partial n} &= \frac{M}{4\pi} \left(K_0(\frac{M}{2}\, r) \sinh(\frac{M}{2}\, r_y) n_y + K_1(\frac{M}{2}\, r) \cosh(\frac{M}{2}\, r_y) \frac{\partial r}{\partial n} \right) \\ \frac{\partial B_1^*}{\partial n} &= \frac{M}{4\pi} \left(K_0(\frac{M}{2}\, r) \cosh(\frac{M}{2}\, r_y) n_y + K_1(\frac{M}{2}\, r) \sinh(\frac{M}{2}\, r_y) \frac{\partial r}{\partial n} \right) . \end{aligned} \tag{3.62}$$

Taking into consideration R as the radius of an infinitely distant upper semi circular boundary Γ_∞ with center at the origin, equations (3.59) and (3.60) can be written containing boundary integrals on both Γ_x and fictitious boundary Γ_∞ where Γ_x is the diameter of the semicircle on the x-axis. The boundary integral equations (3.59) and (3.60) can be restricted only to the boundary Γ_x, if the

following condition be obeyed:

$$\lim_{R\to\infty}\Big[\int_{\Gamma_\infty}(V^*\frac{\partial V}{\partial n}d\Gamma_\infty+\int_{\Gamma_\infty}B^*\frac{\partial B}{\partial n}d\Gamma_\infty+\int_{\Gamma_\infty}(MB^*n_y-\frac{\partial V^*}{\partial n})Vd\Gamma_\infty \\ +\int_{\Gamma_\infty}(MV^*n_y-\frac{\partial B^*}{\partial n})Bd\Gamma_\infty\Big]=0 \tag{3.63}$$

where V^* and B^* replace V_1^* and B_1^* in equations (3.59) and (3.60) respectively. This can be seen from the behaviour of V_1^*, B_1^* and that of their normal derivatives as $R\to\infty$ by the explanation given below.

The replacement of V_1^* or B_1^* in equation (3.63) results in the integrals containing the terms $\frac{1}{2\pi}K_0(M\,r/2)$ multiplied by either $\cosh(M\,r_y/2)$ or $\sinh(Mr_y/2)$, and $\frac{1}{2\pi}K_1(Mr/2)$ multiplied by either $\cosh(Mr_y/2)\frac{\partial r}{\partial n}$ or $\sinh(Mr_y/2)\frac{\partial r}{\partial n}$ as can be seen from equations (3.61)-(3.62). The first two integrals in (3.63) drop as $R\to\infty\,(r\to\infty)$ from the behaviour of modified Bessel functions K_0 and K_1 for large arguments and the behaviour of exponential function.

1. Considering the first integral in (3.63)

$$\begin{aligned}\lim_{R\to\infty}\int_{\Gamma_\infty}V_1^*\frac{\partial V}{\partial n}d\Gamma_\infty &= \lim_{R\to\infty}\int_{\Gamma_\infty}\frac{1}{2\pi}K_0(\frac{M}{2}\,r)\cosh(\frac{M}{2}\,r_y)\frac{\partial V}{\partial n}\,d\Gamma_\infty \\ &= \lim_{R\to\infty}\frac{1}{2\pi}\int_{\Gamma_\infty}\frac{1+e^{-M\,r_y}}{2}e^{\frac{M}{2}\,r_y}\sqrt{\frac{\pi}{2}}\frac{e^{-\frac{M}{2}\,r}}{\sqrt{r}\sqrt{\frac{M}{2}}}\frac{\partial V}{\partial n}\,d\Gamma_\infty \\ &= \lim_{R\to\infty}\frac{1}{4\sqrt{M\pi}}\int_{\Gamma_\infty}(1+e^{-M\,r_y})\frac{e^{-\frac{M}{2}(r-r_y)}}{\sqrt{r}}\frac{\partial V}{\partial n}\,d\Gamma_\infty\,.\end{aligned} \tag{3.64}$$

If $r-r_y\to\infty$ the integral drops obviously. If $r-r_y$ is bounded, so is $e^{-\frac{M}{2}(r-r_y)}$ bounded (except near y-axis) but $1/\sqrt{r}\to 0$ uniformly, which leads to the drop of the integral. However, when x approaches zero in a narrow segment around the y-axis, the integral of the terms $e^{-\frac{M}{2}(r-r_y)}/\sqrt{r}$ has a positive value. But the integral over Γ_∞ still drops since $\partial V/\partial n\to 0$ as $x\to 0$, $y\to\infty$. Similarly, the second integral in (3.63) tends to zero as $R\to\infty$.

2. The third integral in (3.63) can be written as

$$\begin{aligned}\lim_{R\to\infty}\int_{\Gamma_\infty}(MB_1^*n_y-\frac{\partial V_1^*}{\partial n})Vd\Gamma_\infty &= \lim_{R\to\infty}\int_{\Gamma_\infty}\Big[\frac{M}{2\pi}K_0(\frac{M}{2}r)\sinh(\frac{M}{2}r_y)n_y\\ &\quad -\frac{M}{4\pi}K_1(\frac{M}{2}r)\cosh(\frac{M}{2}r_y)\Big(\frac{r_x}{r}n_x+\frac{r_y}{r}n_y\Big)\\ &\quad -\frac{M}{4\pi}K_0(\frac{M}{2}r)\sinh(\frac{M}{2}r_y)n_y\Big]Vd\Gamma_\infty \qquad (3.65)\\ &= \lim_{R\to\infty}\frac{\sqrt{M}}{8\sqrt{\pi}}\int_{\Gamma_\infty}\Big[(1+e^{-Mr_y})\frac{e^{-\frac{M}{2}(r-r_y)}}{\sqrt{r}}\frac{r_y}{r}\\ &\quad -(1-e^{-Mr_y})\frac{e^{-\frac{M}{2}(r-r_y)}}{\sqrt{r}}\Big]Vd\Gamma_\infty\end{aligned}$$

Similar arguments as in Case 1 hold for $r-r_y\to\infty$ and $r-r_y$ is bounded. However again near the y-axis r_y and r are of the same order, i.e. $r_y/r\approx O(1)$. Thus, the integral in (3.65) takes the form $\lim_{R\to\infty}\frac{\sqrt{M}}{4\sqrt{\pi}}\int_{\Gamma_\infty}\frac{e^{-\frac{M}{2}(r+r_y)}}{\sqrt{r}}Vd\Gamma_\infty$, which tends to zero as $R\to\infty$ since V is bounded. Similarly, the last integral in (3.63) also drops as $R\to\infty$.

Thus, equations (3.59) and (3.60) are valid only on the boundary Γ_x and will lead to the following matrix boundary integral equation after the discretization of the boundary Γ_x into N constant boundary elements Γ_j,

$$-c_A\begin{bmatrix}\mathbf{V}(A)\\ \mathbf{B}(A)\end{bmatrix}+\begin{bmatrix}\mathbf{H} & \mathbf{G}\\ \mathbf{G} & \mathbf{H}\end{bmatrix}\begin{bmatrix}\mathbf{V}\\ \mathbf{B}\end{bmatrix}+\begin{bmatrix}\mathbf{H}^1 & \mathbf{G}^1\\ \mathbf{G}^1 & \mathbf{H}^1\end{bmatrix}\begin{bmatrix}\dfrac{\partial\mathbf{V}}{\partial n}\\ \\ \dfrac{\partial\mathbf{B}}{\partial n}\end{bmatrix}=\begin{bmatrix}\mathbf{0}\\ \mathbf{0}\end{bmatrix}. \qquad (3.66)$$

The entries of $\mathbf{H}$, $\mathbf{G}$, $\mathbf{H}^1$ and $\mathbf{G}^1$ become

$$
\begin{aligned}
h_{ij} &= \frac{M}{4\pi}\int_{\Gamma_j}\left(K_0(\frac{M}{2}\,r)\sinh(\frac{M}{2}\,r_y)n_y + K_1(\frac{M}{2}\,r)\cosh(\frac{M}{2}\,r_y)\frac{\partial r}{\partial n}\right)d\Gamma_j \\
g_{ij} &= \frac{M}{4\pi}\int_{\Gamma_j}\left(K_0(\frac{M}{2}\,r)\cosh(\frac{M}{2}\,r_y)n_y + K_1(\frac{M}{2}\,r)\sinh(\frac{M}{2}\,r_y)\frac{\partial r}{\partial n}\right)d\Gamma_j \\
{h^1}_{ij} &= \frac{1}{2\pi}\int_{\Gamma_j} K_0(\frac{M}{2}\,r)\cosh(\frac{M}{2}\,r_y)d\Gamma_j \\
{g^1}_{ij} &= \frac{1}{2\pi}\int_{\Gamma_j} K_0(\frac{M}{2}\,r)\sinh(\frac{M}{2}\,r_y)d\Gamma_j
\end{aligned}
\tag{3.67}
$$

in which the subscripts i and j indicate the fixed node i and the jth element on the boundary Γ_x.

Problem 1

The first example is a simple MHD flow problem on the half plane ($y \geq 0$) defined by equations (3.57) with the boundary conditions

$$
\begin{array}{ll}
V(x,0) = 0 & -\infty < x < \infty \\
B(x,0) = 1 & 0 \leq x < \infty \\
\dfrac{\partial B}{\partial y}(x,0) = 0 & -\infty < x < 0 \\
V \to 0,\ B \to 0 & \text{as } x \to -\infty \\
\left|\dfrac{\partial V}{\partial n}\right| \to 0,\ \left|\dfrac{\partial B}{\partial n}\right| \to 0 & \text{as } x \to 0,\ y \to \infty \\
|V| < \infty,\ |B| < \infty & \text{as } x^2 + y^2 \to \infty \\
\left|\dfrac{\partial V}{\partial n}\right| < \infty,\ \left|\dfrac{\partial B}{\partial n}\right| < \infty & \text{as } x^2 + y^2 \to \infty\,.
\end{array}
$$

The wall $y = 0$ is partly insulated ($x > 0$) and partly perfectly conducting ($x < 0$) as shown in Figure 3.50. An external circuit is connected so that a current enters the fluid at the discontinuity point $(0, 0)$ and leaves at infinity. The boundary $\Gamma_x = [-1, 1]$ is discretized by using $N = 20$, 68 and 100 constant

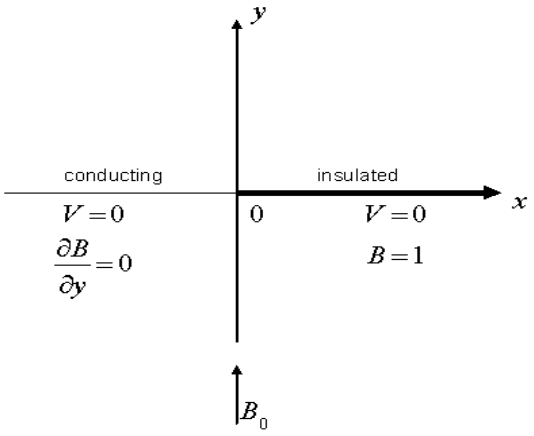

Figure 3.50: Geometry of Problem 1

boundary elements for the calculations with the values of Hartmann number $M = 10$, $M = 300$ and $M = 700$ respectively. It is observed that the higher the Hartmann number is, the more the number of boundary elements is needed. The need of increase in the number of boundary elements results in showing the actions of the velocity and the induced magnetic field clearly near the insulated wall and in the narrow region bounded by the parabola emanating from the origin. However, there is no certain relationship between M and the number of boundary elements in terms of order. The accuracy test is carried by drawing the graphs of $V(xM/M_0,\, yM/M_0)$ and $B(xM/M_0,\, yM/M_0)$ at a fixed point, $(x = .5, y = .5)$, in Figure 3.51 as a function of $dl\, M/M_0$, where M_0 is a fixed Hartmann number value (e.g. $M_0 = 100$) and dl is the length of the boundary elements used in the calculations with M_0. Hartmann number M is ranging between 10 and 250. As can be seen from this figure that as dlM/M_0 decreases the corresponding V and B values are settled down. The same V and B values are drawn in Figure 3.52 as a function of $NdlM/M_0$. This shows the accuracy of the solution with respect to the whole length used on the x-axis in the computations. There is no need to take large interval on the x-axis to see the action.

Figures 3.53-3.54, 3.55-3.56 and 3.59-3.60 show the velocity-induced magnetic field lines for Hartmann numbers M=10, 300 and 700 respectively. In Figures 3.57-3.58 the velocity and induced magnetic field lines are shown in details for

$M = 300$ in a narrow region around the discontinuity point. The condition $\frac{\partial B}{\partial n} = 0$ is clearly satisfied for $x < 0$ (conducting portion). As M increases the boundary layer (Hartmann layer) formation starts taking place near the insulated wall ($x > 0$ and small values of y) for both the velocity field and the induced magnetic field. There is a parabolic boundary layer emanating from the origin for $y > 0$ again for both the velocity and the induced magnetic field. The thickness of the parabolic boundary layer is computed and given at the end of this section. In the figures the parabolas emanating from the discontinuity points are also drawn by dotted lines. Also, one can notice that an increase in M causes a stagnant region for the velocity field in front of the conducting boundary ($y = 0$, $x < 0$). There are hardly any current lines in front of the conducting boundary also as M is increased. The action takes place inside of the parabola in front of the discontinuity point for both the velocity and the induced magnetic field. Since the equal velocity and induced magnetic field lines are drawn on the finite part Γ_x of the x-axis with dimensionless length 2, the lines shown emanating from the end point $x = 1$ indicates that the flow acts just freely when $x \to \infty$. For $x \to -\infty$ both V and B tend to zero.

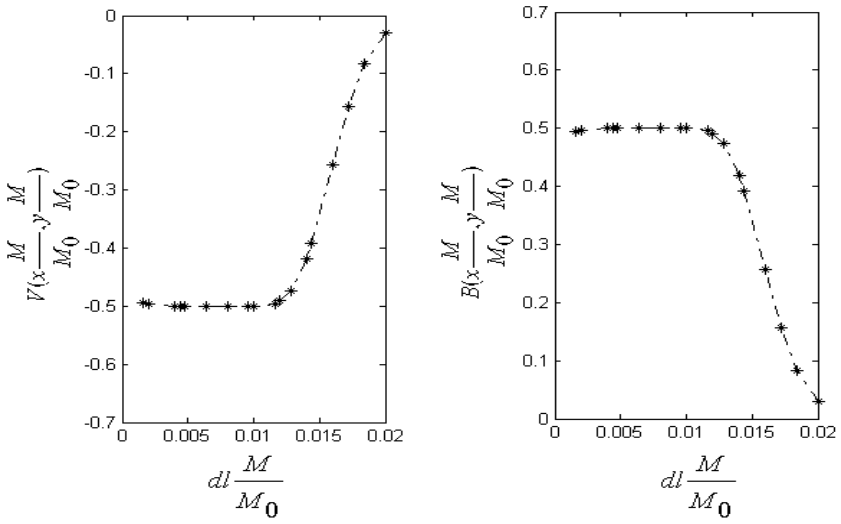

Figure 3.51: Variation of V and B with the length of the boundary elements

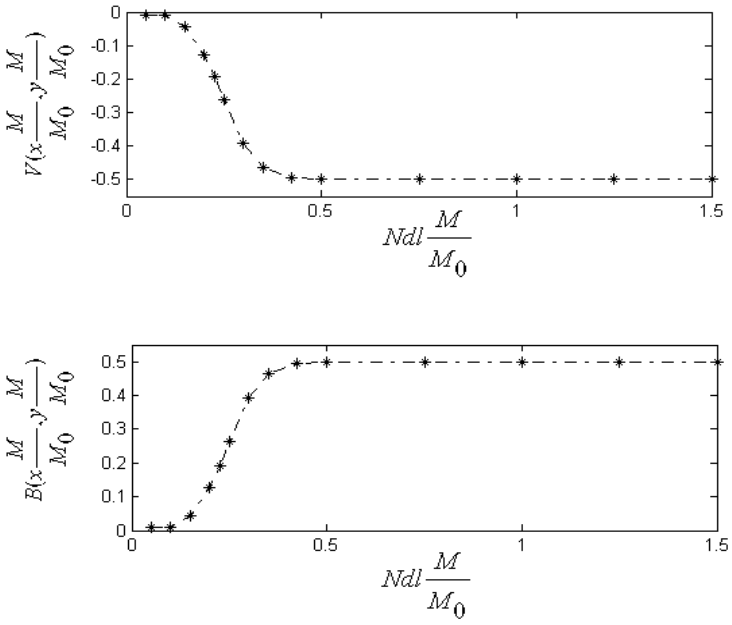

Figure 3.52: Variation of V and B with the length of computational interval on Γ_x

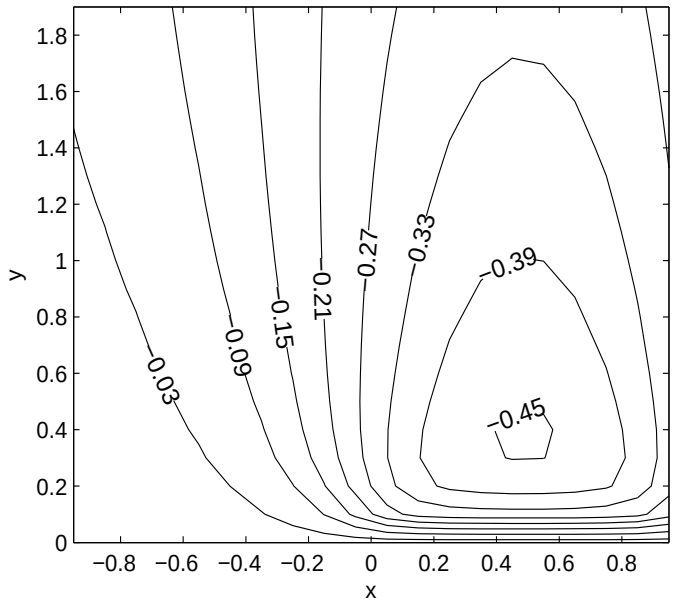

Figure 3.53: Velocity lines for $M = 10$, $N = 20$

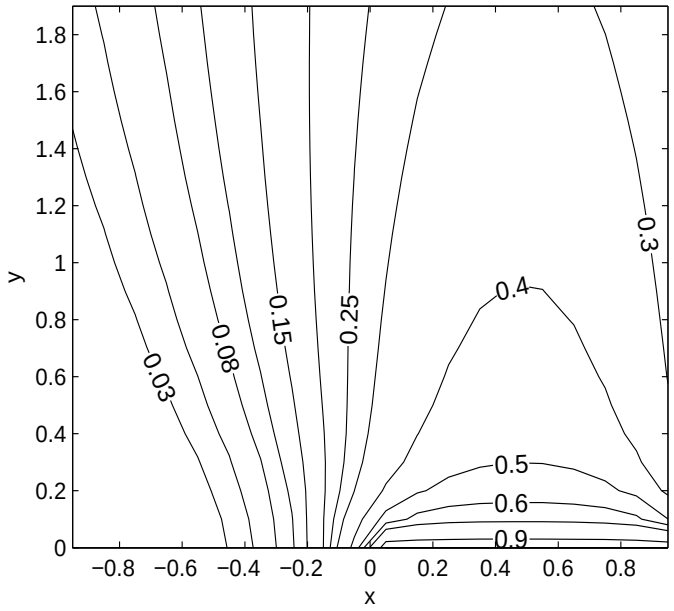

Figure 3.54: Induced magnetic field lines for $M = 10$, $N = 20$

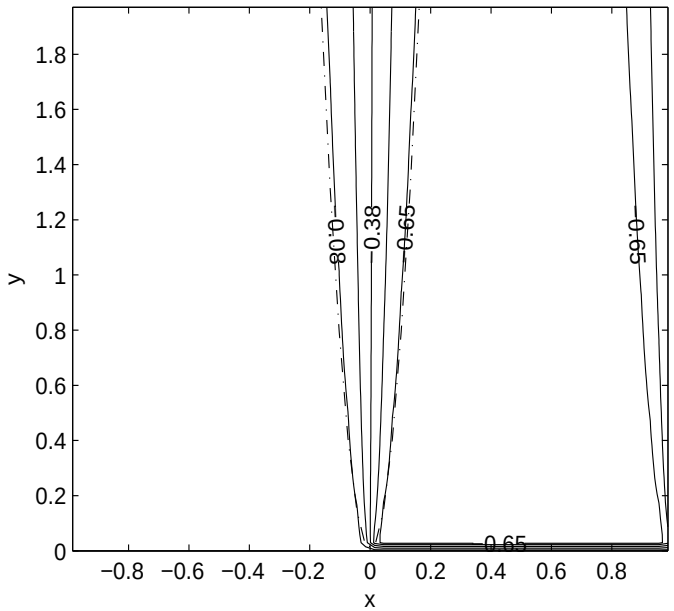

Figure 3.55: Velocity lines for $M = 300$, $N = 68$

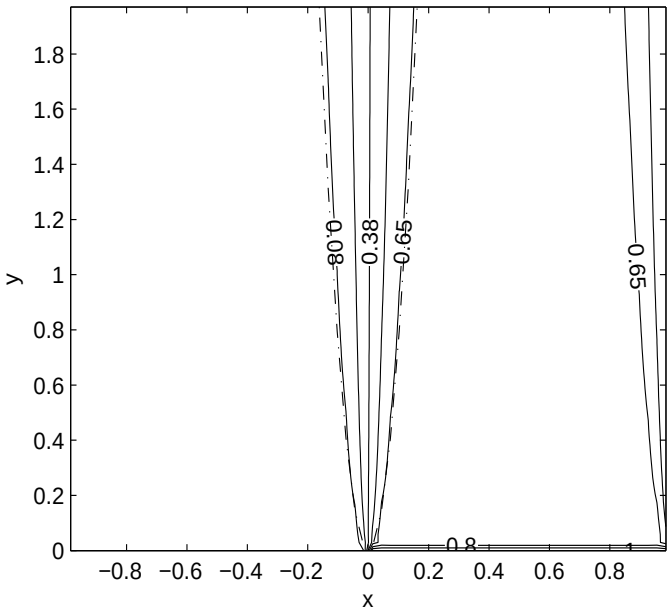

Figure 3.56: Induced magnetic field lines for $M = 300$, $N = 68$

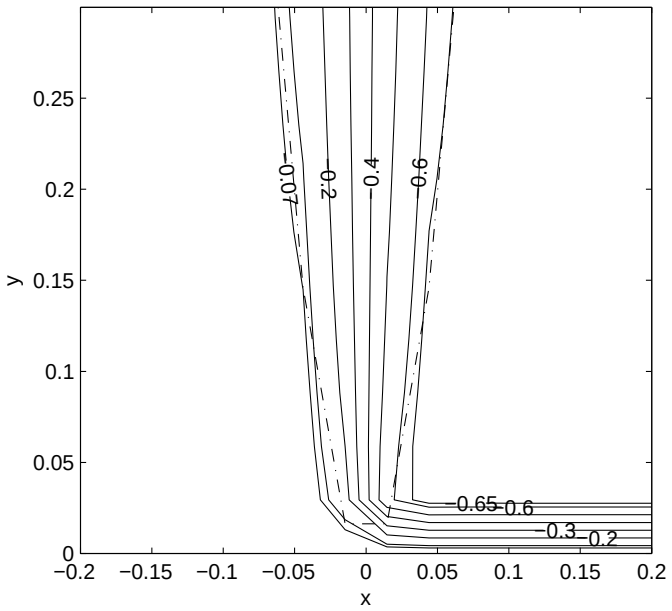

Figure 3.57: Details of Figure 3.55

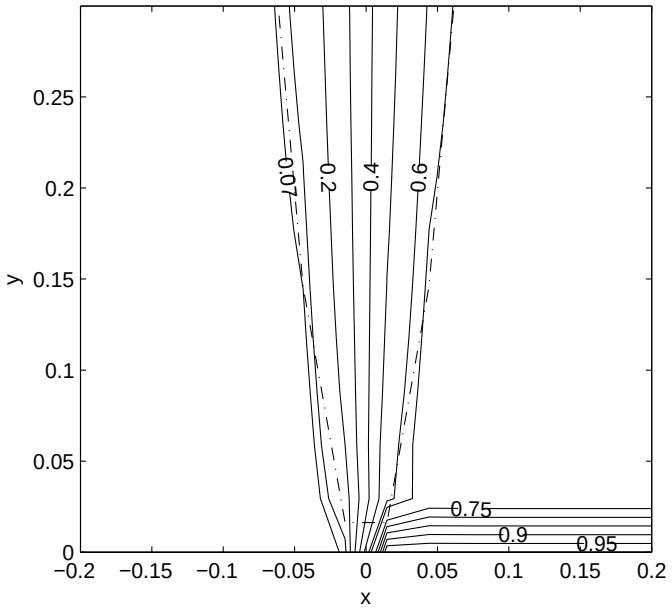

Figure 3.58: Details of Figure 3.56

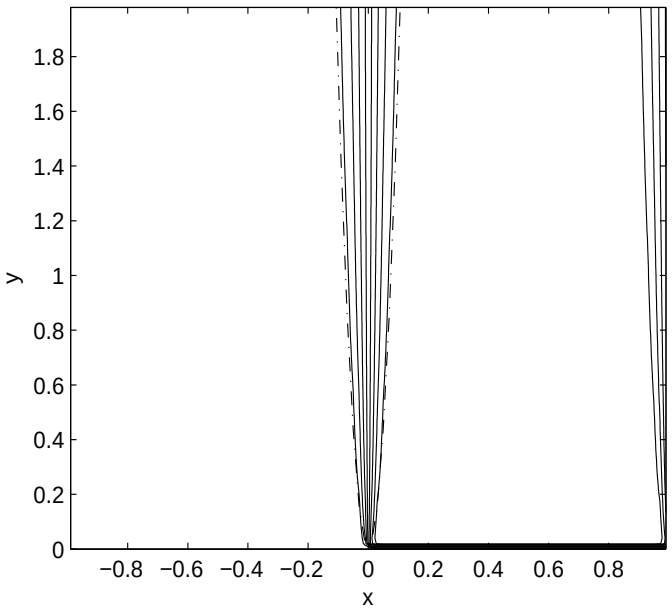

Figure 3.59: Velocity lines for $M = 700$, $N = 100$

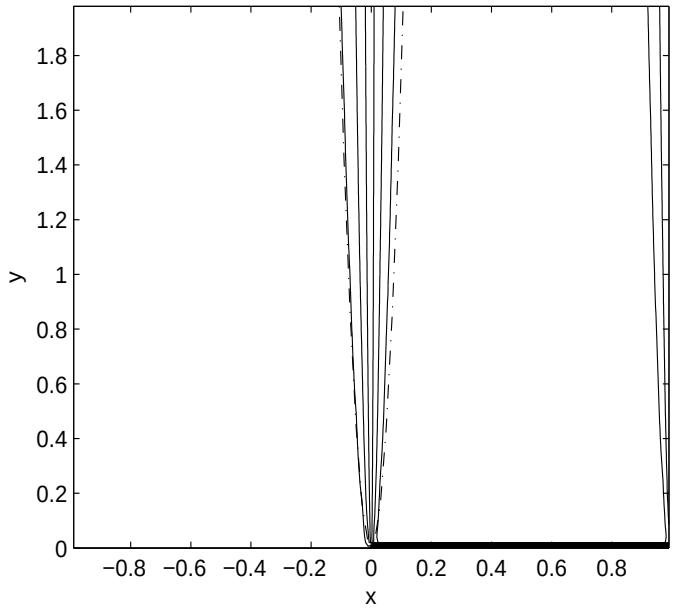

Figure 3.60: Induced magnetic field lines for $M = 700$, $N = 100$

Problem 2

The MHD flow on the upper half of an infinite plate for the case when the flow is driven by the current produced by an electrode of length $2a$, placed in the middle of the plate, therefore conducting, is considered. Imposed electric currents enter the fluid at $x = \pm a$ through external circuits and move up on the plane. The partial differential equations describing the flow are the same as in Problem 1 with the boundary conditions (see Figure 3.61)

$$
\begin{aligned}
&V(x,0)=0 && -\infty<x<\infty\\
&B(x,0)=1 && a<x<\infty\\
&B(x,0)=-1 && -\infty<x<-a\\
&\frac{\partial B}{\partial y}(x,0)=0 && -a<x<a\\
&\left|\frac{\partial V}{\partial n}\right|\to 0,\ \left|\frac{\partial B}{\partial n}\right|\to 0 && \text{as } x\to\pm a,\ y\to\infty\\
&|V|<\infty,\ |B|<\infty && \text{as } x^2+y^2\to\infty\\
&\left|\frac{\partial V}{\partial n}\right|<\infty,\ \left|\frac{\partial B}{\partial n}\right|<\infty && \text{as } x^2+y^2\to\infty\,.
\end{aligned}
$$

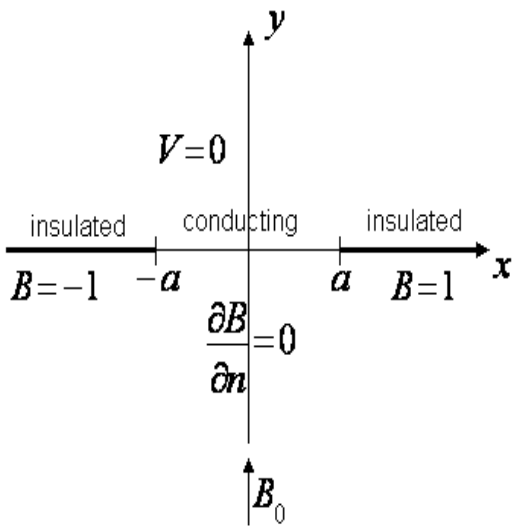

Figure 3.61: Geometry of Problem 2

We present the equal velocity and induced magnetic field lines for $a = 0.1$, 0.3, and for Hartmann numbers 50, 400 and 700 in Figures 3.62-3.65, 3.66-3.69 and 3.70-3.73, respectively again by taking dimensionless finite interval $\Gamma_x = [-1, 1]$. Although we need more boundary elements for large values of Hartmann number there is no relationship between the increase of M and the length of the conducting portion. As M increases boundary layers (Hartmann layers) are

formed near $y = 0$ line for $x > a$ and $x < -a$. It can also be seen from these figures that except for narrow regions near $y = 0$ and $x = \pm a$, the velocity is almost constant and equal to its minimum value. The behaviour of the induced magnetic field lines is similar to that of velocity lines except for $-a < x < a$ and for small values of y, because in this case the magnetic field lines are perpendicular to the x-axis owing to the boundary condition $\partial B/\partial n = 0$. From Figures 3.64 and 3.65 we can see that induced magnetic field lines are antisymmetric with respect to y-axis reaching the values $B = -1$ and $B = 1$ on $-\infty < x < -a$ and $a < x < \infty$ parts, respectively. The velocity is also antisymmetric with respect to y-axis. One can also notice that an increase in the length of the conducting part, a, develops a stagnant region in front of the conducting wall for both of the velocity and the induced magnetic field. There are again parabolic boundary layers (shown by dotted lines in Figures 3.66-3.73) emanating from the discontinuity points $x = \pm a$ for both the velocity and the induced magnetic field.

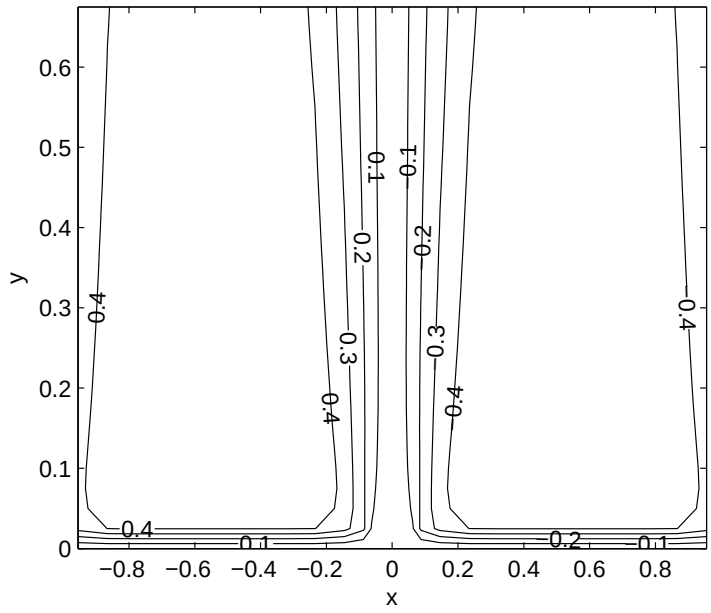

Figure 3.62: Velocity lines for $M = 50$, $N = 28$, $a = 0.1$

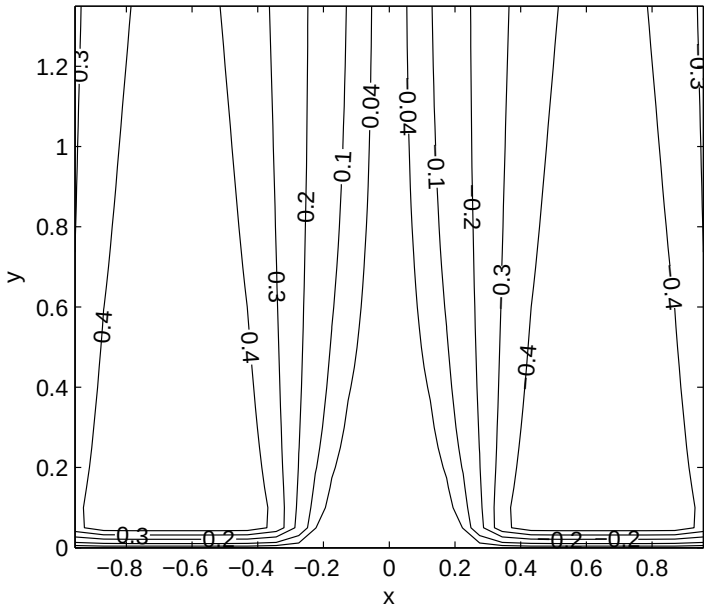

Figure 3.63: Velocity lines for $M = 50$, $N = 28$, $a = 0.3$

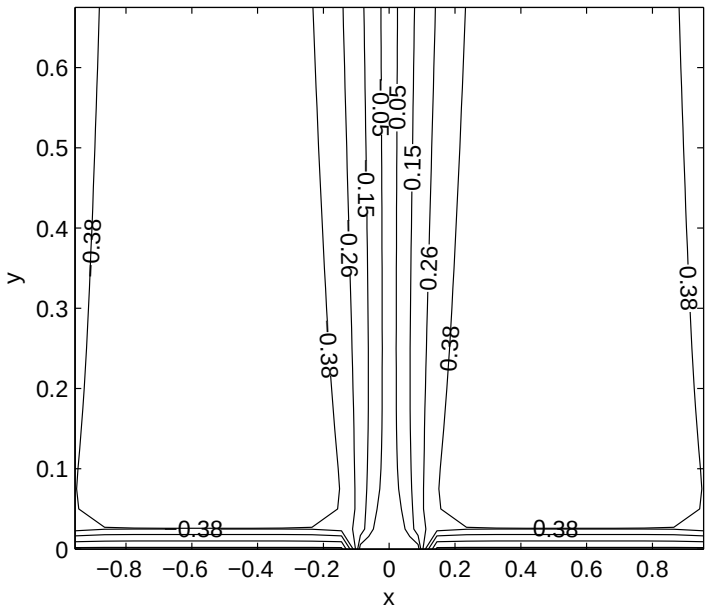

Figure 3.64: Induced magnetic field lines for $M = 50$, $N = 28$, $a = 0.1$

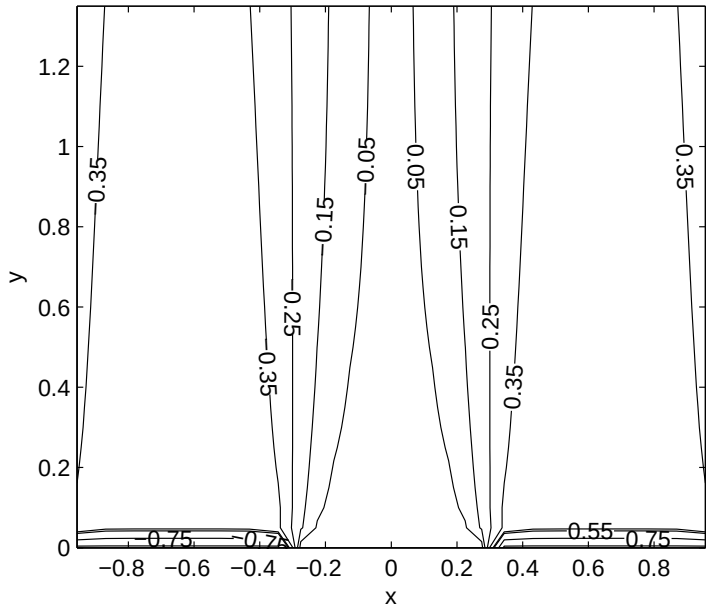

Figure 3.65: Induced magnetic field lines for $M = 50$, $N = 28$, $a = 0.3$

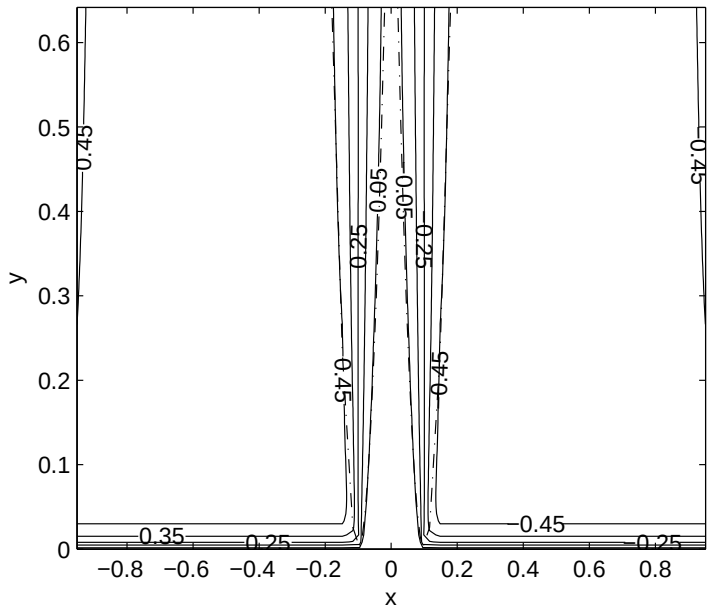

Figure 3.66: Velocity lines for $M = 400$, $N = 80$, $a = 0.1$

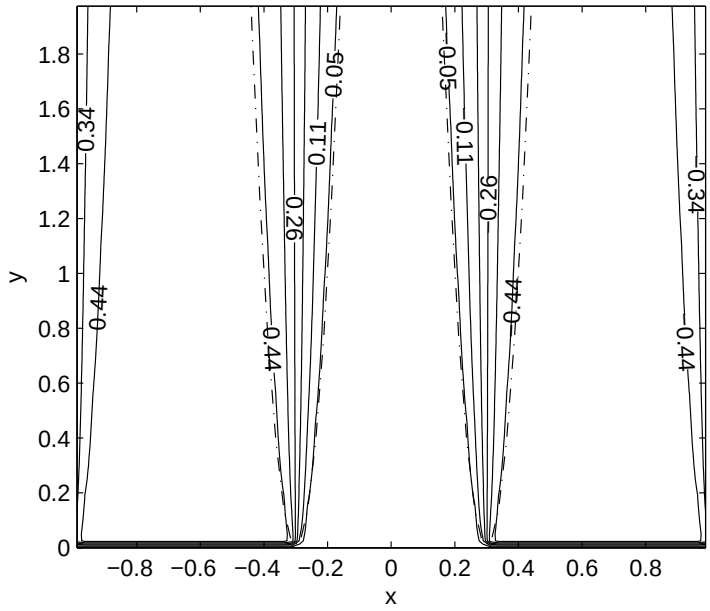

Figure 3.67: Velocity lines for $M = 400$, $N = 80$, $a = 0.3$

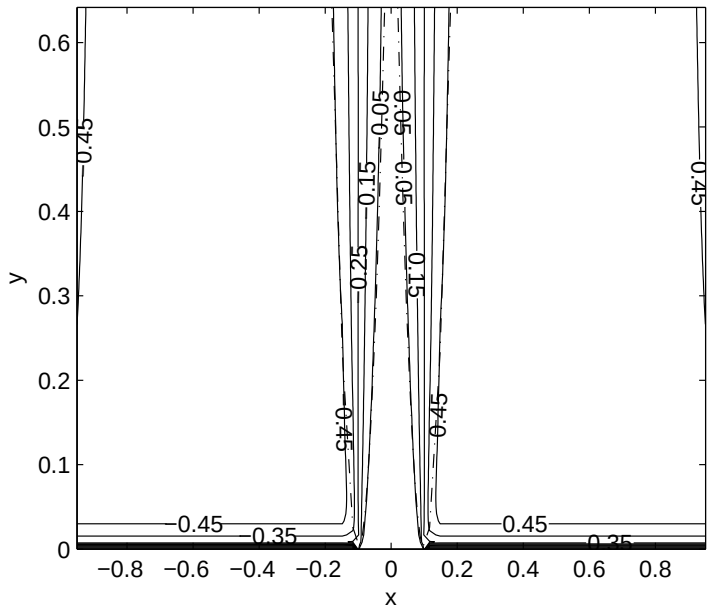

Figure 3.68: Induced magnetic field lines for $M = 400$, $N = 80$, $a = 0.1$

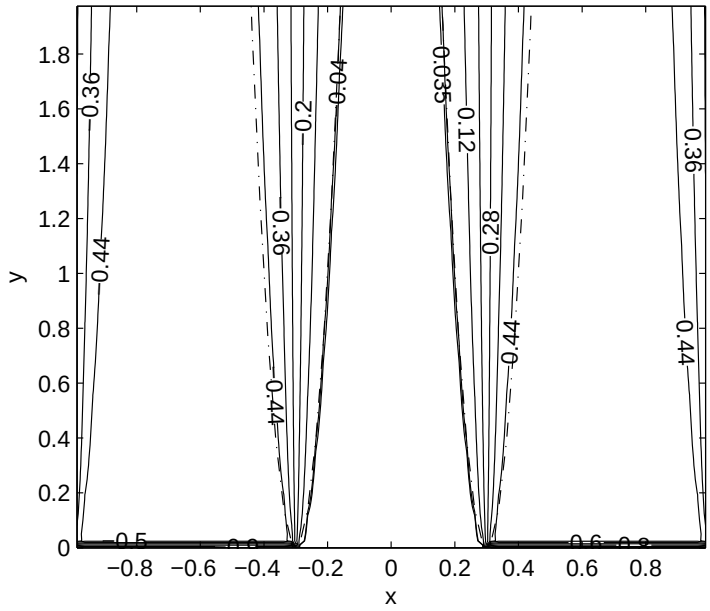

Figure 3.69: Induced magnetic field lines for $M = 400$, $N = 80$, $a = 0.3$

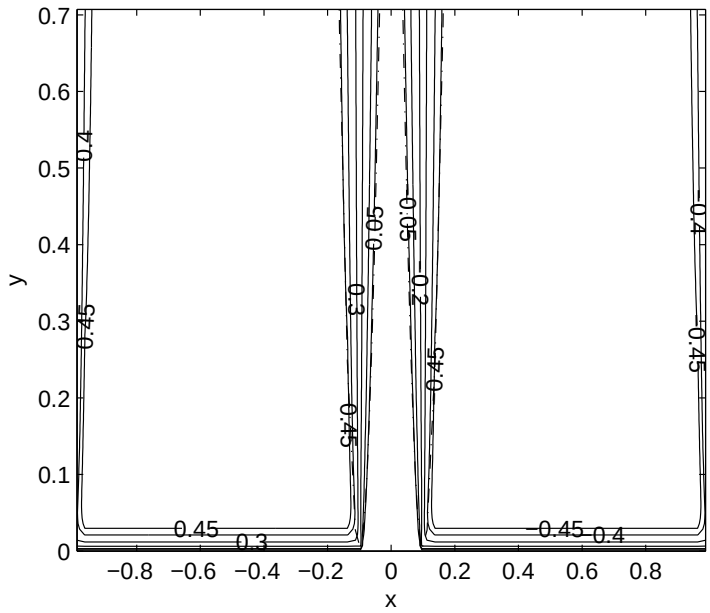

Figure 3.70: Velocity lines for $M = 700$, $N = 100$, $a = 0.1$

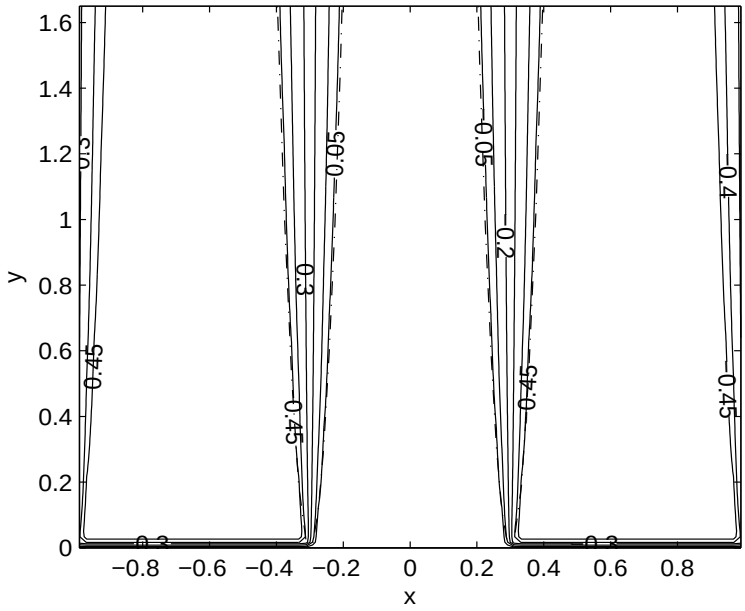

Figure 3.71: Velocity lines for $M = 700$, $N = 100$, $a = 0.3$

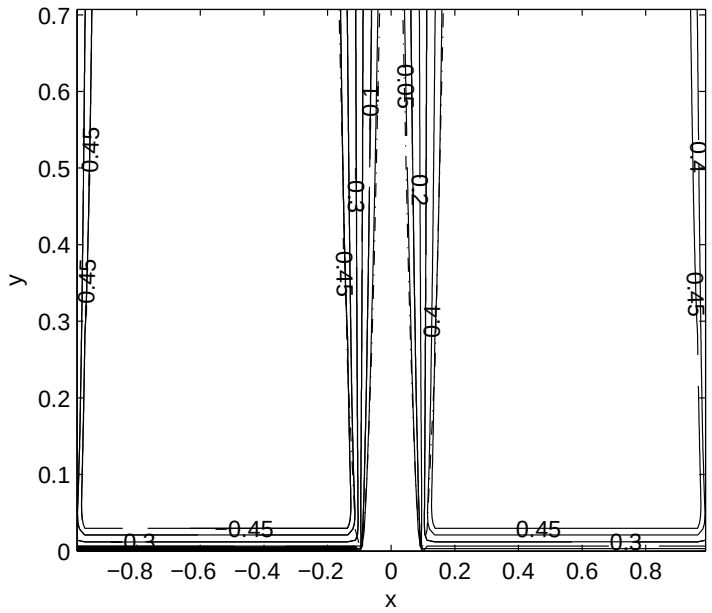

Figure 3.72: Induced magnetic field lines for $M = 700$, $N = 100$, $a = 0.1$

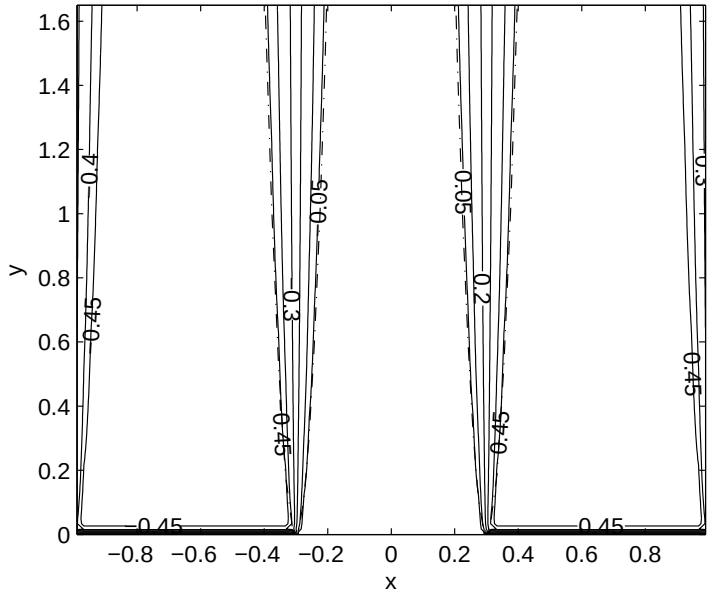

Figure 3.73: Induced magnetic field lines for $M = 700$, $N = 100$, $a = 0.3$

The thickness of the parabolic boundary layer

This part concentrates on the calculation of the thickness of the parabolic boundary layer in the region near the discontinuity points by direct use of the BEM formulations for the velocity and the induced magnetic field.

It is known that there is a boundary layer (Hartmann layer) near the insulated walls which is perpendicular to the applied magnetic field of order $1/M$, [60, 61]. Thus, on the portion of the x-axis where the walls are insulated we have Hartmann layers of order $1/M$ and on the conducting portion the flow is almost stagnant and there are hardly any current lines. This behaviour is depicted in Figure 3.74, which gives the boundary layer thickness versus the Hartmann number M comparing with the function $1/M$.

The integrals can be approximated for large r_y and small $|r_x|$ by using the property of $K_\nu(z) \approx \sqrt{\frac{\pi}{2}}\frac{e^{-z}}{\sqrt{z}}$ for large argument. This case corresponds to the places on the x-axis where the conductivity is changing (discontinuity points) abruptly. Now, the integrals in the entries h_{ij}, g_{ij} and h^1_{ij}, g^1_{ij} contain the products

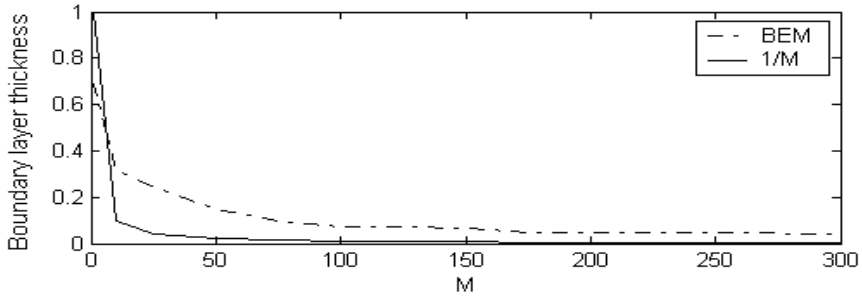

Figure 3.74: Variation of Hartmann boundary layer thickness

of Bessel and hyperbolic fuctions as

$$\begin{aligned} &\int_{\Gamma_j} K_0(\frac{M}{2}\,r)\sinh(\frac{M}{2}\,r_y)d\Gamma_j \quad , \qquad \int_{\Gamma_j} K_0(\frac{M}{2}\,r)\cosh(\frac{M}{2}\,r_y)d\Gamma_j \\ &\int_{\Gamma_j} K_1(\frac{M}{2}\,r)\sinh(\frac{M}{2}\,r_y)\frac{\partial r}{\partial n}d\Gamma_j\,, \qquad \int_{\Gamma_j} K_1(\frac{M}{2}\,r)\cosh(\frac{M}{2}\,r_y)\frac{\partial r}{\partial n}d\Gamma_j \end{aligned} \tag{3.68}$$

and integrations are on the boundary elements Γ_j, thus $d\Gamma_j = dx$.

Each integral in (3.68) can be approximated for $r_y >> r_x$ as

$$\frac{1 \pm e^{-M\,r_y}}{2}\,\frac{\sqrt{\pi}}{\sqrt{M}}\int_{\Gamma_j}\,\frac{e^{\frac{-M}{2}r_y(\sqrt{1+r_x^2/r_y^2}-1)}}{(r_x^2+r_y^2)^{\frac{1}{4}}}\,d\Gamma_x$$

$$= (1 \pm e^{-M\,r_y})\frac{\sqrt{\pi}}{2\sqrt{M}}\int_0^{|x|}\frac{e^{\frac{-M\,r_x^2}{4r_y}}}{\sqrt{r_y}}d\Gamma_x$$

since we consider the boundary layer close to discontinuity points, i.e. in the regions $|x|$ for small r_x. With the change of variable $u = \sqrt{M}r_x/2\sqrt{r_y}$, it can still be transformed to

$$\frac{\pi}{2M}\,(1 \pm e^{-M\,r_y})\,\mathrm{erf}(\frac{\sqrt{M}\,r_x}{2\,\sqrt{r_y}})$$

and with the help of the property of error function $\mathrm{erf}(x)$ for $0 \le x < \infty$ (rational

approximation) it can be written in the form

$$\frac{\pi}{2M}\left(1 \pm e^{-M\,r_y}\right)\left[1 - \frac{a_1}{1+px}\,e^{-\dfrac{M\,r_x^2}{4r_y}} + \cdots\right]$$

$$= \frac{\pi}{2M}\left(1 \pm e^{-M\,r_y}\right)\left[1 - a_1\left(1 - p\frac{\sqrt{M}|r_x|}{2\sqrt{r_y}}\cdots\right)e^{-\dfrac{M\,r_x^2}{4r_y}} + \cdots\right]$$

where a_1 and p are positive constants.

Since r_x and r_y behave like x and y respectively, the thickness of the boundary layer which emanates from the points of discontinuities of boundary conditions on the x-axis and lies on the upper half of the plane $y > 0$, is obtained as $|x| = 2\,\dfrac{\sqrt{y}}{\sqrt{M}}$.

This result is also in accordance with the thickness of the secondary layer on the boundary parallel to the applied magnetic field mentioned by Hunt [60] which is of order $1/\sqrt{M}$. It shows that these type of secondary layers also appear from the points of discontinuity in boundary conditions. The graphs of $|x| = 2\,\dfrac{\sqrt{y}}{\sqrt{M}}$ are superimposed on the velocity and magnetic field lines in the figures. Figure 3.75 also shows the variation of the thickness of the secondary layer (parabolic boundary layer) versus M comparing with the function $1/\sqrt{M}$.

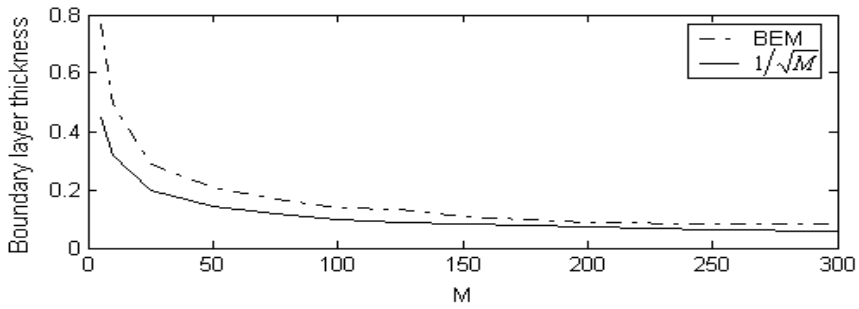

Figure 3.75: Variation of secondary layer thickness

CHAPTER 4

APPLICATION OF DUAL RECIPROCITY BOUNDARY ELEMENT METHOD WITH DIFFERENTIAL QUADRATURE TIME INTEGRATION SCHEME TO THE TRANSIENT CONVECTION-DIFFUSION TYPE EQUATIONS

The numerical solution of transient convection-diffusion type equations is a challenging task because of the occurrence of these equations in many branches of science and engineering. In solving the time dependent problems, classical methods discretize the spatial domain of the problems with one of the known methods such as finite difference, finite element and boundary element methods. Then various time integration schemes, mostly iterative in nature, are applied to the resulting initial value problem represented as a system of ordinary differential equations of the first order for the time domain.

In this chapter, a numerical scheme which is the coupling of the dual reciprocity BEM and the differential quadrature method is introduced for the solution of the two-dimensional transient convection-diffusion type and elastodynamic equations. The theory of the DRBEM is given in Section 4.1. The application of the DRBEM for the Poisson equation with a known right hand side function of position is explained in details through Section 4.1.1. Then, in Section 4.1.2 the method is extended to the Poisson type equation with the right hand side func-

tion involving the unknown itself and its partial derivatives with respect to space and time variables. In the solution procedure, the dual reciprocity BEM is employed to discretize the spatial partial derivatives in the convection-diffusion type equations. The equation is treated as Poisson's type equation keeping the time derivative, the first order space derivatives and the unknown itself as nonhomogeneous terms. BEM idea is applied to the Laplace operator by using fundamental solution of Laplace equation since the equation is diffusion type when all the other terms are considered as the nonhomogeneity. Thus, the resulting matrices contain integrals of logarithmic function or its normal derivative which can be computed quite easily and accurately. The right hand side is approximated using linear and quadratic radial basis functions. DRBEM application to convection-diffusion type equations gives rise to an initial value problem represented by a system of first order ordinary differential equations in time. This system is then solved by the differential quadrature method, the application of which is established in Section 4.2. When the DQM discretizes the system of ordinary differential equations in time direction, we finally obtain a large system of linear equations for the unknown nodal values containing both discretized space and time points. After the imposition of both the initial and the boundary conditions to the final linear system of equations, we end up with a rectangular system, which can be transformed into a square system with the application of least square method. The final system gives the solution vector at any required time level since it contains spatial nodal solution at all time levels between the initial and the required time level. This way, the resulting linear system of equations can be solved by any direct (Gaussian type) or iterative (Gauss-Seidel, SOR) solver without any special treatment like the use of Bartels-Stewart algorithm in the solution of Lyapunov matrix equations, [44]. Also, our solution procedure can be used with large time increments directly in the system of linear equations and does not need an iterative algorithm in the time direction. The other time integration schemes mostly need very small time increments for stability and convergence and thus they are computationally expensive. The applications of the proposed coupled method are considered in Section 4.3 by solving several test problems, such as the transient variable coefficient convection-diffusion equation, the unsteady magnetohydro-

dynamic flow and the elastodynamic problems. In elastodynamic problems the second order time derivative of the solution is involved. Then, this procedure is revised accordingly to have the resulting system of initial value problems of the second order in time.

4.1 Dual Reciprocity Boundary Element Method

The boundary element method always requires a fundamental solution to the original differential equation in order to avoid domain integrals in the formulation of the boundary integral equation, which is one of the drawbacks of the method. Another is that nonhomogeneous and nonlinear terms are incorporated in the formulation by means of domain integrals. The use of cells to evaluate these domain integrals implies an internal discretization which considerably increases the quantity of data necessary to run a problem. Thus, the method loses the attraction of its boundary-only character in relation to the other domain decomposition methods.

One of the several techniques to deal with the domain integrals is the dual reciprocity method (DRM), which is the subject of the present chapter. It is essentially a generalized way of constructing particular solutions that can be used to solve nonlinear and time-dependent problems.

The basic idea behind the dual reciprocity BEM is to employ a fundamental solution corresponding to a simpler equation and to treat the remaining terms, as well as other nonhomogeneous terms in the original equation, through a procedure which involves a series expansion using global approximating functions and the application of reciprocity principles.

In this section, the dual reciprocity method is developed for the Poisson equation in which the nonhomogeneous term is a known function of space. Further, the method is extended to time-dependent cases in which the right hand side of the governing equation is an unknown function of the problem variable as well as a function of space and time.

4.1.1 DRBEM for Poisson equation

The dual reciprocity method is explained for the Poisson equation following the reference [31]

$$\nabla^2 u = b \tag{4.1}$$

where $b = b(x, y)$ is considered to be a known function of position.

The solution to equation (4.1) can be expressed as the sum of the solution of a homogeneous Laplace equation and a particular solution $\hat{u}$ such that

$$\nabla^2 \hat{u} = b \,. \tag{4.2}$$

It is generally difficult to find a particular solution $\hat{u}$, particularly in the case of nonlinear or time-dependent problems. The dual reciprocity method proposes the use of a series of particular solutions $\hat{u}_j$ instead of a single function $\hat{u}$. The number of $\hat{u}_j$ used is equal to the total number of nodes in the problem.

The following approximation for b is then proposed

$$b \approx \sum_{j=1}^{N+L} \alpha_j f_j \tag{4.3}$$

where the α_j are a set of initially unknown coefficients and the f_j are the approximating or interpolating fuctions. The values N and L are the numbers of boundary and internal nodes, respectively. The particular solutions $\hat{u}_j$, and the approximating functions f_j, are linked through the relation

$$\nabla^2 \hat{u}_j = f_j \,. \tag{4.4}$$

The fuctions f_j are only geometry-dependent and there is no restriction on these fuctions. In fact, many different types may be used, each of which results in a different fuction $\hat{u}_j$ as determined from equation (4.4).

Substituting equation (4.4) into equation (4.3) gives

$$b = \sum_{j=1}^{N+L} \alpha_j (\nabla^2 \hat{u}_j) \tag{4.5}$$

which can be substituted into the original equation (4.1) to give the following expression

$$\nabla^2 u = \sum_{j=1}^{N+L} \alpha_j (\nabla^2 \hat{u}_j) \, . \tag{4.6}$$

The procedure explained in Chapter 2 for developing the boundary element method for the Laplace equation can now be applied, [31]. Equation (4.6) is multiplied by the fundamental solution u^* of the Laplace equation and is integrated over the domain Ω, producing

$$\int_\Omega (\nabla^2 u) u^* d\Omega = \sum_{j=1}^{N+L} \alpha_j \int_\Omega (\nabla^2 \hat{u}_j) u^* d\Omega \, . \tag{4.7}$$

Applying Divergence theorem two times in equation (4.7), as in Section 2.2, leads to the following integral equation for each source node i,

$$c_i u_i + \int_\Gamma q^* u d\Gamma - \int_\Gamma u^* q d\Gamma = \sum_{j=1}^{N+L} \alpha_j \left(c_i \hat{u}_{ij} + \int_\Gamma q^* \hat{u}_j d\Gamma - \int_\Gamma u^* \hat{q}_j d\Gamma \right) \tag{4.8}$$

where n is the unit outward normal to the boundary Γ. The term $\hat{q}_j$ is defined as $\hat{q}_j = \partial \hat{u}_j / \partial n$ and can be expanded to

$$\hat{q}_j = \frac{\partial \hat{u}_j}{\partial x} \frac{\partial x}{\partial n} + \frac{\partial \hat{u}_j}{\partial y} \frac{\partial y}{\partial n} \, . \tag{4.9}$$

Note that equation (4.8) involves no domain integrals. The domain integral of the source term b has been substituted by equivalent boundary integrals.

The discretized form of equation (4.8), with summations over the constant

boundary elements replacing the integrals, gives for a source point i the expression

$$\begin{aligned} c_i u_i + \sum_{k=1}^{N} \int_{\Gamma_k} q^* u d\Gamma - \sum_{k=1}^{N} \int_{\Gamma_k} u^* q d\Gamma \\ = \sum_{j=1}^{N+L} \alpha_j \left(c_i \hat{u}_{ij} + \sum_{k=1}^{N} \int_{\Gamma_k} q^* \hat{u}_j d\Gamma - \sum_{k=1}^{N} \int_{\Gamma_k} u^* \hat{q}_j d\Gamma \right) . \end{aligned} \tag{4.10}$$

The functions $\hat{u}_j$ and $\hat{q}_j$ are known once f_j are defined. By introducing the interpolation functions and integrating over each boundary element Γ_k with the substitution of fundamental solution u^* and its normal derivative q^*, equation (4.10) can be written in terms of nodal values as

$$c_i u_i + \sum_{k=1}^{N} H_{ik} u_k - \sum_{k=1}^{N} G_{ik} q_k = \sum_{j=1}^{N+L} \alpha_j \left(c_i \hat{u}_{ij} + \sum_{k=1}^{N} H_{ik} \hat{u}_{kj} - \sum_{k=1}^{N} G_{ik} \hat{q}_{kj} \right) \tag{4.11}$$

where index k is used for the boundary nodes which are the field points. After the application to all boundary nodes using a collocation technique, equation (4.11) can be expressed in matrix form as

$$\mathbf{Hu} - \mathbf{Gq} = \sum_{j=1}^{N+L} \alpha_j (\mathbf{H}\hat{\mathbf{u}}_\mathbf{j} - \mathbf{G}\hat{\mathbf{q}}_\mathbf{j}) \tag{4.12}$$

in which the matrices $\mathbf{H}$ and $\mathbf{G}$ are the same as obtained in Section 2.2.

If each of the vectors $\hat{\mathbf{u}}_\mathbf{j}$ and $\hat{\mathbf{q}}_\mathbf{j}$ is considered to be one column of the matrices $\hat{\mathbf{U}}$ and $\hat{\mathbf{Q}}$ respectively, then equation (4.12) may be written without the summation in the final form as

$$\mathbf{Hu} - \mathbf{Gq} = (\mathbf{H}\hat{\mathbf{U}} - \mathbf{G}\hat{\mathbf{Q}})\boldsymbol{\alpha} \tag{4.13}$$

where $\boldsymbol{\alpha}$ is the vector containing the unknown coefficients α_j.

Equation (4.13) is the basis of the application of the dual reciprocity boundary element method and involves discretization of the boundary only. The definition of interior nodes is not normally necessary to obtain a boundary solution, however,

the solution will be more accurate if a number of such nodes is used. One can calculate the values of u at the internal nodes, by redefining the matrices $\mathbf{H}$ and $\mathbf{G}$ in equation (4.11) in such a way that they contain the point i as an interior node.

The right hand side function b in equation (4.1) is approximated by using the interpolation fuctions f_j as in equation (4.3). By taking the value of b at $(N+L)$ different points, a set of equations is obtained and it may be expressed in matrix form as

$$\mathbf{b} = \mathbf{F}\boldsymbol{\alpha} \tag{4.14}$$

where each column of $\mathbf{F}$ consists of a vector $\mathbf{f_j}$ containing the values of the function f_j at the $(N+L)$ nodes. Thus $\boldsymbol{\alpha}$ is obtained by inverting equation (4.14), that is

$$\boldsymbol{\alpha} = \mathbf{F^{-1}b} \tag{4.15}$$

and when it is substituted back into equation (4.13) we get the system

$$\mathbf{Hu - Gq} = (\mathbf{H\hat{U} - G\hat{Q}})\mathbf{F^{-1}b}\,. \tag{4.16}$$

When this system is arranged after the application of the boundary conditions as given in Section 2.2, we get

$$\mathbf{A}'\mathbf{x} = \mathbf{y} \tag{4.17}$$

where the vector $\mathbf{x}$ contains the N unknown boundary values of u or q.

If the approximating functions f_j are distance or radial basis functions of the form

$$f = 1 + r + r^2 + \ldots + r^m \tag{4.18}$$

where $r^2 = r_x^2 + r_y^2$, in the two-dimensional case, then it can be shown that the corresponding $\hat{u}$ and $\hat{q}$ functions are (from equation (4.4))

$$\hat{u} = \frac{r^2}{4} + \frac{r^3}{9} + \ldots + \frac{r^{m+2}}{(m+2)^2} \tag{4.19}$$

and

$$\hat{q} = \left(r_x \frac{\partial x}{\partial n} + r_y \frac{\partial y}{\partial n} \right) \left(\frac{1}{2} + \frac{r}{3} + \ldots + \frac{r^m}{(m+2)} \right) . \tag{4.20}$$

In principle, any combination of terms may be selected from equation (4.18). In all cases, however, results are found to differ little from those obtained using $f = 1 + r$ which is the simplest alternative.

4.1.2 DRBEM for the equation $\nabla^2 = b(x, y, t, u, u_x, u_y, u_t)$

In the previous section the dual reciprocity BEM is developed for the Poisson type equation in which the right hand side is a known function of the position. In this section, the range of application of the DRBEM is extended to problems governed by the equations [31]

$$\nabla^2 u = b(x, y, t, u, u_x, u_y, u_t) \tag{4.21}$$

where the nonhomogeneous term b now contains the unknown u itself, the convective terms u_x and u_y and the time derivative term u_t. Then, the fuction b can be written as (assuming b is a linear function of u, u_x, u_y and u_t)

$$b = u_t + b_1(x, y) + b_2(x, y)u + b_3(x, y)u_x + b_4(x, y)u_y . \tag{4.22}$$

In this case, the function b is approximated by means of a set of coordinate functions f_j as

$$b = u_t + b_1 + b_2 u + b_3 u_x + b_4 u_y \approx \sum_{j=1}^{N+L} \alpha_j(t) f_j(x, y) \tag{4.23}$$

in which α_j are unknown functions of time. The approximating functions f_j are known functions of geometry and are linked with the particular solutions $\hat{u}_j$ through equation (4.4).

The application of the dual peciprocity method follows the same pattern as

in Section 4.1.1, and produces a matrix equation of the form

$$\mathbf{Hu} - \mathbf{Gq} = (\mathbf{H}\hat{\mathbf{U}} - \mathbf{G}\hat{\mathbf{Q}})\boldsymbol{\alpha} \tag{4.24}$$

where the vector $\boldsymbol{\alpha}$ is obtained from equation (4.23) as

$$\boldsymbol{\alpha} = \mathbf{F}^{-1}(\mathbf{u}_t + \mathbf{b_1} + \mathbf{B_2 u} + \mathbf{B_3 u}_x + \mathbf{B_4 u}_y) \tag{4.25}$$

where $\mathbf{F}$ is the same $(N + L) \times (N + L)$ position matrix, defined in equation (4.14), consisting of the values of f_j at the $(N + L)$ nodal points and $\mathbf{b_1}$ is the vector with components $b_1(x_i, y_i)$ at the nodes $i = 1, \ldots, (N + L)$. The matrices $\mathbf{B_2}$, $\mathbf{B_3}$ and $\mathbf{B_4}$ refer to the diagonal matrices with $b_2(x_i, y_i)$, $b_3(x_i, y_i)$ and $b_4(x_i, y_i)$, $(i = 1, \ldots, (N + L))$, on the diagonals respectively, and of the size $(N + L) \times (N + L)$.

Since the function b contains the values of u and its partial derivatives at the boundary and internal nodes, the vector $\boldsymbol{\alpha}$ can not be calculated explicitly. Therefore during the solution procedure we have to carry it (at least some part) as unknown.

For the solution of the boundary values we have

$$\mathbf{H}^{bs}\mathbf{u} - \mathbf{G}^{bs}\mathbf{q} = (\mathbf{H}^{bs}\hat{\mathbf{U}}^{bs} - \mathbf{G}^{bs}\hat{\mathbf{Q}}^{bs})\boldsymbol{\alpha} \tag{4.26}$$

and for the internal nodes

$$\mathbf{H}^{is}\mathbf{u} - \mathbf{G}^{is}\mathbf{q} = (\mathbf{I}\hat{\mathbf{U}}^{is} + \mathbf{H}^{is}\hat{\mathbf{U}}^{is} - \mathbf{G}^{is}\hat{\mathbf{Q}}^{is})\boldsymbol{\alpha} \tag{4.27}$$

where bs and is refer to boundary and internal solutions, respectively. By the combination of equations (4.26) and (4.27) together at one step, one can get the

following system of equations

$$\begin{bmatrix} \mathbf{H}^{bs} & \mathbf{0} \\ \mathbf{H}^{is} & \mathbf{I} \end{bmatrix} \begin{Bmatrix} \mathbf{u}^{bs} \\ \mathbf{u}^{is} \end{Bmatrix} - \begin{bmatrix} \mathbf{G}^{bs} & \mathbf{0} \\ \mathbf{G}^{is} & \mathbf{0} \end{bmatrix} \begin{Bmatrix} \mathbf{q}^{bs} \\ \mathbf{0} \end{Bmatrix} = \left(\begin{bmatrix} \mathbf{H}^{bs} & \mathbf{0} \\ \mathbf{H}^{is} & \mathbf{I} \end{bmatrix} \begin{Bmatrix} \hat{\mathbf{U}}^{bs} \\ \hat{\mathbf{U}}^{is} \end{Bmatrix} - \begin{bmatrix} \mathbf{G}^{bs} & \mathbf{0} \\ \mathbf{G}^{is} & \mathbf{0} \end{bmatrix} \begin{Bmatrix} \hat{\mathbf{Q}}^{bs} \\ \mathbf{0} \end{Bmatrix} \right) \boldsymbol{\alpha} \tag{4.28}$$

which can be represented in short

$$\mathbf{Hu} - \mathbf{Gq} = (\mathbf{H}\hat{\mathbf{U}} - \mathbf{G}\hat{\mathbf{Q}})\boldsymbol{\alpha} \tag{4.29}$$

in which all the matrices now are of size $(N+L)\times(N+L)$. Thus, it is necessary to use the $(N+L)$ DRBEM collocation points in order to obtain the solution at both boundary and interior nodes.

When the solution u is also approximated by using the same coordinate functions $f_j(x,y)$

$$u \approx \sum_{j=1}^{N+L} \beta_j(t) f_j(x,y) \tag{4.30}$$

where $\beta_j \neq \alpha_j$ are unknown coefficients depending on time, equation (4.30) can also be written in matrix form

$$\mathbf{u} = \mathbf{F}\boldsymbol{\beta}\,. \tag{4.31}$$

Differentiation of equation (4.31) with respect x produces

$$\frac{\partial \mathbf{u}}{\partial x} = \frac{\partial \mathbf{F}}{\partial x}\boldsymbol{\beta} \tag{4.32}$$

and by rewriting equation (4.31) as $\boldsymbol{\beta} = \mathbf{F^{-1}u}$, then (4.32) becomes

$$\frac{\partial \mathbf{u}}{\partial x} = \frac{\partial \mathbf{F}}{\partial x}\mathbf{F^{-1}u}\,. \tag{4.33}$$

Similarly,

$$\frac{\partial \mathbf{u}}{\partial y} = \frac{\partial \mathbf{F}}{\partial y}\mathbf{F^{-1}u}\,. \tag{4.34}$$

With the above approximation of convective terms, equation (4.25) can be rewritten as

$$\boldsymbol{\alpha} = \mathbf{F^{-1}}(\frac{\partial \mathbf{u}}{\partial t} + \mathbf{b_1} + \mathbf{B_2 u} + \mathbf{B_3}\frac{\partial \mathbf{F}}{\partial x}\mathbf{F^{-1}u} + \mathbf{B_4}\frac{\partial \mathbf{F}}{\partial y}\mathbf{F^{-1}u})\,. \tag{4.35}$$

Substituting the vector $\boldsymbol{\alpha}$ back into equation (4.29), one can obtain

$$\mathbf{Hu - Gq} = (\mathbf{H\hat{U} - G\hat{Q}})\mathbf{F^{-1}}(\frac{\partial \mathbf{u}}{\partial t} + \mathbf{b_1} + \mathbf{B_2 u} + \mathbf{B_3}\frac{\partial \mathbf{F}}{\partial x}\mathbf{F^{-1}u} + \mathbf{B_4}\frac{\partial \mathbf{F}}{\partial y}\mathbf{F^{-1}u}) \tag{4.36}$$

and, finally rearranging, the following system of ordinary differential equations is reached

$$\mathbf{C\dot{u}} + (\mathbf{H} + \mathbf{S})\mathbf{u} = \mathbf{Gq} - \mathbf{Cb_1} \tag{4.37}$$

where superscript dot denotes the time derivative. The matrices $\mathbf{C}$ and $\mathbf{S}$ are of size $(N + L) \times (N + L)$ and are given by

$$\begin{aligned} \mathbf{C} &= -(\mathbf{H\hat{U} - G\hat{Q}})\mathbf{F^{-1}} \\ \mathbf{S} &= \mathbf{C}(\mathbf{B_2} + \mathbf{B_3}\frac{\partial \mathbf{F}}{\partial x}\mathbf{F^{-1}} + \mathbf{B_4}\frac{\partial \mathbf{F}}{\partial y}\mathbf{F^{-1}})\,. \end{aligned} \tag{4.38}$$

Now, from equation (4.38) the standard form of the first-order initial value problem is obtained

$$\mathbf{\dot{u}} + \mathbf{Bu} = \mathbf{Dq} - \mathbf{b_1} \tag{4.39}$$

in which $\mathbf{B} = \mathbf{C^{-1}}(\mathbf{H} + \mathbf{S})$ and $\mathbf{D} = \mathbf{C^{-1}G}$. System (4.39) can now be solved by using any time integration scheme.

In elastodynamic problems, the right hand side function b in (4.21) contains u_{tt}, the second order time derivative of the unknown. Thus, the second order time derivative of the unknown vector u also appears in the final system of initial value problem (4.39). Then, this system of second order ordinary differential equations in time will be solved by a proper time integration scheme.

4.2 Differential Quadrature Method

In this section, the DQM is applied to the system of initial value problem (4.39) in order to approximate the first order time derivative of the unknown function. A similar procedure can be carried out for the second order time derivative in elastodynamic problems.

4.2.1 The weighting coefficients in one-dimensional polynomial differential quadrature

The differential quadrature method approximates the derivative of a smooth function with respect to a variable at a grid point by a linear weighted summation of all the functional values in the whole computational domain, [47].

When a function $f(t)$ is approximated at a grid point t_i, $f(t)$ and its first and second order derivatives can be written as

$$f(t_i) = \sum_{j=1}^{K} a_{ij} f(t_j), \qquad i = 1, 2, \ldots, K \tag{4.40}$$

$$\left.\frac{df(t)}{dt}\right|_{t_i} = \sum_{j=1}^{K} a_{ij}^{(1)} f\left(t_j\right), \quad i = 1, 2, \ldots, K \tag{4.41}$$

$$\left.\frac{d^2 f(t)}{d^2 t}\right|_{t_i} = \sum_{j=1}^{K} a_{ij}^{(2)} f\left(t_j\right), \quad i = 1, 2, \ldots, K \tag{4.42}$$

where K is the number of grid points t_i in the variable domain and $a_{ij}^{(1)}$ and $a_{ij}^{(2)}$ are the weighting coefficients for the first and second order derivative approximations of $f(t)$, respectively, to be determined by the polynomial based differential quadrature method. The weighting coefficient are given as, [62]

$$a_{ij}^{(1)} = \frac{M^{(1)}(t_i)}{(t_i - t_j) M^{(1)}(t_j)}, \quad i \neq j \tag{4.43}$$

$$a_{ii}^{(1)} = \frac{M^{(2)}(t_i)}{2M^{(1)}(t_i)} \tag{4.44}$$

$$a_{ij}^{(2)} = 2a_{ij}^{(1)}(a_{ii}^{(1)} - \frac{1}{t_i - t_j}), \quad i \neq j \tag{4.45}$$

$$a_{ii}^{(2)} = \frac{M^{(3)}(t_i)}{3M^{(1)}(t_i)} \tag{4.46}$$

where

$$M^{(1)}(t_k) = \prod_{j=1,\, j\neq k}^{K} (t_k - t_j) \tag{4.47}$$

is the derivative of $M(t)$ given by

$$M(t) = (t - t_1)(t - t_2)\ldots(t - t_K)\,. \tag{4.48}$$

Similarly, $M^{(2)}(t)$ and $M^{(3)}(t)$ are the second and third order derivatives of $M(t)$.

It is observed that if t_i is given, it is easy to compute $M^{(1)}(t_i)$ from equation (4.47) and hence $a_{ij}^{(1)}$, $a_{ij}^{(2)}$ for $i \neq j$. However, the computation of $a_{ii}^{(1)}$ (equation (4.44)) and $a_{ii}^{(2)}$ (equation (4.46)) involve the computation of the second order derivative $M^{(2)}(t_i)$ and the third order derivative $M^{(3)}(t_i)$ which are not easy to compute. This difficulty can be eliminated by the property of the linear vector space.

According to the theory of a linear vector space, one set of base polynomials can be expressed uniquely by another set of base polynomials. Thus, if one set of base polynomials satisfies a linear operator, say equation (4.41) or (4.42), so does another set of base polynomials. As a consequence equations (4.41) and (4.42) should also be satisfied by the second set of base polynomials t^k, $k = 1, 2, \ldots, K-1$. When $k = 0$ this set of base polynomials gives

$$\sum_{j=1}^{K} a_{ij}^{(1)} = 0 \quad \text{or} \quad a_{ii}^{(1)} = -\sum_{j=1,\, j\neq 1}^{K} a_{ij}^{(1)} \tag{4.49}$$

and

$$\sum_{j=1}^{K} a_{ij}^{(2)} = 0 \quad \text{or} \quad a_{ii}^{(2)} = -\sum_{j=1,\, j\neq 1}^{K} a_{ij}^{(2)} \tag{4.50}$$

which are practical to compute once $a_{ij}^{(1)}$, $a_{ij}^{(2)}$ $(i \neq j)$ are known.

4.2.2 DQM for the initial value problems

Now, differential quadrature method is going to be applied to the system of first order initial value problem (4.39) which is the other original contribution of the thesis.

The DQM discretizes the solution $\mathbf{u}$ in the time direction

$$\left.\frac{\partial \mathbf{u}}{\partial t}\right|_{t_i} = \dot{\mathbf{u}}_i = \sum_{j=1}^{K} a_{ij}^{(1)} \mathbf{U}_j, \quad i = 1, 2, \ldots, K \tag{4.51}$$

where $\mathbf{U}_j = \mathbf{u}(t_j)$.

Substituting the approximation (4.51) into equation (4.39) yields

$$\sum_{j=1}^{K} a_{ij}^{(1)} \mathbf{U}_j + \mathbf{B}\mathbf{U}_i = \mathbf{D}\bar{\mathbf{q}}_i - \mathbf{b_1} \quad i = 1, 2, \ldots, K \tag{4.52}$$

where the vectors $\mathbf{U}_i$ and $\bar{\mathbf{q}}_i$ are, infact, the $\mathbf{u}$ and $\mathbf{q}$ vectors respectively

$$\mathbf{u} = \{u_1, u_2, \ldots, u_N, \ldots, u_{N+L}\} \tag{4.53}$$

$$\mathbf{q} = \{q_1, q_2, \ldots, q_N, 0, \ldots, 0\} \tag{4.54}$$

at the ith time level

$$\mathbf{U}_i = \left\{u_{1i}, u_{2i}, \ldots, u_{Ni}, u_{(N+1)i}, \ldots, u_{(N+L)i}\right\} \tag{4.55}$$

$$\bar{\mathbf{q}}_i = \{q_{1i}, q_{2i}, \ldots, q_{Ni}, 0, \ldots, 0\} \tag{4.56}$$

in which $u_{ji} = u_j(t_i)$ and $q_{ji} = q_j(t_i)$.

One can notice that equation (4.52) gives a system of linear equations for each time level t_i $(i = 1, 2, \ldots, K)$

$$a_{i1}^{(1)} \mathbf{U}_1 + a_{i2}^{(1)} \mathbf{U}_2 + \ldots + a_{iK}^{(1)} \mathbf{U}_K + \mathbf{B}\mathbf{U}_i = \mathbf{D}\bar{\mathbf{q}}_i - \mathbf{b_1} \tag{4.57}$$

where $\mathbf{U}_i$ and $\bar{\mathbf{q}}_i$ are the vectors of the size $(N+L)\times 1$. When system (4.57) is written for $i = 1, 2, \ldots, K$, we finally obtain the system of linear equations for the solution of the transient convection-diffusion type problem in the entire time domain

$$\tilde{\mathbf{A}}\tilde{\mathbf{U}} = \tilde{\mathbf{D}}\tilde{\mathbf{q}} - \mathbf{b_1} \tag{4.58}$$

where

$$\tilde{\mathbf{A}} = \mathbf{A} + \tilde{\mathbf{B}}\,. \tag{4.59}$$

The matrices $\mathbf{A}$, $\tilde{\mathbf{B}}$ and $\tilde{\mathbf{D}}$ are expressed as

$$\mathbf{A} = \begin{bmatrix} \mathbf{a}_{11} & \mathbf{a}_{12} & \ldots & \mathbf{a}_{1K} \\ \mathbf{a}_{21} & \mathbf{a}_{22} & \ldots & \mathbf{a}_{2K} \\ \vdots & & & \\ \mathbf{a}_{K1} & \mathbf{a}_{K2} & \ldots & \mathbf{a}_{KK} \end{bmatrix} \tag{4.60}$$

with $(N+L)\times(N+L)$ submatrices $\mathbf{a}_{ij}$ defined as $\mathbf{a}_{ij} = a_{ij}^{(1)}\,\mathbf{I}$ and

$$\tilde{\mathbf{B}} = \begin{bmatrix} \mathbf{B} & & & \\ & \mathbf{B} & & \\ & & \ddots & \\ & & & \mathbf{B} \end{bmatrix}, \qquad \tilde{\mathbf{D}} = \begin{bmatrix} \mathbf{D} & & & \\ & \mathbf{D} & & \\ & & \ddots & \\ & & & \mathbf{D} \end{bmatrix}. \tag{4.61}$$

The sizes of the matrices $\tilde{\mathbf{A}}$, $\tilde{\mathbf{B}}$, $\mathbf{A}$ and $\tilde{\mathbf{D}}$ are $(N+L)\,K\times(N+L)\,K$ and the identity matrix $\mathbf{I}$ is of size $(N+L)\times(N+L)$.

The $(N+L)\,K\times 1$ vectors $\tilde{\mathbf{U}}$ and $\tilde{\mathbf{q}}$ are defined as

$$\begin{aligned}\tilde{\mathbf{U}} = \big\{&u_{11}, u_{21}, \ldots, u_{(N+L)1}; u_{12}, u_{22}, \ldots, u_{(N+L)2}; \ldots \\ &\ldots; u_{1K}, u_{2K}, \ldots, u_{(N+L)K}\big\}\end{aligned} \tag{4.62}$$

$$\begin{aligned}\tilde{\mathbf{q}} = \{&q_{11}, q_{21}, \ldots, q_{N1}, 0, \ldots, 0; q_{12}, \ldots, q_{N2}, 0, \ldots, 0; \ldots \\ &\ldots;\ q_{1K}, \ldots, q_{NK}, 0, \ldots, 0\}\,.\end{aligned} \tag{4.63}$$

In the linear system (4.58) boundary conditions (some of $\tilde{\mathbf{U}}$ and some of $\tilde{\mathbf{q}}$ nodal specified values) are inserted by interchanging the negative of corresponding columns and reordering the solution vector in terms of unknown $\tilde{\mathbf{U}}$ and $\tilde{\mathbf{q}}$ nodal values. When the initial condition is also inserted at the interior plus boundary nodes for the initial time level, system (4.58) finally becomes a rectangular system since known initial $\tilde{\mathbf{U}}$ values are passed to the right hand side leaving less number of unknowns than the number of equations.

The resulting reordered form of system (4.58) is given as

$$\tilde{\tilde{\mathbf{A}}}\ \tilde{\tilde{\mathbf{U}}} = \tilde{\tilde{\mathbf{D}}}\ \tilde{\tilde{\mathbf{q}}} - \mathbf{b_1} \tag{4.64}$$

where the sizes of $\tilde{\tilde{\mathbf{A}}}$, $\tilde{\tilde{\mathbf{U}}}$ are $(N+L)\,K \times ((N+L)\,K - L)$ and $((N+L)\,K - L) \times 1$, respectively if the boundary condition is of Dirichlet type. For Neumann and mixed type of boundary conditions the sizes of $\tilde{\tilde{\mathbf{A}}}$ and $\tilde{\tilde{\mathbf{U}}}$ are appropriately arranged. The sizes of $\tilde{\tilde{\mathbf{D}}}$, $\tilde{\tilde{\mathbf{q}}}$ are the same as the sizes of $\tilde{\mathbf{D}}$ and $\tilde{\mathbf{q}}$. Now $\tilde{\tilde{\mathbf{U}}}$ contains all the unknown values of $\tilde{\mathbf{U}}$ and $\tilde{\mathbf{q}}$ but, $\tilde{\tilde{\mathbf{q}}}$ contains boundary plus initial information.

System (4.64) gives the solution of our transient convection-diffusion problem at all the required time levels directly without the need of a time iteration. But since the system is overdetermined, the least squares method can be employed to obtain the solution.

Application of the least squares method to the overdetermined system (4.64) gives the normal equations

$$\tilde{\tilde{\mathbf{A}}}^{\mathbf{T}}\ \tilde{\tilde{\mathbf{A}}}\ \tilde{\tilde{\mathbf{U}}} = \tilde{\tilde{\mathbf{A}}}^{\mathbf{T}}\ \tilde{\tilde{\mathbf{D}}}\ \tilde{\tilde{\mathbf{q}}} - \tilde{\tilde{\mathbf{A}}}^{\mathbf{T}}\ \mathbf{b_1} \tag{4.65}$$

for the unknown $\tilde{\tilde{\mathbf{U}}}$ which is the solution of transient convection-diffusion equation for the entire domain $\bar{\Omega} \times [0, T]$.

When the initial value problem is of second order a similar procedure will be carried out in Section 4.3.3.

4.3 Numerical Solutions and Discussions

In this section the numerical solutions of the transient convection-diffusion type equations and elastodynamic problems are considered. The equations are discretized by the above proposed tecnique, which involves the coupling of the dual reciprocity BEM in spatial domain with the DQM in the time domain. The discretization of the space variables using the DRBEM in transient convection-diffusion type equations or in elastodynamic equations results in a system of first order or second order initial value problem in time, respectively. Then, this system is discretized in time direction by the use of DQM. After the imposition of both initial and boundary conditions, the problem reduces to a system of linear algebraic equations which gives the solution on the whole computational domain at any required time level at one stroke without the need of iteration in the time direction.

The present section contains the applications of the coupled DRBEM and DQM to mainly three types of equations. These are convection-diffusion equation with variable coefficients, unsteady magnetohydrodynamic flow equations with homogeneous Dirichlet type boundary conditions and the elastodynamic equations. The original unsteady coupled MHD equations can be transformed into two decoupled time dependent convection-diffusion type equations when the walls are insulated. Thus, the proposed method can be applied directly. For the solution of the elastodynamic equations the method is modified for the second order time derivative.

4.3.1 Diffusion and convection-diffusion problems

The equation governing two-dimensional transient convection-diffusion type problems can be expressed as

$$\nu\nabla^2 u = \frac{\partial u}{\partial t} + d_1(x,y)\frac{\partial u}{\partial x} + d_2(x,y)\frac{\partial u}{\partial y} + d_3(x,y)u \tag{4.66}$$

where $(x,y) \in \Omega \subset R^2$, $t > 0$, ν is a constant and d_1, d_2, d_3 are functions of space variables.

Equation (4.66) is supplied with an initial condition

$$u\left(x,y,0\right)=u_0\left(x,y\right) \tag{4.67}$$

and Dirichlet, Neumann or mixed type boundary conditions

$$\begin{aligned} &u\left(x,y,t\right)=\overline{u}\left(x,y,t\right) && (x,y)\in\Gamma_u\\ &q\left(x,y,t\right)=\overline{q}\left(x,y,t\right) && (x,y)\in\Gamma_q\\ &q\left(x,y,t\right)+h\left(x,y,t\right)u\left(x,y,t\right)=0 && (x,y)\in\Gamma_h \end{aligned} \tag{4.68}$$

for obtaining a well-defined problem. Here u_0, $\bar{u}$, $\bar{q}$ and h are given functions and $q=\partial u/\partial n$, (n is the outward normal), $\Gamma=\Gamma_u+\Gamma_q+\Gamma_h$ is the boundary of the region Ω.

Equation (4.66) is in the same form with equation (4.21), by taking $b_1=0$, $b_2=d_3$, $b_3=d_1$ and $b_4=d_2$. Thus, the application of the dual reciprocity BEM transforms the differential equation (4.66) into the boundary integral equations of the form given in equation (4.36), i.e.

$$\nu(\mathbf{Hu}-\mathbf{Gq})=(\mathbf{H\hat{U}}-\mathbf{G\hat{Q}})\mathbf{F^{-1}}(\frac{\partial\mathbf{u}}{\partial t}+\mathbf{d_3u}+\mathbf{d_1}\frac{\partial\mathbf{F}}{\partial x}\mathbf{F^{-1}u}+\mathbf{d_2}\frac{\partial\mathbf{F}}{\partial y}\mathbf{F^{-1}u}). \tag{4.69}$$

When equation (4.69) is rearranged, the following differential equations is obtained

$$\mathbf{C\dot{u}}+(\nu\mathbf{H}+\mathbf{S})\mathbf{u}=\nu\mathbf{Gq} \tag{4.70}$$

where $\mathbf{C}$ is the matrix given in equation (4.38) and the matrix $\mathbf{S}$ of size $(N+L)\times(N+L)$ is as follows

$$\mathbf{S}=\mathbf{C}(\mathbf{d_3}+\mathbf{d_1}\frac{\partial\mathbf{F}}{\partial x}\mathbf{F^{-1}}+\mathbf{d_2}\frac{\partial\mathbf{F}}{\partial y}\mathbf{F^{-1}})\,. \tag{4.71}$$

Thus, the standard form of the first order initial value problem will be

$$\mathbf{\dot{u}}+\mathbf{Bu}=\mathbf{Dq} \tag{4.72}$$

as in equation (4.39) with the initial condition $u(x,y,0)=u_0(x,y)$ where $\mathbf{B}=$

$\mathbf{C}^{-1}(\nu\mathbf{H}+\mathbf{S})$ and $\mathbf{D}=\nu\mathbf{C}^{-1}\mathbf{G}$.

Equation (4.72) now can be discretized in the time direction by using the differential quadrature method which was explained in Section 4.2.2.

We consider both diffusion and convection-diffusion type problems together with Dirichlet, Neumann and/or mixed type boundary conditions. The problem domains are either, a circle, a square or a rectangle in the $(x,\, y)$-plane and the time domain is $[0,\, T]$ where T is a constant. In the DRBEM discretization for the domains, we use constant boundary elements with the numbers ranging from 20 to 240 and some interior nodes for presenting the solution in terms of graphics. For the time domain $(0, T)$ in DQM both equally spaced and Gauss-Chebyshev-Lobatto (GCL) points are used in the discretization. The equally spaced points in the time direction are given by

$$t_i=\frac{i-1}{K-1}T, \qquad i=1,2,\ldots,K$$

for a region $[0, T]$. The GCL points are the Chebyshev collocation points which are the roots of $|T_K(t)|=1$ and given by, [47],

$$t_i=\cos(\frac{i-1}{K-1}\,\pi), \qquad i=1,2,\ldots,K$$

for an interval $[-1, 1]$. For a region on $[0, T]$, they are given by

$$t_i=\frac{T}{2}[1-\cos(\frac{i-1}{K-1}\,\pi)], \qquad i=1,2,\ldots,K\,.$$

Shu and Chen [63] have discussed the optimal selection of the grid points in DQM. They introduced the strectching of GCL points towards boundary to obtain more accurate results. They showed that these points have a faster rate of convergence than the equally spaced points. Since the points are clustered near the end points of a time interval, the value of the solution at the required time level will be captured more accurately. The solution of the test problems are compared with the exact solution and with other studies. The first test problem is the diffusion equation in a circular region of unit radius with mixed

type boundary conditions. The last two applications are convection-diffusion type equations with variable coefficients in rectangular domains with Neumann and/or Dirichlet type boundary conditions.

Diffusion problem in a circular region

The diffusion problem in a circular region of unit radius is described by

$$\frac{\partial u}{\partial t} = \nabla^2 u \qquad 0 \leq r < 1, \qquad t > 0$$

where r is the radius of the circle. The problem is subjected to the mixed type boundary conditions $q = 2(1-u)$ and the initial condition is given as zero.

The circular region is discretized with $N = 24$ constant boundary elements and $L = 10$ internal nodal points. In Figure 4.1, the numerical results are compared with the corresponding analytical values [32] at varying time levels for $r = 0$, $r = 0.5$ and $r = 1.0$, respectively.

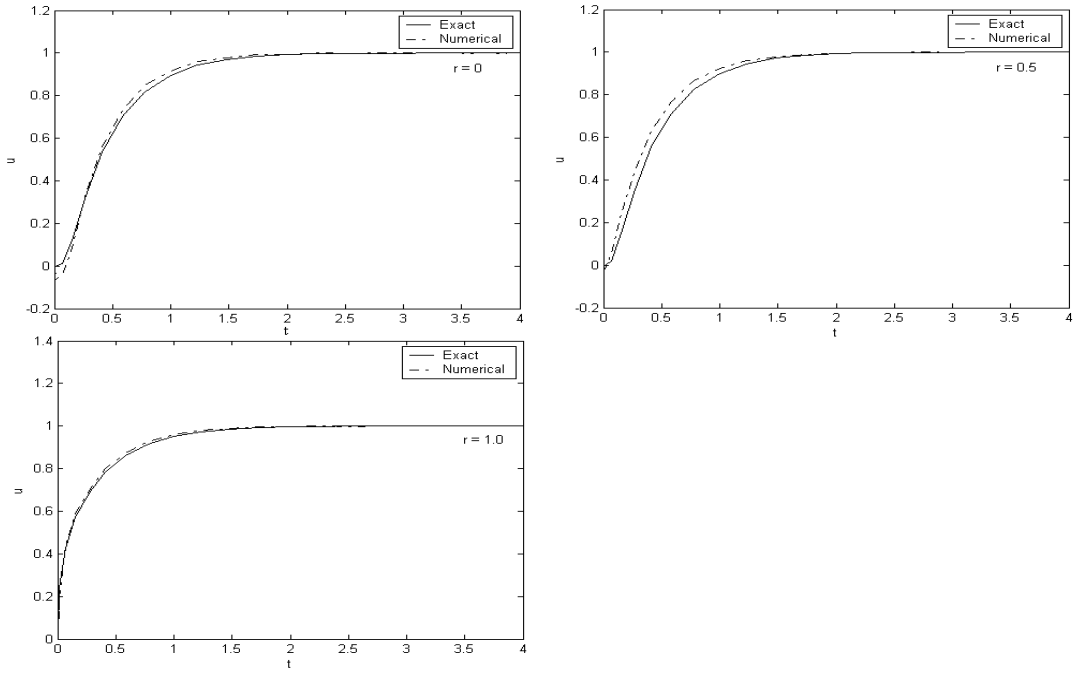

Figure 4.1: Solution of diffusion equation in a circular region at varying time levels for $r = 0$, 0.5 and 1.0 respectively, $N = 24$, $L = 10$

The convection-diffusion type problem (Partridge and Sensale [43])

$$\nabla^2 u = \frac{\partial u}{\partial t} + d_1(x,y)\frac{\partial u}{\partial x} + d_2(x,y)\frac{\partial u}{\partial y} + d_3\, u \qquad \begin{matrix} 0 \le x \le 1 \\ 0 \le y \le 0.7 \end{matrix} , \qquad t > 0$$

where d_3 is the decay parameter and d_1, d_2 are the velocity components defined as

$$\begin{aligned} d_1 &= d_3\, x + log\left(\frac{10}{300}\right) - \frac{d_3}{2} \\ d_2 &= 0\,. \end{aligned}$$

The boundary conditions are

$$\frac{\partial u}{\partial n}(x,0,t) = \frac{\partial u}{\partial n}(x,0.7,t) = 0 \qquad 0 \le x \le 1\,, \quad t > 0$$

$$u(0,y,t) = 300$$

$$0 \le y \le 0.7\,, \quad t > 0$$

$$u(1,y,t) = 10$$

and the initial condition is homogeneous.

The boundary of the region is discretized with $N = 112$, 180 and 240 constant boundary elements for the values of $d_3 = 1$, 20 and 40 with $L = 7$, 20 and 35 interior nodes respectively . $K = 5$ Gauss-Chebyshev-Lobatto points are used in the time direction. The DQM enables us to obtain the solution at any transient and the required time levels. Figure 4.2 gives the behaviour of the DQM solution at the transient levels which converges to steady state exact solution for increasing time levels. The results are also obtained at the steady state level $T = 1.0$ for $d_3 = 20$ and 40. Thus, we are able to compare the obtained numerical results with the steady state exact solution [64]. Figures 4.3 and 4.4 show the agreement of our solution with the steady state exact solution at $y = 0.6$ for $d_3 = 20$ and 40 respectively. It is noticed that for an increased value of d_3, and consequently of d_1, one needs more number of boundary elements. This corresponds to the need of increased discretization for large values of Peclet number.

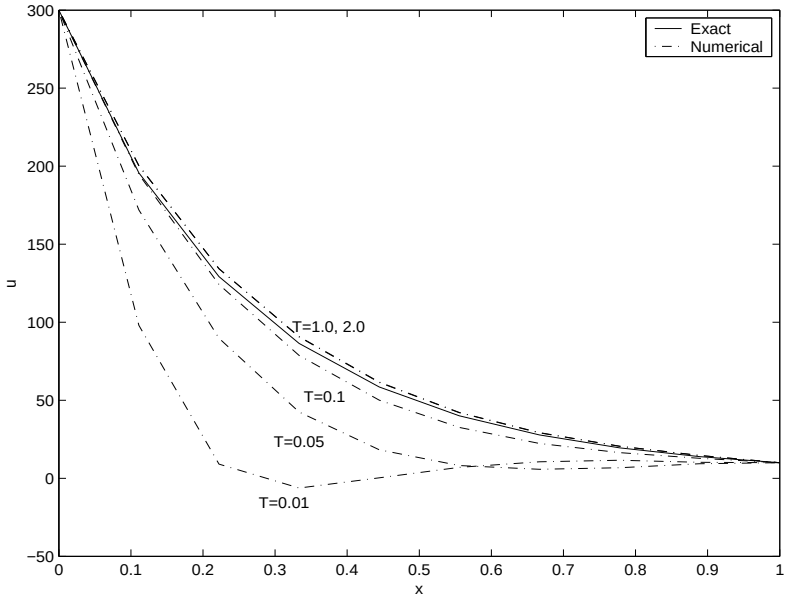

Figure 4.2: Solution of convection-diffusion equation at several T' s for $d_3 = 1$ at $y = 0.6$, $N = 112$

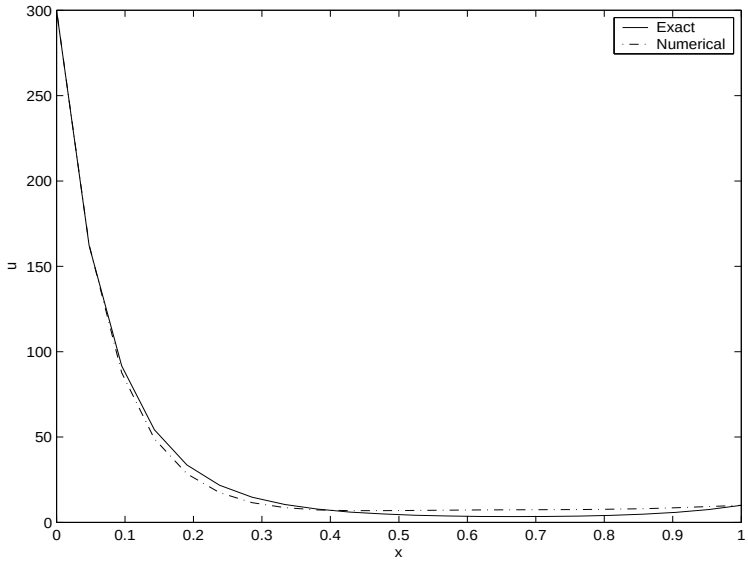

Figure 4.3: Solution of convection-diffusion equation for $d_3 = 20$ at $y = 0.6$, $T = 1.0$, $N = 180$, $L = 20$

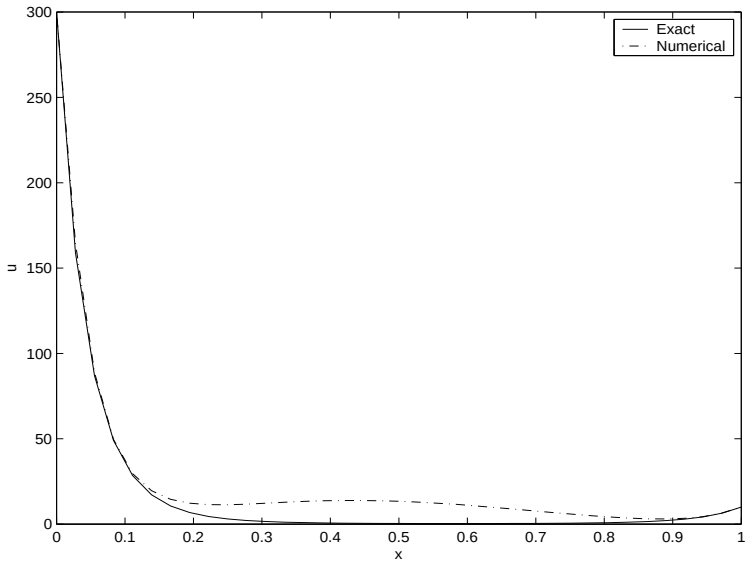

Figure 4.4: Solution of convection-diffusion equation for $d_3 = 40$ at $y = 0.6$, $T = 1.0$, $N = 240$, $L = 35$

Furthermore, this problem has been solved by using the finite difference and the finite element methods for the discretization of the time domain. In the finite difference solution, a general two-level time integration scheme is employed, [65]. Figure 4.5 shows the FDM solution of the problem at the time levels $T = 5$, 10, 15 and 20 by using $K = 15$, 30, 40 and 60 time discretization points, respectively. These results are compared with the solution obtained by the differential quadrature method which uses only $K = 5$ points at each time level, i.e. DQM uses less number of time grid points, and consequently larger time increments, than FDM to reach any required time level with a finer accuracy. It can be also seen in Figure 4.5 that DQM converges to the steady state much faster than finite difference method.

In Figures 4.6 and 4.7 the finite element method solution compared with the DQM solution is drawn by using $K = 5$ time discretization points for the values of $d_3 = 10$ and 20, respectively. They are giving almost the same accuracy, however the implementation of the differential quadrature method is easier than the finite element method.

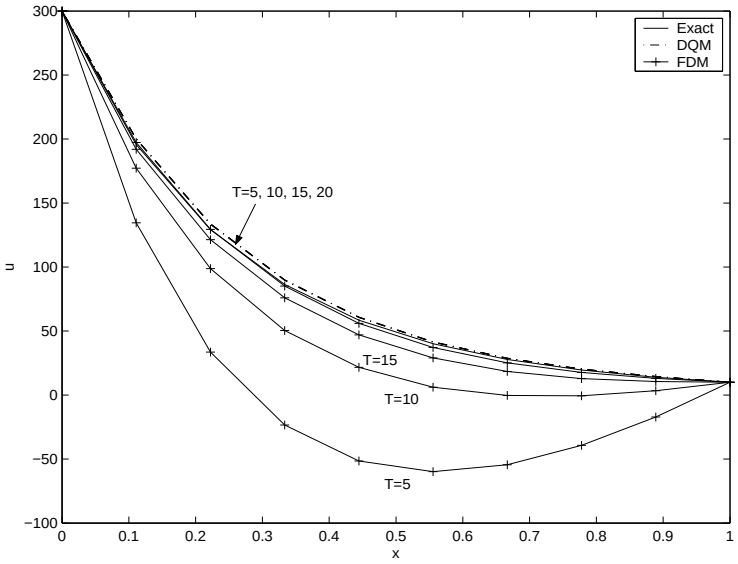

Figure 4.5: Solution of convection-diffusion type equation with FDM and DQM for $d_3 = 1$ at $y = 0.6$, $N = 112$, $L = 7$

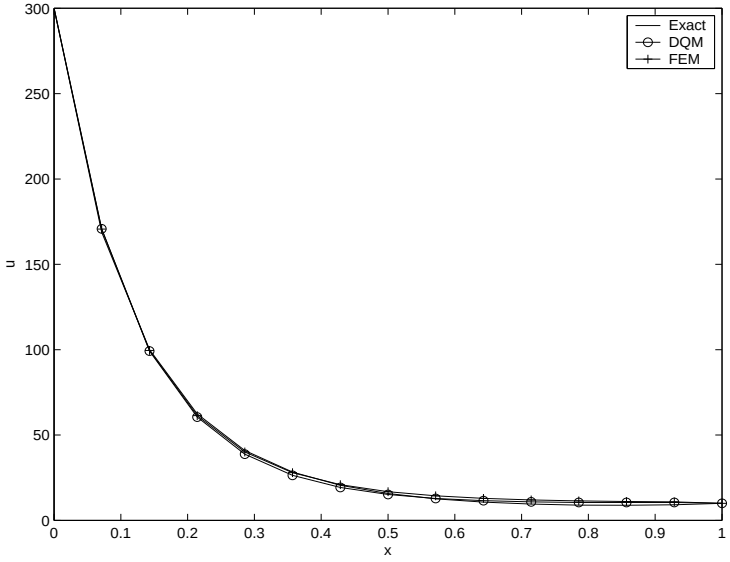

Figure 4.6: Solution of convection-diffusion type equation with FEM and DQM for $d_3 = 10$ at $y = 0.6$, $T = 1.0$, $N = 140$, $L = 13$

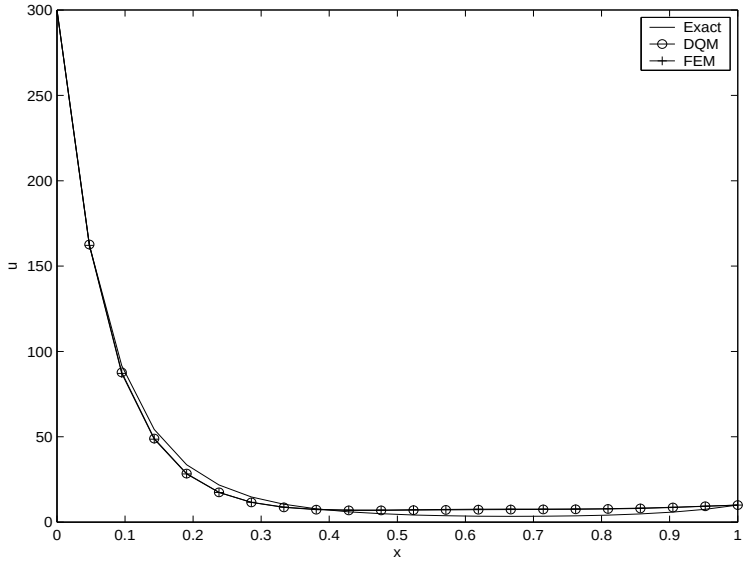

Figure 4.7: Solution of convection-diffusion type equation with FEM and DQM for $d_3 = 20$ at $y = 0.6$, $T = 1.0$, $N = 180$, $L = 20$

The convection-diffusion type problem with variable coefficients (Huerta, Roig and Donea [33])

$$\nu\nabla^2 u + s = \frac{\partial u}{\partial t} + d_1(x,y)\frac{\partial u}{\partial x} + d_2(x,y)\frac{\partial u}{\partial y} + d_3 u \qquad \begin{matrix} -1 \le x \le 1 \\ -1 \le y \le 1 \end{matrix} , \qquad t > 0$$

where $\nu = 5 \times 10^{-5}$, the velocity components $(d_1, d_2) = \phi(\rho)(-y, x)$, $d_3 = 2$, $\rho = \sqrt{x^2 + y^2}$,

$$\phi(\rho) = \begin{cases} 1 - \rho^2 & \text{if} \quad \rho \le 1 \\ 0 & \text{otherwise} \end{cases} \qquad \text{and} \qquad s = \begin{cases} 1 & \text{if} \quad \rho \le 1/2 \\ 0 & \text{otherwise} \end{cases} .$$

This is a rotating pulse problem in the region $\Omega = (-1, 1) \times (-1, 1)$ with homogeneous Dirichlet boundary conditions and zero initial condition. Figure 4.8 shows the solution of the problem at the time levels $T = 0.5$ and $T = 5.0$ respectively which are obtained by taking $N = 200$ and $K = 5$. $T = 5.0$ is

almost the steady state level for the solution and even this solution presents a clear pattern with $u \approx \frac{1}{2}$ if $\rho \leq \frac{1}{2}$ and $u \approx 0$ otherwise, which is the steady state solution behaviour [33].

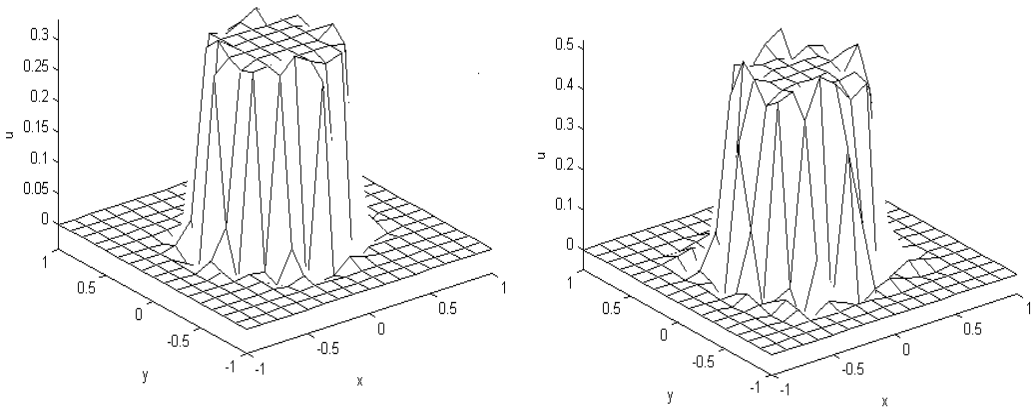

Figure 4.8: Solution of convection-diffusion type equation with variable coefficients at $T = 0.5$ and $T = 5.0$ respectively, $N = 200$, $K = 5$

4.3.2 Unsteady magnetohydrodynamic duct flow

The unsteady, laminar, fully developed flow of viscous, incompressible and electrically conducting fluid in a rectangular duct, subjected to a constant and uniform applied magnetic field B_0 in the direction of x-axis can be put in the following non-dimensional form given by Dragoş, [7],

$$\begin{aligned} \nabla^2 V + M\frac{\partial B}{\partial x} &= -1 + \frac{\partial V}{\partial t} \\ \nabla^2 B + M\frac{\partial V}{\partial x} &= \frac{\partial B}{\partial t} \end{aligned} \tag{4.73}$$

in $\Omega \times [0, \infty)$ with the boundary conditions and the initial condition

$$\begin{aligned} &V(x,y,t) = 0 \qquad B(x,y,t) = 0 \qquad (x,y) \in \Gamma \\ &V(x,y,0) = 0 \qquad B(x,y,0) = 0 \quad (x,y) \in \Omega\,. \end{aligned} \tag{4.74}$$

$V(x,y,t)$, $B(x,y,t)$ are the velocity and the induced magnetic field, respectively, M is the Hartmann number. $V(x,y,t)$, $B(x,y,t)$ are in the z-direction which is the axis of the duct. We take the domain Ω of the problem as a square $|x| \leq 1$, $|y| \leq 1$. The fluid is initially at rest and then starts to move down the duct by the application of a constant pressure gradient. As $t \rightarrow \infty$ we get the steady state solution. Due to the physical and geometrical conditions in which the motion takes place, most of the studies are concentrated not on the original unsteady but on the steady MHD equations which have exact solutions for simple geometry and wall conductivity. However, it is important to see the behaviour of the solution at transient levels as approaching to steady state. Thus, the original unsteady MHD equations are solved here by firstly transforming these coupled equations into decoupled time dependent convection-diffusion type equations with the change of variables

$$U_1 = V + B \quad , \qquad U_2 = V - B \tag{4.75}$$

as

$$\begin{aligned} \nabla^2 U_1 + M\frac{\partial U_1}{\partial x} &= -1 + \frac{\partial U_1}{\partial t} \\ \nabla^2 U_2 - M\frac{\partial U_2}{\partial x} &= -1 + \frac{\partial U_2}{\partial t} \end{aligned} \qquad (x,y,t) \in \Omega \times [0,\infty) \tag{4.76}$$

$$\begin{aligned} &U_1(x,y,t) = 0 \qquad U_2(x,y,t) = 0 \qquad (x,y) \in \Gamma \\ &U_1(x,y,0) = 0 \qquad U_2(x,y,0) = 0 \qquad (x,y) \in \Omega \ . \end{aligned} \tag{4.77}$$

It is possible to go back to the original unknowns V and B through equation (4.75).

Now, both of equations (4.76) are time dependent convection-diffusion type equations with the only difference being $+M$ is replaced with $-M$ in the second equation. After reducing the unsteady coupled MHD equations to the transient convection-diffusion equations we can apply our method described in Sections 4.1 and 4.2.

In the DRBEM discretization in space variables for the square domain, we use constant boundary elements with the number of elements ranging from $N = 92$ to $N = 240$ and some equally spaced interior points for representing the solution in terms of graphics. The distribution of the interior points is arbitrary which is one of the advantage of the DRBEM. We may place more points close to the walls where the most of the action takes place in MHD flow. For the time domain $[0, T]$ in DQM, Gauss-Chebyshev-Lobatto points are used in the discretization. These points are non-uniform and clustered near the boundary which enable us to obtain converged and stable solution for our convection-diffusion type equation [47]. Since we solve the transient MHD equations, we are able to obtain the solution at any required time level. As $t \to \infty$, we get the steady state solution which can be compared with the available exact solution of the steady equations to check the accuracy of the results. Our steady state results for the velocity and the induced magnetic field for small and moderate values of Hartmann number ($5 \leq M \leq 50$) agree with the Shercliff' s, [8], exact solution to roughly three significant digits.

In Figures 4.9 and 4.10 the velocity-induced magnetic field contours are presented at steady state respectively for Hartmann numbers of $M = 5$ and $M = 20$. It is noticed from these figures that as the Hartmann number increases the velocity shows a flattening tendency (contour values are decreased). It is also observed that the boundary layer formation starts near the walls for both the velocity and the induced magnetic field for increasing Hartmann number. This is the well known behaviour of MHD duct flow. For the larger value of M the thickness of the boundary layer is smaller. Velocity becomes uniform at the center of the duct when M is increased and it always has its maximum through the center. When the Hartmann number is increased, the number of boundary elements N must be increased in our computations to get good accuracy. Efficient number of interior points is taken for drawing contours and plots. At the same time we control the total size $((N + L)K - L) \times ((N + L)K - L)$ (K : the number of discretization points in time) of the system with the values of N, L and K not to have difficulties in solving large systems. For this reason we could increase Hartmann number up to $M = 50$ which needs $N = 240$ boundary elements. Further than

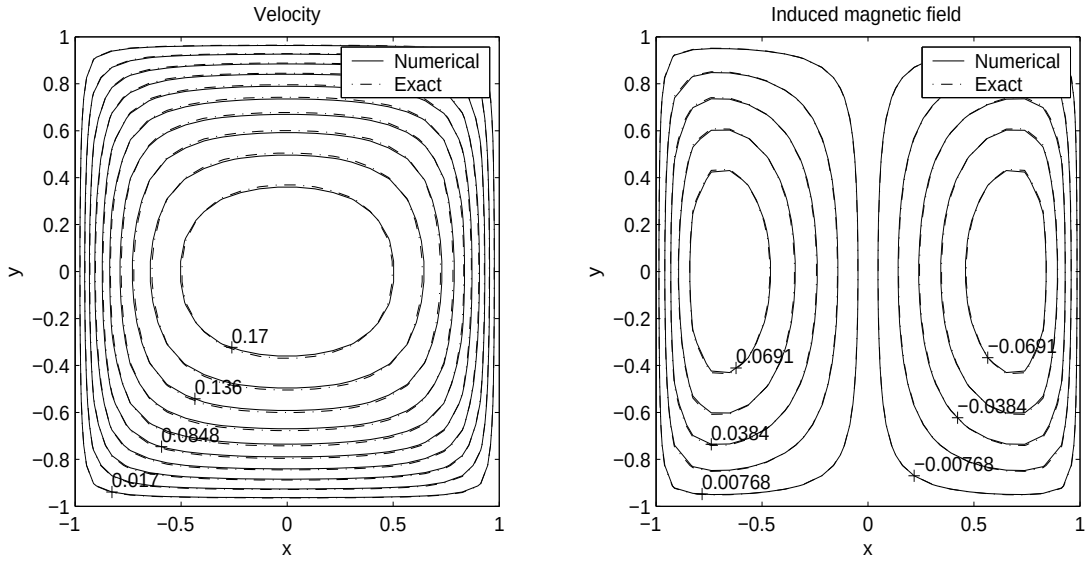

Figure 4.9: Velocity and induced magnetic field lines for $M = 5$, $N = 92$

this Hartmann number, the total size of the system becomes very large due to the large values of especially N, K and L. Figure 4.11 is the velocity-induced magnetic field curves for $M = 50$ at $y = 0$ $(-1 \leq x \leq 1)$ respectively. As we increase Hartmann number M, discrepancies are examined especially for velocity. This may be due to the fact that we need to take more boundary and interior points resulting with a larger sized matrix system. Accumulation of roundoff errors drops accuracy to 10^{-2} especially close to the corners. In Figure 4.11 we notice that the numerical velocity maximum value for $M = 50$ differs from the exact velocity maximum value because of this accuracy drop.

Time discretization points in the DQM application for the time derivative are taken as GCL points which are mostly placed near the boundaries. Since the DQM is stable and convergent for these nonuniform points we don't need to take too many points. In the computations the number of GCL points was taken at most $K = 5$. The other explicit methods need very small time increments in the step by step computation in time.

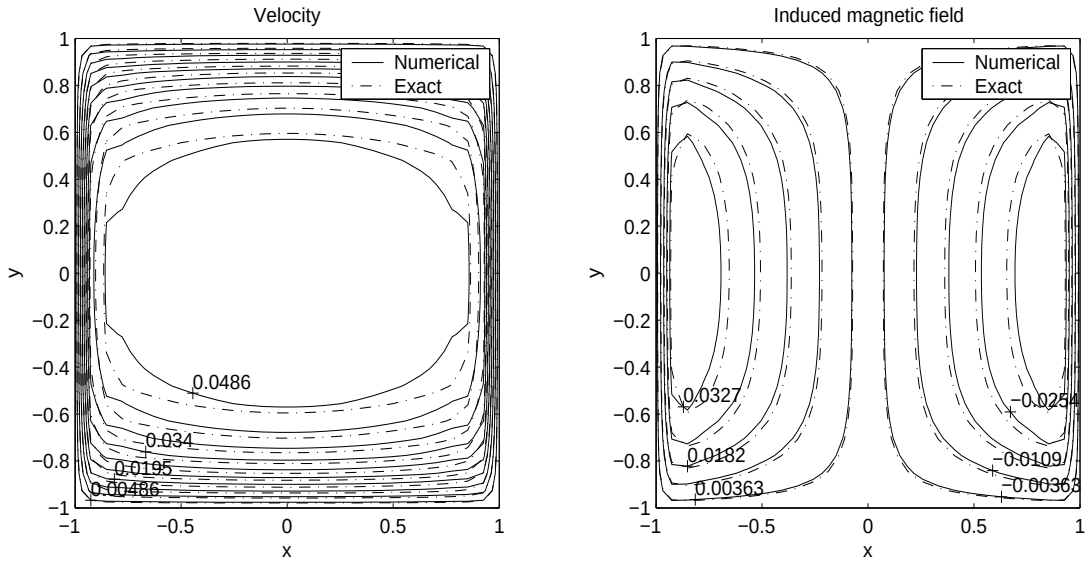

Figure 4.10: Velocity and induced magnetic field lines for $M = 20$, $N = 108$

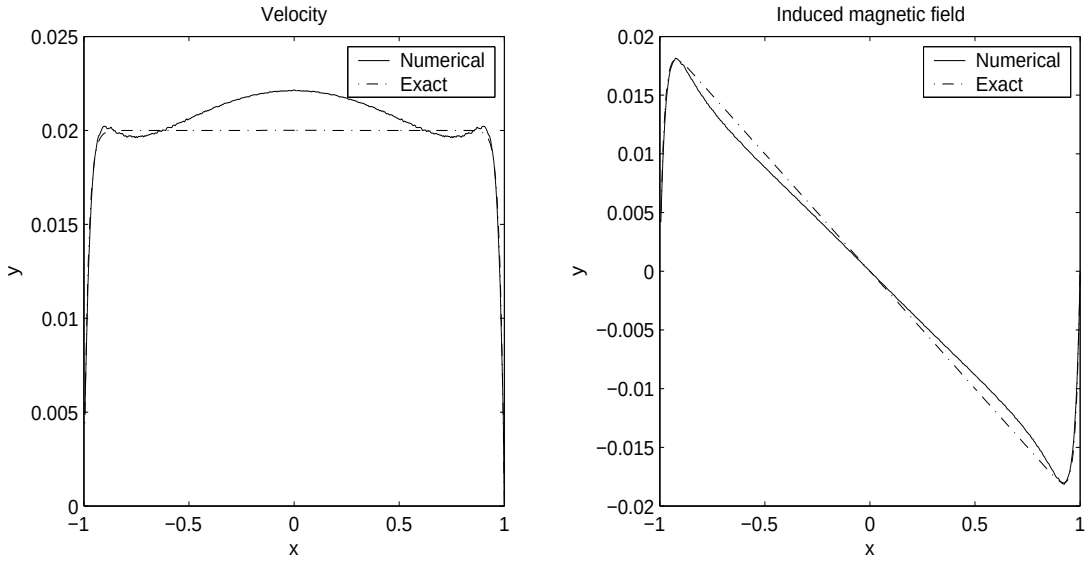

Figure 4.11: Velocity and induced magnetic field lines for $M = 50$, $N = 240$, $y = 0$

4.3.3 Transient elastodynamic problems

In this section, the transient elastodynamic problems are solved by the present numerical method which is the coupling of dual reciprocity BEM with the least squares differential quadrature method. The same procedure has already been applied to the most general type of convection-diffusion problems with variable coefficients in the previous Sections 4.3.1 and 4.3.2. There, the DQM approximated the first order time derivative in the initial value problem obtained by the application of DRBEM to convection-diffusion problems. But when the dual reciprocity BEM is applied to the elastodynamic problems in spatial domain, we end up with a system of second order ordinary differential equations of initial value problem which will be discretized by DQM. Thus, this study can be considered as an extention of the present method to the elastodynamic problems containing both the first and second order time derivatives.

The equation governing the longitudinal vibration of damped plates can be expressed as

$$\nabla^2 u(\mathbf{x},t) = \frac{1}{c^2}\frac{\partial^2 u(\mathbf{x},t)}{\partial t^2} + \lambda \frac{\partial u(\mathbf{x},t)}{\partial t} \ , \qquad \mathbf{x} \in \Omega$$

where λ and c are the coefficient of viscous damping and wave propagation velocity, respectively. To formulate a well-defined problem, boundary and initial conditions must be imposed which specify the state of displacement and velocity as

$$u(\mathbf{x},0) = u_0(\mathbf{x}), \quad \dot{u}(\mathbf{x},0) = v_0(\mathbf{x})$$

at time $t = 0$, where the superimposed dot represents the time derivative. The displacement and traction boundary conditions are given by

$$u(\mathbf{x},t) = \bar{u}(\mathbf{x},t), \qquad \mathbf{x} \in \Gamma_u$$

$$q(\mathbf{x},t) = \bar{q}(\mathbf{x},t), \qquad \mathbf{x} \in \Gamma_q$$

where the spatial domain $\Omega \subset \mathbb{R}^2$ is bounded by a piecewise smooth boundary $\Gamma = \Gamma_u + \Gamma_q$, and $q = \partial u/\partial n$, n is the outward normal on the boundary.

The matrix form of the resulting DRBEM formulation for this elastodynamic problem is obtained as

$$\frac{1}{c^2}\mathbf{C}\ddot{\mathbf{u}} + \lambda\mathbf{C}\dot{\mathbf{u}} + \mathbf{H}\mathbf{u} = \mathbf{G}\mathbf{q} \tag{4.78}$$

where $\mathbf{C}$ is the $(N+L)\times(N+L)$ matrix given in equation (4.38). The matrices $\mathbf{G}$ and $\mathbf{H}$ contain the integrals of the fundamental solution and its normal derivative respectively, which are defined in equation (4.11). By rewriting equation (4.78), the standard form of the second order initial value problem is obtained as

$$\ddot{\mathbf{u}} + \lambda c^2\dot{\mathbf{u}} + \mathbf{B}\mathbf{u} = \mathbf{D}\mathbf{q} \tag{4.79}$$

in which $\mathbf{B} = c^2\mathbf{C}^{-1}\mathbf{H}$ and $\mathbf{D} = c^2\mathbf{C}^{-1}\mathbf{G}$. The sizes of the matrices $\mathbf{B}$ and $\mathbf{D}$ are $(N+L)\times(N+L)$.

When the DQM is applied to the second order initial value problem (4.79) for the approximation of time derivatives, we end up with a linear system of equations for each time level t_i which can be denoted in matrix form similar to (4.58) as

$$\tilde{\mathbf{A}}\tilde{\mathbf{U}} = \tilde{\mathbf{D}}\tilde{\mathbf{q}} \tag{4.80}$$

where $\tilde{\mathbf{A}} = \mathbf{A} + \tilde{\mathbf{B}}$. The $(N+L)K\times(N+L)K$ matrix $\mathbf{A}$ is defined as

$$\mathbf{A} = \begin{bmatrix} \mathbf{a}_{11} & \mathbf{a}_{12} & \dots & \mathbf{a}_{1K} \\ \mathbf{a}_{21} & \mathbf{a}_{22} & \dots & \mathbf{a}_{2K} \\ \vdots & & & \\ \mathbf{a}_{K1} & \mathbf{a}_{K2} & \dots & \mathbf{a}_{KK} \end{bmatrix} \tag{4.81}$$

with the submatrices $\mathbf{a}_{ij} = (a_{ij}^{(2)} + \lambda c^2 a_{ij}^{(1)})\,\mathbf{I}$, where $\mathbf{I}$ is the identity matrix. The matrices $\tilde{\mathbf{B}}$ and $\tilde{\mathbf{D}}$ are the block diagonal matrices containing the matrices $\mathbf{B}$ and $\mathbf{D}$ on the diagonals, respectively.

The procedure outlined here is applied to four types of vibration problems of membranes and plates. The square spatial domain ($0 \le x \le 1$, $0 \le y \le 1$) of the problem is discretized by using $N = 28$ constant boundary elements. For the

discretization of the time domain with the differential quadrature method, $K = 50$ Gauss-Chebyshev-Lobatto points are used. Since the DQM is unconditionally stable, we are allowed to use arbitrarily large time step size to reach a required time level. Thus, the choice of K is arranged accordingly. The number of internal points (L) is taken to depict the behaviour of the solution clearly. Although there is no certain relationship between N, K and L on the accuracy and convergence of the numerical solution, one should be careful in the choice of N, K and L for not having an oversized final linear system of equations for the solution. The use of linear or quadratic radial basis functions in the application of DRBEM does not effect much the accuracy of the numerical results. Thus, for simplicity linear radial basis functions ($f = 1 + r$) are made use of throughout the computations. The last example considered is the longitudinal vibration of plate subjected to Heaviside-type impact load. In this problem, accuracy and convergence properties are studied with respect to the number of points in space and time discretizations.

Free vibration of a square membrane

The free vibration of a square membrane which is released from rest in an initial position and velocity, with homogeneous Dirichlet type boundary conditions $u = 0$ is taken. The initial displacement and the velocity are given by

$$u(x, y, 0) = (x - x^2)(y - y^2), \quad \dot{u}(x, y, 0) = 0 \ .$$

The analytical solution of this problem is, [36],

$$u(x, y, t) = \sum_{m,\, n=1}^{\infty} \Bigg[\frac{16a^2b^2}{\pi^2} \, \frac{1 - (-1)^m}{m^3} \, \frac{1 - (-1)^n}{n^3} \sin(\frac{m\pi x}{a}) \sin(\frac{n\pi y}{b}) \cos(k_{mn} c t) \Bigg]$$

where a and b are the lenghts of the rectangular domain, $k_{mn}^2 = \pi^2 \left(\frac{m^2}{a^2} + \frac{n^2}{b^2} \right)$. $c = \sqrt{T/\rho}$ in which T and ρ are tension and density, respectively.

The numerical results are obtained by using $L = 25$ internal points for $\lambda = 0$. Figures 4.12 and 4.13 show the agreement of the numerical and analytical solutions for the displacement at the center point of the domain and for the traction at the point $(x = 1.0, y = 0.5)$, respectively.

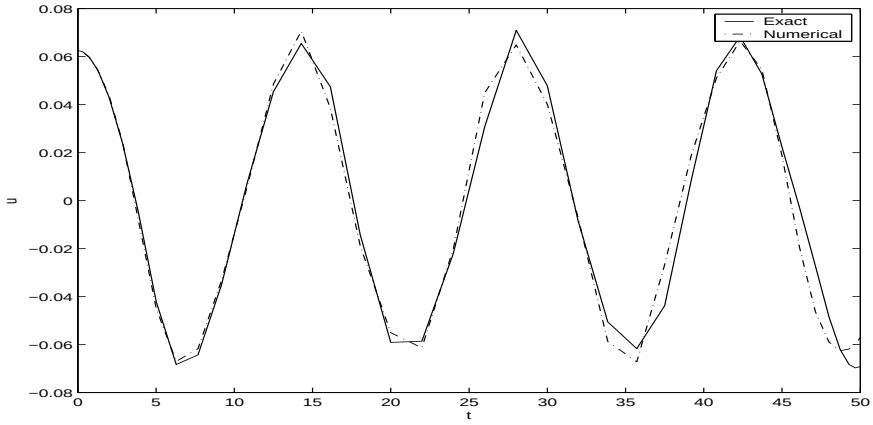

Figure 4.12: Displacement curve at the point (0.5, 0.5) for free vibration of membrane, $\lambda = 0$

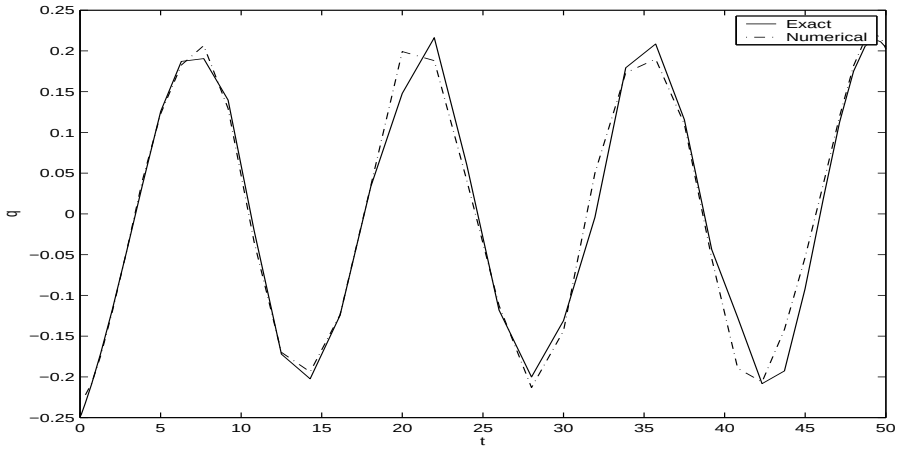

Figure 4.13: Traction curve at the point (1, 0.5) for free vibration of membrane, $\lambda = 0$

Longitudinal vibration of plate subjected to a periodic plane force

The longitudinal vibration of plate subjected to a periodic plane force with zero initial condition is solved. The square plate with edges of length $a = 1$ is fixed along the boundary $x = 1$ and the plane outer force is applied along $x = 0$ (see Figure 4.14). The displacement and traction boundary conditions are as follows,

$$\begin{aligned} u(x, y, t) &= 0 \qquad \text{if } x = 1 \\ q(x, y, t) &= 0 \qquad \text{if } x = 0,\ y = 0,\ 1\ . \end{aligned}$$

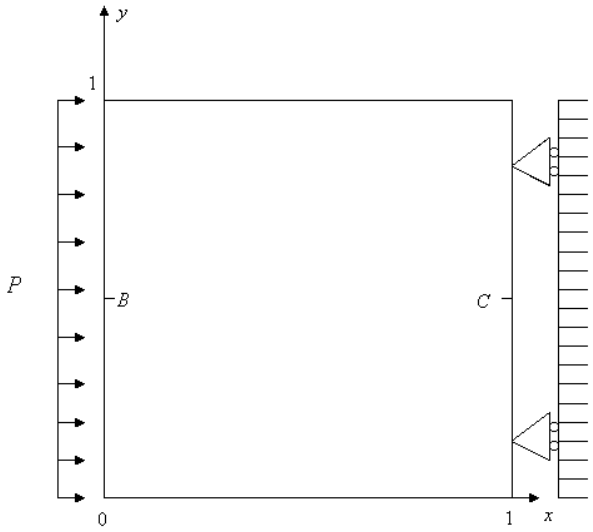

Figure 4.14: Square plate subjected to outer force

The analytical solution

$$u(x, y, t) = \frac{8}{\pi^2}\frac{Pa}{EA}\sum_{i=1}^{\infty}\left\{\frac{(-1)^{i-1}}{(2i-1)^2 - 9/16}\sin\left(\frac{2i-1}{2a}\pi(a-x)\right)\left[\cos\frac{3\pi}{8a}\sqrt{\frac{E}{\rho}}t\right.\right.$$

$$\left.\left. - \cos\frac{2i-1}{2a}\pi\sqrt{\frac{E}{\rho}}t\right]\right\}$$

is obtained when the periodic plane force $p = P\cos\dfrac{3\pi}{8a}\sqrt{\dfrac{E}{\rho}}t$ is applied at the left

side of the plate, [37]. E and ρ are the Young's modulus and the density of the plate material, respectively. A is the area of the cross section.

For the computations $L = 16$ internal points are used and the results are compared with the exact ones in terms of graphics. In Figures 4.15 and 4.16 which show very good agreement with the exact solution, the displacement curve at the point $B(0, 0.5)$ and traction curve at the point $C(1, 0.5)$ versus time are drawn.

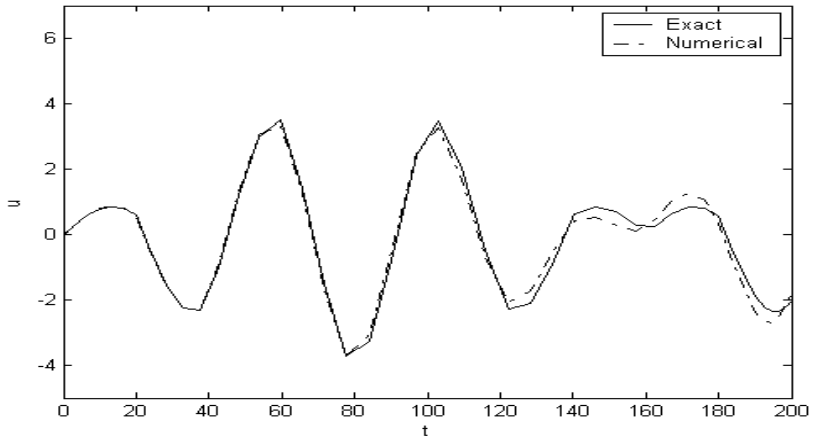

Figure 4.15: Displacement curve at point B, $\lambda = 0$

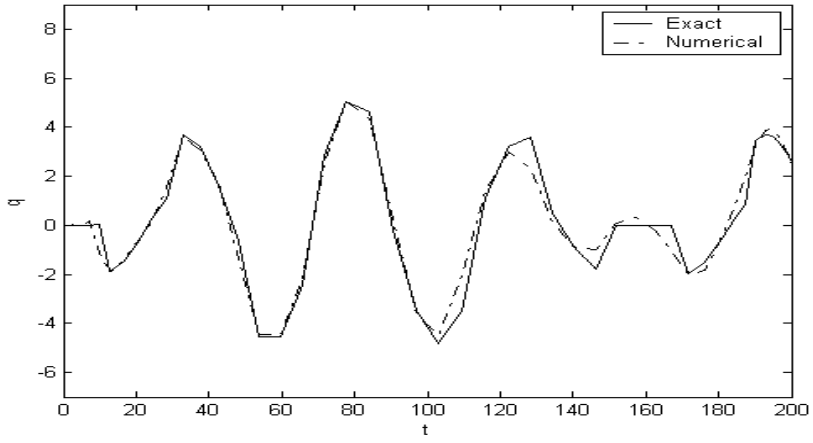

Figure 4.16: Traction curve at point C, $\lambda = 0$

Longitudinal vibration of damped plate subjected to Heaviside impact load

The longitudinal vibration of damped plate subjected to Heaviside impact load is solved for $\lambda = \pi/10$, [38]. Here the initial and boundary conditions and the domain properties (see Figure 4.14) are the same as in the second example, except the applied force. The displacement curve at the point B and the traction curve at the point C are illustrated in Figures 4.17 and 4.18, respectively. As a result of damped factor, the amplitudes of both displacement and traction curves decrease for increasing time levels. There exist oscillations for the traction due to the lack of artificial damping in the application of differential quadrature method. This may be also due to the fact that, it is difficult to represent the derivatives well with constant element DRBEM formulation.

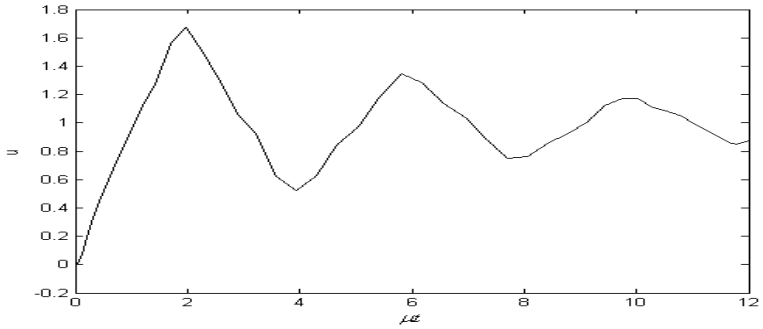

Figure 4.17: Displacement curve at point B, $\lambda = \pi/10$

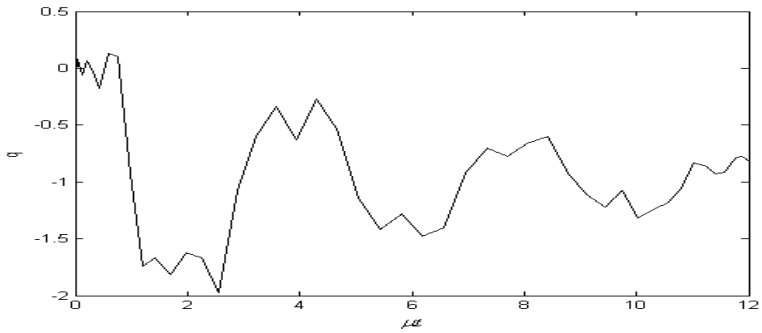

Figure 4.18: Traction curve at point C, $\lambda = \pi/10$

Longitudinal vibration of plate subjected to Heaviside-type impact load

The longitudinal vibration of plate subjected to Heaviside-type impact load is solved. In this case, the $[0,1]\times[0,1]$ square plate is fixed along the left boundary $x=0$ and an impact load of Heaviside-type

$$p = H(t), \quad t \geq 0$$

is enforced at the right wall of the plate $x=1$. The initial and the boundary conditions are given respectively by

$$u(x,y,0) = 0, \qquad \dot{u}(x,y,0) = 0$$

and

$$\begin{aligned} u(x,y,t) &= 0 \qquad \text{if } x = 0 \\ q(x,y,t) &= 0 \qquad \text{if } x = 1,\ y = 0,\ 1\ . \end{aligned}$$

The analytical solution for the displacement of this problem can be expressed as [39]

$$u(x,t) = -\frac{1}{\rho c}\sum_{i=1}^{\infty}(-1)^{i-1}\left[\left(t-\frac{(2i-1)a-x}{c}\right)H\left(t-\frac{(2i-1)a-x}{c}\right)\right.$$

$$\left.-\left(t-\frac{(2i-1)a+x}{c}\right)H\left(t-\frac{(2i-1)a+x}{c}\right)\right]$$

where a and ρ are the same as in the second example. In Figures 4.19 and 4.20, we present the behaviour of the displacement and the relative error at the point ($x=1.0$, $y=0.5$), in a short time interval ($T=1$) with respect to the number of discretization points in space. It is observed that, $N=28$ is the reasonable number of boundary elements since larger values of N do not contribute to the accuracy much. Similarly, Figures 4.21 and 4.22 represent the behaviour of the displacement and the relative error at the same point with respect to time nodal values (number of Gauss-Chebyshev-Lobatto points). $K=$

10 gives quite good accuracy in terms of relative error. For a long time interval K is arranged accordingly. Figure 4.23 represents the long time behaviour of the displacement at the point (1, 0.5), which is in a good agreement with the analytical solution, by using $N = 28$ constant boundary elements, $L = 16$ internal nodes and $K = 38$ time discretization points for the time level $T = 10$.

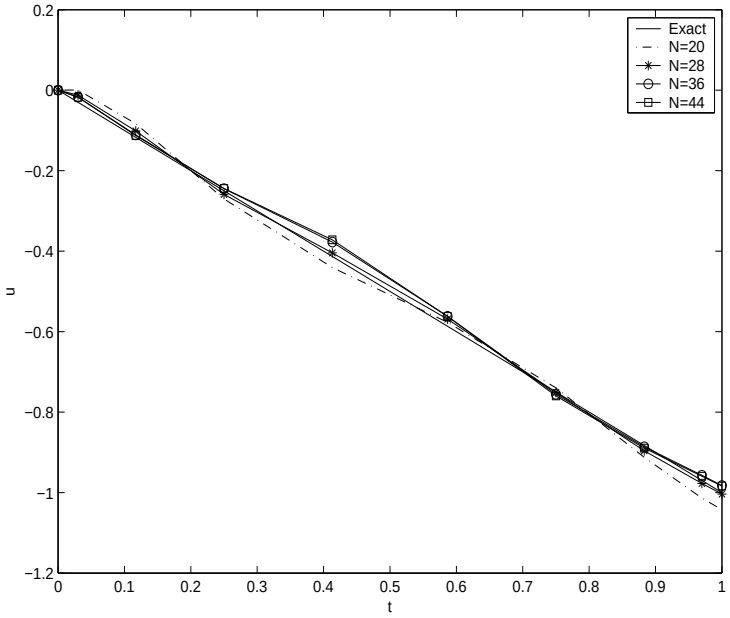

Figure 4.19: Displacement curve for vibration of square plate subjected to Heaviside impact load for several N at the point (1.0, .5), $\lambda = 0$

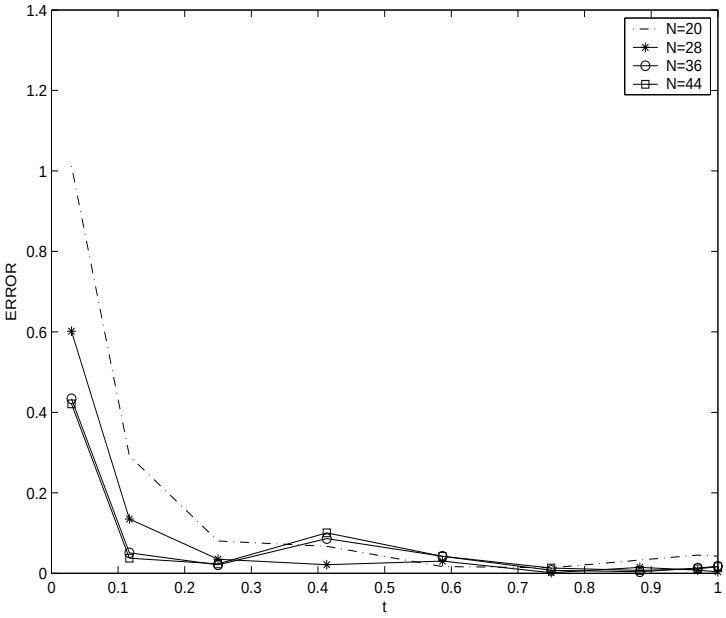

Figure 4.20: Relative error of displacement for several N at the point (1.0, .5), $\lambda = 0$

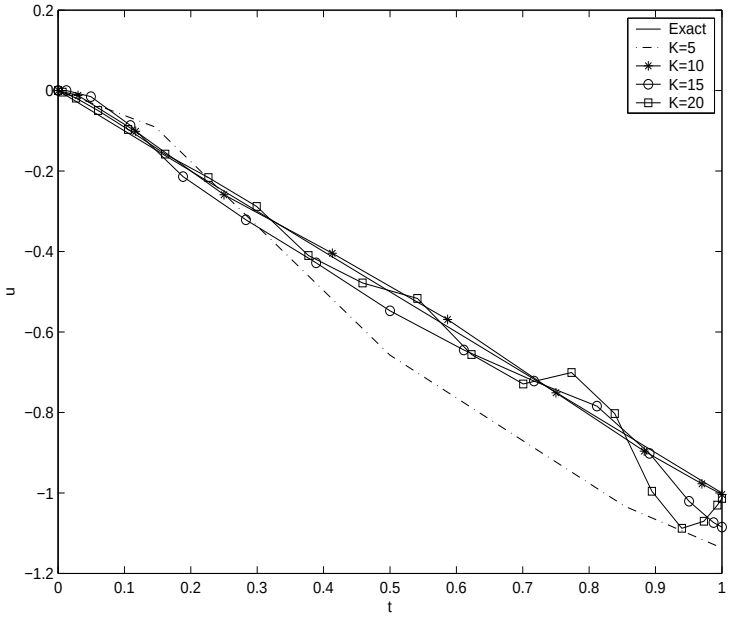

Figure 4.21: Displacement curve for vibration of square plate subjected to Heaviside impact load for several K at the point (1.0, .5), $\lambda = 0$

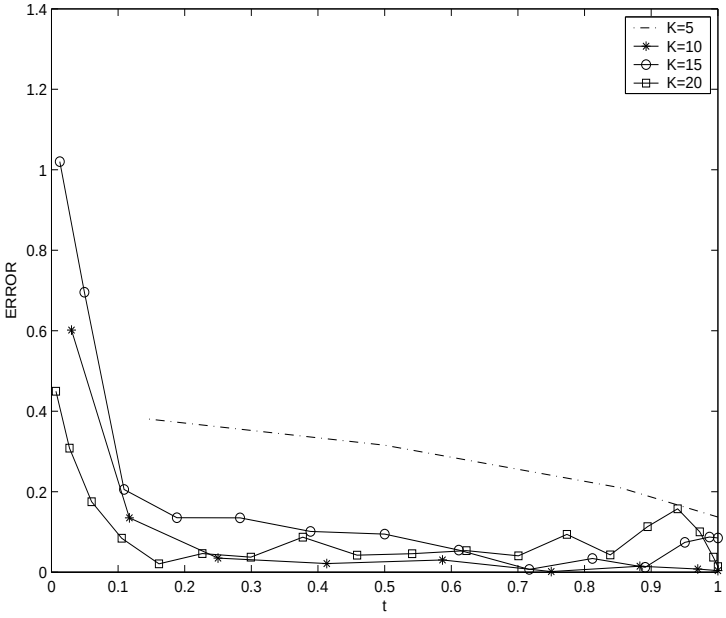

Figure 4.22: Relative error of displacement for several K at the point (1.0, .5), $\lambda = 0$

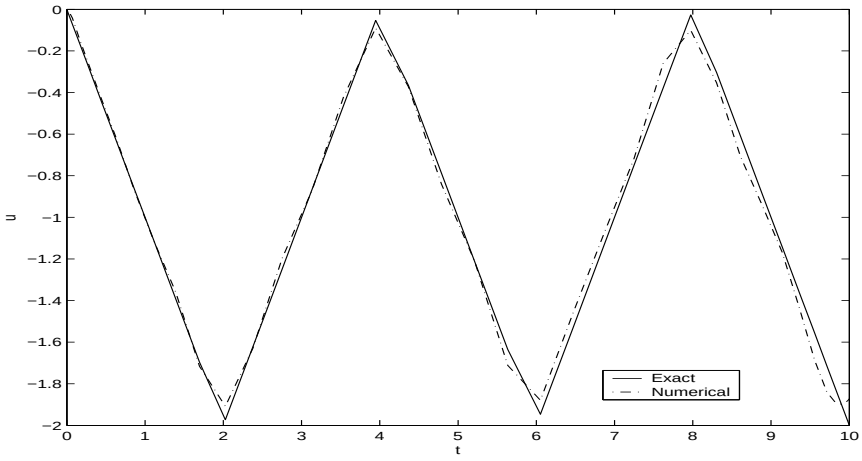

Figure 4.23: Displacement curve at the point (1.0, .5) for vibration of square plate subjected to Heaviside impact load , $\lambda = 0$

As a conclusion, the transient convection-diffusion equations including the unsteady MHD duct flow equations, and the elastodynamic equations which are second order initial value problems in time are solved by using the DRBEM in space - DQM in time procedure in the present chapter. These applications constitute the other original part of the thesis. The DRBEM is applied to Poisson type equation with the fundamental solution of Laplace equation keeping all the other terms as nonhomogeneity, which results in systems of first or second order differential equations in time. These systems are treated by the use of DQM in the discretization of time. The DQM allows us to obtain stable solutions for transient problems although its weighting coefficient matrix is a full matrix. Other time discretization methods as FDM and FEM give block diagonal coefficient matrices despite of using very small time increments

In the next chapter, the same idea will be applied to the unsteady Navier-Stokes equations in terms of stream function and vorticity in which the right hand side functions will contain nonlinear terms also. Therefore, the iterative procedure is made use of between the equations.

CHAPTER 5

SOLUTION OF INCOMPRESSIBLE VISCOUS FLUIDS BY COUPLING OF DIFFERENTIAL QUADRATURE INTEGRATION SCHEME WITH DUAL RECIPROCITY BOUNDARY ELEMENT METHOD

Fluid dynamics deals with the motion of liquids and gases. The flow of most fluids may be analyzed mathematically by the use of two equations. The first one is the *continuity equation* which requires the conservation of mass of a fluid entering a fixed control volume. The other equation is based on the Newton' s law of motion giving the *momentum equations*, or Navier-Stokes equations, which describe the conservation of the momentum. Usually, the term Navier-Stokes equations is used to refer to all of the equations, namely, momentum and continuity equations.

Navier-Stokes equations are one of the most useful sets of equations because they describe the physics of a large number of phenomena of academic and economic interest. They may be used to model weather, the movement of air in the atmosphere, ocean currents, water flow in a pipe, flow around an airfoil, and motion of stars inside a galaxy. As such, these equations in both full and simplified forms, are used in the design of aircraft and cars, the study of blood flow, the design of power stations, the analysis of the effects of pollution, etc. Further,

when they are coupled with Maxwell's equations they can also be used to model and study magnetohydrodynamics as in Chapter 3.

The Navier-Stokes equations for laminar, viscous flow of an incompressible fluid, consist of the momentum equations

$$\rho' \frac{\partial \mathbf{u}'}{\partial t'} + \rho' \mathbf{u}' . \nabla \mathbf{u}' = -\nabla p' + \mu' \nabla^2 \mathbf{u}' + \rho' \mathbf{g}' \tag{5.1}$$

and the continuity equation

$$\nabla . \mathbf{u}' = 0 \tag{5.2}$$

where ρ', μ' and p' are the density, viscosity and pressure, respectively. The vectors $\mathbf{u}'$ and $\mathbf{g}'$ represent respectively the velocity field and the body forces (e.g. gravity).

The Navier-Stokes equations are second order, nonhomogenous, nonlinear partial differential equations, which are extremely difficult to solve in their raw form. However, the equations can be simplified and may admit some numerical solutions.

In this section, the two-dimensional flow of a viscous, incompressible fluid (i.e. a fluid whose density is constant) with a constant viscosity is considered. Thus, the governing Navier-Stokes equations (5.1) and (5.2) can be written in cartesian coordinates as

$$\begin{aligned} \frac{\partial u'}{\partial t'} + u' \frac{\partial u'}{\partial x'} + v' \frac{\partial u'}{\partial y'} &= -\frac{1}{\rho'} \frac{\partial p'}{\partial x'} + \gamma' \left(\frac{\partial^2 u'}{\partial x'^2} + \frac{\partial^2 u'}{\partial y'^2} \right) \\ \frac{\partial v'}{\partial t'} + u' \frac{\partial v'}{\partial x'} + v' \frac{\partial v'}{\partial y'} &= -\frac{1}{\rho'} \frac{\partial p'}{\partial y'} + \gamma' \left(\frac{\partial^2 v'}{\partial x'^2} + \frac{\partial^2 v'}{\partial y'^2} \right) \end{aligned} \tag{5.3}$$

for the momentum equations and the continuity equation takes the form

$$\frac{\partial u'}{\partial x'} + \frac{\partial v'}{\partial y'} = 0 \tag{5.4}$$

in the absence of body force. The constant $\gamma' = \dfrac{\mu'}{\rho'}$ is called as the kinematic viscosity, and $u' = u'(t', x', y')$, $v' = v'(t', x', y')$ are the components of the velocity

field $\mathbf{u}'$.

Equations (5.3) and (5.4) can be written in the nondimensional form by introducing a characteristic length L', a characteristic velocity U', and defining the dimensionless quantities as

$$u = \frac{u'}{U'}, \quad v = \frac{v'}{U'}, \quad x = \frac{x'}{L'}, \quad y = \frac{y'}{L'}, \quad t = \frac{t'}{(L'/U')}, \quad p = \frac{p'}{U'^2\rho'}\,. \tag{5.5}$$

Thus, (5.3) and (5.4) in nondimensional form become

$$\frac{\partial u}{\partial t} + u\frac{\partial u}{\partial x} + v\frac{\partial u}{\partial y} = -\frac{\partial p}{\partial x} + \frac{1}{Re}\left(\frac{\partial^2 u}{\partial x^2} + \frac{\partial^2 u}{\partial y^2}\right) \tag{5.6}$$

$$\frac{\partial v}{\partial t} + u\frac{\partial v}{\partial x} + v\frac{\partial v}{\partial y} = -\frac{\partial p}{\partial y} + \frac{1}{Re}\left(\frac{\partial^2 v}{\partial x^2} + \frac{\partial^2 v}{\partial y^2}\right) \tag{5.7}$$

$$\frac{\partial u}{\partial x} + \frac{\partial v}{\partial y} = 0 \tag{5.8}$$

where

$$Re = \frac{U'L'}{\gamma'} \tag{5.9}$$

is the Reynolds number of the flow.

There are four alternative formulations of the Navier-Stokes equations given earlier. These are (i) the velocity-pressure formulation, (ii) the fourth order stream function equation, (iii) the vorticity-stream function formulation, and (iv) the velocity-vorticity formulation. The advantage of using the velocity-pressure formulation is that we are dealing with the primitive variables. However, in the velocity-pressure formulation it becomes necessary to solve a rather complicated pressure equation, introducing additional difficulties. A second possibility is to solve the fourth order formulation of the Navier-Stokes equations. Although there is only one nonlinear equation that is to be solved, it must be realized that one is now faced with a higher order nonlinear equation. One of the boundary conditions is given in terms of the normal derivatives which also complicates the numerical procedure. For two-dimensional and also for axi-symmetric flows it is convenient to use the vorticity-stream function formulation where the equation of

continuity is automatically satisfied. Of course, the resulting system consists of two coupled equations. Also, the vorticity transport equation is nonlinear. There are several other difficulties associated with the solution of these equations. A major difficulty arises from the boundary conditions of the problem. In practice, only the velocity on the boundaries is prescribed, while for the numerical solution of the equation in the vorticity-stream function formulation we require the values of the vorticity on the boundaries as well.

To obtain the vorticity-stream function formulation of the Navier-Stokes equations (5.6)-(5.8), a stream function ψ satisfying the continuity equation automatically is defined as

$$\frac{\partial \psi}{\partial x} = -v, \qquad \frac{\partial \psi}{\partial y} = u \, . \tag{5.10}$$

The pressure p can be eliminated from equations (5.6) and (5.7) by subtracting the derivative of (5.6) with respect to y from the derivative of (5.7) with respect to x. Then, by introducing the only nonzero component of the vorticity field w as

$$w = \frac{\partial v}{\partial x} - \frac{\partial u}{\partial y} = -\left(\frac{\partial^2 \psi}{\partial x^2} + \frac{\partial^2 \psi}{\partial y^2} \right) = -\nabla^2 \psi \tag{5.11}$$

the momentum equations (5.6) and (5.7) provide a vorticity transport equation,

$$\frac{1}{Re} \nabla^2 w = \frac{\partial w}{\partial t} + u \frac{\partial w}{\partial x} + v \frac{\partial w}{\partial y} \, . \tag{5.12}$$

We are concerned here with the numerical solution of the Navier-Stokes equations in the vorticity-stream function formulation and the required vorticity boundary conditions are obtained from the Taylor series expansion of stream function equation in terms of boundary and interior stream function values. One can observe that equations (5.11) and (5.12) are coupled and equation (5.12) is also a time dependent nonlinear convection-diffusion type equation. In the solution procedure, a combination of the dual reciprocity BEM and the differential quadrature method is used. The spatial domain and time domain are discretized by using DRBEM and DQM, respectively. The stream function equation (5.11) is solved by using DRBEM with an initial vorticity value. The vorticity transport equation (5.12) is solved with the coupling of DRBEM in space-DQM in time domains.

The velocity components in (5.12) are obtained from the stream function values through the relationships (4.33) and (4.34). Thus, equations (5.11) and (5.12) are solved iteratively. This solution procedure for Navier-Stokes equations is also an original contribution in the thesis.

The solution procedure has been tested first on solving Navier-Stokes equations when a force term is present for which an exact solution is available. Then the square cavity problem for which the fluid in the cavity is driven by the motion of one of the walls with a constant velocity is solved for Reynolds number values up to 1000. As a last example the natural convection flow, which involves an additional energy equation because of the heat flux, is considered and it is solved for Rayleigh number values up to 10^5.

5.1 Method of Solution

The Navier-Stokes equations are coupled in terms of vorticity and stream function as shown in equations (5.11) and (5.12). These coupled equations can be solved iteratively. In the solution procedure, firstly the Poisson equation (5.11) is solved for the stream function giving an initial value for the vorticity by using the DRBEM with the fundamental solution of Laplace equation. After obtaining the stream function values for both the boundary and the interior nodal points, the x and y derivatives of the stream function are calculated by using these stream function values through the dual reciprocity boundary element formulation. When we insert these derivative values in the vorticity equation (5.12), it returns into a linear transient convection-diffusion equation with constant coefficients. Thus, this equation can be solved by using the combination of the dual reciprocity BEM for spatial domain and differential quadrature method for the time domain.

5.1.1 Application of DRBEM to vorticity transport and stream function equations

The DRBEM is employed to transform the vorticity transport equation (5.12) and the stream function equation (5.11) into boundary integral equations by using

the fundamental solution of the Laplace equation. The method treats the terms on the right hand sides of these equations as the nonhomogeneity. Thus equations (5.12) and (5.11) are weighted through the domain Ω of the problem as in [31], by the fundamental solution u^* of Laplace equation in two dimensions. Then by using the Green' s second identity, we have

$$\frac{1}{Re}c_i w_i + \int_\Gamma \frac{1}{Re}(q^* w - u^* \frac{\partial w}{\partial n})d\Gamma = -\int_\Omega (\frac{\partial w}{\partial t} + u\frac{\partial w}{\partial x} + v\frac{\partial w}{\partial y})u^* d\Omega \qquad (5.13)$$

and

$$c_i \psi_i + \int_\Gamma (q^* \psi - u^* \frac{\partial \psi}{\partial n})d\Gamma = -\int_\Omega (-w)u^* d\Omega \qquad (5.14)$$

where subscript i denotes the source point, $q^* = \partial u^*/\partial n$ and Γ is the boundary of the domain Ω. The constant $c_i = \theta_i/2\pi$ with the internal angle θ_i at the source point i.

In order to obtain boundary integrals which are equivalent to the domain integrals in equations (5.13) and (5.14), a dual reciprocity approximation is introduced. The basic idea is to expand the terms described as nonhomogeneity in the form,

$$\frac{\partial w}{\partial t} + u\frac{\partial w}{\partial x} + v\frac{\partial w}{\partial y} = \sum_{j=1}^{N+L} \alpha_j(t) f_j(x, y) \qquad (5.15)$$

and

$$-w = \sum_{j=1}^{N+L} \tilde{\alpha}_j f_j(x, y) \qquad (5.16)$$

for equations (5.13) and (5.14), respectively. The above series involve a set of radial basis (coordinate) functions $f_j(x, y)$ which are dependent only on geometry and they are linked with the particular solutions $\hat{u}_j$ of the equation $\nabla^2 \hat{u}_j = f_j$. The unknown coefficients α_j are time dependent whereas $\tilde{\alpha_j}$ are undetermined coefficients. The numbers of boundary and internal nodes are denoted by N and L, respectively. Then, the application of the DRBEM leads to the following

boundary integral equations

$$\frac{1}{Re}\, c_i w_i + \int_\Gamma \frac{1}{Re}(q^* w - u^* \frac{\partial w}{\partial n}) d\Gamma = \sum_{j=1}^{N+L} \alpha_j(t) \left[c_i \hat{u}_{ji} + \int_\Gamma (q^* \hat{u}_j - u^* \hat{q}_j) d\Gamma \right] \quad (5.17)$$

and

$$c_i \psi_i + \int_\Gamma (q^* \psi - u^* \frac{\partial \psi}{\partial n}) d\Gamma = \sum_{j=1}^{N+L} \tilde{\alpha}_j \left[c_i \hat{u}_{ji} + \int_\Gamma (q^* \hat{u}_j - u^* \hat{q}_j) d\Gamma \right] \quad (5.18)$$

where $\hat{q}_j = \dfrac{\partial \hat{u}_j}{\partial n}$.

When constant elements are used for the approximation of ψ, w and their normal derivatives on the boundary, the matrix form of the resulting DRBEM formulation of the vorticity transport and stream function equations are obtained respectively as

$$\frac{1}{Re}(\mathbf{H}\mathbf{w} - \mathbf{G}\frac{\partial \mathbf{w}}{\partial n}) = (\mathbf{H}\hat{\mathbf{U}} - \mathbf{G}\hat{\mathbf{Q}})\boldsymbol{\alpha} \quad (5.19)$$

and

$$\mathbf{H}\boldsymbol{\psi} - \mathbf{G}\frac{\partial \boldsymbol{\psi}}{\partial n} = (\mathbf{H}\hat{\mathbf{U}} - \mathbf{G}\hat{\mathbf{Q}})\tilde{\boldsymbol{\alpha}} \quad (5.20)$$

where $\mathbf{G}$ and $\mathbf{H}$ are the square matrices whose coefficients are calculated by integrating u^* and q^* over each boundary element. Thus, the entries of these matrices are given by

$$H_{ij} = c_i \delta_{ij} + \frac{1}{2\pi} \int_{\Gamma_j} \frac{\partial}{\partial n} \left(\ln(\frac{1}{r}) \right) d\Gamma_j$$

$$G_{ij} = \frac{1}{2\pi} \int_{\Gamma_j} \ln(\frac{1}{r})\, d\Gamma_j$$

where r is the modulus of the distance vector from the point i to the element j, δ_{ij} is the Kronecker delta function and Γ_j is the boundary of the jth element. The matrices $\hat{\mathbf{U}}$ and $\hat{\mathbf{Q}}$ are constructed by taking each vectors $\hat{u}_j$ and $\hat{q}_j$ as columns respectively.

By evaluating expressions (5.15) and (5.16) at all boundary and interior (N+L

points) nodes and inverting, one arrives at

$$\boldsymbol{\alpha} = \mathbf{F}^{-1}\left\{\frac{\partial \mathbf{w}}{\partial t} + \mathbf{u}\frac{\partial \mathbf{w}}{\partial x} + \mathbf{v}\frac{\partial \mathbf{w}}{\partial y}\right\} \tag{5.21}$$

and

$$\tilde{\boldsymbol{\alpha}} = -\mathbf{F}^{-1}\mathbf{w} \tag{5.22}$$

with the $(N+L)\times(N+L)$ matrix $\mathbf{F}$ which contains the coordinate functions f_j' s as column vectors. The substitution of equations (5.21) and (5.22) into equations (5.19) and (5.20) respectively results in

$$\frac{1}{Re}(\mathbf{Hw} - \mathbf{G}\frac{\partial \mathbf{w}}{\partial \mathbf{n}}) = (\mathbf{H}\hat{\mathbf{U}} - \mathbf{G}\hat{\mathbf{Q}})\mathbf{F}^{-1}\left\{\frac{\partial \mathbf{w}}{\partial t} + \mathbf{u}\frac{\partial \mathbf{w}}{\partial x} + \mathbf{v}\frac{\partial \mathbf{w}}{\partial y}\right\} \tag{5.23}$$

and

$$\mathbf{H}\boldsymbol{\psi} - \mathbf{G}\frac{\partial \boldsymbol{\psi}}{\partial n} = (\mathbf{H}\hat{\mathbf{U}} - \mathbf{G}\hat{\mathbf{Q}})\mathbf{F}^{-1}\left\{-\mathbf{w}\right\} . \tag{5.24}$$

Observe that the resulting DRBEM discretization produces coupled equations in vorticity and stream function because of the relationship (5.10). Thus an iterative procedure is necessary to solve them. The iterative procedure proposed here reduces equation (5.23) to a set of ordinary differential equations in time and equation (5.24) to a system of linear algebraic equations in each iteration.

We shall now describe the iterative procedure:

(i) Start with some initial approximations for the vorticity, namely $\mathbf{w^0}$.

(ii) Solve the stream function equation appearing in equation (5.24) with $\mathbf{w} = \mathbf{w^0}$. By this initial vorticity guess the right hand side of equation (5.24) produces a constant vector. Moreover, by the insertion of the boundary conditions for the stream function and its normal derivative and the rearrangement of equation (5.24), we end up with a linear system of equations

$$\tilde{\mathbf{A}}\tilde{\boldsymbol{\psi}} = \tilde{\mathbf{b}} \tag{5.25}$$

where $\tilde{\mathbf{A}}$ is the coefficient matrix of size $(N+L)\times(N+L)$, $\tilde{\mathbf{b}}$ is a known

vector and $\tilde{\boldsymbol{\psi}}$ is the solution vector containing N boundary values of ψ and $\dfrac{\partial \psi}{\partial n}$ plus L interior values of ψ.

(iii) Once the values of stream functions are obtained both on the boundary and inside of the domain, the x and y derivatives of stream function can also be approximated by using the same coordinate functions $f_j(x, y)$, i.e.

$$\psi = \sum_{j=1}^{N+L} \tilde{\beta}_j f_j(x, y) \tag{5.26}$$

where $\tilde{\beta}_j$ are unknown coefficients and this equation can be rewritten as

$$\boldsymbol{\psi} = \mathbf{F}\tilde{\boldsymbol{\beta}} \,. \tag{5.27}$$

Differentiating equation (5.27), we have

$$\frac{\partial \boldsymbol{\psi}}{\partial x} = \frac{\partial \mathbf{F}}{\partial x}\mathbf{F}^{-1}\boldsymbol{\psi} \,, \qquad \frac{\partial \boldsymbol{\psi}}{\partial y} = \frac{\partial \mathbf{F}}{\partial y}\mathbf{F}^{-1}\boldsymbol{\psi} \tag{5.28}$$

since $\tilde{\boldsymbol{\beta}} = \mathbf{F}^{-1}\boldsymbol{\psi}$. Thus, the velocity components u and v given in equation (5.10) in terms of derivatives of stream function at the required nodal points can be found by using equation (5.28). These obtained values of u and v will be used as constants in the solution of vorticity tranport equation.

(iv) Solve the vorticity transport equation (5.23). Since equation (5.23) involves $\dfrac{\partial \mathbf{w}}{\partial t}$, the vorticity is approximated by using the same coordinate function $f_j(x, y)$ as

$$w = \sum_{j=1}^{N+L} \beta_j(t) f_j(x, y) \tag{5.29}$$

where $\beta_j(t) = -\tilde{\alpha}_j$ are time dependent unknown coefficients as given in equation (5.16) and the system $\mathbf{w} = \mathbf{F}\boldsymbol{\beta}$ leads to the convective terms of

the vorticity

$$\frac{\partial \mathbf{w}}{\partial x} = \frac{\partial \mathbf{F}}{\partial x}\mathbf{F}^{-1}\mathbf{w}\,, \qquad \frac{\partial \mathbf{w}}{\partial y} = \frac{\partial \mathbf{F}}{\partial y}\mathbf{F}^{-1}\mathbf{w} \tag{5.30}$$

since $\boldsymbol{\beta} = \mathbf{F}^{-1}\mathbf{w}$.

Substituting convection terms back into equation (5.23) one can obtain

$$\frac{1}{Re}(\mathbf{H}\mathbf{w} - \mathbf{G}\frac{\partial \mathbf{w}}{\partial n}) = (\mathbf{H}\hat{\mathbf{U}} - \mathbf{G}\hat{\mathbf{Q}})\mathbf{F}^{-1}\left\{\frac{\partial \mathbf{w}}{\partial t} + u\frac{\partial \mathbf{F}}{\partial x}\mathbf{F}^{-1}\mathbf{w} + \mathbf{v}\frac{\partial \mathbf{F}}{\partial y}\mathbf{F}^{-1}\mathbf{w}\right\} \tag{5.31}$$

and finally rearranging, we end up with the following system of ordinary differential equations

$$\mathbf{C}\dot{\mathbf{w}} + \tilde{\mathbf{H}}\mathbf{w} - \tilde{\mathbf{G}}\frac{\partial \mathbf{w}}{\partial n} = 0 \tag{5.32}$$

where the matrices $\mathbf{C}$, $\tilde{\mathbf{H}}$ and $\tilde{\mathbf{G}}$ are

$$\begin{aligned} \mathbf{C} &= -(\mathbf{H}\hat{\mathbf{U}} - \mathbf{G}\hat{\mathbf{Q}})\mathbf{F}^{-1} \\ \tilde{\mathbf{H}} &= \frac{1}{Re}\,\mathbf{H} + \mathbf{C}\mathbf{R_1} + \mathbf{C}\mathbf{R_2} \\ \tilde{\mathbf{G}} &= \frac{1}{Re}\,\mathbf{G} \end{aligned} \tag{5.33}$$

and

$$\mathbf{R_1} = u\frac{\partial \mathbf{F}}{\partial x}\mathbf{F}^{-1}\,, \qquad \mathbf{R_2} = v\frac{\partial \mathbf{F}}{\partial y}\mathbf{F}^{-1}\,. \tag{5.34}$$

Now, from equation (5.32), the standard form of the first order initial value problem

$$\dot{\mathbf{w}} + \mathbf{B}\mathbf{w} = \mathbf{D}\frac{\partial \mathbf{w}}{\partial n} \tag{5.35}$$

is obtained, in which $\mathbf{B} = \mathbf{C}^{-1}\tilde{\mathbf{H}}$, $\mathbf{D} = \mathbf{C}^{-1}\tilde{\mathbf{G}}$ and superscript dot denotes the time derivative. Then, system (5.35) is integrated in time using differential quadrature method which enables us to obtain vorticity values at any required time level.

(v) Repeat steps (ii)-(iv) until the convergence is obtained. In our calculations we terminate the procedure when the difference between the values of ψ and w at two successive iterates in L_∞ norm is less than a preassigned tolerance.

5.1.2 Application of the DQM to vorticity transport equation

The differential quadrature method approximates the derivative of a smooth function at a grid point by a linear weighted summation of all the functional values in the whole computational domain, [47]. In this study DQM is employed to discretize the time derivative of $\mathbf{w}$ in equation (5.35).

The DQM analogue of the first order derivative of a function $f(t)$ at a grid point t_i can be expressed as

$$\left.\frac{df(t)}{dt}\right|_{t_i} = \sum_{j=1}^{K} a_{ij}^{(1)} f(t_j) \tag{5.36}$$

where $i = 1, 2, \ldots, K$ is the number of grid points t_i in the time direction and $a_{ij}^{(1)}$ are the weighting coefficients for the first order derivative approximations of $f(t)$, which are determined in Section 4.2.1 by using the polynomial based differential quadrature method [47, 62].

The weighting coefficients for the first order derivative are given as

$$a_{ij}^{(1)} = \frac{M^{(1)}(t_i)}{(t_i - t_j)\, M^{(1)}(t_j)} \qquad i \neq j\ ,\ \ i, j = 1, 2, \ldots, K \tag{5.37}$$

$$a_{ii}^{(1)} = -\sum_{j=1,\, j\neq i}^{K} a_{ij}^{(1)} \tag{5.38}$$

where

$$M^{(1)}(t_j) = \prod_{k=1,\, k\neq j}^{K} (t_j - t_k) \tag{5.39}$$

and

$$a_{ij}^{(1)} = a_j^{(1)}(t_i) \quad .$$

By using the DQM time approximation, the first order initial value problem (5.35) for vorticity w becomes

$$\sum_{j=1}^{K} a_{ij}^{(1)} \mathbf{w}_j + \mathbf{B}\mathbf{w}_i = \mathbf{D}\mathbf{q}_i \,, \qquad i = 1, 2, \ldots, K \tag{5.40}$$

where the vectors $\mathbf{w}_i$ and $\mathbf{q}_i$ are, infact, the vectors containing the values of vorticity w and $\dfrac{\partial w}{\partial n}$ respectively at the ith time level and they are given as

$$\begin{aligned} \mathbf{w}_i &= \left\{ w_{1i}, w_{2i}, \ldots, w_{Ni}, w_{(N+1)i}, \ldots, w_{(N+L)i} \right\} \\ \mathbf{q}_i &= \left\{ \left.\frac{\partial w}{\partial n}\right|_{1i}, \left.\frac{\partial w}{\partial n}\right|_{2i}, \ldots, \left.\frac{\partial w}{\partial n}\right|_{Ni}, 0, \ldots, 0 \right\} \end{aligned} \tag{5.41}$$

in which $w_{ji} = w_j(t_i)$ and $\left.\dfrac{\partial w}{\partial n}\right|_{ji} = \left.\dfrac{\partial w}{\partial n}\right|_{j} (t_i)$.

Equation (5.40) gives a system of linear equations for each time level t_i which can be denoted in matrix vector form

$$\mathbf{S}\tilde{\mathbf{W}} = \tilde{\mathbf{D}}\tilde{\mathbf{q}} \tag{5.42}$$

where

$$\mathbf{S} = \mathbf{A} + \tilde{\mathbf{B}} \ . \tag{5.43}$$

The matrices $\mathbf{A}$, $\tilde{\mathbf{B}}$ and $\tilde{\mathbf{D}}$ are expressed as

$$\mathbf{A} = \begin{bmatrix} \mathbf{a}_{11} & \mathbf{a}_{12} & \ldots & \mathbf{a}_{1K} \\ \mathbf{a}_{21} & \mathbf{a}_{22} & \ldots & \mathbf{a}_{2K} \\ \vdots & & & \\ \mathbf{a}_{K1} & \mathbf{a}_{K2} & \ldots & \mathbf{a}_{KK} \end{bmatrix} \tag{5.44}$$

with $(N+L) \times (N+L)$ submatrices $\mathbf{a}_{ij}$ defined as

$$\mathbf{a}_{ij} = a_{ij}^{(1)} \ \mathbf{I} \ ,$$

and

$$\tilde{\mathbf{B}} = \begin{bmatrix} \mathbf{B} & & & \\ & \mathbf{B} & & \\ & & \ddots & \\ & & & \mathbf{B} \end{bmatrix}, \qquad \tilde{\mathbf{D}} = \begin{bmatrix} \mathbf{D} & & & \\ & \mathbf{D} & & \\ & & \ddots & \\ & & & \mathbf{D} \end{bmatrix}. \tag{5.45}$$

The sizes of the matrices $\mathbf{S}$, $\tilde{\mathbf{B}}$, $\mathbf{A}$ and $\tilde{\mathbf{D}}$ are $(N+L)\,K \times (N+L)\,K$ and the identity matrix $\mathbf{I}$ is of size $(N+L) \times (N+L)$.

The $(N+L)\,K \times 1$ vectors $\tilde{\mathbf{W}}$ and $\bar{\mathbf{q}}$ are defined as

$$\tilde{\mathbf{W}} = \{w_{11}, w_{21}, \ldots, w_{(N+L)1}; w_{12}, w_{22}, \ldots, w_{(N+L)2}; \ldots \\ ; \ldots; w_{1K}, w_{2K}, \ldots, w_{(N+L)K}\} \tag{5.46}$$

$$\bar{\mathbf{q}} = \left\{ \left.\frac{\partial w}{\partial n}\right|_{11}, \left.\frac{\partial w}{\partial n}\right|_{21}, \ldots, \left.\frac{\partial w}{\partial n}\right|_{N1}, 0, \ldots, 0; \left.\frac{\partial w}{\partial n}\right|_{12}, \ldots, \left.\frac{\partial w}{\partial n}\right|_{N2}, 0, \ldots, 0; \ldots \right.$$

$$\left. ; \ldots; \left.\frac{\partial w}{\partial n}\right|_{1K}, \ldots, \left.\frac{\partial w}{\partial n}\right|_{NK}, 0, \ldots, 0 \right\}. \tag{5.47}$$

In the linear system (5.42) boundary conditions (some of $\tilde{\mathbf{W}}$ and some of $\tilde{\mathbf{q}}$ nodal specified values) are inserted by interchanging the negative of corresponding columns and reordering the solution vector in terms of unknown $\tilde{\mathbf{W}}$ and $\tilde{\mathbf{q}}$ nodal values. When the initial condition is also inserted at the interior plus boundary nodes for the initial time level, system (5.42) finally becomes a rectangular system since known initial $\tilde{\mathbf{W}}$ values are passed to the right hand side leaving less number of unknowns than the number of equations.

The resulting reordered form of system (5.42) is given as

$$\tilde{\mathbf{S}}\mathbf{X} = \mathbf{Y} \tag{5.48}$$

where the size of the matrix $\tilde{\mathbf{S}}$ is $((N+L)\,K - L) \times ((N+L)\,K - L)$. The

vectors $\mathbf{X}$ and $\mathbf{Y}$ are of the size $((N+L)\,K-L)\times 1$ if the boundary condition is of Dirichlet type. For Neumann type of boundary conditions the sizes of $\tilde{\mathbf{S}}$, $\mathbf{X}$ and $\mathbf{Y}$ are appropriately arranged. The vector $\mathbf{X}$ contains the unknown values of w and its normal derivative for each nodal points at all the required time levels whereas $\mathbf{Y}$ contains all boundary plus initial information. Therefore, once system (5.48) is solved, one can obtain the solution for vorticity on the entire domain at any time level at one stroke and then iteratively at steady state.

5.2 Numerical Results

Three test problems are considered. As a first example, the Navier-Stokes equations in a square domain ($0 \leq x,\, y \leq 1$), when an external force is present, is solved to see the accuracy and efficiency of present numerical method since the exact solution is available. The second example is the lid-driven cavity problem for which the fluid in the cavity is driven by the motion of the upper wall with a constant velocity. In the DRBEM discretization for the spatial domains, we use suitable number of constant boundary elements and some interior nodes for presenting the solution in terms of graphics. For the time domain Gauss-Chebyshev-Lobatto points are used in the differential quadrature discretization. The two-dimensional natural convection problem in a square cavity is also solved as a third application with the proposed iterative procedure. Now, the Navier-Stokes equations include the buoyancy force generated as a result of fluid density difference caused by the temperature difference. The buoyancy term is computed based on the Boussinesq approximation.

5.2.1 Navier-Stokes equations in a square

The aim of this first problem is to verify the accuracy of the proposed method. The equations now include a force term f as

$$\begin{aligned} \frac{\partial w}{\partial t} + u\frac{\partial w}{\partial x} + v\frac{\partial w}{\partial y} &= \frac{1}{Re}\nabla^2 w + f \\ \nabla^2 \psi &= w \end{aligned} \tag{5.49}$$

with no slip boundary conditions for the stream function (i.e. $\psi|_\Gamma = 0$) and $\frac{\partial \psi}{\partial n}|_\Gamma = 0$, where Γ is the boundary of the square domain $0 \leq x,\, y \leq 1$. Here the velocity field is given by $u = -\partial\psi/\partial y$ and $v = \partial\psi/\partial x$. Boundary conditions for the vorticity are taken from the exact solution, [66],

$$\begin{aligned} \psi &= -\sin t \sin^2 \pi x \sin^2 \pi y \\ w &= -\pi^2 \sin t(\cos 2\pi x + \cos 2\pi y - 2\cos 2\pi x \cos 2\pi y) \\ u &= \pi \sin t \sin 2\pi y \sin^2 \pi x \\ v &= -\pi \sin t \sin 2\pi x \sin^2 \pi y \end{aligned} \tag{5.50}$$

and the force is given by

$$\begin{aligned} f = \; & -\pi^2 \cos t(\cos 2\pi x + \cos 2\pi y - 2\cos 2\pi x \cos 2\pi y) \\ & +\pi^4 \sin^2 t \sin 2\pi x \sin 2\pi y(\cos 2\pi x - \cos 2\pi y) \\ & -\frac{4}{Re}\pi^4 \sin t(\cos 2\pi x + \cos 2\pi y - 4\cos 2\pi x \cos 2\pi y)\,. \end{aligned} \tag{5.51}$$

In the DRBEM discretization we use N constant boundary elements ranging from $N = 64$ to 80 and $K = 4$ GCL points are taken in the time discretization for DQM. In Figures 5.1, 5.2 and 5.3 the agreement of numerical solutions with exact ones is depicted for both the stream function and the vorticity in terms of contours at several time levels for the Reynolds number $Re = 500$, 1500 and 2000 respectively. It is noted that this viscous flow problem has the particularity of having a flow pattern, which is independent of the Reynolds number.

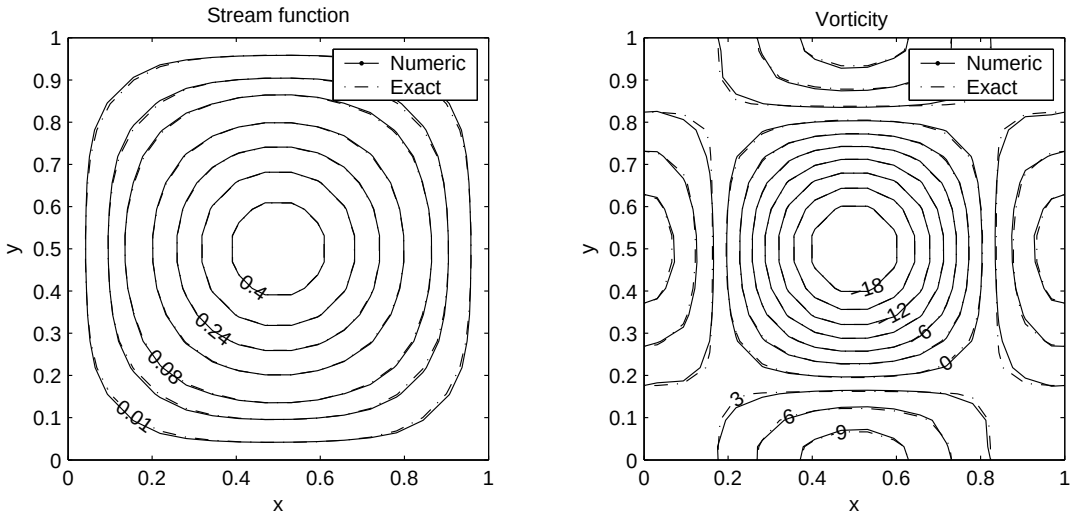

Figure 5.1: Stream function and vorticity contours for $Re = 500$, $N = 64$, $K = 4$, $T = 10$

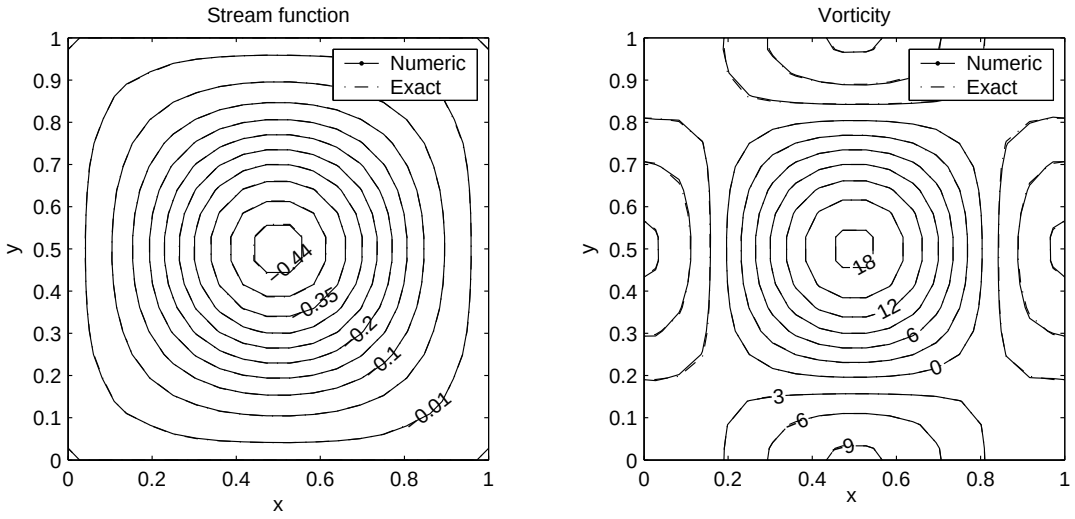

Figure 5.2: Stream function and vorticity contours for $Re = 1500$, $N = 72$, $K = 4$, $T = .5$

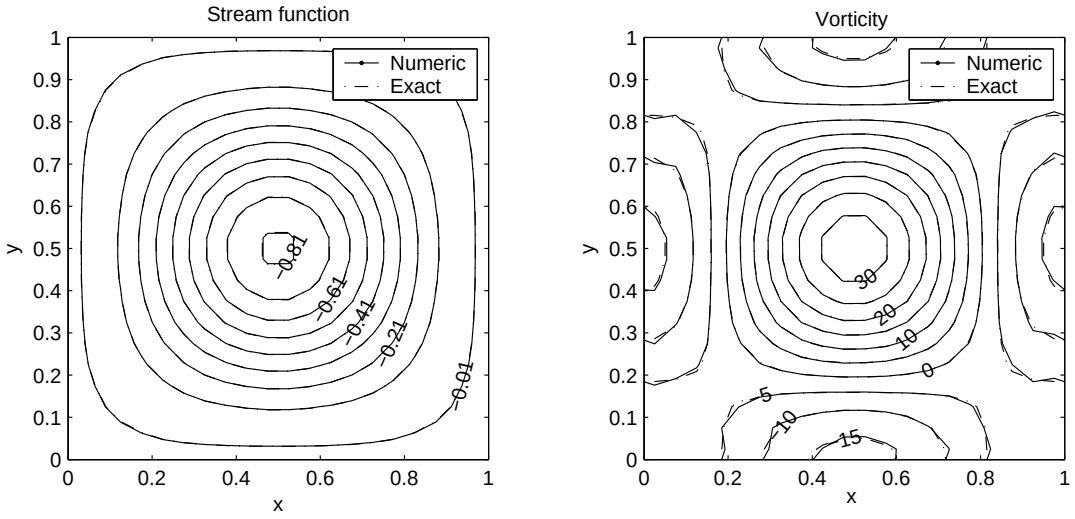

Figure 5.3: Stream function and vorticity contours for $Re = 2000$, $N = 80$, $K = 4$, $T = 1$

5.2.2 Lid-driven cavity flow

The second problem is the classical lid-driven cavity flow in a square domain $\Omega = [0, 1] \times [0, 1]$ containing a recirculating flow induced by the motion of the lid, [67].

We consider the equations governing the transient, laminar flow of a viscous incompressible fluid in a square cavity. The fluid in the cavity is driven by the motion of the upper wall which is assumed to move with a constant velocity $u = -1$. The governing equations are given by

$$\frac{1}{Re}\nabla^2 w = \frac{\partial w}{\partial t} + u\frac{\partial w}{\partial x} + v\frac{\partial w}{\partial y}$$

$$\nabla^2 \psi = -w\,.$$

The velocities and the stream function are prescribed on the boundaries of the square cavity (Figure 5.4) bounded by three motionless walls and by fourth wall moving in its own plane. These boundary conditions are used for the solution of the stream function.

In order to solve the vorticity transport equation, vorticity boundary con-

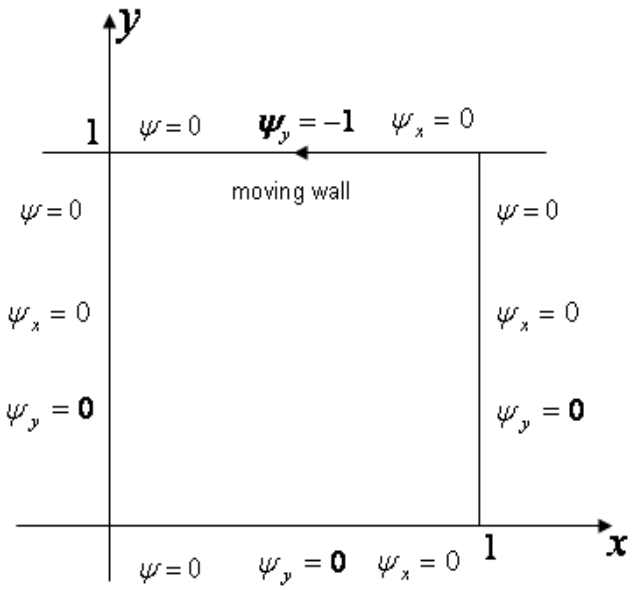

Figure 5.4: Boundary conditions for the lid-driven cavity problem

ditions are required and these values can be approximated from the discretized stream function equation using the relation

$$w_{i,j} = -\nabla^2 \psi_{i,j} \, . \tag{5.52}$$

The boundary approximation for w is obtained on any boundary by taking

$$\psi_{nn}|_0 = \alpha_0 \psi_0 + \alpha_1 \psi_p + \alpha_2 \psi_q + \alpha_3 \psi_n|_0 \tag{5.53}$$

where subscripts 0, p and q indicate ψ values on the boundary mesh point, ph and qh distances away from the boundary respectively, as shown in Figure 5.5.

The expansion of ψ_p and ψ_q into Taylor series about the mesh point numbered

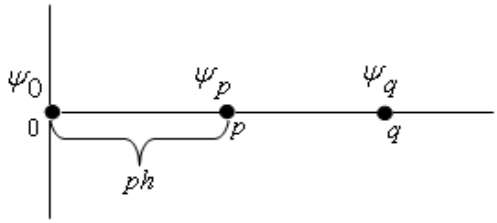

Figure 5.5: ψ values on the boundary mesh points

0 and reorganization of terms gives

$$\begin{aligned}\psi_{nn}|_0 = \psi_0(\alpha_0+\alpha_1+\alpha_2) + \psi_n|_0(ph\alpha_1 + qh\alpha_2 + \alpha_3) \\ +\psi_{nn}|_0(\frac{p^2h^2}{2}\alpha_1 + \frac{q^2h^2}{2}\alpha_2) + \dots .\end{aligned} \tag{5.54}$$

In this latter equality, by setting the corresponding terms equal we obtain the solution

$$\begin{aligned}\alpha_0 &= \frac{-2(p^3-q^3)}{h^2p^2q^2(p-q)}, \qquad \alpha_1 = \frac{-2q}{h^2p^2(p-q)} \\ \alpha_2 &= \frac{-2p}{h^2q^2(p-q)}, \qquad \alpha_3 = \frac{-2(p+q)}{hpq}\end{aligned} \tag{5.55}$$

where p and q are positive integers and $p \neq q$. Thus, the boundary approximation becomes

$$\begin{aligned}w_0 = -h^{-2}\Bigg[-\frac{2(p^3-q^3)}{p^2q^2(p-q)}\psi_0 - \frac{2q}{p^2(p-q)}\psi_p \\ +\frac{2p}{q^2(p-q)}\psi_q - \frac{2h(p+q)}{pq}\psi_n|_0\Bigg]\end{aligned} \tag{5.56}$$

which involves the unknown ψ values at distances ph and qh along the normal and has a truncation error of order h^2. Since boundary values of ψ, ψ_x, ψ_y for the cavity flow are given, the boundary values of w can be obtained from equation (5.56).

In the computations $p = 2$ and $q = 1$ are taken. We use $N = 56$, 88 and 112 constant boundary elements and $K = 3$, 2 and 2 time discretization points for the values of Reynolds number $Re = 100$, 500 and 1000, respectively. The steady state stream function and the vorticity values are obtained after 59, 116 and 200 iterations with an accuracy 10^{-4} for the Reynolds number $Re = 100$, 500 and 1000 and these results are presented, respectively in Figures 5.6, 5.7 and 5.8.

At a Reynolds number of around 100, the streamline primary vortex moves towards the left hand wall. At Reynolds numbers of $Re = 500$ and $Re = 1000$ the primary vortex starts to move towards the cavity center. As the Reynolds number increases up to 500 the recirculations appear at the lower corners for the streamlines. At $Re = 1000$ the recirculation close to upper right corner shows up since the fluid movement is affected with the velocity of the lid which moves to the left. As Re increases, the vorticity contours move away from the cavity center towards the cavity walls indicating that strong vorticity gradients develop on the lid and the cavity walls (especially $x = 0$ wall). The fluid begins to rotate with a constant angular velocity. These behaviours are in good agreement with the behaviours observed in [54, 68, 69].

The numbers of the boundary elements N and the time points K for one time block are so small that the whole procedure is still more economical than the FDM which has to use very small time increment for stability. Although, there is no certain relationship between N, K and L on the accuracy and the convergence of the numerical solution, one should be careful in the choice of N, K and L for not having an oversized final linear system of equations for the solution. Thus, the application of the present method to the three-dimensional problems is not recommended since one has to deal with much larger matrices.

Figures 5.9 and 5.10 show the velocity profiles for u along vertical line ($x = 0.5$) and v along horizontal line ($y = 0.5$) passing through the geometric center of the cavity for the values of Reynolds number $Re = 100$ and 400. The numerical results obtained by the coupling of the DRBEM and DQM is compared with the results of Ghia [67] (by taking $u = 1$ on the upper lid as is done in [67]) and it is observed that they are in good agreement.

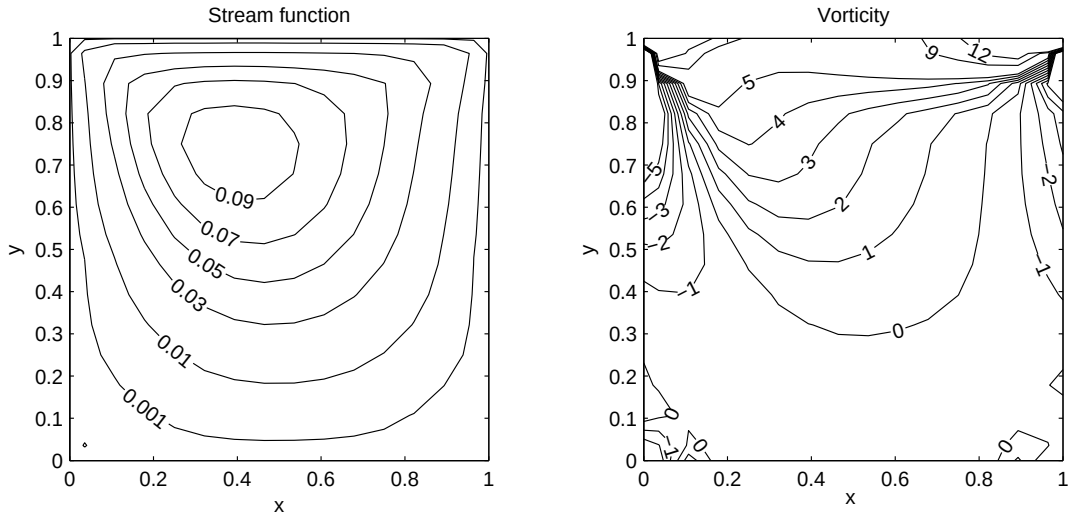

Figure 5.6: Stream function and vorticity contours for $Re = 100$, $N = 56$, $K = 3$

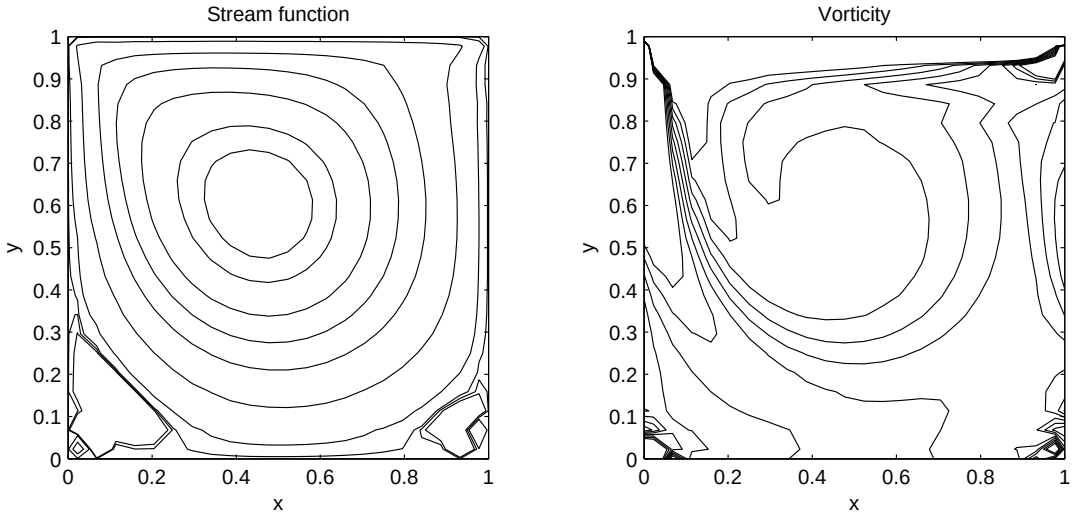

Figure 5.7: Stream function and vorticity contours for $Re = 500$, $N = 88$, $K = 2$

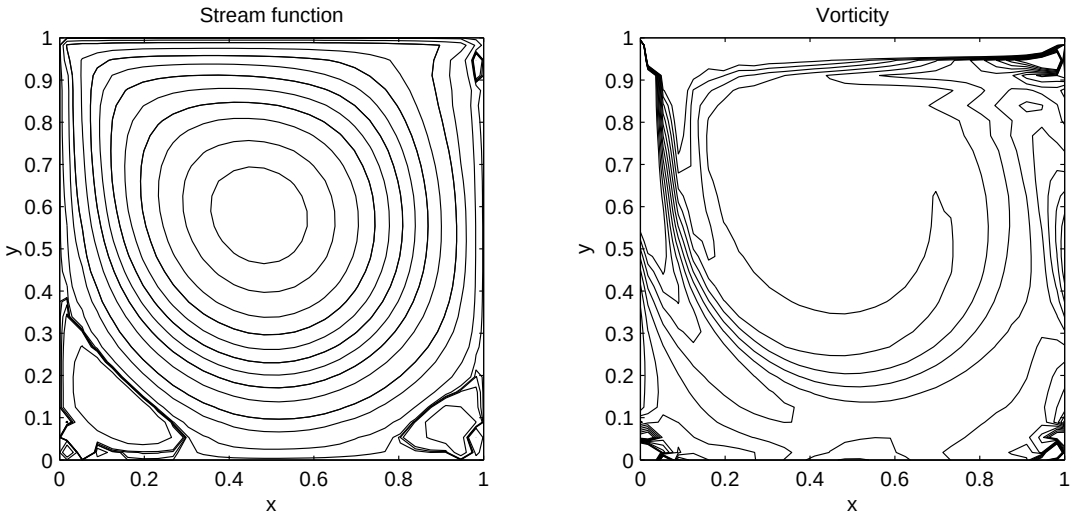

Figure 5.8: Stream function and vorticity contours for $Re = 1000$, $N = 112$, $K = 2$

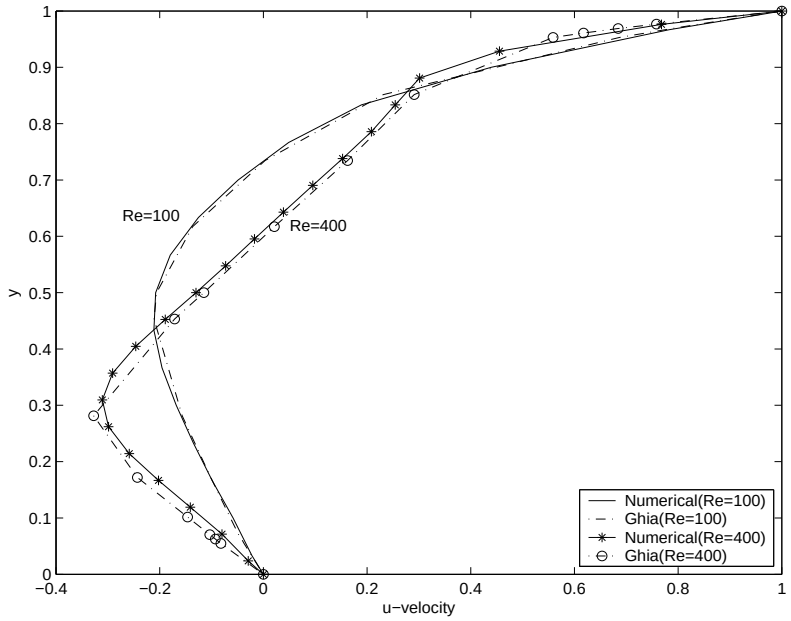

Figure 5.9: u-velocity along vertical line ($x = 0.5$)

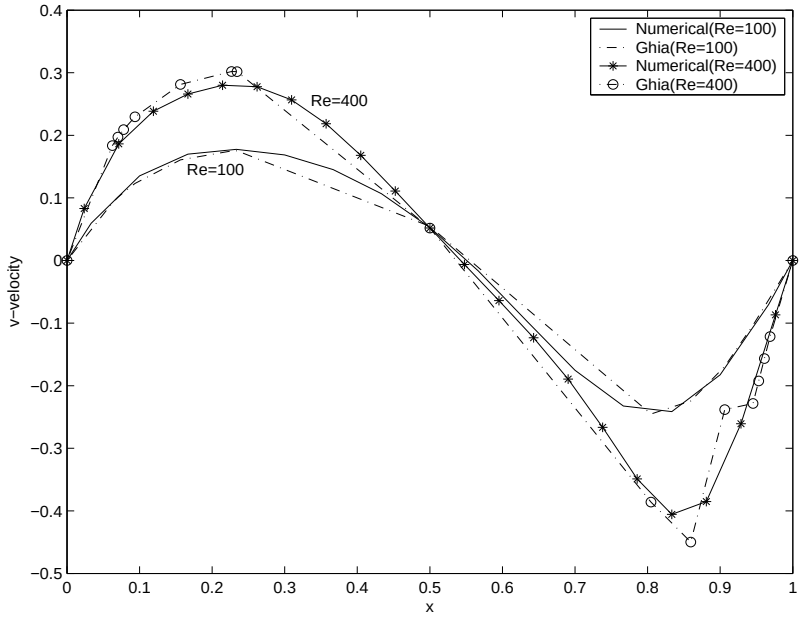

Figure 5.10: v-velocity along horizontal line (y=0.5)

5.2.3 Natural convection in a square cavity

In situations where the fluid may be treated as incompressible and temperature differences are small, momentum equations (5.3) and the continuity equation (5.4) are sufficient to specify the velocities and pressure. If heat flux occurs (temperature not constant), at least one additional equation is required. In some of these instances, the energy equation may be used. Natural convection in a differentially heated enclosure which is a popular problem as testing any proposed numerical scheme is added here since the governing equations can be treated easily with the proposed method. The vorticity transport equation is coupled to the energy equation through the buoyancy force $RaPr\dfrac{\partial T}{\partial x}$ and the energy equation is exactly in the same form (convection term multipliers are the velocity components) of vorticity transport equation for the Navier-Stokes equations.

The equations are given as, [55, 57],

$$\begin{aligned} \frac{\partial w}{\partial t} + u\frac{\partial w}{\partial x} + v\frac{\partial w}{\partial y} &= Pr\nabla^2 w + RaPr\frac{\partial T}{\partial x} \\ \nabla^2 \psi &= w \\ \frac{\partial T}{\partial t} + u\frac{\partial T}{\partial x} + v\frac{\partial T}{\partial y} &= \nabla^2 T \end{aligned} \tag{5.57}$$

where $L^{'}$, $\alpha/L^{'}$, $\alpha/L^{'^2}$, $L^{'^2}/\alpha$ and $T = (\theta^{'} - \theta_c^{'})/(\theta_h^{'} - \theta_c^{'})$ are used as scaled factors for length, velocity, vorticity, time and temperature in the above nondimensional form of the governing equations. The nondimensional parameters are defined as Rayleigh number, $Ra = g\beta(T_s - T_\infty)L^{'3}/\alpha\nu$, and Prandtl number, $Pr = \nu/\alpha$. Here α is the thermal diffusivity, g gravitational acceleration, β is the coefficient of thermal expansion, T_s is the temperature of wall and T_∞ is the fluid temperature far from the surface of the object.

Equation (5.57) is subjected to initial conditions

$$w = T = 0\,. \tag{5.58}$$

The no-slip boundary conditions of the velocity at boundary walls are assumed. Temperature has Dirichlet type conditions as 1 and 0 at the left and right walls of the cavity $[0,1]\times[0,1]$ whereas adiabatic conditions $\dfrac{\partial T}{\partial y} = 0$ are imposed on the top and bottom (see Figure 5.11). The proposed coupled numerical algorithm is applied to determine the stream function, vorticity and temperature variations with the given initial values iteratively.

In Figure 5.12 we present streamlines, vorticity and temperature contours at steady state for $Ra = 10^3$, 10^4 and 10^5 with the number of constant boundary elements $N = 48$, 64 and 80 respectively. As the Rayleigh number increases the boundary layer formation starts for all the variables stream function, vorticity and isotherms near the walls $x = 0$ and $x = 1$. It is also observed from isotherms that the temperature contours undergo an inversion at the central region of the cavity. The primary vortex of the stream lines tends to seperate and form two

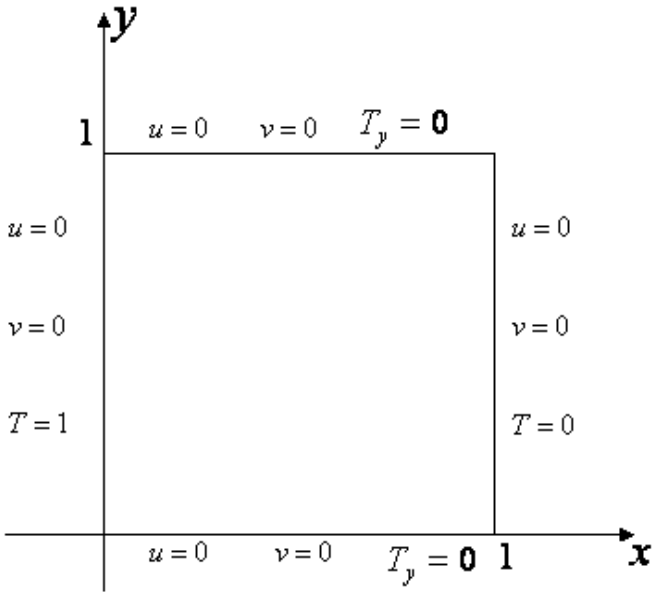

Figure 5.11: Boundary conditions for the natural convection flow

vortices through the corners $(0, 1)$ and $(1, 0)$ as the Rayleigh number increases. These behaviours are in good agreement with the previously published results [55, 56, 57]. The obtained results indicate that present method is capable of handling high Rayleigh number without difficulties and with a considerable small number of mesh points.

In Table 5.1, the values of the Nusselt number on the vertical boundary at $x = 0$, Nu_0, and the average Nusselt number throughout the cavity, $\overline{Nu}$, obtained by the present study are compared with the benchmark solution given by Davis, [70], for $Ra = 10^3$, 10^4 and 10^5. As Rayleigh number increases we need to take more boundary elements to obtain better accuracy. Although there are some differences in the values in Table 5.1, the flow patterns obtained by the coupling of the DRBEM and DQM show no distinguishable difference.

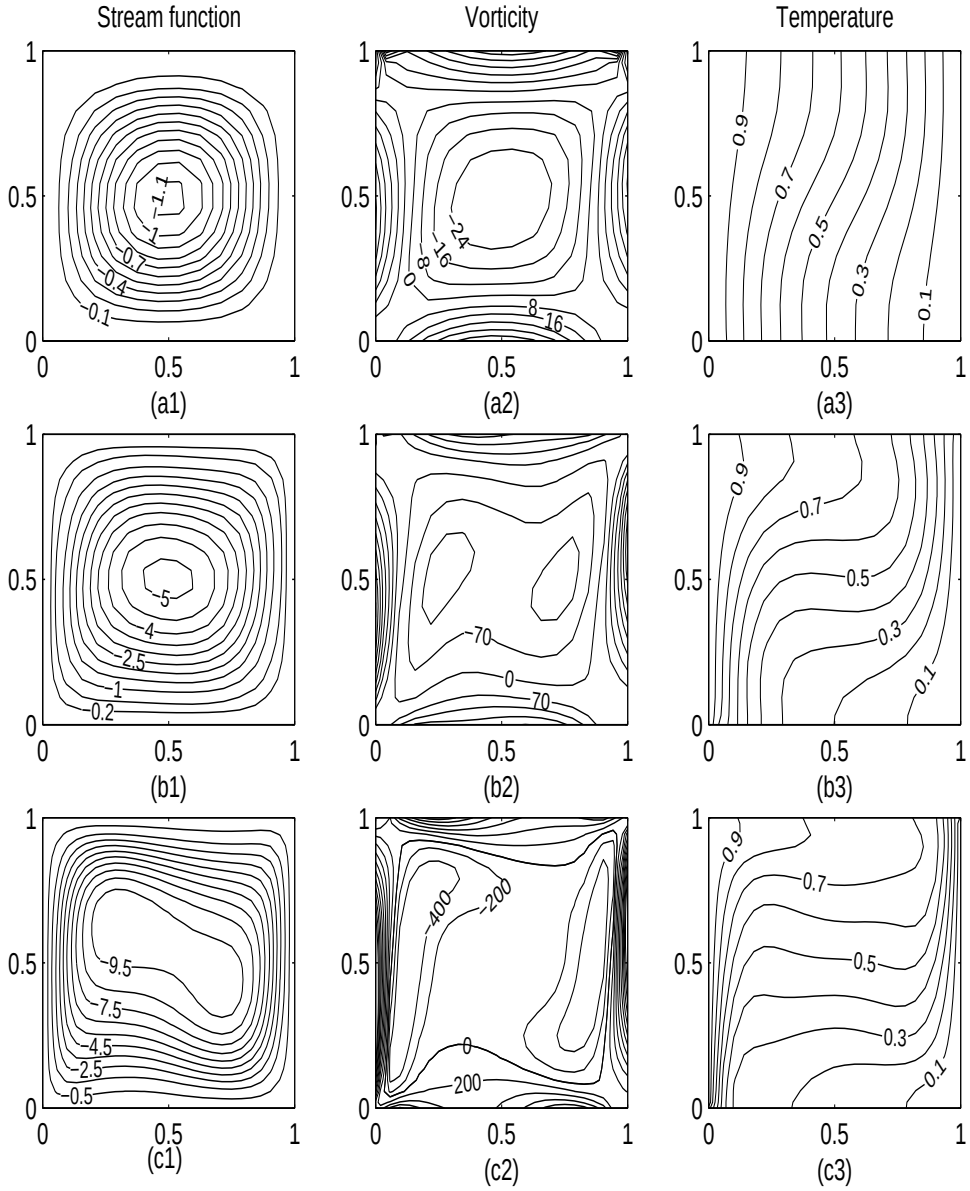

Figure 5.12: Stream function, vorticity and temperature contours: $(a1 - a3)$ $Ra = 10^3$, $N = 48$, $K = 3$; $(b1 - b3)$ $Ra = 10^4$, $N = 64$, $K = 2$ and $(c1 - c3)$ $Ra = 10^5$, $N = 100$, $K = 2$

Table 5.1: Numerical results of natural convection for $Ra = 10^3$, 10^4 and 10^5

	$Ra = 10^3$		$Ra = 10^4$		$Ra = 10^5$	
	Nu_0	$\overline{Nu}$	Nu_0	$\overline{Nu}$	Nu_0	$\overline{Nu}$
DRBEM&DQM	1.118	1.105	2.274	2.352	4.376	4.369
Davis[70]	1.117	1.118	2.238	2.243	4.509	4.519

As a result, the transient two-dimensional Navier-Stokes equations in stream function-vorticity form are solved by using the dual reciprocity BEM in spatial and DQM in time domains. The DQM discretization in time direction results in a system of linear algebraic equations which gives the solution vector for vorticity at the required time levels at one stroke. The vorticity boundary conditions are computed by a finite difference formula which uses both the boundary and interior stream fuction values. The proposed numerical algorithm is also applicable for the solution of natural convection in a square cavity. It gives very good accuracy with a considerable small number of mesh points in both space and time directions.

CHAPTER 6

CONCLUSION

This thesis, in general, is devoted to the numerical solutions of convection-diffusion type equations using the boundary element method. We consider the problems in two groups, mainly steady and unsteady differential equations, and solve by using the direct BEM and the dual reciprocity BEM, respectively.

First, the fundamental solution of steady magnetohydrodynamic flow equations in the original coupled form which are convection-diffusion type is established to be able to apply the BEM directly with the most general form of wall conductivities. The applications are given for the pressure driven MHD flows in rectangular ducts with insulating and/or conducting, partly insulating partly conducting walls, and then for electrically driven MHD flows in infinite regions. The case of inclined applied external magnetic field is also considered. As the value of the Hartmann number M, increases boundary layer formation starts to take place at the insulated parts of the boundary. With the increase in the length of the conducting part, a stagnant region develops and the induced magnetic field has its maximum value in front of the conducting portion. These are the well known characteristics of the MHD duct flow. Also, as M increases parabolic boundary layers form emanating from the points of discontinuities. For the MHD flow on the upper half plane with mixed boundary conditions on the x-axis, similar results are observed for increasing M and the length of the conducting portion. The boundary layer thicknesses are also computed directly from the boundary element formulations of MHD flow in infinite regions. The thickness of the boundary layer (Hartmann layer) near the insulated walls, which are perpendicular to the applied magnetic field, is of order $1/M$. The thickness of the parabolic boundary layer which emanates from the point where the conductivity changes is computed and found to be of order $1/\sqrt{M}$. This is also in accordance

with the secondary boundary layer in rectangular ducts. It is also noticed that an increase in M needs more boundary elements for obtaining accurate solutions. The BEM application with the derived fundamental solution also enables one to obtain solutions for high values of Hartmann number.

In the second part of the thesis, the unsteady differential equations are solved by a numerical scheme which is the coupling of the dual reciprocity BEM with the differential quadrature method. The DRBEM and DQM are used in the discretization of spatial and time domains, respectively. The DRBEM is preferred since it gives the flexibility of using fundamental solution of Laplace equation which is rather simple to implement. Thus, it is possible to treat the space and the time derivatives of the unknown as well as the unknown itself, and the nonlinear terms in the equation as the nonhomogeneity. The DRBEM application results in a system of initial value problems in time which is going to be solved by a time integration scheme. Then, the application of the DQM for the time derivatives in these ordinary differential equations gives an algebraic system of equations to be solved for the unknown nodal values containing both discretized space and time points on the whole computational domain. Thus, one can obtain the solution at any required time level including steady state at one stroke and without the need of a time iteration which usually needs very small time increments for stability. Another advantage is that the DQM allows one to use large step sizes since it is unconditionally stable. The proposed method is general in the sense that it is applicable to both linear and nonlinear equations. The diffusion equation in a circle with mixed type boundary conditions, variable coefficient convection-diffusion equations, and also unsteady MHD duct flow equations with insulating walls conditions are solved giving very good accuracy and the solutions are stable. Elastodynamic problems containing second order time derivatives are also solved since DQM is suitable for higher order derivatives. Finally, the solution of the Navier-Stokes equations which are nonlinear in nature is able to be obtained with this procedure. Applications are on the lid-driven cavity flow and natural convection flow in a square cavity. One is able to obtain solutions for the values of Reynolds number up to 1000 in the Navier-Stokes equations and Rayleigh number values up to 10^5 in natural convection flow.

Further investigations could be concentrated on obtaining solutions for higher values of Reynolds and Rayleigh numbers in solving Navier-Stokes and natural convection equations respectively. We also believe that the procedure outlined in Chapter 3 for deriving the fundamental solution of coupled MHD equations, can be extended for the derivation of fundamental solution of Navier-Stokes equations. Since the Navier-Stokes equations are coupled and nonlinear in nature, this needs further studies on coupled partial differential equations.

REFERENCES

[1] Brebbia, C.A. *The Boundary Element Method for Engineers*, Pentech Press, London, (1978).

[2] Brebbia, C.A., Telles, J.C.F. and Wrobel, L.C. *Boundary Element Techniques*, Springer-Verlag, Berlin and New York, (1984).

[3] Brebbia, C.A. and Dominguez, J. *Boundary Elements: An Introductory Course*, Computational Mechanics Publications, Southampton and McGraw-Hill, New York, (1989).

[4] Banerjee, P.K. and Butterfield, R. *Boundary Element Methods in Engineering Science*, McGraw-Hill, London, (1981).

[5] Kythe, Prem K. *Fundamental Solutions for Differential Operators and Applications*, The Maple Press Company, Boston: Birkhäuser, (1996).

[6] Pozrikidis, C. *A Practical Quide to Boundary Element Method with The Software Library BEMLIB*, Chapman and Hall, (2002).

[7] Dragoş, L. *Magneto-Fluid dynamics*, Abacus Press: England, (1975).

[8] Shercliff, J.A. *Steady motion of conducting fluids in pipes under transverse fields*, Proc. Camb. Phil. Soc., **49**, 136-144, (1953).

[9] Singh, B. and Lal, J. *MHD axial flow in a triangular pipe under transverse magnetic field*, Indian J. Pure Appl. Math., **9(2)**, 101-115, (1978).

[10] Singh, B. and Lal, J. *MHD axial flow in a triangular pipe under transverse magnetic field parallel to a side of the triangle*, Indian J. Tech., **17**, 184-189, (1979).

[11] Singh, B. and Lal, J. *Finite element method in magnetohydrodynamic channel flow problems*, Int. J. Numer. Meth. Engng., **18(7)**, 1104-1111, (1982).

[12] Singh, B. and Lal, J. *Finite element method for unsteady MHD flow through pipes with arbitrary wall conductivity*, Int. J. Numer. Meth. Fluids, **4**, 291-302, (1984).

[13] Gardner, L.R.T. and Gardner, G.A. *A two dimensional bi-cubic B-spline finite element: used in a study of MHD-duct flow*, Comput. Methods Appl. Mech. Engng. , **124(4)**, 365-375, (1995).

[14] Tezer-Sezgin, M. and Köksal, S. *Finite element method for solving MHD flow in a rectangular duct*, Int. J. Numer. Meth. Engng., **28**, 445-459, (1989).

[15] Demendy, Z. and Nagy, T. *A new algorithm for solution of equations of MHD channel flows at moderate Hartmann numbers*, Acta Mech., **123**, 135-149, (1997).

[16] Barrett K.E., *Duct flow with a transverse magnetic field at high Hartmann numbers*, Int. J. Numer. Meth. Engng., **50**, 1893-1906, (2001).

[17] Neslitürk, A.I. and Tezer-Sezgin, M. *The finite element method for MHD flow at high Hartmann numbers*, Comput. Meth. Appl. Mech. Engng., **194**, 1201-1224, (2005).

[18] Neslitürk, A.I. and Tezer-Sezgin, M. *Finite element method solution of electrically driven magnetohydrodynamic flow*, J. Comput. Appl. Math., **192(2)**, 339-352, (2006).

[19] Singh, B. and Agarwal, P.K. *Numerical solution of a singular integral equation appearing in magnetohydrodynamics*, ZAMP, **35**, 760-770, (1984).

[20] Tezer-Sezgin, M. *Boundary element method solution of MHD flow in a rectangular duct*, Int. J. Numer. Meth. Fluids, **18**, 937-952, (1994).

[21] Liu, H.W. and Zhu, S.P. *The dual reciprocity boundary element method for magnetohydrodynamic channel flows*, ANZIAM J., **44(2)**, 305-322, (2002).

[22] Tezer-Sezgin, M. and Aydın, S.H. *Dual reciprocity BEM for MHD flows using radial basis functions*, Int. J. Comput. Fluid Dyns., **16(1)**, 49-63, (2002).

[23] Carabineanu, A., Dinu, A. and Oprea, I. *The application of the boundary element method to the magnetohydrodynamic duct flow*, ZAMP, **46**, 971-981, (1995).

[24] Carrer, J.A.M. and Mansur, W.J. *Time-domain BEM analysis for the 2D scalar wave equation: initial conditions contributions to space and time derivatives*, Int. J. Numer. Meth. Engng., **39**, 2169-2188, (1996).

[25] Mansur, W.J., Carrer, J.A.M. and Siqueria, E.F.N. *Time discontinuous linear traction approximation in time-domain BEM scalar wave propagation analysis*, Int. J. Numer. Meth. Engng., **42**, 667-683, (1998).

[26] Carrer, J.A.M. and Mansur, W.J. *Time-dependent fundamental solution generated by a not impulsive source in the boundary element method analysis of the 2D scalar wave equation*, Commun. Numer. Meth. Engng, **18**, 277-285, (2002).

[27] Nardini, D. and Brebbia, C.A. *A new approach to free vibration analysis using boundary elements*, Boundary Element Methods in Engineering, Computational Mechanics Publications, Southampton and Springer-Verlag, Berlin and New York, (1982).

[28] Wrobel, L.C., Brebbia, C.A. and Nardini, D. *The dual reciprocity boundary element method formulation for transient heat conduction*, Finite Elements in Water Resources VI, Computational Mechanics Publications, Southampton and Springer-Verlag, Berlin and New York, (1986).

[29] Partridge, P.W. and Brebbia, C.A. *Computer Implementation of the BEM dual reciprocity method for the solution of Poisson type equations*, Software for Engineering Workstations, **5(4)**, 199-206, (1989).

[30] Partridge, P.W. and Wrobel, L.C. *The dual reciprocity boundary element method for spontaneous ignition*, Int. J. Numer. Meth. Engng., **30**, (1990).

[31] Brebbia, C.A., Partridge, P.W. and Wrobel, L.C. *The Dual Reciprocity Boundary Element Method*, Computational Mechanics Publications, Southampton Boston, (1992).

[32] Carslaw, H.S. and Jaeger, J.C. *Conduction of Heat in Solids*, Clarendon Press, Oxford, (1959).

[33] Huerta, M., Roig, B. and Donea, J.S. *Time-accurate solution of stabilized convection-diffusion-reaction equations: II-accuracy analysis and examples*, Commun. Numer. Meth. Engng. **18**, 575-584, (2002).

[34] Nardini, D. and Brebbia, C.A. *A new approach to free vibration analysis using boundary elements*, Appl. Math. Model., **7**, 157-162, (1983).

[35] Nardini, D. and Brebbia, C.A. *Transient dynamic analysis by boundary element method*, Boundary Elements, Brebbia CA (ed). Springer: Berlin, 719-730, (1983).

[36] Tanaka, M. and Chen, W. *Dual reciprocity BEM applied to transient elastodynamic problems with differential quadrature method in time*, Comput. Method Appl. Mech. Engng. **190**, 2331-2347, (2001).

[37] Timoshenko, S., Young, D.H. and Weaver, W. *Vibration Problems in Engineering*, John Wiley & Sons, New York, (1974).

[38] Chen, W. and Tanaka, M. *A study on time schemes for DRBEM analysis of elastic impact wave*, Comput. Mech., **28**, 331-338, (2002).

[39] Gaul, L. *The influence of damping on waves and vibrations*, Mech. Syst. Signal Pr., **13(1)**, 1-30, (1999).

[40] Singh, K.M. and Kalra, S. *Time integration in the dual reciprocity boundary element analysis of transient diffusion*, Eng. Anal. Bound. Elem., **18**, 73-102, (1996).

[41] Singh, K.M. and Kalra, S. *Least-squares finite element schemes in the time domain*, Comput. Methods Appl. Mech. Engng., **190**, 111-131, (2000).

[42] Chawla, M.M. and Al-Zanaidi, M.A. *An extended trapezoidal formula for the diffusion equation in two space dimensions*, Int. J. Computs. Maths. Appl., **42**, 157-168, (2001).

[43] Partridge, P.W. and Sensale, B. *The method of fundamental solutions with dual reciprocity for diffusion and diffusion-convection using subdomains*, Eng. Anal. Bound. Elem., **24**, 633-641, (2000).

[44] Tanaka, M. and Chen, W. *Coupling dual reciprocity BEM and differential quadrature method for time-dependent diffusion problems*, Appl. Math. Model., **25**, 257-268, (2001).

[45] Loeffler, C.F. and Mansur, W.J. *Analysis of time integration schemes for boundary element applications to transient wave propagation problems*, In BETECH' 87, Computational Mechanics Publication, Southampton, (1987).

[46] Chien, C.C., Chen, Y.A. and Chueng, C.C. *Dual reciprocity BEM analysis of 2D transient elastodynamic problems by time discontinuous Galerkin FEM*, Eng. Anal. Bound. Elem., **27**, 611-624, (2003).

[47] Shu, C. *Differential Quadrature and Its Applications in Engineering*, Springer-Verlag London Limited, (2000).

[48] Bellman, R.E., Kashef, B.G. and Casti, J. *Differential quadrature: a technique for the rapid solution of nonlinear partial differential equations*, J. Comput. Phys., **10**, 40-52, (1972).

[49] Shu, C. and Chew, Y.T. *Fourier expansion-based differential quadrature and its application to Helmholtz eigenvalue problems*, Commun. Numer. Meth. Engng., **13(8)**, 643-653, (1997).

[50] Wong, J.C.F. and Chan, M.K.H. *A consistent splitting scheme for unsteady incompressible viscous flows I. Dirichlet boundary condition and applications*, Int. J. Numer. Meth. Fluids, **51**, 385-424, (2006).

[51] Erturk, E., Corke, T.C. and Gökçöl, C. *Numerical solutions of 2-D incompressible driven cavity flow at high Reynolds numbers*, Int. J. Numer. Meth. Fluids, **48**, 747-774, (2005).

[52] Wu, Y. and Liao, S. *Solving high Reynolds-number viscous flows by the general BEM and domain decomposition method*, Int. J. Numer. Meth. Fluids, **47**, 185-199, (2005).

[53] Sousa, E. and Sobey, I.J. *Effect of boundary vorticity discretization on explicit stream-function vorticity calculations*, Int. J. Numer. Meth. Fluids, **49**, 371-393, (2005).

[54] Ghadi, F., Ruas, V. and Wakrim, M. *Numerical solution of the time-dependent incompressible Navier-Stokes equations by piecewise linear finite elements*, J. Comput. Appl. Maths., **215**, 429-437, (2008).

[55] Lo, D.C. and Young, D.L., Tsai, C.C. *High resolution of 2D natural convection in a cavity by the DQ method*, J. Comp. Appl. Math., **203**, 219-236, (2007).

[56] Ding H., Shu C., Yeo, K.S., Xu D. *Development of least-square-based two dimensional finite-difference schemes and their application to simulate natural convection in a cavity*, Comput. & Fluids, **33**, 137-154, (2004).

[57] Shu, C. and Xue, H. *Comparison of two approaches for implementing stream function boundary conditions in DQ simulation of natural convection in a square cavity*, Int. J. Heat Fluid Fl., **19**, 59-68, (1998).

[58] Kobayashi, M.H. and Pereira, J.M. *A computational stream function method for two-dimensional incompressible viscous flows*, Int. J. Numer. Meth. Engng, **62**, 1950-1981, (2005).

[59] John, F. *Partial Differential Equations*, 4th Edition, Springer-Verlag: New York, (1982).

[60] Hunt, J.C.R. *Magnetohydrodynamic flow in rectangular ducts*, J. Fluid Mech., **21**, 577-590, (1965).

[61] Hunt, J.C.R. and Shercliff, J.A. *Magnetohydrodynamics at high Hartmann number*, Annual Review of Fluid Mechanics, **3**, 37-62, (1971).

[62] Shu, C. and Richards, B.E. *Application of generalized differential quadrature to solve two-dimensional incompressible Navier-Stokes equations*, Int. J. Numer. Meth. Fluids, **15**, 791-798, (1992).

[63] Shu, C. and Chen, W. *On optimal selection of interior points for applying discretized boundary conditions in DQ vibration analysis of beams and plates*, J. Sound Vib., **222(2)**, 239-257, (1999).

[64] DeFigueiredo, D.B. *Boundary Element Analysis of Convection Diffusion Problems*, Lecture Notes in Engineering Series. Berlin: Springer, (1991).

[65] Wrobel, L.C., Telles, J.C.F and Brebbia, C.A. *A dual reciprocity boundary element formulation for axisymmetric diffusion problems*, Boundary Elements VIII Conf., pp. 59-69, Springer-Verlag, Comp. Mech. Pub., (1986).

[66] Yun-Xin, Z. and Yong-Ji, T. *Meshless schemes for unsteady Navier-Stokes equations in vorticity formulation using radial basis functions*, J. Comput. Appl. Maths., **192**, 328-338, (2006).

[67] Ghia, U., Ghia, N., and Shin, C.T. *High-Re solutions for incompressible flow using the Navier-Stokes equations and a multigrid method*, J. Comput. Phys., **48**, 387-411, (1982).

[68] Şahin, M. and Owens, R.G. *A novel fully implicit finite volume method applied to lid-driven cavity problem – Part I: High Reynolds number flow calculations*, Int. J. Numer. Meth. Fluids, **42**, 57-77, (2003).

[69] Wu, J.S. and Shao, Y.L. *Simulation of lid-driven cavity flows by parallel lattice Boltzmann method using multi-relaxation-time scheme*, Int. J. Numer. Meth. Fluids, **46**, 921-937, (2004).

[70] De Vahl Davis, G. *Natural convection of air in a square cavity: a benchmark numerical solution*, Int. J. Numer. Meth. Fluids, **3**, 249-264, (1983).

CURRICULUM VITAE

PERSONAL INFORMATION

Surname, Name: Bozkaya, Canan
Date and Place of Birth: 10 December 1979, Ankara
email: bcanan@metu.edu.tr

EDUCATION

Degree	Institution	Year of Graduation
MS	METU, Mathematics	2004
BS	METU, Mathematics	2002
High School	Konya Atatürk Girl High School	1998

FOREIGN INSTITUTE EXPERIENCE

Institution	Year
Institute of Applied Mechanics Technical University of Braunschweig Braunschweig, Germany	2005-2006

AWARDS

- Travel grant for IABEM 2006 Conference, Graz, Austria
- **The Scientific and Technical Research Council of Turkey (TUBITAK)**
  - The Integrated Ph.D. Scholarship, 2003-2007
  - Scholarship for Master of Science, 2002-2003

WORK EXPERIENCE

Year	Place	Enrollment
2002-present	METU, Mathematics Department	Research Assistant

FOREIGN LANGUAGES

English(fluent), German(basic)

PUBLICATIONS

1. C. Bozkaya, *Least squares differential quadrature time integration scheme in the DRBEM solution of convection-diffusion problems*, WIT Transaction on Modelling and Simulation, Online Journal, **39** (2005).

2. C. Bozkaya, M. Tezer-Sezgin, *Boundary element solution of unsteady MHD duct flow with differential quadrature time integration scheme*, Int. J. Numer. Meth. Fluids, **51** (2006), 567-584.

3. C. Bozkaya, *Least squares differential quadrature time integration scheme in the DRBEM solution of convection-diffusion problems*, Eng. Anal. Bound. Elem., **31** (2007), 83-93.

4. C. Bozkaya, M. Tezer-Sezgin, *Fundamental solution for coupled MHD flow equations*, J. Comput. Appl. Math., **203** (2007), 125-144.

5. C. Bozkaya, M. Tezer-Sezgin, *Boundary element method solution of magnetohydrodynamic flow in a rectangular duct with conducting walls parallel to applied magnetic field*, Comput. Mech., **41**(6) (2008), 769-775.

6. C. Bozkaya, *A coupled numerical scheme of dual reciprocity BEM with DQM for the transient elastodynamic problems*, Int. J. Numer. Meth. Engng., (in press).

7. C. Bozkaya, M. Tezer-Sezgin, *Solution of transient Navier-Stokes equations by the coupling of differential quadrature time integration scheme with dual reciprocity boundary element method*, Int. J. Numer. Meth. Fluids, (in press).

8. M. Tezer-Sezgin, C. Bozkaya, *The boundary element solution of magnetohydrodynamic flow in an infinite region*, (revised version is submitted to the J. Comput. Appl. Math.)

CONFERENCE PAPERS

1. C. Bozkaya, *Least squares differential quadrature time integration scheme in the dual reciprocity boundary element method solution of convection-diffusion problems* , in: Proc. of BEM/MRM 27 Inter. Confr., 15-17 March 2005, Orlando, USA, pp. 123-131.

2. C. Bozkaya, *Fundamental solution for some equations in magnetohydrodynamic flow*, in: Proc. of UKBIM5 Inter. Confr., 12-13 September 2005, Liverpool, England, pp. 90-99.

3. C. Bozkaya, *Application of dual reciprocity BEM coupled with least squares differential quadrature time integration scheme to transient elastodynamic problems*, in: Proc. of IABEM 2006 Inter. Confr., 10-12 July 2006, Graz, Austria, pp. 67-70.

4. M. Tezer-Sezgin, C. Bozkaya, *Boundary element method solution of magnetohydrodynamic flow in a rectangular duct with conducting walls parallel to applied magnetic field*, in: Proc. of IABEM 2006 Inter. Confr., 10-12 July 2006, Graz, Austria, pp. 337-340.

5. C. Bozkaya, M. Tezer-Sezgin, *DRBEM solution of natural convection flow with DQ time integration scheme*, in: Proc. of UKBIM6 Confr., 17-18 September 2007, Durham, UK, pp. 89-98.

6. M. Tezer-Sezgin, C. Bozkaya, *BEM solution of coupled MHD equations on the halfplane*, in: Proc. of UKBIM6 Confr., 17-18 September 2007, Durham, UK, pp. 129-138.

CONFERENCE PRESENTATIONS

1. C. Bozkaya, *Differential quadrature solution of Schrödinger equation*, Dynamical Systems Confr., 23-24 April 2004, Izmir, Turkey.

2. C. Bozkaya, *A coupled differential quadrature time integration scheme with dual reciprocity boundary element method applied to the unsteady Navier-Stokes equations*, NA07 Confr., 26-29 July 2007, Dundee, Scotland, UK.